Fakultät für Medizin
Lehrstuhl Epigenetik der Hautalterung

Study of Isolation, Analysis, and Use of Skin-Derived Precursor Cells

Leithe Budel

Vollständiger Abdruck der von der Fakultät für Medizin der Technischen Universität München
zur Erlangung des akademischen Grades eines
Doktors der Naturwissenschaften (Dr. rer. nat.)
genehmigten Dissertation.

Vorsitzender: Prof. Dr. Carsten Schmidt-Weber

Prüfer der Dissertation:

1. Prof. Dr. Karima Djabali
2. Prof. Dr. Burkhard Rost

Die Dissertation wurde am 30.07.2018 bei der Technischen Universität München eingereicht und durch die Fakultät für Medizin am 20.02.2019 angenommen.

Thesis abstract

Stem cells have generated much attention and insight over the last decade and have become a hot topic. These cells are the source for development and maintenance of the human body. Key characteristics include the ability to renew themselves but also to differentiate into other cell types. Such properties have been recognized as imperative tools for research and therapy development. However, while recent stem cell research has shown an increasing variety of different stem cell types, methods to obtain them remain scarce and often cumbersome. In this doctoral thesis, I discuss the 3.5 years of research I spent on developing a novel method to obtain multipotent stem cells in an easy, reproducible, and fast manner. The developed method, discussed in Chapter 1, uses a 30-min low pH stress step on pre-established dermal fibroblasts to obtain multipotent skin-derived precursor (SKP) cells, termed pH-SKPs, after only 5 days. These isolated cells showed all the stemness characteristics of multipotent stem cells. Additionally, during the development of this method, two novel imaging methods were developed to improve the analysis of the spherical SKP cultures. These methods were termed motorized mosaic imaging and video mosaic imaging and are described in Chapter 2. They offer a low-cost and easy mosaic imaging method for macro-scale imaging of microscopic targets. Finally, the findings and progress of the pH-SKP isolation method were applied to cells affected by the rare disease Hutchinson-Gilford progeria syndrome (HGPS) and are described in Chapter 3. From pre-established HGPS fibroblasts, multipotent HGPS pH-SKP stem cells were successfully obtained after only 5 days of culture. Overall, the successful development and application of pH-SKP multipotent stem cells will accelerate stem cell research and promote the development of novel therapies.

Table of Contents

Chapter 1

Rapid Isolation and Expansion of Skin-Derived Precursor Cells from Human Primary Fibroblasts Cultures

Rapid isolation and amplification of skin-derived precursor cells from primary human fibroblasts by low pH stress treatment.

1.0.1 Abstract

Skin-derived precursor (SKP) cells have self-renewal and multipotent abilities and are found in the dermis. SKP cells have been isolated previously from pre-established dermal fibroblast cultures. In these procedures, long-term culture and low yield remain the crucial aspects requiring improvement. In this study, we exposed pre-established dermal fibroblasts to a 30-min acid stress step prior to isolating SKP cells (termed pH-SKPs) and compared the yield to the previously published trypsin- and no-stress isolation methods. Spheroid formation was confirmed and analyzed at days 3, 5, and 7. Stemness was investigated by immunohisto-chemistry for the following stem cell markers: nestin, CD9, Sox2, Oct4, NANOG, vimentin, and NG2. Multipotency was investigated by differentiation into adipocytes, smooth muscle cells, and fibroblasts. Our results showed that the pH-SKP spheroid yield at day 5 was 4- and 5-fold higher than those obtained using the trypsin- and no-stress methods, respectively. The expression of stem cell markers was significantly expressed in pH-SKPs compared to their fibroblast origin. Successful pH-SKP spheroid formation and differentiation were achieved and validated in 11 distinct human primary fibroblast lines. Overall, these results demonstrate that acute acidic stress treatment of dermal fibroblast cultures greatly improves SKP isolation, growth, yield, and multipotency compared to previous methods.

Keywords: acidic stress, adult stem cells, human fibroblast, multipotent, skin-derived precursor cells

1.0.2 Abbreviations

Abbreviation	Meaning
CTRL	control
Dex	dexamethasone
DMEM	Dulbecco's modified Eagle medium
DNA	deoxyribonucleic acid
EGF	epidermal growth factor
FACE-1	farnesylated-proteins converting enzyme 1
FBS	fetal bovine serum
FGF	fibroblast growth factor
h	hours
HGPS	Hutchinson-Gilford progeria syndrome
HSC	hematopoietic stem cell
IBMX	3-IsoButyl-1-MethylXanthine
ICMT	isoprenylcysteine carboxyl methyltransferase
IHC	immunohistochemistry
min	minutes
MMI	motorized mosaic imaging
mRNA	messenger ribonucleic acid
NS-SKP	no-stress SKP
ORO	oil red O
P4HD	prolyl-4-hydroxylase beta
PBS	phosphate buffered saline
PFA	paraformaldehyde
pH-SKP	low pH isolated skin-derived precursor cells
RCE-1	ras converting CAAX endopeptidase 1
RT	room temperature
s	seconds
SKP	skin-derived Precursor
SMC	smooth muscle cells
SM-MHC	smooth muscle myosin heavy chain
Tr-SKP	trypsin-SKP
ZmpSte24	zinc metallopeptidase STE24 homolog

1.1 Background and Introduction

In this subchapter, the general information, basic components, and related investigative techniques are discussed for Chapter 1. The purpose of this subchapter is to provide fundamental information for readers unfamiliar in the field and provide means to increase their comprehension of the thesis' content and conclusions. The discussed topics will provide various answers to certain questions: "What are mammalian cells?" "How are they cultured?" "Why are they used?" etc. Additionally, the principles behind investigative techniques, such as skin-derived precursor (SKP) stem cell isolation, polymerase chain reaction (PCR), and immunohistochemistry (IHC), are also shortly discussed in a fundamental perspective. However, details such as step-by-step protocols, material references, or machine models are not discussed in this subchapter. For this information, I kindly refer to the Materials and Methods subchapter of this chapter.

1.1.1 Tissue culture of mammalian cells

In the scientific field of biology and medicine, mammalian cells are often a crucial component for research development and investigation. The use of these cells outside the host organism for culture, analysis, and manipulation is termed *in vitro* cell research. If the investigation or manipulation of cells would occur in a host organism itself, it is termed *in vivo* research. For this thesis, I only used *in vitro* cell research with human primary skin fibroblasts as mammalian cells. The advantage of *in vitro* cell research is that a very stable environment can be created for more consistent results than would be possible within the host due to additional influential factors (e.g., other host cells or pathogens). For the standard *in vitro* cell research, an incubator is often used providing an environment of 37°C and 5% CO_2 for optimal temperature and pH conditions for the cells. Furthermore, the possibility of hurting or losing the host by death is not a factor for *in vitro* studies, eliminating certain ethical limitations for research. Together, *in vitro* cell research provides the opportunity for broad manipulation and investigation options with high reproducibility.

Mammalian cells, such as skin fibroblasts, can be grown after isolation from a host. The cells used in this study were primary skin fibroblasts from humans. The adjective "primary" is added as they are original cells obtained by isolation from skin tissue biopsy material (Fig. 1). This means that the cells are highly similar to the ones located in the host and have a finite number of times they can duplicate before reaching the Hayflick limit and becoming senescent [68]. Cells that have become senescent cannot duplicate anymore, and this occurrence is a primary cause for aging [175]. Cells that would be immortalized lose the primary adjective and can be grown indefinitely [65, 143]. However, such cells do not represent the host cells well because of cancer-like properties and DNA mutations compared to primary cells [85, 96].

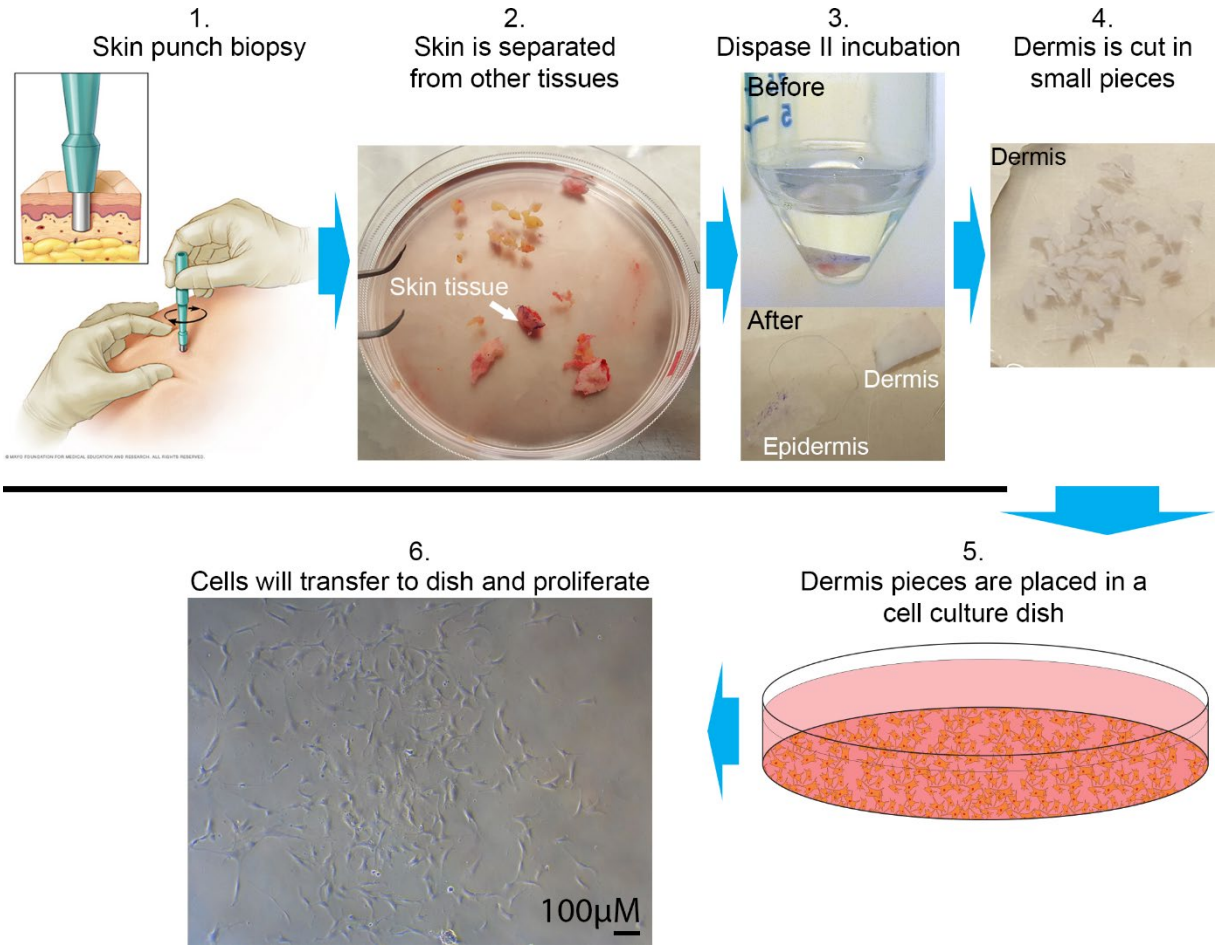

Fig. 1. Representation of skin punch biopsy and the isolation of primary fibroblasts. (**1**) with a circular blade, the deeper layers of the skin are obtained (all image rights of the schematic punch biopsy are reserved to the Mayo clinic). (**2**) After the skin biopsy, other tissue types such as fat or muscle are removed from the skin. (**3**) The skin is then incubated with an enzyme called Dispase II. This enzyme separates the epidermis and dermis layers from each other. (**4**) The dermis layer is then cut into small pieces and (**5**) placed in a cell culture dish with Dulbecco's modified Eagle medium. (**6**) After 1–2 weeks, fibroblast cells have transferred and adhered to the dish's plastic surface and started to proliferate.

Primary fibroblasts are cells that can synthesize extracellular matrix and collagen and represent essential roles in organ and tissue structure but also in wound healing [172, 189]. Fibroblasts are highly present in connective tissue, and therefore, can be isolated in high quantities from skin (Fig. 1) [147]. After isolation, the cells are grown in a medium called Dulbecco's modified Eagle medium (DMEM), which contains necessary nutrients for cell culture such as glucose, amino acids, vitamins, and other elements. Additionally, fetal bovine serum (FBS) and antibiotics (e.g., pen/strep and gentamycin) are added to improve cell growth and add protection against potential pathogens, respectively. In this complete medium, the cells will proliferate and can eventually be passaged (e.g., splitting one dish to five new ones) when 70–90% confluent (the amount of cell-covered surface) with the use of an enzyme called trypsin. Trypsin is required as fibroblasts are adherent cells and attach themselves to the

plastic surface of the culture dish. This attachment is made possible by specific anchoring proteins. Here, trypsin is a serine protease enzyme that cleaves these anchors, resulting in single, detached cells floating in the medium. By repeating this process of proliferation and splitting with trypsin, more cells are obtained with each passage over time.

The above-described cell isolation and culture process is widely applied in the life sciences. Commercial companies such as Coriell Institute and American Type Culture Collection (ATCC) Biorepositories have optimized these protocols and offer culture-ready cells cryogenically frozen and stored in vials at −180°C. After thawing, these cells can directly be placed in a cell culture dish for culture. The used cells for this chapter are a combination of commercially obtained and self-isolated primary fibroblast cell lines (Table 1).

Table 1. Human primary dermal fibroblast cell lines used in Chapter 1.

Name	Condition	Passage	Donor	Skin biopsy	Source
GM05565	Normal	P13	3 YR/M	Inguinal area	Coriell
GM01652	Normal	P16	11 YR/F	Arm	Coriell
GM03349	Normal	P15	10 YR/M	Unspecified	Coriell
GM01582	Normal	P16	11 YR/F	Arm	Coriell
GM03165	Normal	P15	8 YR/M	Unspecified	Coriell
GM01651	Normal	P15	13 YR/F	Arm	Coriell
PDF070	Normal	P11	30YR/F	Forehead	[115]
GM02036	Normal	P15	11 YR/F	Unspecified	Coriell
PDF142	Normal	P12	53 YR/M	Scalp	[115]
PDF323	Normal	P16	41 YR/F	Cheek	[115]
Foreskin	Normal	P7	<10 YR/M	Foreskin	-

1.1.2 Stem cell origin and promise

Before discussing the various type of stem cells, it is helpful to understand what stem cells are and what they can do. Firstly, stem cells are cells that can renew themselves in high numbers, and secondly, keep the ability to differentiate (specialize) into one of the 225 different human cell types currently known (e.g., neuron, muscle, fat, etc.) [54, 188]. There are in total four classes of stem cells, each with a different range of capabilities. **The first class, totipotent stem cells**, is a cell type only present during early embryogenesis and can differentiate into every human cell type known, including placenta related cells [121]. **The Second class, pluripotent stem cells**, includes cell types originating from totipotent cells, are present during late embryogenesis and can also differentiate into every human cell type known, excluding placenta related cells [121]. Additionally, some claim that these cells are also found during adulthood [7, 104]. **Then the third class, multipotent cells**, includes cell types originating from pluripotent cells. These cells are present during adulthood and can only differentiate into a limited set of other cell types. Hematopoietic stem cells (found in bone marrow), for example, are multipotent and can differentiate only into blood-related cells (e.g., erythrocytes, granulocytes, lymphocytes, etc.) [34]. **Finally, the fourth class**, **unipotent or somatic cells**, includes cell types originating from multipotent cells and can only become one specific cell type [16]. Together, all stem cell classes regulate the source and variety of cell types found in the development and maintenance of the human body.

On top of the four classes of stem cells, another level of organization can be found during embryogenesis and includes the so-called three germ layers. For humans, these layers include the endoderm, mesoderm, and ectoderm. For more details about information, described in this paragraph, please see the book *Developmental Biology*, 6th edition [56]. Each of these germ layers consists of different classed cells, such as pluripotent and multipotent stem cells, which will then specialize and differentiate into a certain area of the body during embryogenesis. First, there is **the endoderm layer**, which is responsible for forming the stomach, colon, liver, pancreas, and other main organs. Then, there is **the mesoderm layer**, which is responsible for forming among others the dermis, muscles, bones, circulatory system, and adipose tissue. And finally, there is **the ectoderm layer**, which forms among others the epidermis, hairs, lenses of the eyes, brain, and peripheral nervous system. Together, starting at the embryogenesis, the four classes of stem cells and the organization of three germ layers regulate the development and growth of the human body. In this study, the focus was primarily on the multipotent class stem cells originating from the mesoderm layer (dermis from skin).

Multipotent stem cells are a class of stem cells present at various body sites (e.g., skin, bone marrow, fat, intestines, brain, etc.) during adulthood and are often termed “adult stem cells” [34, 105, 146, 155, 170, 174]. During adulthood, the main functions of these cells are to sustain, replenish, and repair old, damaged, or lost cells. For example, erythrocytes (red blood cells) are generally replaced in the body after three months of function by new ones generated via differentiation of multipotent blood stem cells [34]. Similarly, after incurrence of damage—as is seen with wounds to the skin—the tissue heals by generating new cells to repair the lost ones. However, while these multipotent stem cells can repair or replace tissue in the aforementioned situations, with other damages—such as spinal cord injury and brain damage by stroke or diseases such as diabetes—the repairs are mostly absent or incomplete. While this is the case *in vivo*, studies have shown that *in vitro* the multipotent stem cells are actually capable of differentiation into neurons or islet-type insulin-producing cells, when under the right conditions with the right differentiation cocktails [66, 81]. Such obtained cells *in vitro* are required to repair or cure damages or diseases not repairable naturally *in vivo*. This discovery led to the research field of cell-based therapy, offering a myriad of possibilities in future treatments. These possibilities envision the isolation of multipotent stem cells from the human body to first differentiate them *in vitro* into any desired cell type. Then, these cells could be used to repair extraordinary damages, such as spinal cord injury *in vivo*. However, finding the right type of multipotent stem cells, methods of isolation and propagation, and differentiation cocktails leave significant steps to be explored and optimized for future cell-based therapies.

1.1.3 Skin-derived precursor cells

In the scientific and medical field, there is an increasing interest in human multipotent stem cells derived from the skin, coined as skin-derived precursor (SKP) cells. These type of multipotent stem cells are present throughout adulthood, reside accessibly within the dermis of the skin, can self-renew, and express stem cell markers [5, 49, 97, 122, 138, 167, 169]. More will be discussed later about stem cell markers. Additionally, SKPs can be readily isolated and expanded from skin biopsy independent of the subject's age, site of biopsy, or disease [82, 173]. Together, these factors have made SKPs a topic of great interest as studies continue to find increasing potential in their multipotent ability to become other cell types.

Several studies have shown that SKPs can differentiate into various mesodermal and ectodermal cell types, such as smooth muscle cells, fibroblasts, neuronal cells, osteocytes, Schwann cells, and adipocytes [11, 77, 91, 92, 158, 163]. Recently, SKPs were shown to even differentiate into endodermal-like functional insulin-producing islet-like cells *in vitro* [10, 118]. These results suggest that SKPs could be used as a new tool for diabetes research and possible treatment. Another study demonstrated the scalability of SKPs for large expansion and differentiation into Schwann cells [183]. Such cells could then be used in axon/nerve

regeneration research or as cell therapy for neurological injuries, such as spinal cord injury [88, 124, 177, 198], but also for a disease such as multiple sclerosis [191]. In addition to their multipotent ability, SKPs have also shown promising results for stroke treatment thanks to their secreted fibroblast growth factors (FGF) and vascular endothelial growth factors, which are known to promote angiogenesis and neural stem cell proliferation [111]. Consequently, SKPs are becoming attractive tools for disease modeling and therapy development as they are present during adulthood, multipotent, secrete a wide range of growth factors, and have great regenerative potential.

1.1.4 Classical isolation of skin-derived precursor cells

The isolation of SKP cells from human skin biopsy has been well established [1-3]. For this method, the isolation of dermis from biopsied skin is required (Fig. 1). This dermis is directly used to isolate cells from with protease enzymes such as trypsin or collagenase IX (Fig. 2). Both these enzymes cleave peptide chains and dissociate the tissue into single cells. The

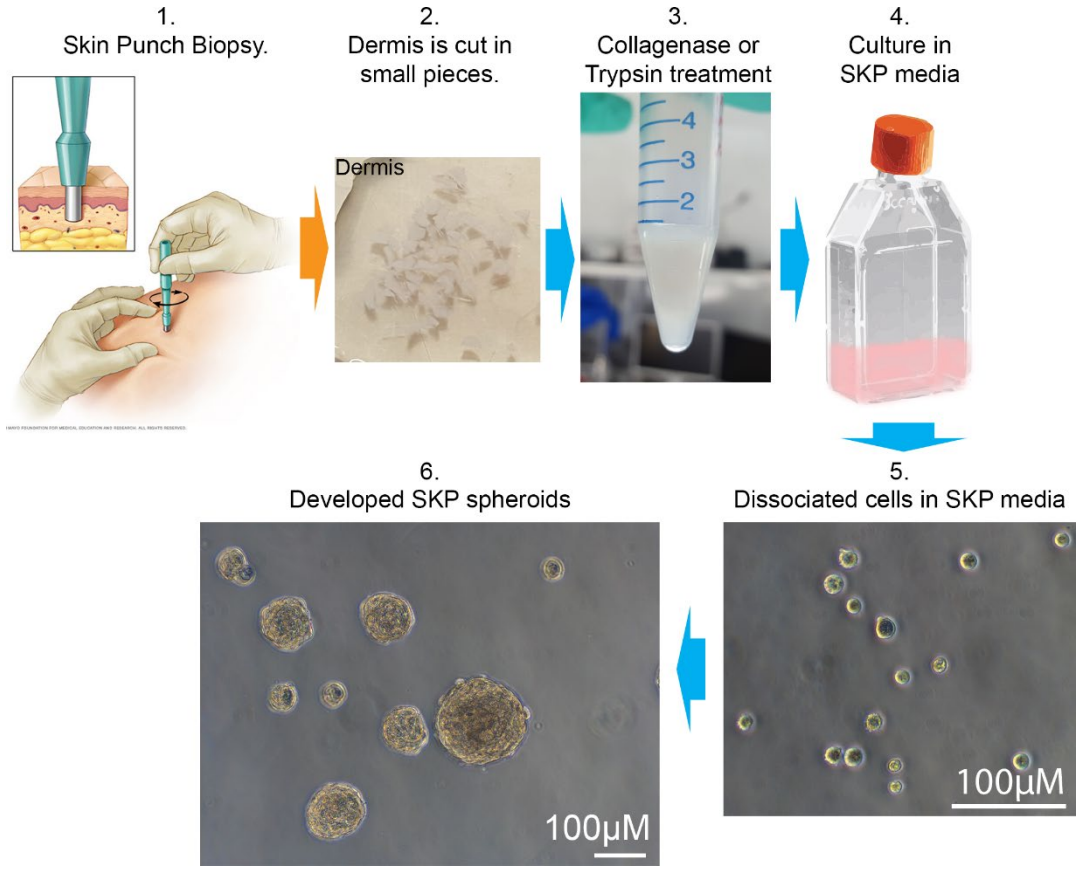

Fig. 2. Representation of classical SKP isolation from the skin. (**1**) With a circular blade the deeper layers of the skin are obtained (all image rights of the schematic punch biopsy are reserved to the Mayo clinic). (**2**) After preparing the skin (by removing the epidermis), the dermis is cut into pieces. (**3**) These pieces are then incubated in trypsin or collagenase, which dissociates the tissue into a single-cell suspension. (**4**) Dissociated cells are then transferred into SKP medium containing EGF and FGF and are (**5**) further cultured in a T25 non-treated flask in suspension. (**6**) After 2–3 weeks, the cells will develop into SKP spheroids.

dissociated dermis cells are then further cultured and expanded in a medium containing epidermal growth factor (EGF) and fibroblast growth factor 2 (FGF2 or FGF), resulting in a suspension culture of SKP spheroids over time (Fig. 2). Both EGF and FGF are growth factor proteins that maintain and stimulate the stem cell properties and growth of these SKP cells [48, 168, 170].

The main limitation of the classical SKP isolation method is the necessity of obtaining fresh skin biopsies for dermis tissue each time to isolate the SKPs. It increases the technical difficulty and decreases availability and accessibility for the study and use of SKPs because access to human skin samples is limited and requires ethical committee approval. In addition, large-scale expansion of SKP cultures rapidly increases cost due to the required essential growth factors. Therefore, alternative methods were sought for.

1.1.5 Trypsin-stress based SKP isolation

An alternative approach was investigated for SKP isolation, which was one that uses pre-established dermal primary fibroblast cultures to circumvent the limitations inherent to the classic SKP isolation method. Here, pre-established cultures are cells originally isolated from a biopsy but then further grown in culture as primary fibroblasts. These cells are grown in a monolayer configuration and can be easily expanded into large quantities. They are also inexpensive to culture as they only need standard medium (without costly growth factors) to grow. On top of that, they can be easily preserved for decades via cryogenic storage. Thanks to these properties, pre-established cultures can also be easily obtained from commercial cell banks such as Coriell Institute and ATCC Biorepositories, who offer a wide range of culture-ready cells with normal and disease conditions. Since pre-established fibroblast cultures originate from the skin dermis, the thought is that SKP cells might still be present in them [185]. Therefore, pre-established primary fibroblast cultures were thought to represent an attractive alternative for skin to isolate SKPs from.

The first method that successfully isolated SKP-like cells (from here on just SKP cells) from pre-establish fibroblast cultures was developed by Wenzel et al. [185]. With this isolation method, trypsin is used as a temporary cellular stressor on pre-established fibroblasts, followed by a 21-day culture in conventional SKP medium. Normally, trypsin is only used for 10 min on cultured cells with the purpose to detach them forcibly from the culture dish. This process exposes the cells to high stress as exterior anchoring membrane proteins are cleaved, forcing the cells into suspension [144]. For the trypsin-SKP isolation method, cells are placed for 16 h in trypsin at 37°C to induce high stress levels resulting in large numbers of cell death. The rationale behind the stress is that stem cells, such as the SKPs, are more robust, can survive high stress conditions, and can also renew into large numbers, while somatic fibroblast

cells cannot. Then, by placing the stressed cells into SKP medium, further stem cell isolation and proliferation is stimulated. As a result, after 21 days of culture in SKP medium, SKP spheroids develop (termed Tr-SKPs) and are capable of differentiation [185].

Additional to Tr-SKPs, a second method was published shortly after by Hill et al. [71]. In that method, similar results for SKP cell isolation from pre-established fibroblasts were reported but without the application of any stress. However, no clear results were presented concerning the purity of SKPs after the isolation.

Currently, only the two previous studies mentioned above have reported an alternative isolation method for SKP cells from primary fibroblast cultures. Both methods remain subject to certain limitations and unclear factors. These include the reduced multipotency of SKPs isolated from fibroblast cultures at high passage, the long period needed to grow SKPs, the unknown differentiation efficiencies, and the low yields of SKPs. Such limitations must be addressed via either improved methods or alternative approaches for SKP isolation so that the great promise SKPs hold become significantly closer to realization.

1.1.6 Acidic-stress based SKP isolation

The main topic of investigation I discuss is an alternative novel SKP isolation method that uses acidity as a stressor. Topics such as the finding, the analysis, and establishment of this method will be described in detail. The foundation of our hypothesis for the acid SKP isolation method was based on previous observations of which acidic pH affected certain cellular properties such as proliferation and differentiation [51]. We then hypothesized that temporary acidic stress on pre-established primary fibroblast cultures would improve and accelerate the isolation and proliferation of SKP cells *in vitro*.

Via experimentation, a final method was designed in which acute acidic stress exposure to pre-established fibroblast resulted in accelerated SKP isolation. Additionally, strong spheroid growth after only 5 days was seen with high yield. These SKP spheroids also exhibited multipotent ability independent of the fibroblast line of origin or passage number *in vitro*. Therefore, this novel strategy provides an improved alternative method for SKP isolation from pre-established primary fibroblasts.

1.2 Methodology Used

Various methods and analysis approaches were employed to test the hypothesis and establish a novel SKP isolation protocol. In this subchapter, the background and principles behind those approaches are shortly discussed. After this subchapter, a detailed step-by-step protocol for each method mentioned in this chapter is followed. The protocols include exact material references to provide the means and full understanding for repetition and validation by other scientists.

The cell culture method was the most fundamental method used, where primary fibroblast cell lines were cultured to gain testing material. These cells were then used for the various treatments to attempt isolation of SKP cells, including the trypsin-stress based, no-stress based and low pH stress-based methods. To determine the presence and efficiency of each method to isolate SKP cells, the following analysis approaches and protocols were used: cell culture, immunohistochemistry, flow cytometry analysis, motorized mosaic imaging, ribonucleic acid (RNA) expression analysis, cryosectioning, protein expression analysis via western blot and antibody staining, and adipocyte, smooth muscle cell, and fibroblast differentiation.

1.2.1 Immunohistochemistry labeling

Immunohistochemistry labeling is a technique that allows visualization of specific proteins present in or on the cell and can be made visible thanks to the use of antibodies. These antibodies are Y-shaped glycoproteins (or immunoglobins), high in molecular weight, and able to bind specifically to other molecules and proteins (Fig. 3A). This principle functions as each protein has its unique conformation of amino acids, creating various points (so-called epitopes) to which an antibody can bind. Antibodies themselves are generated by injecting the target protein (or only the epitope) into a host animal. Since the injected material is foreign to the immune system of the host, the host will start to produce B cells against it. These can produce and secrete a specific antibody against the foreign material, similar as it would against a virus to neutralize it. For further information regarding antibody function and creation, I kindly refer to the book *Molecular Biology of the Cell*, 4th edition, chapter 24, subchapter B, Cells and Antibodies.

After generation of B cells in the host animal, antibodies can be further modified. By adding a protein with a fluorophore, called a fluorescent protein (e.g., green fluorescent protein), the antibody can be visualized by laser excitation (Fig. 3B). When the laser light of the fluorescent microscope hits the fluorophore, a light signal is released. The modified antibody is then added to the cells, which will then bind to its target in or on the cells. Each acquired signal with the microscope would then represent the protein of interest and represents its location and concentration. A similar second technique uses the addition of a secondary antibody. Here, the primary antibody can only bind to the protein of interest and the secondary antibody containing the fluorophore only to the primary one (Fig. 3C). The advantage is that multiple secondary antibodies can bind to one primary antibody. As a result, there is a stronger fluorescent light signal per protein of interest obtained, which produces a better image for

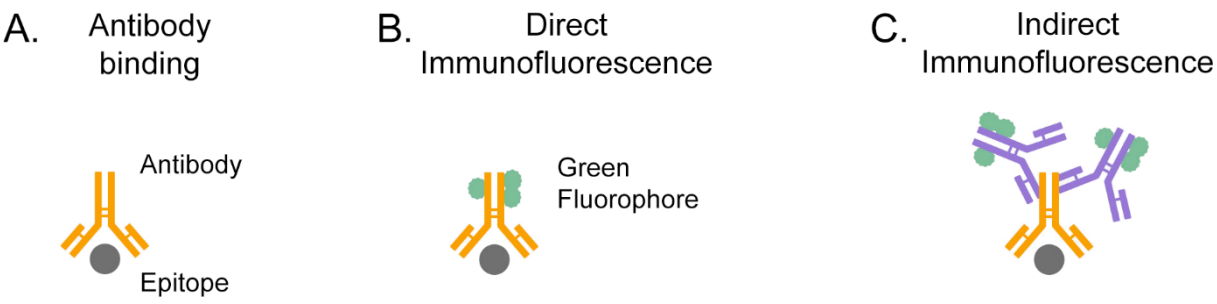

Fig. 3. Antibody principle and fluorescent labeling. (**A**) An antibody is a Y-shaped immunoglobin protein originally generated by the immune system and can bind to an epitope. (**B**) For direct immunofluorescence, a fluorophore is attached to the antibody, which can be visualized by light. (**C**) For indirect fluorescence, a secondary antibody can be used. The secondary antibody binds to the primary one and increases the signal intensity.

proteins present in low concentrations. Above antibody and fluorescence principles, have been highly modernized and commercialized by specialized companies such as Abcam (Cambridge, United Kingdom) and Santa Cruz Biotechnology (Dallas, USA). They offer a plethora of antibodies for research, of which each can bind to a specific target protein of interest. There are various fluorescent proteins with different colors thanks to alternative fluorophores. Each of these antibodies can then be used to visualize a broad range of specific proteins. Overall, this cell protein visualization process is termed immunohistochemistry and also known in the nomenclature as immunofluorescent staining or fluorescent labeling. In this study, immunohistochemistry techniques were mainly used to visualize proteins previously identified as stem cell markers to detect stem cells. Specific antibodies were also used to visualize proteins that represent a specific differentiated cell type, such as smooth muscle cells or fibroblasts.

1.2.2 Flow cytometry analysis

Flow cytometry analysis was applied to evaluate the cells of interest. It analyses the number of dead cells versus the number of living cells to determine overall cell viability of a sample. To do this, the technique uses fluorescent labeling of a specific target from which the levels are then detected via a laser excitation source. The fluorescent labeling for viable cells is different compared to the immunohistochemistry labeling described previously. Instead of antibodies, a fluorescent dye is used that binds to DNA. Then, in the flow cytometer apparatus, each cell is separately measured for its signal. After counting a set number of cells, a percentage per category (live or dead) can be given, representing the viability state of one sample.

There are many flow cytometers with the purpose to detect fluorescent signals. In this thesis, the Muse Cell Analyzer from Millipore Merck was used (Fig. 4A). At the right of the device, there is an arm that holds the sample placed in an Eppendorf tube. The viability reagent of Millipore Merck is added and incubated for 5 min with the sample in order to determine the number of dead and live cells. More details of these steps will be described in the step-by-step protocol subchapter located further below. The viability reagent of Millipore Merck contains two fluorescent dyes. The first dye is a yellow DNA-binding dye. This dye can only stain the DNA if the outer membrane and nuclear membrane of the cell have lost their integrity (e.g., damaged and permeable). Thus, the dye only enters and stains dead and dying cells. In contrast, live cells with intact cell membranes cannot be stained with the first dye. However, the second dye is a membrane-permeant red DNA-binding dye. This dye can permeate through intact membranes and stain the DNA. Together, the two dyes represent dead, dying, living, and nucleated cells (Fig. 4B). By counting 5,000 to 10,000 cells, a very accurate viability assay can be performed. Thanks to the two dyes, two main groups will form in the analysis plot. One

group contains the live cells and the other the dead cells (Fig. 4C). The viability assay was used to determine the cell number and viability before and after the various SKP isolation methods.

A.

B.

Two dyes:
1. Yellow non-membrane permeable DNA-binding dye.
2. Red membrane permeable DNA-binding dye.

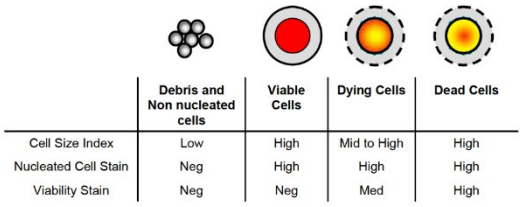

	Debris and Non nucleated cells	Viable Cells	Dying Cells	Dead Cells
Cell Size Index	Low	High	Mid to High	High
Nucleated Cell Stain	Neg	High	High	High
Viability Stain	Neg	Neg	Med	High

C.

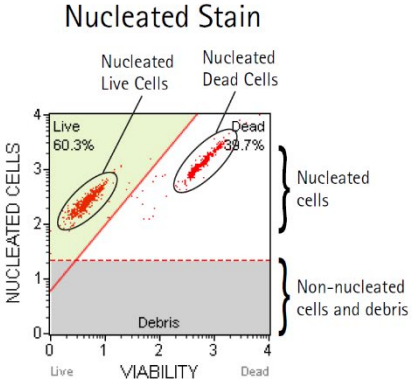

Fig. 4. Muse Cell Analyzer and cell viability assay. (**A**) The Muse Cell Analyzer from Millipore Merck is a small convenient device with only a footprint of 20 × 25 cm, a green excitation laser, and a multitude of pre-configured analysis options such as the viability assay. (**B**) With the use of the two dyes, one yellow non-membrane permeable DNA-binding dye and one red membrane permeable DNA-binding dye, live cells can be separated from dead and dying ones. (**C**) A plot is given of live and dead cells after analysis.

1.2.3 Motorized mosaic imaging

After the treatment of cells with the no-stress, trypsin-stress, and low pH stress conditions, spheroid development was investigated. For all SKP isolation methods, the cells go from a single-cell suspension state to a three-dimensional spherical suspension state. This process occurs via a combination of cellular proliferation and amalgamation, increasing the total cell number and the formation of cellular spheroids. These spheroids represent the yield of a particular SKP isolation method. For previous studies, either the spheroid number or average spheroid size (based on an average small sampling number) was reported as a yield indicator of the isolation method [70, 186]. Such an approach has the disadvantage that if for example method A resulted in 100 spheroids and method B in 150, method B is chosen as the best method. This without knowing whether method A had 100 spheroids of 1,000 µm in diameter size and method B 150 of 50 µm. In that case method A should have been chosen as the best.

Similarly, if the average spheroid size of method A would be 500 µm and 250 µm for method B, method A is chosen as the best method. This without knowing whether method A produced 50 spheroids averaging 500 µm and method B 1,000 spheroids of 250 µm. In that case method B should have been chosen as the best method. To circumvent these issues, the total amount of SKP spheroids was determined, factoring in both the total number and size of each spheroid, to represent the total yield.

To determine the total yield, including the total spheroid number and the size of each individual spheroid, a novel imaging and analysis method was developed. The development, functions, and other potential uses of this method will be further described in detail in Chapter 2, pages 93 to 127. For Chapter 1 only the novel method, termed motorized mosaic imaging (MMI), was used, and its principles will be shortly explained here.

As mentioned above, SKP preparations are cultured in T25 non-treated flasks. The cells and spheroids are in suspension with an approximate volume of 3 mL. For the novel MMI technique, this whole volume containing all the spheroids is transferred and divided over two 48-well-plate wells and then imaged. The MMI technique uses a motorized table connected to a microscope with a computer and a camera. With this setup and the appropriate objective, a magnified image can be obtained at a specific point of the 48-well-plate well. The first magnified image is acquired from the top left corner of the well. Then, with the use of the motorized table, the sample is moved, and another image is acquired below the first image. The second image is positioned in such a way that it is partially overlapping with the first. This process is repeated for the whole well via programmed imaging and positioning. By acquiring these magnified images of the whole well in an overlapping fashion, mosaic software (Autopano Giga, Kolor) can be used. The mosaic software uses the overlapping parts of images to stitch them together into one large mosaic image. For further methodological principles and details, I kindly refer to Chapter 2, pages 95 to 110. As a result, a whole-well mosaic image of each well is obtained containing all the spheroids at high magnification (Fig. 5).

With the use of mosaic imaging, all the data of the complete sample is obtained. The total spheroid number and each spheroid size are captured in a digital image. Via further image processing with Photoshop CC and analysis by ImageJ, discussed further in the Materials and Methods section of Chapter 1 (page 37 and 38), numerical data can be obtained. This data includes values for the spheroid number and size. By combining both values, a total yield per SKP preparation can be calculated. In this chapter, the MMI method was applied to analyze the total yield of SKP preparations at culture days 3, 5, and 7 for no-stress, trypsin-stress, and low pH stress SKPs (referred to as pH-SKPs from here on).

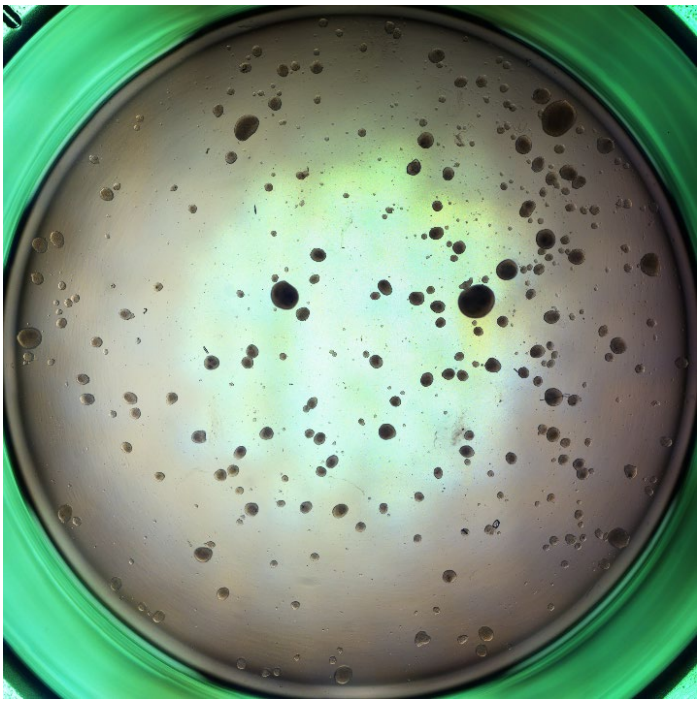

Fig. 5. Whole-well mosaic image. This image was obtained via the MMI method. In the mosaic image, all the spheroids in the 48-well-plate well from an SKP preparation can be seen. The high-resolution image makes it possible to zoom in and visualize microscopic particles (for more details please see Chapter 2).

1.2.4 RNA expression analysis

One of the techniques to determine the stem cell status of SKP spheroids is via messenger RNA (mRNA) expression analysis. Each different class of stem cell type (totipotent, pluripotent, multipotent, and unipotent) express different stem cell-related proteins to maintain their stemness and differentiation capabilities. These proteins are transcribed from genes located in the DNA resulting in mRNA. This mRNA is then translated into peptide chains representing the protein. Therefore, by isolating the RNA, one can determine the expression level of a particular protein based on its mRNA expression. In the case of my projects, mRNA expression of stem cell-related proteins was compared between normal fibroblasts and SKP cells after pH-SKP isolation. Together, the two values present an x-fold of change, in which a positive value represents a higher value of protein expression for the pH-SKP cells. When the value is significantly higher, it indicates their status as multipotent stem cells.

The literature was thoroughly investigated to select the protein targets expressed in SKPs. Based on existing literature, there are currently 23 publications stating expression of the protein Oct4 [28, 30, 37, 43, 66, 70, 76, 89, 98, 100, 101, 104, 134, 135, 152, 164, 166, 182, 186, 193, 196, 197, 201] and 16 for NANOG [28, 30, 70, 76, 89, 104, 134, 135, 152, 157, 166, 182, 186, 193, 199, 201, 202] in SKPs or similar derived from the skin. From this literature collection, nine publications [70, 89, 104, 134, 166, 182, 186, 197, 199] discuss the use of established primary fibroblast cultures to obtain stem cells. Furthermore, two of those publications clearly stated the fold change in expression between fibroblasts and the obtained stem cells from them [166, 186]. With Oct4 ranging between 1.2–15-fold and NANOG 2–20-fold of increase compared to fibroblasts (both for human). Both Oct4 and NANOG are proteins of interest as they have classically been known to be expressed in totipotent and pluripotent stem cells [203].

However, the above-found literature for Oct4 and NANOG also indicate that they play a role in multipotent stem cells. Higher expression of these proteins indicates the stemness and multipotent ability of the cells. For this reason, the mRNA expression of these proteins was included as stem cell markers for pH-SKPs. Additionally, other proteins known to be expressed in SKPs are nestin [97], Sox2 [5], CD9 [80, 98], C-Myc [30] and Klf4 [30], which were all analyzed for their expression in pH-SKP cells versus the origin fibroblast cells.

To analyze the mRNA expression of genes, a technique called quantitative real-time quantitative PCR (qPCR) can be applied. Here, cDNA is used, which is a complementary strand from the mRNA, synthesized via molecular biological techniques (described further in the Materials and Methods section). In regard to SKP spheroids, they will be collected and used to isolate the total RNA. For a full description regarding RNA isolation, see the step-by-step protocol in the next Materials and Methods subchapter. After the total RNA is isolated, it is converted into cDNA with the use of reverse transcriptase. Then, an oligonucleotide primer pair of each approximately 18 to 25 nucleotides is designed to fit and amplify the gene of interest. These primers are then added in a cDNA mixture with other components required for the PCR process (see Materials and Methods). PCR itself involves a series of heating and cooling to activate various reactions. During the PCR reaction, one primer binds onto the DNA of the gene of interest present in the cDNA. As a result, the cDNA strand of the gene will be complemented by the polymerase enzyme, creating double-stranded DNA. By heating the mixture, the double-stranded DNA separates again. To one strand the first primer can bind again, and to the other complementary strand, primer two can bind. Both strands will be complemented again by the polymerase enzyme, followed by denaturing, followed by primer binding, etc. With one of the components in the PCR mix, the double-stranded DNA can be visualized for detection. This component is a fluorescent marker called Sybr Green and only binds to double-stranded DNA due to its intercalating properties. When present in double-stranded DNA, the Sybr Green marker emits a signal when excited by a laser. This is then detected by the device, which plots a graph of the intensity at different intervals. Samples that have higher gene expression will be faster detectable compared to low gene expression. The expression value of the origin fibroblasts can then be compared with the pH-SKPs.

Additional to the real-time qPCR, there is also the classical PCR. The advantage of this method is that it is less prone to error—in exchange for lower sensitivity. Here, the cDNA is amplified similarly as with the real-time qPCR, but the amplification product is placed on an agarose gel instead. This gel is then run under a voltage causing the DNA fragments to separate from each other based on their molecular size. The separation provides an additional benefit in which only the gene of interest is analyzed because with real-time qPCR the signal does not differentiate between different DNA amplicon products. This separation is especially helpful with difficult-to-amplify DNA fragments, in which non-specific amplification could occur,

potentially resulting in false positives. To detect the DNA in the agarose gel, it contains a DNA intercalating agent that becomes detectable under an ultraviolet (UV) source. The visualized DNA bands are then imaged and compared between samples. A thicker band indicates higher gene expression. With specialized image analyzing software differences in band thickness can be accurately determined. This difference represents the x-fold change in (mRNA) protein expression.

1.2.5 Cryosectioning of spheroids

The pH-SKP spheroid first need to be sectioned in order to apply the immunohistochemistry protocols as discussed previously. After the desired number of days in culture, the spheroids are transferred into optimal cutting medium (OCT) and then frozen and stored at −80°C. The freezing preserves the spheroids and makes it possible to section them while frozen. The sectioning occurs in a specialized apparatus called a cryostat that maintains a temperature between −15°C and −30°C. The spheroids are then sectioned at a thickness of 5 µm. This section is then attached to a coverslip and immediately fixated in ice-cold methanol (−20°C) for 10 min. For further descriptions regarding cryosectioning, please see the following Materials and Methods subchapter. After the fixation, samples can be either stored or used for immunohistochemistry purposes to visualize the proteins of interest. The following proteins were investigated in spheroids: nestin, lamin A, CD9, Sox2, Oct4, NANOG, vimentin, NG2, and fibronectin.

1.2.6 Differentiation of SKP cells

One of the most important and applicable potentials of stem cells is their ability to differentiate into different cell types. SKPs are known to be able to differentiate into various types of cells. The focus in this chapter was placed on the differentiation into adipocytes, smooth muscle cells, and fibroblast cells. Various pathways need to be activated to start the wanted differentiation to differentiate the cells. For this purpose, special differentiation mixes have been developed and optimized during this study. Further information concerning reagents and specific protocols can be found in the next subchapter.

The pH-SKP cells are in a spheroid formation and have to change their conformation for the differentiation protocols. Therefore, for all differentiation protocols, spheroids were first adhered to a plastic surface. The adherence causes the cells to flatten and spread, providing better access to the differentiation mix for each cell. For some differentiation cell types, a higher or lower cell density was required. For example, the pH-SKP cells required a high cell density to successfully differentiate into adipocytes, while for smooth muscle cell and fibroblast differentiation, a low cell density was required instead.

1.3 Materials and Methods

In this paragraph, the materials and methods used in this chapter are described in detail. First in an overview and then as an exact step-by-step protocol. The step-by-step protocol is provided because the focus of this thesis lays on method and technique development. Knowledge for precise execution is therefore required. By following the step-by-step protocol, one can exactly repeat the performed experiments. In addition to the step-by-step protocol, the specific reagents and media will also be provided.

1.3.1 Cell culture

In general, cells were first thawed from a cryogenic vial. Note, only vials were used for this thesis. Therefore, the step-by-step protocol regarding cell culture will start based on the material contained in a vial. All other cell lines can be cultured based on this protocol.
The human primary dermal fibroblast lines GM05565, GM05757, GM01652, GM03349, GM01582, GM03165, GM01651, and GM02036 were all obtained from Coriell Institute (New Jersey, USA). PDF070, PDF142, and PDF323 were obtained from a previous study [116]. The above cell lines were all originally established from skin biopsies of unaffected individuals (Table 1). The human mesenchymal cell line, bone marrow mesenchymal stem cells (BM-MSC), was kindly provided by Toguchida Junya and Aoyama Tomoki from the Kyoto University [131]. A comparison between the no-stress SKP (NS-SKP), Tr-SKP, and pH-SKP isolation methods was performed with normal dermal primary fibroblasts originally isolated from foreskin, as described previously [185]. All fibroblast cell lines were cultured as monocultures in DMEM (Sigma, D6429) supplemented with 15% FBS (ThermoFisher-Gibco, 10270106), 1% L-glutamine (ThermoFisher-Gibco 25030081), 1% penicillin/streptomycin (ThermoFisher-Gibco, 1514022), and 0.4% gentamycin (ThermoFisher-Gibco, 15710049). Fibroblasts were sub-cultured and used when they were approximately 80% confluent because the use of confluent cultures resulted in poor SKP isolation and reduced viability. Furthermore, all fibroblast cultures in this study were used at passage numbers ranging from 7 to 21. All cultures were performed in a cell incubator (Binder, 9140-0046) with a humidified chamber at 37°C and 5% CO_2.

Cell culture: step-by-step protocol.

Required medium:

Fibroblast culture medium:
The following was added to a bottle of 500 mL of DMEM (Sigma, D6429): 75 mL of FBS (final concentration 15%), 5 mL of penicillin/streptomycin (final concentration 1%), 5 mL of glutamine (final concentration 1%), and 2 mL of gentamycin (final concentration 0.4%). All the contents were mixed, and the bottle then stored at 4°C until use.

Cell culture:

1. The vial containing the cells was taken out of the cryogenic storage and placed at room temperature (RT) to thaw. After approximately 10 to 15 min, the cells were transferred into a 50-mL tube containing 5 mL of fibroblast culture medium.
2. The emptied vial was then rinsed once with 5 mL of culture medium. This volume was added to the 50-mL tube.
3. The 50-mL tube containing all the cells from the vial was then centrifuged at 450 × g for 5 min at RT to pellet the cells.
4. After centrifugation, the supernatant was aspirated. About 10 to 20 mL of sterile phosphate buffered saline (PBS) was added to wash the cells once. The previous centrifugation step was repeated.
5. After the second centrifugation step, the supernatant was aspirated, and the cells resuspended in fibroblast culture medium. The volume of this medium depended on the number of dishes prepared for culture. In general, one vial was divided over five cell culture dishes or between 2×10^5 and 3×10^5 cells per dish. In this step, 10 mL of fibroblast culture medium was added to the cell pellet for resuspension and was then divided into 2 mL aliquots per dish. Before adding the cells, 6 mL of fibroblast culture medium was added to each new dish. The final volume including cells equaled 8 mL.
6. After adding the cells to the dishes, the dishes were gently agitated by a swirling motion to homogenize the cells throughout the medium and spread them over the dish.
7. The culture dishes were then placed into the cell incubator. This incubator was set at 37°C and 5% CO_2. Every Monday, Wednesday, and Friday, the medium was aspirated and refreshed with 8 mL of fresh fibroblast culture medium.
8. When the cells became approximately 80% confluent, they were either divided into more dishes or used for experimentation.

Dividing one cell culture population from one culture dish into multiple:

1. The dishes containing the cells were taken out of the cell incubator and placed in the biosafety cabinet that maintained a sterile working area.
2. The medium was aspirated from each dish, and 8 mL of sterile PBS was added to wash the cells and remove any FBS residue.
3. The dish with PBS was gently agitated via a swirling motion followed by aspiration.
4. Then, 0.5 mL of trypsin was added directly on top of the cells. The trypsin was spread over the whole dish by tilting it in all directions. The dishes with trypsin were then incubated for 10 min in a cell incubator at 37°C.
5. After incubation with the trypsin, fibroblast culture medium was added to each dish to stop the trypsin's enzymatic reaction and collect the cells. In general, 9 to 10 mL of fibroblast culture medium was added to the first dish. With this volume, the dish was gently sprayed to collect the cells and detach any remaining cells. The same suspension was then used for the next two or three dishes for cell collection. After those dishes, a fresh volume of 9 to 10 mL culture medium was added to the next dish. The same process was repeated for all dishes. The total cell suspension of one cell line was then collected into a 50-mL tube.
6. After collecting all the cells, they were centrifuged 450 × g for 5 min at RT.
7. The supernatant was aspirated and the cells resuspended in fresh fibroblast culture medium. The amount of volume depended on the number of dishes prepared. For each newly prepared dish, 2 mL of fibroblast culture medium was added to the cell pellet. For each new dish, 6 mL of fresh fibroblast culture medium was pre-deposited. In general, either 1 dish with cells was divided over 3 to 5 new ones (depending on the proliferation speed of the culture) or between 2×10^5 and 3×10^5 cells per dish. After mixing the cells in the freshly added culture medium via careful pipetting with a 5- or 10-mL pipet, 2 mL of the cell mixture was added to a new dish containing the pre-deposited fresh 6 mL medium. This mixture was then mixed via careful swirling.
8. The new dishes with cells were placed in the cell incubator providing 37°C and 5% CO_2. When 80% confluent, either above steps were completely repeated, or the cells were used for experimentation after step six.

1.3.2 Isolation protocols of SKPs

1.3.2a Trypsin-SKP isolation and culture

Trypsin-based isolation of SKP cells (Tr-SKP) was performed based on a previously described method [185]. Briefly, 80% confluent fibroblast cultures were washed with sterile PBS and incubated in 5 mL of 0.25% trypsin-EDTA (ThermoFisher-Gibco, 25200056) for 16 to 18 h in a cell incubator at 37°C and 5% CO_2. The cells were then pelleted (450 × g 5 min at RT) and washed in standard DMEM containing 15% FBS, followed by a PBS wash. One million cells were resuspended in 6 mL of classic SKP medium [169] ([4:1 – DMEM [ThermoFisher-Gibco, 21885025]: F12 [ThermoFisher-Gibco, 21765029], 20 ng/mL EGF [ThermoFisher-Gibco, PHG0311], 40 ng/mL bFGF [ThermoFisher-Gibco, PHG0021], 2% v/v B27 [ThermoFisher-Gibco, 17504044], 0.5 µg/mL Fungizone [ThermoFisher-Gibco, 15290018] and 100 U/100 µg/mL penicillin/streptomycin [ThermoFisher-Gibco, 1514022]) and equally divided over two T25 non-treated flasks (Fisher Scientific-Falcon, 10112732, USA). Cultures were fed every other day with 10× SKP medium (SKP medium with 10× concentrated EGF, bFGF, and B27) diluted to a final concentration of 1× in culture medium and agitated daily by pipetting up and down to prevent clumping and cell adherence to the plastic flask.

Trypsin isolation and culture (Tr-SKPs): step-by-step protocol.

Required media:

Table 2. 1× SKP medium – used for SKP isolation.

	Total volume	10,000	µL		
	Times concentrated	1			
	Material			**End concentration**	
1	DMEM (low glucose) Gibco, 21885-025	7,255.5	µL		
2	F12 Gibco, 21765-029	2,418.5	µL		
3	EGF (0.1 mg/mL) ThermoFisher-Gibco, PHG0311	2	µL	20	ng/mL
4	bFGF (0.1 mg/mL) ThermoFisher-Gibco, PHG0021	4	µL	40	ng/mL
5	B27 ThermoFisher-Gibco, 17504044	200	µL	2%	v/v
6	Fungizone (250 µg/mL) ThermoFisher-Gibco, 15290018	20	µL	0.5	µg/mL
7	Pen/Strep (10,000 U/10,000 µg/mL) ThermoFisher-Gibco, 1514022	100	µL	100 U/100	µg/mL

Table 3. 10× SKP medium – used for SKP feeding.

	Total volume	10,000	µL		
	Times concentrated	10			
	Material			**End concentration**	
1	DMEM (low glucose) Gibco, 21885-025	5,865	µL		
2	F12 Gibco, 21765-029	1,955	µL		
3	EGF (0.1 mg/mL) ThermoFisher-Gibco, PHG0311	20	µL	200	ng/mL
4	bFGF (0.1 mg/mL) ThermoFisher-Gibco, PHG0021	40	µL	400	ng/mL
5	B27 ThermoFisher-Gibco, 17504044	2,000	µL	20%	v/v
6	Fungizone (250 µg/mL) ThermoFisher-Gibco, 15290018	20	µL	0.5	µg/mL
7	Pen/Strep (10,000 U/10,000 µg/mL) ThermoFisher-Gibco, 1514022	100	µL	100 U/100	µg/mL

Stock preparation notes for SKP medium:

The master and working stocks are given with their concentrations and can be scaled up linearly (e.g., add twice as much of everything to have twice as much stock material).

EGF master stock – 1 mg/mL:

1. The EGF was delivered in a vial containing 100 µg lyophilized powder (ThermoFisher-Gibco, PHG0311). With this powder, it is recommended to store it at 2–8°C until stock preparations.
2. The EGF vial was placed in a 50-mL tube and centrifuged at the fastest centrifugation speed possible for 5 min at RT to pellet the content. All further steps were performed under sterile conditions.
3. The vial was carefully opened inside the biosafety cabinet, and 100 µL of sterile PBS was added (final concentration: 1 mg/mL). The content was carefully reconstituted by pipetting while avoiding any bubble formation.
4. The solution was then aliquoted in 10 µL portions and stored at −20°C.

EGF working stock – 0.1 mg/mL:

1. To prepare a working stock, a total of 90 µL of DMEM (low glucose, Gibco, 21885-025) was added to 10 µL of master stock (final concentration: 0.1 mg/mL).
2. The content was carefully mixed by pipetting while avoiding any bubble formation.
3. The solution was then aliquoted in 10 µL portions and stored at −20°C.
4. Freeze-thaw cycles were avoided, and the working stock was placed back into the freezer immediately after use.

FGF master stock – 1 mg/mL:

5. The FGF was delivered in a vial containing 100 µg lyophilized powder (for catalog ThermoFisher-Gibco, PHG0021). With this powder it is recommended to store the powder at 2–8°C until stock preparations.
1. The FGF vial was placed in a 50-mL tube and centrifuged at the fastest centrifugation speed possible for 5 min at RT to pellet the content. All further steps were performed under sterile conditions.
2. The vial was carefully opened inside a sterile biosafety cabinet, and 200 µL of sterile demineralized water was added (final concentration: 0.5 mg/mL). The content was carefully reconstituted by pipetting while avoiding any bubble formation.
3. The solution was then aliquoted in 20 µL portions and stored at −20°C.

FGF working stock – 0.1 mg/mL:

1. To prepare a working stock, 80 µL of DMEM (low glucose) was added to 20 µL master stock (final concentration: 0.1 mg/mL).
2. The content was carefully mixed by pipetting while avoiding any bubble formation.
3. The solution was then aliquoted in 20 µL portions and stored at −20°C.
4. Freeze-thaw cycles were avoided, and the working stock was placed back into the freezer immediately after use.

Trypsin-stress SKP protocol (Tr-SKPs):

1. Primary fibroblasts were used and cultured with normal fibroblast medium DMEM (15% FBS, 1% Glutamine, 1% Pen/Strep (10,000 U/10,000 µg/mL), and 2 mL Gentamicin).
2. The cells used for SKP isolation were at least 60% confluent and not above 80%. Importantly, for all SKP conditions, the monoculture cells never reached or had reached a confluent state above 90% in their culture history.
3. When the cells were ready, they were detached via the trypsin protocol, described previously (page 27 and 28). Briefly, the culture medium in the cell culture dish was aspirated followed by the addition of 8 mL of sterile PBS. The dish was rinsed by carefully tilting it. Then, the PBS was aspirated, and 0.5 mL of trypsin was added to each dish. All dishes were then placed into the cell incubator providing 37°C. After 10 min of incubation, the cells were collected in fibroblast culture medium, transferred to a 50-mL tube, and centrifuged 450 × g for 5 min at RT.
4. The supernatant was aspirated, and the cells were resuspended in sterile PBS. The volume of PBS was usually around 20 mL per tube. This cell suspension was then used to determine the cell concentration via a cell hemocytometer, which was either via the Muse viability assay according to the manufacturer’s instructions or a counting

chamber (Neubauer Chamber), in which 5 µL of cell suspension was inserted to each side.

5. After determining the cell concentration, the cells were centrifuged 450 × g for 5 min at RT. The supernatant was aspirated.
6. The cells were resuspended in 1 mL of trypsin per one million cells. This suspension was transferred to a cell culture dish and placed into the cell incubator at 37°C for 16 to 18 h. This was done to expose the cells to the trypsin-stress.
7. After the trypsin-stress period, the cells were collected in standard fibroblast medium including 15% FBS to inhibit the trypsin. This step was followed by centrifugation of 450 × g for 5 min at RT to pellet the cells.
8. The supernatant was aspirated and the pellet resuspended in sterile PBS to remove any residual FBS. The PBS cell suspension was then divided over 15-mL tubes with one million cells per tube. This step was followed again by a centrifugation step of 450 × g for 5 min at RT.
9. The supernatant was aspirated, and the cells resuspended in 6 mL of 1× SKP medium per 15-mL tube (Table 2). From this suspension, 3 mL was transferred into a non-treated T25-flask.
10. The caps of the flasks were left partially unscrewed to allow air circulation into the flask. The flasks were then placed into a cell incubator for culture providing 37°C and 5% CO_2.
11. Every day the cells were resuspended once by using a 5- or 10-mL pipet and gently spraying the medium over the bottom of the flask to promote a suspension culture.
12. After 2 days of culture, the cells were fed by adding 10× concentrated SKP medium (including 10× EGF, FGF, and B27, see Table 3) by diluting it with the main previously volume (e.g., 3 mL previous volume + 333 µL 10× SKP medium). The feeding was repeated every other day.
13. At days 3, 5, and 7, the spheroids were taken out for mosaic imaging analysis to determine the culture yield.

1.3.2b Low pH SKP isolation and culture

Primary fibroblast cultures (≤80% confluent) were collected by trypsin, and the cell suspension pelleted at 450 × g for 5 min at RT followed by a wash with sterile PBS. One million cells were resuspended in 500 µL of pH-adjusted Hank's balanced salt solution (HBSS, ThermoFisher-Gibco, 14175053) buffer. The pH of the HBSS buffer was adjusted with hydrochloric acid (HCl, Merck, 1.00319.2500, Hohenbrunn, Germany) to the following pH values: 7.0, 6.7, 6.3, 6.0, 5.7, 5.3, 5.0, and 2.5. Cells resuspended in HBSS at the indicated pH were incubated for 25 min at 37°C and 5% CO_2 and agitated every 5 min. After that, the cell suspensions were centrifuged for 5 min (450 × g at RT). The cells were exposed to the indicated pH in HBSS for a total of 30 min, which included the 25-min incubation and 5-min centrifugation steps. Next, each pellet (containing one million cells) was resuspended in 6 mL of classic SKP medium and divided equally into two T25 non-treated flasks (Fisher Scientific, 10112732, USA). The cultures were then maintained as described for the Tr-SKP condition.

<u>Low pH SKP isolation and culture (pH-SKPs): step-by-step protocol.</u>

Required media:
For SKP medium, see Table 2 and 3 (page 30 and 31).

HBSS pH 5.7

1. The pH of the HBSS (Gibco, Life Technologies, 14175-053) was adjusted to 7.0, 6.7, 6.3, 6.0, 5.7, 5.3, 5.0, and 2.5 by using HCl (Merck, 1.00319.2500, Hohenbrunn, Germany). Please note that the following steps could take 1 to 2 days.
2. A 500-mL HBSS bottle was emptied into a 1-L beaker, and HCl was added until the first pH level was reached (pH 7.0). After reaching the desired pH, the next 15 min were observed to confirm a stable pH. Then, 50 mL of pH-adjusted HBSS volume was collected into a 50-mL tube.
3. Step 2 was repeated for all remaining pH levels.
4. The collected solutions were filtered with a 0.2 µm Minisart (Sartorius Stedim, 16534) filter to sterilize the solution.
5. The filtered HBSS was then aliquoted in 50- and 15-mL tubes and stored at 4°C until use. It is recommended to re-measure the pH after 1 year of storage.

Low pH SKP protocol (pH-SKPs):

1. At least 2 days before following the pH-SKP isolation protocol, pH-adjusted HBSS was prepared, see above.
2. Before starting the isolation protocol, pH-adjusted HBSS was placed at RT to acclimatize.

3. Primary fibroblasts were used that were previously cultured with normal fibroblast medium (DMEM: 15% FBS, 1% Glutamine, 1% Pen/Strep [10,000 U/10,000 µg/mL], and 2 mL Gentamicin).
4. The used cells for SKP isolation were at least 60% confluent and not above 80%. Importantly, for all SKP conditions the monoculture cells never reached or had reached a confluent state of above 90% in their culture history.
5. When the cells were ready, they were detached via the trypsin protocol, described previously (page 29). Briefly, the culture medium in the cell culture dish was aspirated followed by the addition of 8 mL of sterile PBS. The dish was rinsed by carefully tilting it. Then the PBS was aspirated, and to each dish, 0.5 mL of trypsin was added. All dishes were then placed into the cell incubator providing 37°C. After 10 min of incubation, the cells were collected in fibroblast culture medium, transferred to a 50-mL tube and centrifuged 450 × g for 5 min at RT.
6. The supernatant was aspirated, and the cells were resuspended in sterile PBS. The volume of PBS was usually around 20 mL per tube. This cell suspension was then used to determine the cell concentration via a cell hemocytometer. This was done either via the Muse viability assay according to the manufacturer's instructions or a counting chamber (Neubauer Chamber) in which 5 µL of cell suspension was inserted to each side.
7. After determining the cell concentration, the cells were transferred with one million per 15-mL tube. These cells were then centrifuged 450 × g for 5 min at RT. The supernatant was then aspirated.
8. The cells were resuspended in 500 µL of HBSS and carefully mixed with a 1000-µL pipet tip while avoiding any bubble formation. The 15-mL tubes were then placed vertically into a cell incubator at 37°C and 5% CO_2.
9. The cells were agitated every 5 min to homogenize the descended cells again.
10. After 25 min, the cells were placed in a centrifuge and centrifuged 450 × g for 5 min at RT. In sum, the total incubation time in pH-adjusted HBSS solution was in total 30 min.
11. After centrifugation, the acidic supernatant was carefully removed via aspiration. The cells were then gently resuspended in 6 mL of SKP medium per 15-mL tube (see Table 2). Per T25 flask, 3 mL of the cell suspension was transferred, totaling the cell number at 0.5 million per flask.
12. The cap of the flasks was left partially unscrewed to allow air circulation. The flasks were then placed into a cell incubator for culture.
13. Every day the cells were resuspended once by using a 5- or 10-mL pipet and gently spraying the medium over the bottom of the flask to promote a suspension culture.

14. After 2 days of culture, the cells were fed by adding 10× concentrated SKP medium (including 10× EGF, FGF and B27, see Table 3) by diluting it with the main previously volume (e.g., 3 mL previous volume + 333 µL 10× SKP medium). The feeding was repeated every other day.
15. At days 3, 5, and 7, the spheroids were taken out for mosaic imaging analysis to determine the culture yield.

1.3.2c No-stress SKP isolation and culture

Fibroblast cultures (≤80% confluent) were collected by trypsin of which the pellets were washed with DMEM containing 15% FBS, followed by two washes with sterile PBS. Then, one million cells were resuspended in 6 mL of SKP medium, equally divided into two T25 non-treated flasks and cultivated the same as Tr-SKP and pH-SKPs.

<u>No-stress SKP (NS-SKPs) isolation: step-by-step protocol.</u>

Required media:
For SKP medium see Table 2 and 3 (page 29 and 30).

No-stress SKP isolation protocol:

1. Primary fibroblasts were used and cultured with normal fibroblast medium DMEM (15% FBS, 1% Glutamine, 1% Pen/Strep (10,000 U/10,000 µg/mL), 2 mL Gentamicin).
2. The used cells for SKP isolation were at least 60% confluent and not above 80%. Importantly, for all SKP conditions the monoculture cells never reached or had reached a confluent state of above 90% in their culture history.
3. When the cells were ready, they were detached via the trypsin protocol, described previously (page 27 and 28). Briefly, the culture medium in the cell culture dish was aspirated followed by the addition of 8 mL of sterile PBS. The dish was rinsed by carefully tilting it. Then the PBS was aspirated, and 0.5 mL of trypsin was added to each dish. All dishes were then placed into the cell incubator providing 37°C. After 10 min of incubation, the cells were collected in fibroblast culture medium, transferred to a 50-mL tube, and centrifuged 450 × g for 5 min at RT.
4. The supernatant was aspirated, and the cells were resuspended in sterile PBS. The volume of PBS was usually around 20 mL per tube. This cell suspension was then used to determine the cell concentration via a cell hemocytometer. Which was either via the Muse viability assay according to the manufacturer's instructions or a counting chamber (Neubauer Chamber), in which 5 µL of cell suspension was inserted to each side.

5. After determining the cell concentration, the cells were transferred with one million per 15-mL tube. The cells were then centrifuged 450 × g for 5 min at RT. The supernatant was aspirated.
6. The cells were resuspended in 6 mL of 1 × SKP medium per 15-mL tube (Table 2). From this cell suspension, 3 mL was transferred into a non-treated T25-flask.
7. The caps of the flasks were left partially unscrewed to allow air circulation into the flask. The flasks were then placed into a cell incubator for culture.
8. Every day the cells were resuspended once by using a 5- or 10-mL pipet and gently spraying the medium over the bottom of the flask to promote a suspension culture.
9. After 2 days of culture, the cells were fed by adding 10× concentrated SKP medium (including 10× EGF, FGF and B27, see Table 3) by diluting it with the main previously volume (e.g., 3 mL previous volume + 333 µL 10× SKP medium). The feeding was repeated every other day.
10. At days 3, 5, and 7, the spheroids were taken out for mosaic imaging analysis to determine the culture yield.

1.3.3 SKP spheroid analysis by mosaic imaging

Spheroid formation was determined by measuring individual spheroids via a whole-well mosaic image obtained via MMI. Spheroids from one flask were temporarily divided into two wells of a 48-well plate and placed in an Axiovert 200M microscope chamber adjusted to 37°C and 5% CO_2. Additionally, evaporative demineralized water was added to sustain a high humidity similar as in a cell incubator. A complete mosaic image was generated with the 5× objective for each well using the Zeiss Multidimensional Acquisition software (Axiovision 4.8.2). For further detailed information regarding MMI, please refer to Chapter 2, pages 103 to 107. After MMI acquisition of the well, the captured image was cropped on the edges and resized to 5000 × 5000 pixels in Photoshop CC (Adobe). The spheroids in the mosaic image were manually isolated with the Photoshop CC selection tool. Cellular objects smaller than 20 pixels were ignored. The selected spheroids were colored in black, while the background was colored white. These images were then processed in ImageJ. Each image was processed using the watershed tool and then analyzed with the particle analysis tool (scale was set to 0.5 pixels = 1.2 µm). Obtained data included the spheroid number and surface size of each spheroid per sample. The size frequency was calculated in Excel 2013 (Microsoft).

SKP spheroid analysis: step-by-step protocol.

1. The following protocol describes the imaging of one flask with the MMI method. This method can be used for multiple flasks but recommended is not to use more than six per day for imaging. Optimally, two groups of three flasks were imaged, in which the first three flasks were switched after completion with the other three (in a new well). This because long imaging times resulted in spheroid attachment to the plastic surface of the well or each other.
2. At the designated day (days 3, 5, or 7), the flasks containing the SKP spheroids were collected from the incubator and placed in a sterile biosafety cabinet.
3. With a 5-mL pipet, the medium inside the flask was taken and used to carefully spray the plastic bottom surface to detach any attached spheroid. Then, the complete solution was collected in the 5-mL pipet and divided over two 48-well-plate wells. Depending on the culture day, the total volume to divide was between 3 and 3.5 mL.
4. After the transfer of spheroids into the 48-well plate, they were allowed to descend to the bottom of the well. Depending on the spheroid size, this would take approximately 1 to 3 min.
5. After the spheroids descended, approximately 1 mL of each well's medium was taken back into the 5-mL pipet. This medium was used to rinse the flasks again and collect any remaining spheroids. These remaining spheroids (the suspension) were divided over the same two wells.
6. The spheroids were mixed in each well with a 1000-µL pipet tip to promote a homogenous spread over the surface of the well. Then, the spheroids were allowed to descend again. The remaining bubbles on top of the liquid's surface were removed with a 1000-µL pipet tip to obtain the best imaging quality. The volume level was also made equal among all wells.
7. With the spheroids ready in each well, MMI was performed. For further detailed instructions, see Chapter 2, Materials and Methods.
8. After imaging, the spheroids were first detached by using a 1000-µL pipet tip. The spheroids were then collected in a 5-mL pipet. Both wells were collected and transferred back into their respective flask.
9. The flask containing the spheroids was then placed back into the cell incubator for the continuation of spheroid culture.

1.3.4 Gene expression analysis via RT-PCR, PCR, and real-time qPCR

Total RNA was first isolated from cell pellets to analyze gene expression using the RNeasy Plus Mini Kit (Qiagen, 74136). Total RNA was converted via reverse transcriptase PCR (RT-PCR) to cDNA with Omniscript Reverse Transcriptase (Omniscript RT Kit, Qiagen, 205113), oligo-dT primers (Qiagen, 79237), and RNase inhibitor (Qiagen, 129916). They were all used according to the manufacturer's instructions.

Normal PCR was used to amplify the target of interest. PCR reactions were performed in a total volume of 25 µL containing 20 ng of cDNA template together with Taq DNA Polymerase (1 unit), 10× Key buffer, 1.5 mM $MgCL_2$, and 0.2 mM deoxyribonucleotide triphosphates (dNTPs, with each dNTP), all from VWR Chemicals (Cat. No.: 733-1311). The corresponding primers (Table 4) were all from ThermoFisher. Amplification was performed using a PCR machine (Bio-Rad, iCycler thermal cycler) programmed with an initial 3-min denaturing cycle at 95°C and X cycles (depending on the primer target, see Table 4) of 20 s denaturing at 95°C, 40 s annealing at 60°C, and 30 s of elongation at 72°C. GAPDH was included and used for normalization between samples. For all primers, an appropriate cycle number was used below the PCR plateau phase to visualize expression differences between samples (Table 4). Relative changes in gene expression were determined by agarose gel analysis. Briefly, 5 µL of PCR product and 5 µL of Orange G loading dye (ThermoFisher, R0631) were loaded on a 1.5% agarose (ThermoFisher, Ref. 16500) gel containing 1:10,000 GelRed (VWR 89139-138) nucleic acid gel stain. The gel ran at 150 V for 40 to 45 min in TBE buffer (89 mM Tris, pH 7.6 [Sigma, T1503], 89 mM boric acid [Carl Roth, 6943.3], and 2 mM EDTA, pH 8 [Carl Roth, 200-449-4]). Images were captured with the Chemidoc MP (Bio-Rad) apparatus, and DNA bands of interest in the gel were analyzed with Image Lab (V5.2.1 Bio-Rad).

Table 4. Primer design and cycle number for optimal PCR reaction.

Primer (5' to 3')	Target Gene	Product Size (base pairs)	Primers (nM)	Cycles	Info
FW: ACCAGCTCGCAGACCTACAT REV: ATGTGTGAGAGGGGCAGTGT	Sox2	320	200 200	36	[153]
FW: GCGGGCTACTGAAAAGTTCC REV: GAGGGTCCTGTACGTGGC	Nestin	154	300 300	32	Designed in Primer3
FW: TTTTGGTACCCCAGGCTATG REV: GCAGGCACCTCAGTTTGAAT	Oct4	136	450 450	33	[153]
FW: ACCTTGGCTGCCGTCTCTGG REV: AGCAAAGCCTCCCAATCCCAAACA	NANOG	151	250 250	41	[153]
FW: ATGATGCTGGTGGGCTTC REV: GCTCATCCTTGGTTTTCAGC	CD9	205	250 250	29	[75]
FW: AAACACAAACTTGAACAGCTAC REV: ATTTGAGGCAGTTTACATTATGG	C-Myc	188	350 350	26	[108]
FW: ACCAGGCACTACCGTAAACACA REV: GGTCCGACCTGGAAAATGCT	Klf4	79	300 300	30	[108]
FW: CTCTGCTCCTCCTGTTCGA REV: TTAAAAGCAGCCCTGGTGAC	GAPDH	144	300 300	26	[59]

cDNA preparation: spheroid preparation for RNA isolation, step-by-step protocol.

1. Spheroids were collected for RNA isolation on the designated day. Collecting was always done on day 5 of SKP culture. Furthermore, a minimum of four flasks was used per RNA isolation to obtain sufficient material. As a control for SKPs, the origin fibroblasts used for the SKP isolation were included for cDNA preparation.
2. For the monoculture, the cells were first detached via the trypsin protocol as previously described (page 29). They were then washed in fibroblast culture medium followed by the addition of sterile PBS and not used further until step 5.
3. For SKP spheroids, the flasks were taken from the incubator and placed in a sterile biosafety cabinet.
4. The spheroids were collected with a 5-mL pipet and transferred into a 50-mL tube. Approximately 5 mL of sterile PBS was added to each flask, to detach any remaining spheroids by spraying the flask's surface. The remaining spheroids were then transferred into the same 50-mL tube.
5. The spheroids or cells were then centrifuged 450 × g for 5 min at 4°C. The material was kept at low temperatures for all following steps in order to preserve the RNA integrity.
6. The supernatant was removed, and another 25 mL of sterile PBS was added. The previous centrifugation step was repeated. This step removes the residual salts or other possible interfering components present in the SKP or fibroblast culture medium.
7. A part of the supernatant was removed by leaving 1 mL of supernatant. The complete solution with the spheroids or cells was then transferred to a 1.5-mL Eppendorf tube. The tube was then centrifuged again with 450 × g for 5 min at 4°C to pellet the cells and spheroids.
8. The complete supernatant was removed as much as possible without disturbing the spheroids or cell pellet. From this point, the spheroids or cells could be either immediately used for RNA isolation or prepared for long-term storage. See the next step-by-step protocol for the RNA isolation protocol.
9. To prepare spheroids or cells for long-term storage, 300 µL of PBS was added to the pellet together with 200 µL of RNAlater solution (Life Technologies, AM7020). This was gently mixed and then placed overnight at 4°C to incubate. This incubation step allowed the preservation agent (RNAlater) to permeate into the spheroids or cells to preserve the RNA.

   Note: It was found best to add and mix the PBS and RNAlater solution carefully. Heavily pipetting caused the spheroids or cells to stick inside the pipet tip.
10. After the preservation step, the RNAlater cell mixtures were stored at −20°C. In this state, the RNA can be preserved for multiple years.

cDNA preparation: RNA isolation, step-by-step protocol.

The RNeasy Plus Mini Kit from Qiagen (74136) was used to isolate RNA. This kit follows a standardized protocol with optimized reagents for optimal RNA isolation. Before starting the RNA isolation, specific reagents were required to be mixed and other materials to be prepared first.

Required kit material:

- RW1 buffer
- RLT Plus buffer (requires 10 µL β-mercaptoethanol [β-ME or 2-ME, Bio-Rad Cat #161-0710] per 1 mL of buffer, which can be used for 1 month)
- RPE buffer (for the first time, 4 volumes of 99.9% cell-grade ethanol was added to 1 volume of RPE buffer)

Required non-kit material:

- Fresh cells or cells prepared in RNAlater
- 14.3 molar (M) β-ME
- RNase-free filter pipet tips
- Centrifuge for Eppendorf tubes (2 mL)
- 99.9% Cell-grade ethanol (VWR chemicals, 2082.33)
- Disposable safety gloves
- Vortex
- QIAshredder homogenizer (Qiagen, 79654)

RNA isolation protocol:

1. When using cells stored in RNAlater at −20°C, the cells were first placed at RT for about 30 min. This step was required because too low temperatures inhibit the RNA isolation process. Therefore, the kit recommends to work at RT, but also to work as swiftly as possible. Long durations of temperatures above 4°C should be avoided due to the degradation sensitivity of RNA. Cell pellets that had been prepared freshly on the same day could be placed on ice until use.
2. The RTL Plus buffer was prepared by adding 100 µL of β-ME to 10 mL of RLT Plus buffer together in a chemical fume hood. This mixture could be stored for one month at RT. Additionally, a 70% ethanol solution was made by mixing 35 mL of 99.9% cell-grade ethanol with 15 mL of demineralized water. This ethanol mixture could be stored at RT until completely used. Both mixes were used for RNA isolation.

3. For cells prepared in RNAlater, PBS was added until the Eppendorf tube was almost completely filled. This step was added to dilute and wash away the RNAlater solution. All the cells were then centrifuged 450 × g for 5 min at RT.
   Note: During each centrifugation step, the required tubes of the kit were collected and labeled by a marker with the sample names to save time and improve efficiency.
4. After centrifugation, the supernatant was carefully removed with a 1000-µL pipet tip. Care had to be taken with samples previously stored in RNAlater because the RNAlater solution was more viscous. The increased viscosity caused the cells to form a less dense pellet, making it easier to disrupt and lose material.
5. After removing the supernatant, PBS was added again until the Eppendorf tube was filled. The cells were centrifuged 450 × g again for 5 min at RT.
6. Steps 4 and 5 were repeated once.
7. The freshly prepared cellular material could now directly be used for RNA isolation. The cells previously stored in RNAlater were washed once more via steps 4 and 5 to completely remove the RNAlater solution.
8. Then, 350 µL of RLT Plus buffer was added to the cell pellet and mixed adequately while avoiding bubble formation. The RLT buffer induces cell lysis and prepares them for further steps of the kit.
9. The lysed cells in RLT buffer were then transferred into a QIAshredder spin column, which was placed in a 2-mL collection tube. This tube was centrifuged for 2 min at full speed (≥10,000 rpm RT). In this step, the cells are further disrupted to break free the RNA.
10. The spin column was discarded, and the flow-through transferred into a gDNA eliminator spin column, which was placed in a 2-mL collection tube. These were then centrifuged for 30 s at ≥10,000 rpm RT.
11. The flow-through was kept, and one volume of 70% ethanol (usually around 350 µL) was added to the sample and mixed well by pipetting.
12. Up to 700 µL of the sample, including any precipitate that may have formed, was transferred to an RNeasy spin column placed in a 2-mL collection tube and centrifuged for 15 s at ≥10,000 rpm RT. Because of the 70% ethanol, the RNA binds to the membrane of the spin column. Therefore, the flow-through is discarded and the spin column kept for further steps.
13. Then, 700 µL of RW1 buffer was added to the RNeasy spin column to wash the column. This was centrifuged for 15 s at ≥10,000 rpm RT. The flow-through was discarded.
14. A total of 500 µL RPE buffer was added to the RNeasy spin column and centrifuged again for 15 s at ≥10,000 rpm RT. The flow-through was discarded.

15. Another 500 µL of RPE buffer was added to the RNeasy spin column. The column was then centrifuged for 2 min at ≥10,000 rpm RT.
16. As a final step to remove any possible residue of RPE buffer, the RNeasy spin column was placed in a new 2-mL collection tube for a final centrifugation step at full speed for 1 min at RT to dry the column.
17. The RNeasy spin column was then placed in a new 1.5-mL collection tube. Then, 30 to 50 µL of RNase-free water was directly added to the spin column membrane to elute the bound RNA. Care was taken to not directly touch the membrane with the pipet tip. For fibroblast material, 50 µL of water was usually added, and for SKP spheroid material, this was 35 µL.
18. After carefully adding the water, the columns were centrifuged for 1 min at ≥10,000 rpm RT to collect the RNA.
19. These samples were then placed directly on ice for later determination of the RNA concentration, see the step-by-step protocol below.

Nanodrop – RNA concentration measurement: step-by-step protocol.

1. The concentration of total RNA was determined with the Nanodrop apparatus. The material to be measured could be either freshly prepared RNA or RNA previously stored at −80°C. For both conditions, the RNA was placed on ice before measurement.
2. The Nanodrop software was started, and the RNA measurement setting selected. The software then requests a drop of (1 µL) RNase-free water. After placing the water on the sensor, the button “OK” was pressed, and the device would measure the water to set its settings. Then, the button “Blank” was pressed with the water sample still on top of the sensor. This was done to create a baseline without any RNA material.
3. The water sample was removed by just wiping over the sensor with a soft paper tissue. Then, 1 µL of the sample was placed on top of the sensor. The button “Measure” was clicked. The device then measured the RNA concentration. The given concentration was presented in ng/µL. Noteworthy here is that the values A280 and A230 should be above 2 or higher as these values indicate the purity of the sample.
4. After all measurements were completed, the RNA samples were either used for cDNA synthesis or stored at −80°C.

cDNA preparation: cDNA conversion, step-by-step protocol.

After isolation and determination of the RNA concentration, the material was converted into cDNA with the use of the Omniscript reverse transcriptase kit (Qiagen, 205113). Below are the required materials to successfully convert RNA into cDNA.

Required kit material (Qiagen, 205113):

- 10× RT Buffer
- dNTP Mix (5 mM of each dNTP)
- Omniscript Reverse Transcriptase (4 units per 20 µL, we have 4 U/µL)

Required non-kit material:

- RNA samples (at least 1,000 ng within a volume of 10.5 µL)
- Oligo-dT-primer (10 µM) (Qiagen, 79237)
- RNase Inhibitor (10 units per 20 µL, we have 4U/µL) (Qiagen, 129916)
- RNase-free water

Table 5. RNA to cDNA synthesis mix.

RNA to cDNA synthesis	**2 µg RNA (1×)**	**Total for … (+1) reactions**
10× RT Buffer	2,0 µL	µL
dNTP Mix (5 mM of each dNTP)	2,0 µL	µL
Oligo-dT-Primer (10 µM)	2,0 µL	µL
RNase Inhibitor (10 units per 20 µL, we have 4U/µL)	2,5 µL	µL
Omniscript Reverse Transcriptase (4 units per 20 µL, we have 4 U/µL)	1,0 µL	µL
Subtotal	**9,5 µL**	µL
H_2O + RNA material (50 ng – 2 µg)	11,5 µL	XXX
Total	**20,0 µL**	**XXX**

cDNA conversion protocol:

1. If the RNA was stored at −80°C, it was first placed on ice to thaw. The following materials were also placed at RT to thaw: oligo-dT-primer, 10× RT Buffer, and dNTP mix.
2. A 10.5 µL mixture of RNA with RNase-free water was prepared for each sample to contain 2,000 ng of RNA in one PCR tube.
3. The master mix was prepared, and 9.5 µL was added to the 10.5 µL RNA solution containing the 2,000 ng RNA. The mix was then centrifuged quickly via the quick spin centrifuge for a short centrifuge spin to collect the drops together at the bottom of the

tube followed by mixing with the vortex. The drops were then collected again on the bottom of the tube via a short centrifuge spin.

4. The PCR tubes containing the RNA material and Omniscript mixture were placed in a PCR machine (Bio-Rad, iCycler thermal cycler) and run **without a hot start** for 60 min at 37°C with a continuous end cycle at 4°C.
5. After the incubation period, the samples could be further processed. Since a total of 2,000 ng of RNA was used in 20 µL, the final estimated concentration of cDNA was 100 ng/µL. The word “estimated” is used here as the exact RNA to cDNA conversion rate was unknown and is assumed to be 100%. For further PCR reactions, a final concentration of 20 ng/µL was used. To achieve this, 80 µL of RNase-free water was added to the cDNA mixture after conversion, resulting in 100 µL of 20 ng/µL estimated cDNA.
6. The samples were then stored at −20°C for long-term storage. However, when planning to use the samples often (within three months), it was better to store them at 4°C to prevent freeze-thaw cycles.

1.3.4A Classic PCR sample amplification

To amplify the target of interest, specific oligonucleotides were designed to bind the cDNA of interest during the PCR reaction (Table 5). A PCR kit, containing all the required reagents, was obtained from VWR Chemicals (Cat. No.: 733-1311). The mRNA of the targeted gene was indirectly (via cDNA conversion) amplified for future analysis purposes to determine gene expression levels.

Classic PCR: step-by-step protocol.

Required kit material (Cat. No.: 733-1311):

- 10× Buffer
- 25 mM MgCl2
- 5 mM dNTP mix (each)
- Taq DNA Polymerase (5 U/µL)

Required non-kit material:

- DNase and RNase-free water
- Reverse primer of targeted gene
- Forward primer of targeted gene
- cDNA of interest
- PCR apparatus

Table 6. PCR master mix example for 10 samples.

Sample number	10			
+1 for pipet errors	**11**			
Components	**Volume for 1 reaction (µL)**	**Volume for 11 Reactions (µL)**	**Final concentration per reaction**	**Info**
10× buffer	2.5	27.5	1 ×	
25 mM MgCl2	1.5	16.5	1.5 mM	0.5–5 mM
5 mM dNTP mix (of each)	1	11.0	0.2 mM	Of each dNTP
Taq DNA polymerase (5 U/µL)	0.2	2.20	1 unit	1–5 units
Primer reverse and forward (each 4 µM)	1.88	20.6	0.45 nM	0.1–1.0 uM
Total volume	7.08			
Volume for cDNA mix	17.92			

Other general information:

20 ng of estimated cDNA was used per reaction in a total reaction volume of 25 µL.

Table 7. PCR program.

Step	**Cycles**	**Temperature**	**Time**	**Description/Step**
1	1	95°C	180 s	Denature
2	x number of cycles depended on each primer (Table 4)	95°C	20 s	Denature
3		60°C	40 s	Annealing
4		72°C	30 s	Elongation
5 (optional)		4°C	Indefinite	Preservation

1. Before starting with the PCR arrangements, the ordered primers were reconstituted (in general the primers were delivered lyophilized) and working solutions prepared.
2. The primer manufacturer would report the primer amount in nmol. Then, to make a stock solution of 100 µM, the number of nmol was multiplied by 10, which then represented the water volume (µL) required for reconstitution. For example, a primer amount of 29.5 nmol needs to be reconstituted in 295 µL of water to obtain a 100 µM solution of that primer.
3. This stock solution is then used to make the working stock solution. The reverse and forward primer were combined in the working stock to reduce the steps necessary to make the PCR master mix.
4. For a 500 µL working stock (containing 4 µM), 40 µL of the forward primer (100 µM) and 40 µL of the reverse primer (100 µM) were added to 420 µL water. This solution was then mixed on the vortex. The total volume could be aliquoted in smaller volumes and stored at −20°C until use to reduce freeze-thaw cycles.

For the PCR amplification protocol, the following components of the master mix were thawed at RT: 10× buffer, $MgCl_2$, dNTP mix, and primer work solutions. The cDNA solutions were placed on ice until use. Often it occurred that each primer pair required its custom master mix as in general—during primer concentration optimization—a specific concentration was required. This entails that gene 1 might require 100 nmol of each primer per reaction and that gene 2 requires 500 nmol of each primer per reaction. So, the end volume of the master mix was influenced based on the primer amount required per gene of interest; thus, requiring more or less volume of water compensation. Therefore, the amount of remaining volume to add of cDNA and water equaled 25 µL (total reaction volume) − master mix volume (including primers). In the example above (see Table 6), the master mix volume equaled 7.08 µL, resulting in a 17.92 µL volume to add of cDNA and water. With an estimated cDNA concentration of 20 ng/µL, only 1 µL of cDNA has to be added to 16.92 µL water to create a total volume of 17.92 µL of 20 ng cDNA in water. Finally, to this volume, the master mix of 7.08 µL was added to represent the total volume of 25 µL containing all the necessary components for the PCR reaction.

1. The cDNA mixtures were made while thawing the master mix components. For the master mixes containing 450 nM of each primer, as shown in the example (Table 6) above, 17.92 µL of cDNA with water had to be added.
2. In a 250-µL PCR tube, 16.92 µL of water was added. A pipetting technique called reverse pipetting was applied to optimize the handling of repetitive handling of the same reagent. Briefly, the volume of the pipet was set, and the volume controller pressed down completely (through the second stop). The pipet tip was placed in the liquid followed by completely releasing the pipet controller. The pipet tip was then placed at a 45° angle against the inner upper side of the PCR tube, followed by pressing the pipet controller down until the first stop. While holding at the first stop, the same pipet tip was used to take up the same liquid again by placing it inside the liquid and releasing the pipet controller up. This process was repeated for each PCR tube.
3. With a 10-µL pipet, 1 µL of cDNA was added to the opposite side of the inner upside of the PCR tube. The left-over volume inside the pipet tip was returned to the cDNA tube. For each different cDNA sample, a different pipet tip was used.
4. The PCR tubes containing the cDNA mixture and water were centrifuged for a few seconds to collect the drops. The cDNA samples were then placed shortly on the vortex to mix. This was followed again by a quick centrifugation step. The PCR tubes were then placed on ice.
5. The PCR master mix was made according to Table 6. For each component, a new pipet tip was used. The Taq polymerase was added as last.

6. The master mix was then centrifuged for a few seconds to collect all the drops together. This was followed by placing it shortly on the vortex to mix the components.
7. The master mix was centrifuged again for a few seconds.
8. When the cDNA for each sample was only required to determine the expression of one gene (e.g., only nestin), the same PCR tube containing the 20 ng of cDNA material, was used to add the PCR master mix. In this example, 7.08 µL of PCR master mix was directly added to the cDNA tube. Continue to step 10.
9. If the cDNA was required for multiple gene expression determinations (e.g., Oct4, nestin, Sox2, etc.), the cDNA was transferred to a new PCR tube to which also the PCR master mix (a mix for each marker, e.g., Oct4) would then be transferred. In this example, 17.92 µL of cDNA and water would be transferred into a new PCR tube together with 7.08 µL of PCR master mix. Again, each addition would be done by pressing the pipet tip to an unused opposite side of the inner side of the tube. This to avoid contamination between mixtures and improve workflow.
10. The PCR tubes containing the cDNA and the master mix were shortly centrifuged for a few seconds to collect all the liquid at the bottom of the tube. This was followed again by mixing on the vortex and a repetition of the centrifugation step.
11. The PCR tubes were then placed in the PCR apparatus that would follow the PCR schedule shown in Table 7. As a final but optional step, a preservation step in the PCR schedule was added leaving the samples indefinitely (until removed) at 4°C. This option could be used when the PCR was started at the end of the day and allowed the post-PCR samples to be left in the apparatus overnight.
12. After completion of the PCR program, the samples were stored at 4°C until further use or analysis.

<u>Classic PCR: PCR product separation, step-by-step protocol.</u>

After the completion of the targeted gene amplification, the resulting PCR product could be used for analysis and gene expression determination. For this purpose, a 1.5% agarose gel was made to separate the DNA fragments based on their molecular weight and base pair (bp) size (more base pairs = higher molecular weight). While in theory, the PCR should only amplify the mRNA of one gene of interest, the separation of the agarose gel will rule out any possible unspecific amplification in the final analysis. Additionally, gelRed was used for analysis of agarose gels as an alternative to ethidium bromide. Both reagents intercalate with DNA and emit light when excited with a UV source. However, gelRed cannot penetrate cell membranes whereas ethidium bromide can. This makes gelRed significantly safer to use and requires less strict safety regulations. Additionally, gelRed provided a stronger signal.

Making the agarose gel (1.5%):

Table 8. 0.5 M EDTA solution (500 mL).

Component	**Amount**
EDTA (Sigma, ED2SS)	93.05 g
Add 200 mL of demineralized water and mix with a stirrer	
Adjust volume to 500 mL with demineralized water	
Adjust pH to 8	

Table 9. 10× TBE buffer (1,000 mL).

Component	**Amount**
Tris (Trizma Base, Sigma T1503)	108 g
Boric Acid (Roth, 6943.1)	55 g
Add 900 mL demineralized water and mix	
Add 40 mL of 0.5 M EDTA (pH 8)	
Adjust volume to 1 L with demineralized water and mix	

1. The 0.5 M EDTA solution was made, see Table 8.
2. The 10× TBE buffer was prepared, see Table 9.
3. A total of 1.05 g agarose powder was placed in an Erlenmeyer (one that fits in the microwave).
4. Then, 70 mL of 1× TBE buffer (7 mL 10× TBE + 63 mL H_2O) was added to the agarose. This amount was enough to make two small gels. For one large gel, 90 mL was required. More volume can be made when a thicker gel is desired.
5. The mixture was heated for 3 to 5 min in a microwave. The Erlenmeyer was regularly taken out to mix the contents by swirling, or when the mixture produced too many bubbles due to the heat.
6. After the agarose powder was completely dissolved and the mixture had become a clear solution, the gel was ready to be poured.
7. The agarose solution was allowed to cool down until the bottom of the Erlenmeyer could be pressed against your hand (wearing a latex glove) for 5 s. During this time, the running chamber was prepared and the combs placed. It was made sure that the running chamber was cleaned and free from any previous residues.
8. Then, 1:10,000 of gelRed was added to the liquid gel. For a 70-mL agarose solution, this was 7 µL. After adding the gelRed, the content was mixed by swirling the flask.
9. The agarose solution was poured into the running chamber. All remaining bubbles were removed by using a 10-µL pipet tip.
10. The agarose gel was allowed to polymerize for at least 1 h at RT. During this time the PCR samples were prepared as described below.
11. The PCR samples were vortexed and centrifuged to mix the sample liquid.

12. In new PCR tubes, 6 µL of Orange G solution was added, followed by 6 µL of PCR product. The mixtures were each centrifuged, vortexed for 3 s, and centrifuged again. The samples were now ready to be loaded into the gel.
13. When the agarose gel was completely polymerized, the combs were removed, and the gel positioned correctly with the slots near the + side.
14. The running chamber was filled with 1× TBE buffer (diluted in Milli Q [MQ]) until the gel was submerged with approximately 2 to 5 mm of liquid on top.
15. With a 10-µL pipet, 10 µL of Orange G/PCR sample was added per slot in the gel; one or two slots per row were left free for the DNA marker.
16. After filling all the slots with the samples, 5 µL of diluted 100 bp DNA marker was added.
17. The cables were connected, and the gel was run at 100 to 120 V for 30 to 40 min. This voltage was suitable for a small gel (40 mL). For a large gel (90–100 mL), a voltage of 120 to 150 V could be used and run for 45 to 50 min. In general, the recommended voltage is between 4 and 10 V/cm of the distance between electrodes.
    Note: DNA always runs toward the positive side because it is negative by itself due to the phosphate groups located in its backbone.
18. The running was completed when the Orange G marker line reached the end of the gel or the next slots.
19. The gel was imaged and analyzed with the Chemidoc MP (Bio-Rad) apparatus. After imaging, the bands of interest in the gel were analyzed with the Image Lab (V5.2.1 Bio-Rad) software.

1.3.4B Real-time quantitative PCR of NHE1

Table 10. Primer design.

Primer (5' to 3')	**Target Gene**	**Product Size (base pairs)**	**Primers (nM)**	**Info**
FW: CTCTGCTCCTCCTGTTCGA REV: TTAAAAGCAGCCCTGGTGAC	GAPDH	144	300 300	[59]
FW: CCAGCTCATTGCCTTCTACC REV: TGTGTCTGTTGTAGGACCGC	NHE1*	249	300 300	[27]

*Abbreviation NHE1: Sodium-Hydrogen Exchanger 1.

For the real-time qPCR, the reaction occurred in a volume of 15 µL and was divided into two parts. One part contained the primers and reaction mix SsoFast EvaGreen (Table 11) and the other cDNA and water (Table 12). Additionally, in each 15 µL of volume, 20 ng of estimated cDNA was included per reaction as starting material for the PCR amplification.

Table 11. Real-time qPCR master mix, primers, and SsoFast EvaGreen.

All primers for 48 wells (calculate with 50)					
Each primer's stock is 4 µM, both are 8 µM.					
Primer	**nM**	**Dilution factor**	**µL primer**	**µL SSO Fast**	**Per well**
GAPDH	300	13.33	56.3	375.0	8.63
NHE1	300	13.33	56.3	375.0	8.63

Table 11 is based on all the samples used for GAPDH and NHE1 analysis. There are in total five unique samples per primer, each n = 3 and in triplicate, resulting in 5 × 3 × 3 = 45 PCR reactions. Each primer pair also included three wells as a negative control, resulting in a total of 48 reactions. Additionally, to compensate for pipetting errors, 50 reactions were used per primer pair for calculation.

In Table 11, the nM (nanomolar) represents the desired concentration of primer—300 nM forward and 300 nM reverse. The primer work stock consisted out of 8 µM per primer pair (4 µM forward and 4 µM reverse). Therefore, the dilution factor required is 13.33 (8,000 / 13.33 = 600 nM [including 300 nM forward and 300 nM reverse]). One reaction per well of 15 µL in total requires then 1.13 µL (15 / 13.33) of primer working stock, and 56.3 µL is required for all 50 reactions. Then, the SsoFast EvaGreen has to be 1:1 diluted (according to the manufacturer's instructions). Based on a volume of 15 µL, this equals 7.5 µL of SsoFast EvaGreen mix per reaction, which is 375 µL for all 50 reactions. Together, one reaction well requires 8.63 µL, including 1.13 µL primer working stock and 7.5 µL SsoFast EvaGreen. As such, a remaining 6.38 µL volume is left for the cDNA and water to make a total of 15 µL (Table 12).

Table 12. cDNA and water master mix.

cDNA dilutions/sample				
1×	1×	7×	7×	-
cDNA 20 ng	H_2O	cDNA 20 ng	H_2O	Per well
1.00	5.38	7.00	37.63	6.38

The above table is based per sample and its triplicates (so sample n1 results in three reactions etc.). The amount of cDNA required per sample for both primers equals then six (three triplicates for GAPDH and three for NHE1). To compensate for pipetting errors, a number of seven reactions was used for calculation. Together, 6.38 µL of cDNA and water per reaction well was added to 8.63 µL of primer with SsoFast EvaGreen mix, resulting in 15 µL of reaction mix with all components adequately diluted to the desired concentrations.

Table 13. Real-time qPCR program.

Step	Cycles	Temperature	Time	Description/Step
1	1	95°C	180 s	Denature
2	40	95°C	5 s	Denature
3		60°C	20 s	Annealing – Read end
4	1	95°C	5 s	Denature
5		60°C	20 s	Annealing
6	1	95°C	-	Melting curve – Read all

Real-time qPCR: step-by-step protocol.

1. The ordered primers were reconstituted (the primers were generally delivered lyophilized) first and working solutions prepared beforehand.
2. For the real-time qPCR amplification protocol, the cDNA and SsoFast EvaGreen were placed on ice to thaw until use. The required primer working stocks were placed at RT until thawed.
3. In a 250-µL PCR tube, 37.63 µL of water was added. This was done 15 times (5 unique samples in total, each n = 3). Reverse pipetting was applied to optimize the handling of this process for repetitive handling of the same reagent or sample.
4. With a 10-µL pipet, 7 µL of cDNA for each sample was added to the opposite side of the inner upside of a PCR tube (previously used to fill with water). This was also done with the reverse pipetting technique as this technique prevents bubble insertion and improves accuracy. The left-over volume inside the pipet tip was returned to the cDNA tube. A different pipet tip was used for each different cDNA sample.
5. The PCR tubes containing the cDNA mixture and water were centrifuged for a few seconds to collect the drops on the bottom of the tube. Then, the cDNA samples were shortly placed on the vortex to mix. This was followed again by the quick centrifugation step. The PCR tubes were then placed on ice.
6. The PCR primer and SsoFast EvaGreen mix were made according to Table 11. For each reagent or component, a new pipet tip was used. The primers were added as last.
7. The master mix was then centrifuged for a few seconds to collect all the drops together. This was followed by placing it on the vortex to shortly mix the components.
8. The master mix was centrifuged again for a few seconds.
9. The prepared volumes were then pipetted into the 96-well plate: 8.63 µL of the primer mix with SsoFast EvaGreen and 6.38 µL of cDNA and water mix. Care was taken not to place the drops too high in the well due to the placement of the lid later.
10. The lid was placed on top of the wells to close them.
11. The 96-well plate was 3 to 5 min centrifuged at the fastest speed possible to collect the drops at the bottom.

12. The plate was carefully vortexed to mix the contents followed by centrifugation again (see step 11).
13. Then, the plate was placed in the real-time qPCR apparatus (Mx3000P, Agilent Genomics), and the program set according to Table 13.
14. After completion of the PCR program, the samples were stored at 4°C for other possible uses, such as agarose gel electrophoresis as described previously.

1.3.5 Cryosections and fixation of pH-SKPs

Cryosections of pH-SKP spheroids were made for immunohistochemistry protocols. Briefly, spheroids were collected and washed in PBS and then pelleted by centrifugation of 450 × g for 5 min at RT. The supernatant was removed and the spheroid pellet resuspended in 30% sucrose (Sigma, 84097) PBS. A 10- to 15-µL aliquot of the spheroid suspension was embedded in optimal cutting temperature compound (OCT, Sakura, 4583) and fast frozen in a −80°C cooled 99% isopropanol (Carl Roth, T910.1) bath. The pH-SKP spheroids were then sectioned with a cryostat at a 5-µm thickness (Leica, CMM3050S). Sections were attached to glass slides and immediately fixated in ice-cold 100% methanol for 10 min at −20°C. They were then allowed to dry under the chemical fume hood for 5–10 min. The slides could be placed in the fridge for short-term storage or in the −20°C or −80°C for long-term storage.

Cryosections and fixation of SKP spheroids, freezing: step-by-step protocol.

1. Prior to any step, a container was filled with isopropanol (also known as 2-propanol, Carl Roth, T910.1) and placed the day before in a freezer providing −80°C. This container would be used to fast-freeze spheroid samples.
   Note: When freezing spheroids, the container would remain in the −80°C freezer.
2. The SKP cultures were taken out of the incubator on the desired day.
3. The spheroids of each flask were collected and washed similarly as the RNA protocol steps (page 40).
4. When the spheroids were pelleted in a PBS solution, the supernatant would be aspirated and resuspended in 10 to 30 µL of 30% sucrose PBS solution.
5. OCT medium was added in a 1 × 1 cm cryosection mold. All bubbles were removed with a 100-µL pipet tip.
6. Then, 10 µL of the spheroid solution was dropped on the OCT present in the mold. This drop would slowly sink through the OCT medium to the bottom of the mold. When the spheroid drop would be in the middle of the OCT, the whole mold was carefully placed in the pre-cooled isopropanol bath. By carefully placing the molds in the isopropanol, the mold would float on top while the content froze.

7. After a few seconds, the OCT medium in the mold would turn white. The mold was left for at least three more minutes in the −80°C isopropanol bath.
8. The mold was then removed from the isopropanol bath and placed on top of a paper tissue to remove any residual isopropanol.
   Important note: All was done and left in −80°C freezing temperature environment to prevent thawing.
9. The molds containing the SKP spheroids were then placed together with a piece of paper tissue in a plastic sealed bag. The paper tissue was added to absorb any residual isopropanol. By placing the frozen molds in a plastic sealed bag, dehydration was reduced to improve preservation of the sample.
10. The samples were left in the −80°C for at least 24 h before sectioning.

Cryosections and fixation of SKP spheroids, sectioning: step-by-step protocol.

1. The frozen OCT mold containing the SKP spheroids was placed inside the cryostat, of which the chamber temperature was set to −20°C. The mold was acclimatized for at least 1 h.
2. The OCT block was then pressed out of the plastic mold. A large drop of OCT medium was placed on top of a cryo-adapter, and the frozen OCT block containing the sample was immediately pressed on top of this drop.
   Note: The uneven and rough side of the OCT block was pressed downwards on the new OCT drop, not vice versa.
3. The new OCT drop was allowed to freeze completely. The freezing would be complete when the fresh OCT was not glossy anymore by the ambient light but mat.
4. The adapter with the OCT block was then placed on the sectioning head. The sectioning head was set at a temperature of −18°C. The adapter and OCT block were allowed to acclimatize for another 15 min.
5. The sectioning head was then brought forward toward the blade until the OCT block almost touched it.
6. The trim section rate was set to 30 µm. This rate was used to trim away OCT material that did not contain any sample. When the spheroids would be vaguely seen through the OCT, the trim would be deactivated and the section rate set to 5 µm.
7. A sectioned piece would be placed onto a cryo-suitable glass slide when the spheroid depth was thought to be reached.
   Note: Sometimes the slides would be very static and cause trouble for placement of the sections. When this happened, all the slides to be used were shortly touched by water from a running crane. The slides could then be wiped or air-dried until use.

8. After placement of the section on the slide, it would be inspected with a microscope for any presence of spheroids. If spheroids were detected, the following consecutive sections were used for sample obtainment.
   Notes: Usually two to four sections were placed on one slide. Between each section placed on the same slide, approximately 2 to 5 mm of space was left in between. This space was added for future immunohistochemistry labeling to prevent spillovers when two different first antibodies would be used on the same slide.
9. After the placement of the sections, the slide was immediately placed into a −20°C cooled methanol bath for 10 min to fixate.
   Note: Six to eight sections were prepared in the freezing chamber of the cryostat at once. Then, two slides with each three or four sections were nearly simultaneously prepared. Directly after placement of the sections, they were placed in the methanol bath for fixation.
10. After 10 min of incubation, the slides were carefully removed and placed in a chemical fume hood on top of some paper tissues. In the fume hood, the methanol would evaporate quickly.
11. After completely drying the slides, they were stored at either 4°C for short-term storage or −20°C and −80°C for long-term storage.
12. When the desired number of slides had been obtained, and there was still sample material left to section, fresh OCT medium was placed on top of the cutting area to prevent dehydration during continued storage at −80°C.

1.3.6 Immunohistochemistry

Cells grown on coverslips or slides containing spheroid sections were fixated with 4% paraformaldehyde (Merck, 1.04005) for 15 min at RT and then permeabilized with 0.3% Triton X-100 (Applichem, A1388.0500) in PBS for 10 min at RT. Samples were blocked in PBS containing 15% FBS and 0.25% Tween-20 (Applichem, A4974.0500) for 1 h at RT. The samples were then incubated with primary antibodies, either for 1 h at RT or overnight at 4°C as indicated in Table 14. After several washes in blocking buffer, the corresponding secondary antibodies (Table 14) were added for 1 h at RT. Samples were counterstained and mounted with VectaShield containing 4',6-diamidino-2-phenylindole (DAPI, Vector Laboratories – H1200).

Immunohistochemistry, methanol fixated samples: step-by-step protocol.

Required reagents:

0.3% Triton X-100 (Applichem, A1388.0500)
(e.g., 75 µL Triton + 25 mL PBS)

0.25% phosphate buffered saline with tween (PBST, Tween-20, Applichem, A4974.0500)
(e.g., 125 µL Tween + 50 mL PBS)

15% FBS/PBST (Blocking buffer) made fresh
(e.g., 4.5 mL FBS (Gibco, 10270–106) + 35.5 mL PBST)

Table 14. Antibody list and incubation information. Abbreviations, PFA: paraformaldehyde.

Primary antibodies	**Fixation**	**Species**	**Dilution and incubation time**	**Supplier**
Stem cell markers	Methanol			
anti-nestin		Mouse	1:400 – 1 h RT	Abcam, ab22035
anti-CD9		Mouse	1:400 – o/n 4°C	Millipore, MAB4427
anti-melanoma-associated chondroitin sulfate proteoglycan / neuron-glial antigen 2 (NG2/MCSP)		Mouse	1:200 – 1 h RT	R&D, MAB2585
anti-vimentin		Mouse	1:200 – o/n 4°C	Millipore, CBL202
Smooth muscle cell markers	PFA			
anti-calponin		Mouse	1:100 – o/n 4°C	Dako, M^{3}556
anti-α-smooth muscle actin (αSMA)		Mouse	1:100 – o/n 4°C	Dako, M0851
anti-smooth muscle myosin heavy chain (SM-MHC)		Mouse	1:200 – o/n 4°C	Abcam, Ab683
Fibroblast marker	PFA			
anti-prolyl-4-hydroxylase beta (P4HD)		Mouse	1:400 – o/n 4°C	Acrys, AF0910–1
Other	Methanol			
anti-fibronectin		Rabbit	1:400 – 1 h RT	Sigma, F3648
anti-lamin A		Mouse	1:200 – 1 h RT	Abcam, ab8980
Secondary antibodies	-			
anti-mouse IgG (H + L)		Donkey	1:400 – 1 h RT	ThermoFisher, A-21202
anti-rabbit IgG (H + L)		Donkey	1:800 – 1 h RT	ThermoFisher, A-31572

1. For all prefixed samples, the samples were first allowed to acclimatized to RT for about 15 min. The required solutions were made during the acclimatization time, including the 0.25% PBST and 15% blocking buffer as described above.
2. For section samples, a circular or square-shaped outline was drawn with a hydrophobic PAP pen around the sample to prevent cross spilling of liquids.

3. Next, an incubation chamber was prepared. This chamber was a metal box with a removable lid. The filter paper was cut to the size of the box and was added to the bottom. Additionally, a piece of parafilm was placed on top of the filter paper.
4. After the acclimatization period, the samples were placed on top of the parafilm. Appropriate markings were made to be able to distinguish between samples.
5. A drop of PBS was added on top of each sample to hydrate it and was incubated for 5 min.
6. This was repeated for two more times to wash the sample.
7. A drop covering the whole sample of blocking buffer was then added and incubated for 60 min at RT. During this step, unspecific binding of the primary antibody was blocked or reduced for later steps.
8. Approximately 5 min before the end of the blocking incubation, the primary antibody solution was prepared in blocking buffer according to Table 14.
9. After the complete incubation period of the blocking buffer, the buffer was aspirated, and the primary antibody added. The volume of added antibody was between 60 to 80 µL, depending on sample size, for a 1-h RT staining. For samples that required staining overnight at 4°C, at least 80 µL was used per sample. This to prevent drying out of the sample.
10. After adding the primary antibody to each sample, demineralized water was added to the filter paper to further protect against evaporation.
11. After the primary antibody incubation, either 1 h at RT or overnight at 4°C, the liquid was aspirated. Then, the sample was covered with a drop of blocking buffer to start washing away the remaining and unbound antibodies.
12. The drop of blocking buffer was aspirated immediately followed by placing a fresh one to incubate it for 3 to 5 min at RT. This was repeated for three times in total.
13. Before the end of the final washing step, the secondary antibody was prepared in 15% blocking buffer according to Table 14.
14. After aspirating the final wash of blocking buffer, the secondary antibody was added in a volume of 60 µL and incubated for 1 h at RT.
    Note: All steps involved during and after the secondary antibody were executed in an as dark as possible environment.
15. After the incubation period with the secondary antibody, the liquid was aspirated and the sample washed by adding a drop of PBST. This was immediately aspirated and repeated two more times.
16. The washing step was repeated with 3 to 5 min of incubation between each aspiration.
17. Next, three times of a quick wash with just PBS was performed.

18. Any remaining liquid on top of the sample was aspirated, and a small drop of approximately 10 µL of DAPI was added. For coverslips, this drop was placed on the slide to which the coverslip was turned upside down on. For slides containing sections, the drop was placed directly on top of the sample. Then a large square coverslip was placed on top.
19. The DAPI was allowed to incubate for at least 30 min before any imaging by immunofluorescent microscopy. Samples were stored either in a slide container or a slide box at 4°C. Best was to image directly after finishing the staining protocol or otherwise usually maximally 1 to 2 days after.

Immunohistochemistry, paraformaldehyde-fixated samples: step-by-step protocol.

1. Steps 1 to 6 of the methanol fixated samples were also followed for the paraformaldehyde-fixated samples.
2. After the washing steps, 0.3% Triton X-100 was added to the samples. This step permeabilized the samples to provide access for the antibodies and was necessary for all paraformaldehyde-fixated samples.
3. The Triton was aspirated, and a PBS drop was added. This was followed by immediate aspiration.
4. A drop of PBS was added on top of the samples and incubated for 3 to 5 min. This was repeated for a total of 3 times.
5. Step 7 to 19 of the methanol fixated samples (see above protocol) was followed from hereon after.

1.3.7 Differentiation of pH-SKPs

For all differentiation methods, pH-SKPs were first collected, placed in adherence medium (SKP medium supplemented with 5% FBS), and allowed to adhere in a 6-well plate for 16 to 18 h at 37°C and 5% CO_2; BM-MSCs were treated similarly.

1.3.7A SKP adipocyte differentiation

Adhered pH-SKPs were washed once with sterile PBS, and 3 mL of adipocyte differentiation medium (DMEM with 1 g/L glucose [ThermoFisher – Gibco, 21885025], 0.5 mM 3-isobutyl-1-methylxanthine [IBMX, Sigma, I7018, stock in absolute ethanol {VWR chemicals, 20821.33}], 10 µg/mL insulin [Sigma, I2643, stock in 0.01 M HCL {Merck, 1.00319.2500} in Ultra-Pure water from Milli Q {MQ}], 1 µM dexamethasone [Sigma, D4902, stock in absolute ethanol], 10% FBS, 0.5 µg/mL Fungizone, 50 µM indomethacin [Sigma, I7378, stock in 100% DMSO {Sigma, D2650}], and 100 U/100 µg/mL penicillin/streptomycin [ThermoFisher-Gibco, 1514022]) was added and completely refreshed every 2 to 3 days.

<u>Differentiation of pH-SKPs to adipocytes: step-by-step protocol.</u>

Required media:

Table 15. SKP adherence medium – used to adhere and flatten SKP spheroids to a surface.

	Total Volume (X µL)	10,000	µL		
	Material			**End concentration**	
1	DMEM (low glucose) Gibco, 21885–025	6,880.5	µL		
2	F12 Gibco, 21765–029	2,293.5	µL		
3	EGF (0.1 mg/mL) ThermoFisher-Gibco, PHG0311	2	µL	20	ng/mL
4	bFGF (0.1 mg/mL) ThermoFisher-Gibco, PHG0021	4	µL	40	ng/mL
5	B27 ThermoFisher-Gibco, 17504044	200	µL	2%	v/v
6	Fungizone (250 µg/mL) ThermoFisher-Gibco, 15290018	20	µL	0.5	µg/mL
7	Pen/Strep (10,000 U/10,000 µg/mL) ThermoFisher-Gibco, 1514022	100	µL	100 U/100 µg/mL	
8	FBS Gibco, 10270–106	500	µL	5.0%	v/v

Stock preparation notes for the adipocyte differentiation medium:
The stocks are given in the amount they need to be diluted to (e.g., 100× or 250×), but also in molarity, and the weight/volume concentration. All solutions can be scaled up linearly (e.g., add twice as much of everything to have twice as much stock material).

IBMX (3-isobutyl-1-methylxanthine) stock – 100× / 50 mM / 11,11 mg/mL:

1. A total of 22.22 mg IBMX powder was weighed under a chemical fume hood.
2. This was transferred to a 50-mL tube, and 2 mL of 99% cell-grade ethanol was added.
3. This was repeatedly pipetted (with a 5-mL or 1000-µL pipet tip) until the powder dissolved completely (this could take some time: 10–15 min).
4. The solution was filtered through a 0.22 um filter to sterilize.
5. Aliquots of 500 µL were made and stored at −20°C.

Insulin stock – 100× / 1 mg/mL:

1. A total of 5 mg insulin powder was weighed under a chemical fume hood.
2. This was transferred to a 50-mL tube, and 5 mL of HCl (0.01 M) was added.
3. It was resuspended with a 5-mL pipet until clear (this went fast in general).
4. The solution was filtered through a 0.22 um filter to sterilize.
5. Aliquots of 500 µL were made and stored at −20°C.

Dexamethasone stock – 250× / 25 µM / 9.8 µg/mL:

1. A total of 5 mg dexamethasone powder was weighed under a chemical fume hood.
2. This was transferred to a 50-mL tube, and 50 mL of 99% cell-grade ethanol was added (it usually dissolved very fast).
3. The solution was filtered through a 0.22 um filter to sterilize. This was a pre-stock and had to be stored at −20C.
4. For the working stock, it was further diluted 1:10 in sterile PBS. Example: 100 µL pre-stock plus 900 µL PBS. The end solution was 250× / 25 µM / 9.8 µg/mL. It was stored at −20°C as well.

Indomethacin stock – 800× / 40 mM / 14.3 mg/mL:

1. A total of 28.62 mg indomethacin powder (very toxic) was weighed under the fume hood and transferred to a 50-mL tube. Then, 2 mL of 100% DMSO was added.
2. This was resuspended with a 1000-µL pipet. The liquid would become a clear yellow-green solution.
3. The solution was filtered through a 0.22 um filter to sterilize.
4. Aliquots of 300–500 µL were made and stored for long-term at −80°C and short-term at −20°C (no longer than 6 months).

Table 16. Adipocyte differentiation medium (shortened as ADI+) – used to differentiate pH-SKP spheroid cells into adipocytes.

	Total Volume (X µL)	10,000	µL		
	Material			**End concentration**	
1	DMEM (1 g/L glucose) Gibco, 21885-025	8,628	µL		
2	IBMX (100 × / 50 mM / 11.11 mg/mL) I7018-250MG Sigma	100	µL	0.5	mM
3	Insulin (100 × / 1.0 mg/mL) I2643-50MG Sigma	100	µL	10	µg/mL
4	Dexamethasone (250 × / 25 µM / 9.8 µg/mL) D4902-100MG Sigma	40	µL	1	µM
5	Indomethacin (800 × / 40 mM / 14.3 mg/mL) I7378-5G Sigma	12.5	µL	50	µM
6	Fungizone (250 µg/mL) ThermoFisher-Gibco, 15290018	20	µL	0.5	µg/mL
7	Pen/Strep (10,000 U/10,000 µg/mL) ThermoFisher-Gibco, 1514022	100	µL	100 U/100 µg/mL	
8	FBS Gibco, 10270-106	1,000	µL	10%	v/v

SKP spheroid adherence protocol:

1. A few days before starting, the reagent stocks were made as shown above (page 60).
2. The SKP adherence medium was made (Table 15) on the day of usage.
   Note: Thawing the reagents at RT took approximately 5 to 15 min.
3. For differentiation designed to take place on coverslips, the coverslips were first placed in 99% cell-grade ethanol to sterilize. The coverslips were then placed either in a 24-well plate or a 6-well plate. Only one coverslip would fit in a 24-well-plate well and five in a 6-well-plate well.
4. The coverslips were allowed to dry inside a sterile biosafety cabinet. This took approximately 10 to 15 min (with the lid half open).
5. For the differentiation, 5-day-old pH-SKPs were used for experimentation and to obtain data for publication purposes. However, 3-day-old pH-SKPs were also tested and found successful (5-day-old were used to have more material grown).
6. The spheroids were collected from their respective flasks and transferred into a 50-mL tube. The flask was washed with 10 mL of sterile PBS to collect any remaining or attached spheroids and was added to the 50-mL tube with the other spheroids. The 50-mL tube was then centrifuged at 450 × g for 5 min at RT.
7. The supernatant was carefully aspirated, and 5 mL of SKP adherence medium was added to resuspend the spheroids.
   Note: Depending on the number of spheroids, more or less SKP adherence medium volume could be added. For small experiments, 1 mL would suffice.

8. With a 100-µL yellow pipet tip, one to five spheroids were collected from the spheroid mixture in an 80 µL volume and placed as a drop in the center of the coverslip. Care had to be taken to prevent shaking or disturbing the drop as too much disturbance would result in the spilling of the liquid next to the coverslip.
9. The plate with the spheroid drops was then placed in the cell incubator, which maintained 37°C and 5% CO_2, for minimally 16 h, or until the spheroids had attached and flattened sufficiently onto the coverslip.
10. The SKP spheroids were now ready for further differentiation steps. For all differentiation types used in this study, this adherence protocol was first executed.

SKP adipocyte differentiation: step-by-step protocol.

1. The reagents required for the adipocyte differentiation medium were taken out of their respective storage places to acclimatize at RT. For the reagent IBMX, repeatedly pipetting with a 1000-µL pipet tip was done to promote the dissolving of formed crystals during storage. This would take between 5 to 10 min and would go much faster when acclimatized to RT first.
2. The adipocyte differentiation medium was prepared, see Table 16. The required volume depended on the number of wells targeted for differentiation. For a 24-well plate, each well would receive 500 µL of differentiation medium. A 6-well-plate well would receive 3 mL of medium. Additionally, sufficient medium would be made for aliquots for 2 weeks of future adipocyte feeding. These aliquots were stored in the −20°C freezer.
3. Prior to differentiation initiation, the attached spheroids were washed by carefully adding 2 mL of sterile PBS to each 24-well-plate well and 5 mL to each 6-well-plate well.

   Note: Care must be taken when adding new liquids to the wells containing attached spheroids. This because the flow of liquid could disrupt their attachment.
4. After washing the spheroids, adipocyte medium was added to each well (500 µL per 24 well-plate well and 3 mL per 6 well-plate well). For each experiment, controls were included by using standard fibroblast culture medium on spheroids. These spheroids should not develop adipocytes.
5. The plate was then placed in the cell incubator set at 37°C and 5% CO_2.
6. All the cells were fed every 3–4 days, by refreshing the medium completely. In general, micro lipids became visible after 2 or 3 days, starting first in and around the center of the attached spheroid.
7. After 3 to 4 weeks, lipids were present in most cells.

8. The adipocytes were fixated after the desired culture days.
9. The cultures were removed from the incubator and placed in a sterile biosafety cabinet.
10. The media was aspirated from the wells (always from the control first), followed by a careful wash with sterile PBS. The volume of the PBS was 2 mL for a 24-well-plate well and 5 mL for a 6-well-plate well.
    Note: The washing was done with utmost care as adipocytes are very fragile.
11. The PBS was removed, and 500 µL of 4% PFA (Merck, 1.04005) was added to each well for a 24-well-plate well and 3 mL for a 6-well-plate well.
12. For immunohistochemistry labeling, the incubation time of fixation was between 10 to 15 min at RT. For oil red O (ORO) staining, the incubation time of fixation was 30 to 45 min at RT.
    Note: All fixations with PFA were performed under a chemical fume hood.
13. After fixation, the PFA was aspirated, and the wells were rinsed carefully with PBS or demineralized water. PBS was used for samples intended for immunohistochemistry and demineralized water for ORO staining. This was repeated for a total of 3 times. Similarly, utmost care was taken to prevent the detachment of adipocytes.
14. The adipocytes were now ready for either immunohistochemistry protocols (pages 55–58) or the ORO staining protocol (pages 68–69).

1.3.7B SKP smooth muscle cell (SMC) differentiation

Adhered spheroids were dissociated by trypsin and seeded at a low density (2×10^4 cells/well) in SKP medium supplemented with 5% FBS for 18 h in a 6-well-plate well. Fibroblasts and NS-SKPs (no-stress SKPs) were used in parallel as a control. The cells were washed once with sterile PBS. Then, 3 mL of SMC differentiation medium (4:1 – DMEM [Sigma, D6429]: F12 and 2.5 ng/mL transforming growth factor beta [TGF-β1, ThermoFisher, PHG9214], 0.5% FBS and 100 U/100 µg/mL penicillin-streptomycin [ThermoFisher-Gibco, 1514022]) was added to each well. The complete medium was changed every 4 days for a period of 8 to 12 days. SMC differentiation was confirmed by immunolabeling of the SMC markers calponin, αSMA and SM-MHC (Table 14).

SKP SMC differentiation: step-by-step protocol.

Required reagents:

TGF-β1 (transforming growth factor beta 1) stock – 10 µg/mL.

1. All following steps were performed under sterile conditions.
2. The product was contained in a vial when delivered. It was shortly centrifuged at high speed (3,000–4,000 rpm 5 min at RT) to bring the contents to the bottom.
3. The vial was opened, and the lyophilized protein reconstituted in a sterile acidic buffer such as 40 mM acetic acid or 4 mM HCl, both containing 0.1% bovine serum albumin. The volume of solvent to add was equal to create a final concentration of 10 µg/mL. For the product "Thermo Fisher PHG9214," 10 µg of material is provided in the vial, and therefore, 1 mL of solvent was added.
4. The solution was pipetted multiple times to reconstitute the protein completely. Note: The solution should not be vortexed.
5. Aliquots of 100 µL portions were made to reduce freeze/thaw cycles, which were stored at −20C.

Table 17. Smooth muscle cell differentiation medium (shortened as SKP SMC differentiation medium) – used to differentiate SKP cells into smooth muscle cells.

	Total Volume (X µL)	10,000	µL		
	Material			**End concentration**	
1	DMEM (4.5 g/L glucose) Sigma, D6429	7,348	µL		
2	F12 Gibco, 21765-029	2,449	µL	0.5	mM
3	Pen/Strep (10,000 U/10,000 µg/mL) ThermoFisher-Gibco, 1514022	100	µL	100 U/100 µg/mL	
4	FBS Gibco, 10270–106	100	µL	1%	v/v
5	TGF-β1 (10 µg/mL) Thermo Fisher, PHG9214	2.5	µL	2.5	ng/mL

1. The spheroids were adhered according to the spheroid adherence protocol (page 61 and 62).
2. The samples were taken out of the cell incubator, and the adherence medium was aspirated.
3. A total of 500 µL sterile PBS was added for a 24-well-plate well and 5 mL for a 6-well-plate well to wash the adhered cells.
4. The PBS was aspirated, and 100 µL of trypsin was added for a 24-well-plate well and 500 µL for a 6-well-plate well. This was incubated in the cell incubator at 37°C for 10 min to dissociate and detach the cells.

5. Sterile coverslips were placed in the intended wells during incubation for later single-cell attachment for differentiation.
6. The dissociated cells were then collected by adding standard fibroblast culture medium and transferring it into a 50-mL tube. Then, additional medium was added to collect all remaining cells from the wells.
7. The cells in the 50-mL tube were centrifuged at 450 × g for 5 min at RT.
8. The supernatant was aspirated, and approximately 20 to 40 mL of sterile PBS was added in order to wash the cells and remove any remaining FBS residue. The volume of PBS to add depended on the amount of space left in the 50-mL tube.
9. Step seven was repeated.
10. The supernatant was aspirated, and 1 to 5 mL of sterile PBS was added to resuspend the cells. The amount of PBS volume depended on the number of estimated cells or wells used to collect cells from—if many wells or cells were expected, a higher volume was used and vice versa.
11. The cells were then counted to determine the concentration. This was done with the use of a counting chamber (Neubauer Chamber).
12. After determining the total amount of cells, the cells were centrifuged again, similarly as step seven.
13. The supernatant was aspirated, and SKP medium supplemented with 5% FBS was added to obtain a concentration of 1×10^4 cells/mL.
14. From the cell suspension, either 250 µL was added per 24-well-plate well or 2 mL per 6-well-plate well.
15. The plate containing the cells was then placed into the cell incubator maintaining 37°C and 5% CO_2. The cells were incubated for at least 18 h in order to adhere to the surface.
16. After incubation, the adherence medium was aspirated, and the cells washed with the appropriate volume as described above with PBS.
17. The PBS was aspirated, and 500 µL of SMC differentiation medium (Table 17) was added for a 24-well-plate well and to 3 mL for a 6-well-plate well.
18. The plates were then placed back into the cell incubator.
19. The cells were fed on day 4 and 8 by refreshing the complete medium after aspiration of the old medium.
20. Usually, after 5 to 8 days, the cells showed flattening and enlargement, which indicated SMC differentiation.
21. Generally, the cells were fixated between days 10 and 12. This was done by aspirating the media and washing with the appropriate volume of PBS. Then, a 4% PFA solution (500 µL 24-well-plate well and 3 mL 5-well-plate well) was added to fixate the cells for

10 min at RT. The PFA was aspirated, and the cells washed 3 times with PBS. This was then aspirated, followed by the addition of fresh PBS to keep the cells hydrated.

22. Prepared cells could then be placed in the fridge at 4°C or immediately used for immunohistochemistry protocols.
23. Identification of SMC cells was done via the immunohistochemistry protocol and the following antibodies: anti-Calponin, αSMA (anti-α-smooth muscle actin), and SM-MHC (anti-smooth muscle myosin heavy chain), see Table 14.

1.3.7C SKP fibroblast differentiation

For fibroblasts differentiation, pH-SKP spheroids were allowed to adhere for 18 h and then reseeded at low density as described for the SMC differentiation protocol. Cells were fed with standard fibroblast culture medium (DMEM/15% FBS) every 2 to 3 days. The cells were passaged three to five times before immunohistochemistry labeling with P4HD (anti-prolyl-4-hydroxylase beta), a fibroblast marker (Table 14).

SKP fibroblast differentiation: step-by-step protocol.

1. The spheroids were adhered according to the spheroid adherence protocol (page 61 and 62).
2. The samples were taken out of the cell incubator, and the adherence medium was aspirated.
3. A total of 500 µL sterile PBS was added for a 24-well-plate well and 5 mL for a 6-well-plate well to wash the adhered cells.
4. The PBS was aspirated, and 100 µL of trypsin was added for a 24-well-plate well and 500 µL for a 6-well-plate well. This was incubated in the cell incubator at 37°C for 10 min in order to dissociate and detach the cells.
5. During incubation, sterile coverslips were placed in the intended wells to use for differentiation.
6. The dissociated cells were then collected by adding standard fibroblast culture medium and for transfer into a 50-mL tube. Then, additional medium was added to collect all the remaining cells from the wells.
7. The cells in the 50-mL tube were then centrifuged 450 × g for 5 min at RT.
8. The supernatant was aspirated, and approximately 20 to 40 mL of sterile PBS was added in order to wash the cells and remove any remaining FBS residue. The volume depended on the amount of space left in the 50-mL tube.
9. Step 7 was repeated.

10. The supernatant was aspirated, and 1 to 5 mL of sterile PBS was added to resuspend the cells. The amount of volume depended on the number of estimated cells or wells used to collect cells from—if many wells or cells were expected, a higher volume was used and vice versa.
11. The cells were then counted to determine the concentration. This was done with the use of a counting chamber (Neubauer Chamber).
12. The cells were centrifuged again, similar as in step 7.
13. The supernatant was aspirated, and SKP medium supplemented with 5% FBS was added to obtain a concentration of 1×10^4 cells/mL.
14. From the cell suspension, 3 mL per 6-well-plate well was added.
15. The plate containing the cells was then placed into the cell incubator maintaining 37°C and 5% CO_2. This was incubated for at least 18 h to adhere the cells to the surface.
16. After incubation, the adherence medium was aspirated and the cells washed with 5 mL of sterile PBS.
17. The PBS was aspirated, and 3 mL of fibroblast culture medium was added per well.
18. The plates were then placed back into the cell incubator.
19. The cells were fed every Monday, Wednesday, and Friday by aspirating the old medium and adding 2 mL of fresh fibroblasts culture medium.
20. When the cells became ~80% confluent, they were dissociated and detached from the well via the trypsin protocol. After detachment, they were seeded again by dividing one 6-well-plate well over three 10-cm cell culture dishes in a total volume of 8 mL per dish. This would account for passage 1.
21. The cells were then fed every Monday, Wednesday, and Friday again by aspirating the old media and adding 8 mL of fresh fibroblasts culture medium.
22. When the cells became ~80% confluent again, the cells would be split again according to step 19; however, a splitting ratio of 1:5 was used instead. This accounted for passage 2.
23. Steps 19 to 21 were repeated up to four to five passages. With the last intended passage, before placing the cells back into the cell culture dish, sterile coverslips were placed in the dish for the cells to adhere on top of it.
24. The cells were then ready for analysis of the fibroblast differentiation. This was done by fixating the cells with 4% PFA for 10 min at RT (5 mL for a 10-cm dish). After the fixation, the cells were washed once by PBS (8 mL/dish) followed by aspiration. Eight mL of PBS was then added to keep the cells hydrated.
25. Prepared cells could then be placed in the fridge at 4°C or immediately used for immunohistochemistry protocols.

26. Identification of fibroblast cells was done via the immunohistochemistry protocol by using the following antibody as fibroblast marker: anti-prolyl-4-hydroxylase beta (P4HD), see Table 14.

1.3.8 Oil red O staining and analysis

ORO staining, following the ThermoScientific SC protocol 00011, confirmed adipocyte differentiation. ORO staining was observed by bright field microscopy, of which a red staining indicated intracytoplasmic lipids.
After ORO staining, digital image analysis of ORO-stained adipocytes was performed to obtain a quantitative value of pH-SKP spheroids that had differentiated into adipocytes. Here, bright field images were acquired with a 10× objective providing an 879 µm × 658 µm field of interest. The images were processed and analyzed via a simplified method based on Deutsch et al. [42]. Briefly, via red color thresholding, cellular lipids stained by ORO were digitally isolated, followed by binarization of the image for digital analysis. ImageJ was used to calculate the percentage of the white color of the total image, which represented the percentage of adipocyte lipids. Three different image locations with the highest concentrated adipocyte areas per ORO-stained sample were analyzed. This procedure was performed with a total of three samples per cell line to obtain a mean value with standard deviation.

<u>Oil red O staining: step-by-step protocol.</u>

Required reagents and materials:

- Oil red O powder (Sigma, O0625)
- 99% isopropyl alcohol or 99% 2-propanol (Carl Roth, Art. -nr. T910.1)
- Demineralized water
- Tap water
- Whatman Filter paper (Fisher 09–845)

1. An ORO stock solution was prepared by weighing 150 mg of ORO powder under a chemical fume food. This was transferred to a 50-mL tube, followed by the addition of 50 mL of 99% 2-propanol to solve and mix it.
   Note: This stock solution is stable for one year from the date it is made.
2. A 60% 2-propanol solution was made by adding 30 mL of 99% 2-propanol to 20 mL of demineralized water into a 50-mL tube. This was stored at RT and had no apparent expiration date.
3. If the adipocyte samples were fixated previously and stored in the fridge, they were first taken out into RT to acclimatize. If the samples were not fixated yet, they were first

fixated by PFA. Briefly, the culture media was removed by aspiration, and the samples washed once by adding PBS and aspirating again. Then, 4% PFA solution was added to each sample. The samples were incubated for 30 min at RT under a fume hood. The next steps could be performed during this incubation period.

4. Under a chemical fume food, three parts of ORO stock solution were mixed with two parts of demineralized water in a 50-mL tube. The amount of ORO solution needed depended on the number of samples. For a 24-well-plate well, a minimum of 300 µL was used, but 500 µL was optimal. For a 6-well-plate well, a minimum of 1 mL was used, but 2–3 mL was optimal. Care had to be taken with the calculation because during the filtration step approximately 20 to 30% of the volume would be lost.
5. This working solution was then incubated for 10 min at RT. The working solution is stable for only 2 h and has to be used within this period.
6. After incubation, the work stock was filtered by pouring it through a Whatman filter paper, which was placed in a new 50-mL tube. This process was done under a chemical fume hood and required approximately 15 to 20 min for the liquid to pass entirely.
7. After the fixation period, the PFA was removed, and the samples gently washed with demineralized water. The volume of water to add was 500 µL for the 24-well-plate wells and 2 mL for the 6-well-plate wells. For any further directions of adding liquids or reagents, the same volumes were used.
8. The aspirated water was removed as PFA waste.
9. Then, 60% 2-propanol was added to each well and incubated for 5 min RT.
10. The 2-propanol was removed, and the ORO work solution was added to each well. Note: It was made sure that the liquid covered the entire monolayer.
11. The ORO solution on the samples was incubated for 5 min at RT.
12. It was then removed and the cultures rinsed with RT tap water. For a 24-well plate, it was practical to use a 10-mL pipet and add 2 mL per well. The same pipet was then used to aspirate the liquid. For a 6-well plate, a 25-mL pipet was used, and a volume of 8 mL was added per well. The whole process was repeated until the aspirated water was clear of color.
13. In the final step, 500 µL of demineralized water was added to each well for a 24-well plate and 2 mL for a 6-well plate. This to prevent any dehydration during storage. However, care had to be taken for long-term storage in the fridge because usually the water would be evaporated within 1 to 2 months. Some water was simply added to prevent this.
14. The samples were ready for microscopy analysis.

Digital image analysis or ORO: step-by-step protocol.

1. The ORO-stained samples were taken out of the fridge to acclimatize to RT prior to microscopic imaging.
2. With a standard microscope (Zeiss Axiovert 40 CFL inverted), camera (AxioCam MRc5, Zeiss), and 10× objective, bright field images were acquired of the samples. The camera was used via the AxioVision software (AxioVs40×64 V4.8.3.0) and images were only taken of the highest density ORO-stained positive cells. This provided an 879 µm × 658 µm field of interest containing positively stained cells.
3. Step 2 was in total 3 times repeated for each well, where each time a unique field was used.
4. Step 2 and 3 were repeated for two other wells containing the same sample to provide an n = 3.
5. The obtained images were then processed by ImageJ (Fiji) to determine the percentage of positively stained adipocytes as described above in the overview protocol.
6. The processing steps of the digital image analysis overview protocol were translated into a macro code to automate the analysis of multiple images. In the program, the “Process” tab, then “Batch,” then “Macro,” the following code was used and inserted into the large field:

```
// Color Thresholder 2.0.0-rc-43/1.51a
// Autogenerated macro, single images only!
min=newArray(3);
max=newArray(3);
filter=newArray(3);
a=getTitle();
run("HSB Stack");
run("Convert Stack to Images");
selectWindow("Hue");
rename("0");
selectWindow("Saturation");
rename("1");
selectWindow("Brightness");
rename("2");
min[0]=20;
max[0]=240;
```

```
filter[0]="pass";
min[1]=0;
max[1]=255;
filter[1]="pass";
min[2]=0;
max[2]=255;
filter[2]="pass";
for (i=0;i<3;i++){
  selectWindow(""+i);
  setThreshold(min[i], max[i]);
  run("Convert to Mask");
  if (filter[i]=="stop")  run("Invert");
}
imageCalculator("AND create", "0","1");
imageCalculator("AND create", "Result of 0","2");
for (i=0;i<3;i++){
  selectWindow(""+i);
  close();
}
selectWindow("Result of 0");
close();
selectWindow("Result of Result of 0");
rename(a);
// Color Thresholding----------

setOption("BlackBackground", true);
run("Make Binary");

dir = getDirectory("image");
name = getTitle;
index = lastIndexOf(name, ".");
if (index!=-1) name = substring(name, 0, index);
name = name + ".csv";

run("Measure");
saveAs("Results", dir+name);
print(dir+name);
```

7. In the same window, the folder containing all the ORO-stained images was chosen as an input folder, and an empty folder was chosen as an output folder. All the processed images would be located in the output folder after running the code. The output format was set to JPEG, and in the “field name contains” field JPEG or JPG was inserted.
8. The button “process” was selected to run the analysis.
9. After the processing was finished, multiple Excel files were created in the ImageJ folder—the folder where ImageJ is installed or located on the hard drive. From these Excel files, only the most recent one (with the latest date) was taken, and the others deleted. The latest file contained all the samples, while the first generated file only contained the 1st sample. The second file contained the 1st and 2nd, etc.
10. In the Excel file, all the values concerning the positive percentage of ORO-stained cells for each sample could be viewed and processed for graphical presentation.
    Note: The value represents the percentage of staining and not the actual percentage of cell number.

1.3.9 Statistical analysis

Results are presented as the mean ± standard deviation (SD). Comparisons were performed using the Student’s t-test. *P* values less than 0.05 were considered statistically significant. The sample sizes are indicated in the figure legends.

1.4 Results

To test our hypothesis that acute acidic stress on pre-established primary fibroblast monocultures would permit the rapid isolation and expansion of SKP cells, we established an acidic stress isolation method and compared this with the previously published trypsin-based isolation method and no-stress method by examining SKP growth [71, 185]. The stemness of the isolated SKP spheroids was then further investigated.

1.4.1 Defining the acidic pH stress for the novel SKP isolation method

To determine the optimal acidic stress, we first investigated the effect of low acidic stress on primary dermal fibroblasts using a pH range from 7 to 5 in HBSS. Standard HBSS (pH 7.4) was used as a control, and pH 2.5-adjusted HBSS was used to induce cell death (Fig. 6). Fibroblasts were incubated in suspension for 30 min in HBSS buffer with varying pH at 37°C and 5% CO_2 and were, after removal of the HBSS buffer, transferred into classic SKP culture medium (see Chapter 1, Materials and Methods). After treatment, cell viability was determined by fluorescence-activated cell sorting (FACS). The viability of standard HBSS-treated fibroblasts showed that the direct effect of the experimental conditions resulted in a total cell death of ~4.5% at 0-h post-treatment to ~20% at 2-h, with no further reduction at 20-h post-treatment (Fig. 6). Fibroblast suspensions exposed to pH 7.0 and below showed high levels of cell death at 20-h post-treatment (Fig. 6). Interestingly, the percentage of cell death between pH 6.7 and pH 5.3 reached a plateau at ~34% but increased significantly at pH 5.0 (~45% cell death) (Fig. 6). These findings indicate that an average of 66% of the fibroblast suspension remained viable at 20-h post-treatment between pH 6.7 and pH 5.3. To assess the effect of acidic pH stress on SKP isolation from primary fibroblast cultures, we selected pH 5.7.

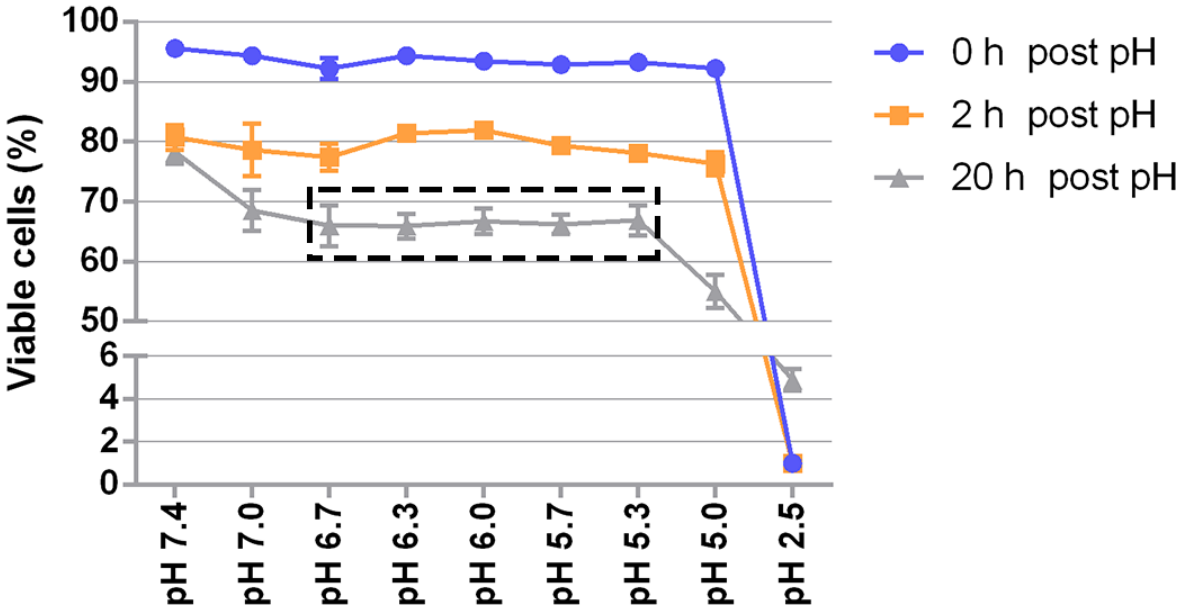

Fig. 6. Primary dermal fibroblasts exposed to low pH from 6.7 to 5.3 exhibit a similar range of cell death. A viability assay graph based on FACS analysis of primary foreskin fibroblasts treated in suspension for 30 min at 37°C with HBSS of different pH values as indicated. The percentages of viable cells at time points 0-, 2- and 20-h post-treatment are shown as the mean ± SD (n = 3). Abbreviations used: h = hours, FACS = fluorescence-activated cell sorting.

1.4.2 Acidic stress at pH level 5.7 activates NHE1 expression

The expression of the sodium-hydrogen exchanger 1 (NHE1) was investigated next. NHE1 is known as the main regulator of intracellular pH (pHi) and is located in the plasma membrane. It functions via the exchange of a proton for an extracellular sodium ion when the pHi drops below a certain threshold level [3, 86, 160]. NHE1 affects various cell functions, such as cell survival, proliferation, and cytoskeleton and actin filament assembly [41, 84, 119].

Fibroblasts treated with the acidic stress of pH level 5.7 for 30 min were assessed for NHE1 expression with real-time qPCR after stress exposure. Various post-treatment time points were investigated for NHE1 protein expression. These included 0- (immediately after 30 min of pH 5.7 exposure), 4-, and 20-h post-treatment (Fig. 7). Results showed that immediately after exposure (0 h), NHE1 expression was activated and that the expression was highest at 20-h post-treatment. These data are in line with the cell viability seen at 20-h post-treatment, previously shown in Fig. 6. Here, between pH 6.7 and pH 5.3, cell death at 20 h did not increase further. In sum, our data suggest a significant role of NHE1 expression in cells under acidic stress for their survival and adaptation.

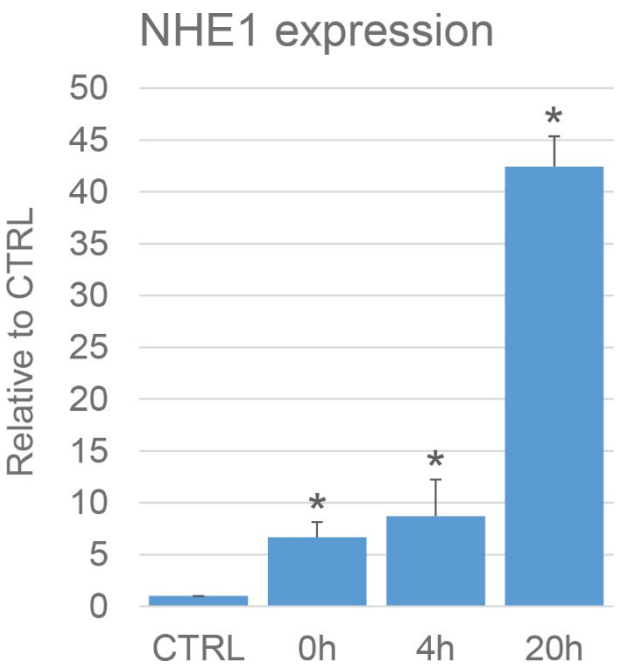

Fig. 7. NHE1 expression is highest in fibroblasts at 20-h post-treatment of acidic stress. Real-time qPCR evaluation of NHE1 RNA expression in GM05565. The fibroblasts were treated with 30 min of pH 5.7 for 0, 4, and 20 h. Data are shown as the expression in acidic stress-treated fibroblasts relative to non-treated cells (CTRL, which equals 1). Values represent the mean + SD (*P < 0.05, n = 3). Abbreviations used: CTRL = control, and h = hours.

1.4.3 Acidic stress treatment on primary dermal fibroblasts induces rapid spheroid formation and growth

To assess the effect of low acidity on SKP isolation, a 30-min acidic stress treatment of pH 5.7 in HBSS buffer at 37°C was used on pre-established dermal primary fibroblasts derived from foreskin. These cultures were compared to cultures subjected to no-stress or trypsin-stress conditions as described previously (Materials and Methods and [185]). After treatment, all groups were cultured in SKP medium and termed NS-SKP (no-stress based), Tr-SKP (trypsin-based), and pH-SKP (low pH-based) (Fig. 8A).

Images of all SKP cultures were acquired at various days to monitor spheroid formation and growth. Clear spheroid formation in pH-SKP cultures was detected by day 3, and further analysis showed that 5 days was sufficient for pH-SKP to form numerous large spheroids (Fig. 8B). In contrast, the no-stress and trypsin-based methods produced fewer spheroids and required longer culture periods (up to 21 days) to form numerous larger spheroids, which was consistent with previous reports [71, 185]. These differences indicated that spheroid development under pH-SKP isolation conditions was significantly faster compared to the other isolation conditions.

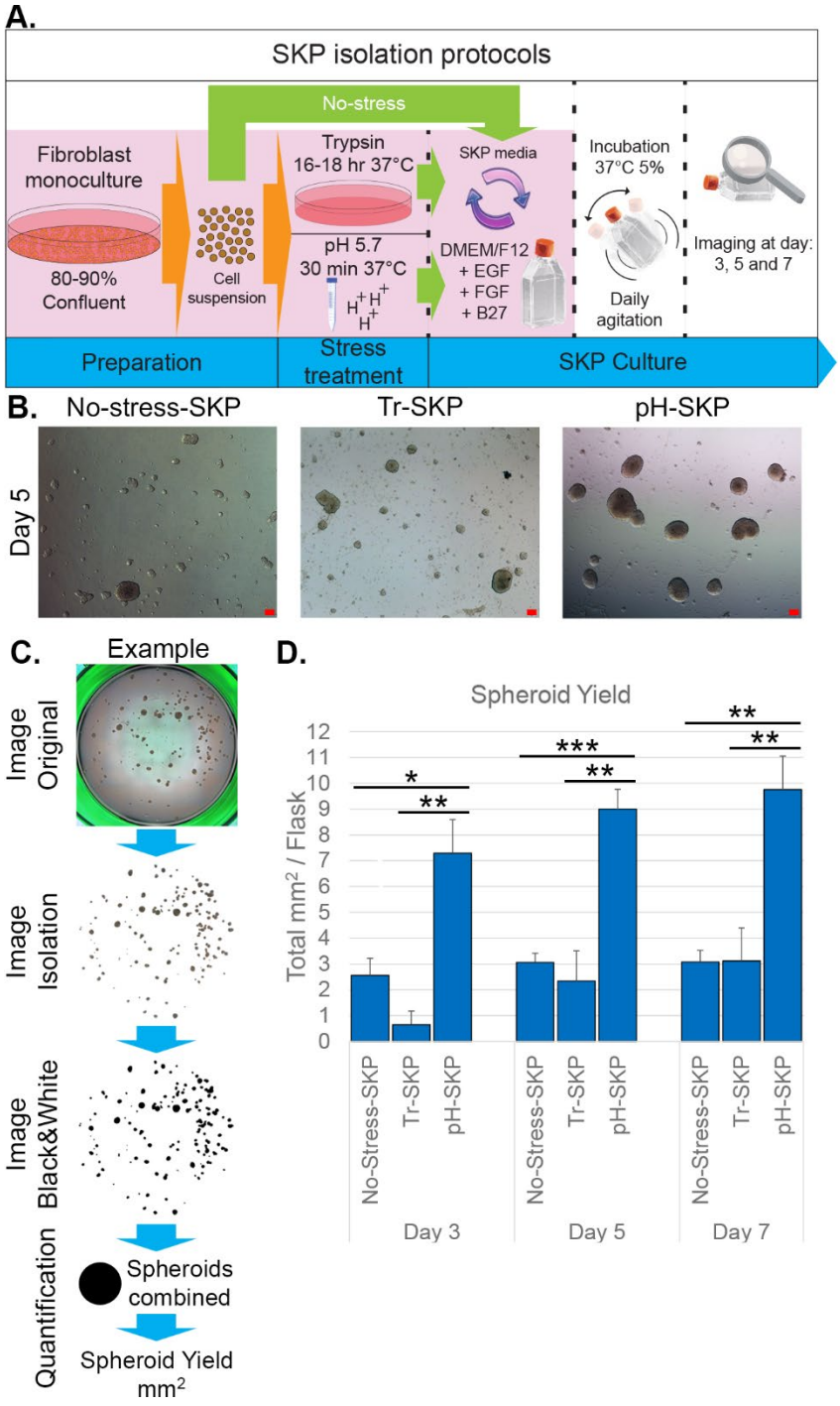

Fig. 8. Acute exposure of primary fibroblasts to pH 5.7 induces rapid SKP spheroid formation and growth. (**A**) Schematic representation of methods of SKP isolation from primary fibroblasts using no-stress, trypsin-stress (Tr-SKP), and acidic stress (pH-SKP). (**B**) Representative images of SKP spheroid are shown of cultures on day 5 using the no-stress, trypsin-stress, and low pH stress (n = 6). Scale bar: 100 µm. (**C**) This panel outlines the spheroid quantification process starting from a whole-well image of a whole SKP culture. Briefly, spheroids are isolated from the image original, and black color is then overlaid for binarization. All spheroid numbers and sizes are combined to calculate the spheroid yield per culture. (**D**) The graph represents the spheroid yield at days 3, 5, and 7 in mm^2. Data are expressed as the mean ± SD (***P < 0.005, **P < 0.01, *P < 0.05; n = 3).

To further determine the effect of low pH treatment on global spheroid culture, the spheroid number and size were quantified for all conditions. The entire cultures were collected in 48-well plates, and images of the complete wells were acquired as described in the Materials and Methods (Fig. 8C). The spheroids were first digitally isolated from the original image, followed by black and white adjustment for binarization and quantification of each spheroid by ImageJ (Fig. 8C). The numbers and sizes of spheroids were combined to give the total spheroid yield per culture and condition (Fig. 8D). The total spheroid yield was much higher using pH-SKP conditions compared to no-stress or Tr-SKP cultures (Fig. 8D). A clear difference was already apparent on day 3. Importantly, when typical large spheroids were detected on day 5, the pH-

SKP spheroid yield was 3- and 4-fold higher than those observed under no-stress and trypsin-stress conditions, respectively (Fig. 8D). Collectively, these findings indicate that exposure of primary fibroblast cells to acute acidic stress (pH 5.7) induce more efficient spheroid formation and growth than previously reported methods.

1.4.4 pH-SKP spheroids express multipotent stem cell markers

The expression of stem cell markers was evaluated by immunohistochemistry to determine the stemness of pH-SKP spheroid cells of day 5 pH-SKP spheroid cryosections. Sections were positive for the neuronal crest marker nestin [97] and multipotent markers Sox2 [5], Oct4 [138], NANOG [122], and TG30 (an antibody highly specific for embryonic stem cell marker CD9) [80] (Fig. 9A). Furthermore, the neuron-glial antigen 2 (NG2), also known as melanoma chondroitin sulfate proteoglycan (MCSP), a marker for glial precursor and epidermal stem cells [95, 162], was positively labeled in pH-SKP spheroids. In addition to stem cell markers, positive labeling was found for lamin A, vimentin, and fibronectin (Fig. 9A), showing that pH-SKP spheroids also express proteins that are present in fibroblast cells.

Next, expression of mRNA—encoding various stem cell markers in pH-SKPs—was determined by RT-PCR analysis. Total RNA was isolated from pH-SKP cultures on day 5. The mRNA expression of stem cell markers nestin, Sox2, Oct4, NANOG, CD9, C-Myc, and Klf4 was determined using targeted PCR amplification and by comparing the pH-SKP spheroids with the corresponding origin fibroblasts (Fig. 9B). All analyzed stem cell markers showed a significant increase in expression in pH-SKP samples, with $P < 0.0005$ for nestin, NANOG, C-Myc, and Klf4; $P < 0.005$ for Sox2 and CD9; and $P < 0.05$ for Oct4. Together, these findings show that pH-SKP spheroids at day 5 of culture expressed stem cell markers at both the mRNA and protein level, indicating that these pH-SKP cells exhibit multipotent properties.

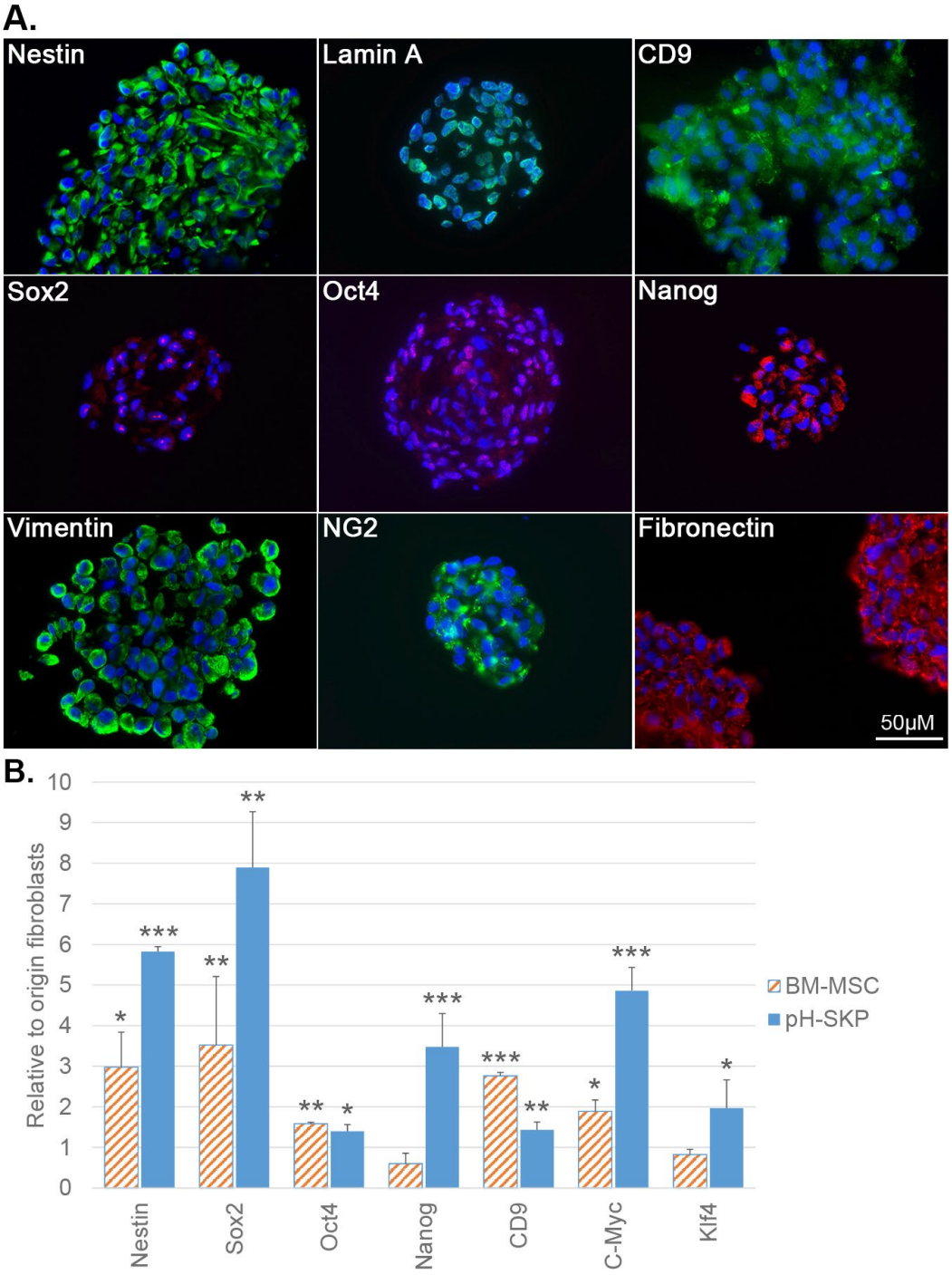

Fig. 9. Day 5 pH-SKPs express the neuronal crest and multipotent stem cell markers. (**A**) Immunohistochemistry of stem cell markers of day 5 pH-SKP spheroids obtained from cell line GM05565 at passage 12. The following stem cell markers were evaluated and labeled on 5-µm thick spheroid cryosections: nestin (green), CD9 (green), Sox2 (red), Oct4 (red), NANOG (red), and NG2 (green). The nuclear lamina marker lamin A (green), vimentin (green), and fibronectin (red) were labeled as well. All cryosections were counterstained for DNA with DAPI (blue). (**B**) PCR evaluation of stem cell marker expression of day 5 pH-SKP spheroids obtained from cell line GM05565 at passage 12. RNA expression was determined of nestin, Sox2, Oct4, NANOG, CD9, C-Myc, and Klf4. Data are shown as the expression in pH-SKP cells relative to the expression in corresponding origin fibroblasts. Values represent the mean + SD (***$P < 0.0005$, **$P < 0.005$, *$P < 0.05$; n = 6).

1.4.5 pH-SKPs can be isolated from human primary fibroblast cultures derived from all ages, body sites, and passage numbers

To further investigate the potential of the acidic stress method for SKP isolation, various primary fibroblast lines were used for a proof of concept. In total, 11 primary fibroblast cell lines—with passage numbers between 7 and 16 and originating from various body sites, including the inguinal area, arm, and foreskin—were used to isolate pH-SKPs (Table 1). After acidic treatment, the cells were cultured in suspension for 5 days in SKP medium. On day 3 and 5, successful formation of spheroids was observed for all cell lines (Fig. 10A).

Further measurements of the spheroids revealed several differences among the cell lines. The spheroid number showed the largest variance, with an average of 678 spheroids among all cell lines and a SD of 490, which represents a 72% variance (Fig. 10B, spheroid number). These results indicate that the number of spheroids obtained during isolation is dependent on the starting material but has no apparent correlation with skin biopsy site, passage number, or donor age. This suggests that the number of formed spheroids is cell line- and experiment-dependent. However, the variance in the measured spheroid size was lower. Here, an average diameter of 155 µm with a SD of 30 µm was observed, representing a variance in spheroid size of only 19% among all cell lines (Fig. 10B, spheroid size).

Collectively, these findings indicate that acidic stress treatment at pH 5.7 successfully induced SKP isolation from primary fibroblast cultures, independent of donor age, skin biopsy site, or passage number. To further characterize the multipotent properties of these pH-SKP spheroids, we evaluated their differentiation potential.

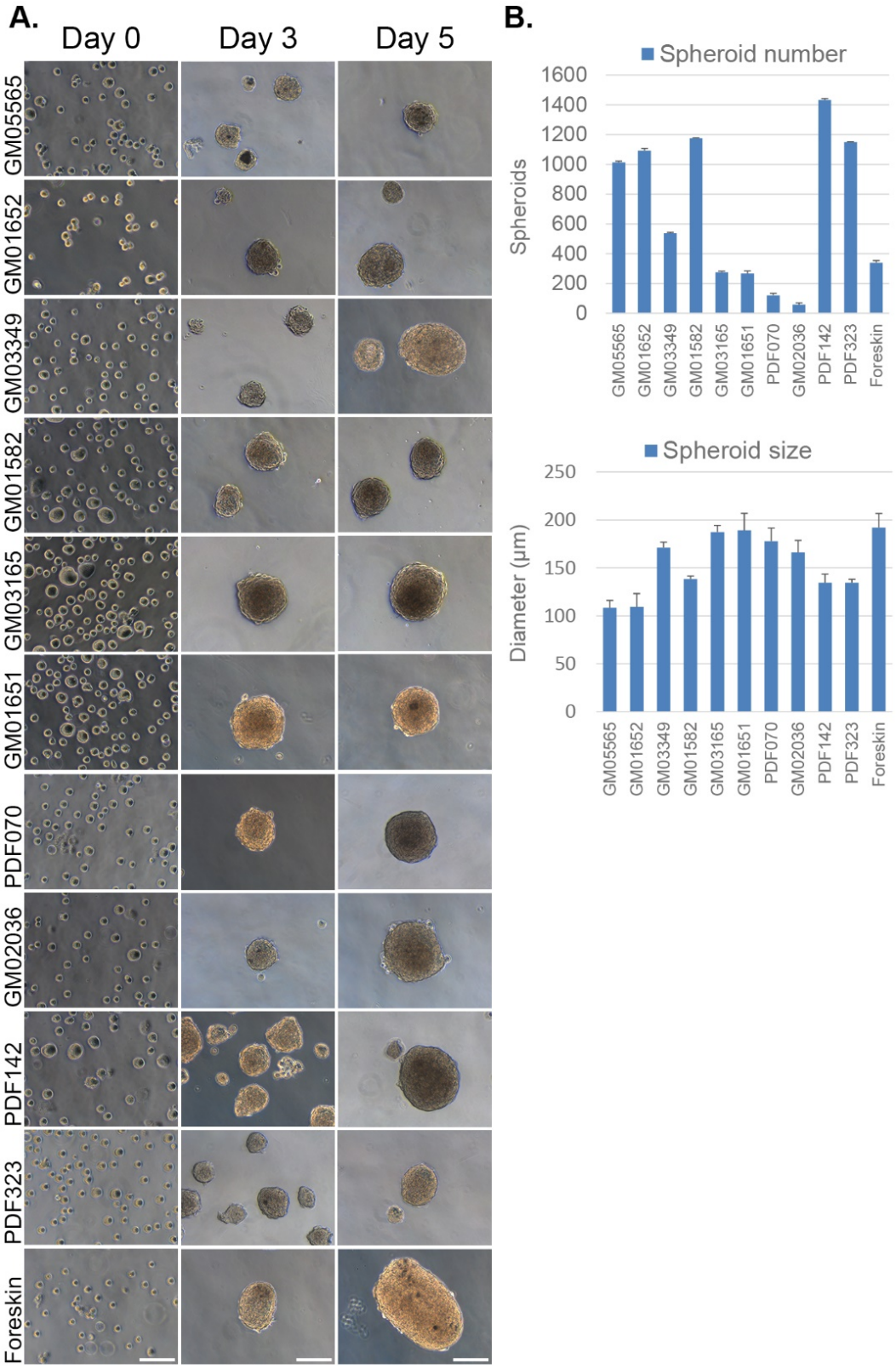

Fig. 10. Efficient isolation of pH-SKP spheroids from 11 primary fibroblast cell lines. (**A**) Images show a representative 5-day growth overview of pH-SKP spheroids from the 11 primary fibroblast cell lines at days 0, 3, and 5 in SKP medium (n = 3). Scale bar: 100 µm. (**B**) The graph illustrates day 5 measurements of pH-SKP spheroids for each cell line representing in the upper panel the spheroid number (n = 3) and the lower panel the spheroid size in diameter. Both panels were based on 50 random spheroid measurements (n = 5). Data are expressed as the mean ± SD.

1.4.6 pH-SKP cells differentiate into adipocytes

To assess the multipotent potential of pH-SKP cells, adipocyte differentiation was induced as outlined in the schematic representation of the adipocyte differentiation protocol (Fig. 11A). Briefly, pH-SKP spheroids at day 5 were first allowed to adhere in 5% FBS-supplemented SKP medium for a period of 16 to 18 h. Then, the medium was replaced with differentiation medium containing adipocyte-inducing factors (10% FBS, IBMX, dexamethasone, insulin, and indomethacin as indicated in Chapter 1, Materials and Methods, page 60 and 61). This time point was considered day 0 of adipocyte induction. Lipid vesicle formation was monitored and visualized by oil red O (ORO) staining on day 28.

At day 5, pH-SKP spheroids from 11 distinct primary fibroblast cell lines (Table 1) were directed to differentiate into adipocytes for a period of 28 days (Fig. 11B). The formation of lipid triglycerides in a range of three to eight small lipid vesicles could generally be detected in cells at 2 days post-induction by standard bright field microscopy (Fig. 11B, first column). Here, pH-SKP cells derived from all cell lines between passage 7 to 16 showed lipid formation, with the earliest detection on day 2 and the latest at day 6 post-induction. In addition, SKPs derived from passage 21 fibroblast cultures were also able to differentiate into adipocytes (Fig. 12). From days 7 to 28 in adipocyte differentiation medium, cells from all cultures showed increasing numbers of lipid droplets of increasing size (Fig. 11B).

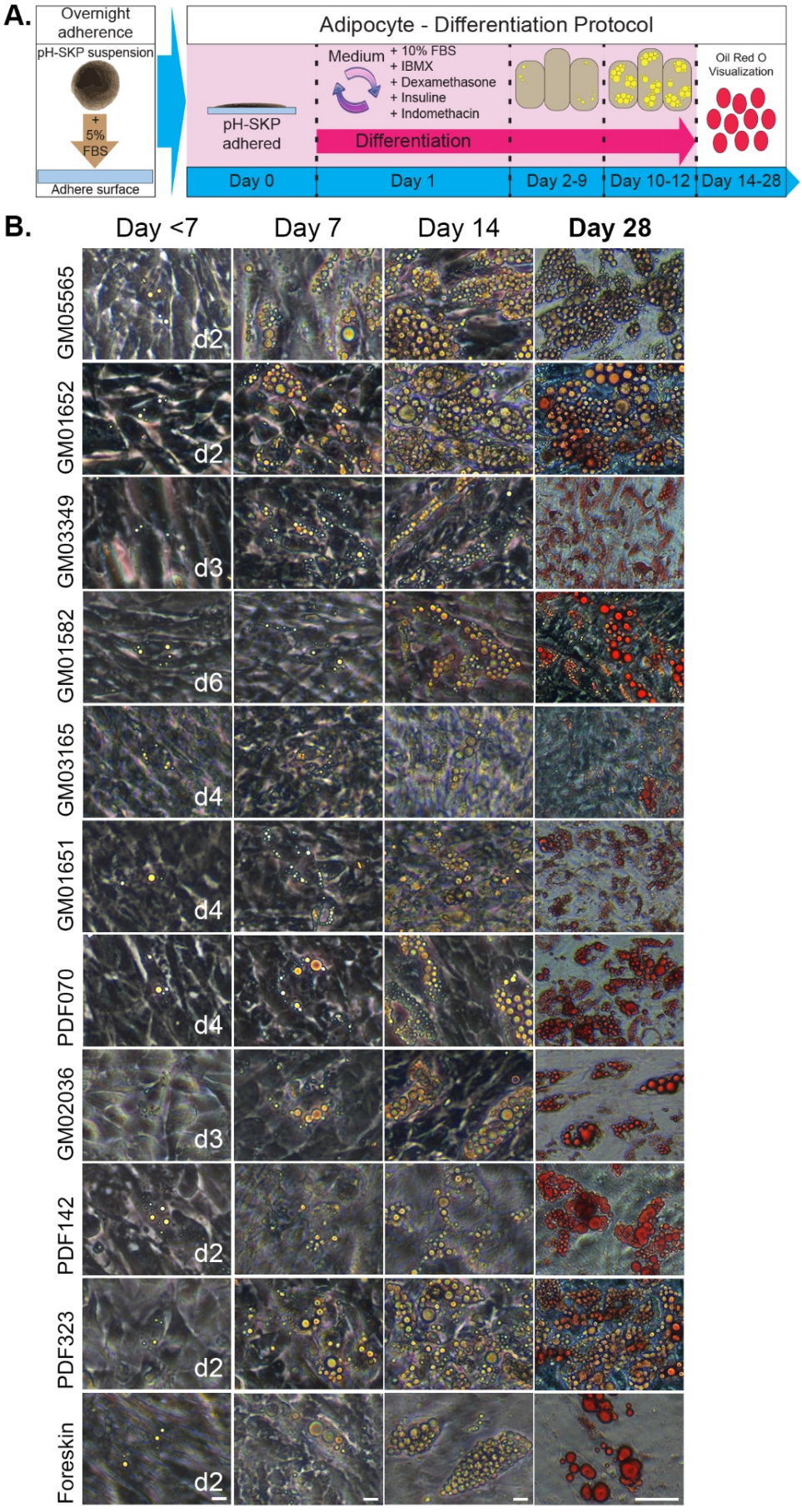

Fig. 11. The pH-SKP spheroids of multiple cell lines can differentiate into adipocytes. (**A**) Schematic overview outlines the pH-SKP adipocyte differentiation protocol. Briefly, pH-SKP spheroids were adhered overnight in SKP medium supplemented with 5% FBS, followed by (day 0) incubation in adipocyte differentiation medium for 14 to 28 days. Then, oil red O (ORO) staining was performed. (**B**) ORO staining was performed on the indicated days on pH-SKPs differentiated into adipocytes. Scale bar: first to third column: 10 µm; fourth column: 50 µm; n = 3.

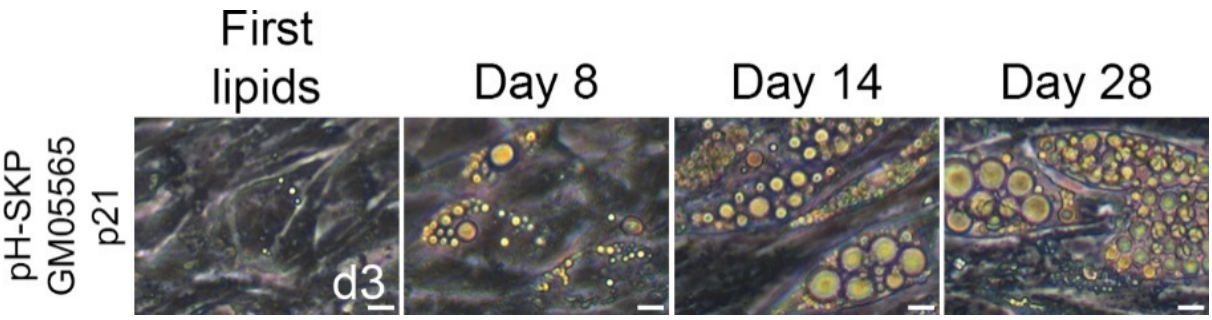

Fig. 12. Adipocyte differentiation of pH-SKP spheroids isolated from primary fibroblasts at passage 21. Adipocyte differentiation of pH-SKP spheroids isolated from cell line GM05565 at *in vitro* passage 21. The first column shows the first lipid detection on day 3, followed by days 7, 14, and 28 of adipocyte development. Scale bars: 10 µm.

The lipid presence was estimated per cell line via digital image analysis to quantify the adipocyte differentiation potential of each culture. A simplified image analysis method based on the report of Deutsch et al. was applied [42]. Here, via red color thresholding, stained cellular lipids were digitally isolated, which was followed by the binarization of the image to make it suitable for digital analysis (Fig. 13A). Raw images for digital ORO analysis were obtained by imaging three different locations with the highest lipid density per cell line with a 10× objective. This resulted in a total acquired image field of 879 µm × 658 µm of which the color percentage was determined (Fig. 13B). The values of BM-MSC-derived adipocytes served as a positive control and were set as 100% (Fig. 13A).

Overall, the pH-SKP samples showed a higher tendency to differentiate into adipocytes relative to BM-MSC (Fig. 13B). Besides GM03165 and foreskin pH-SKP samples, all the other samples exhibited an average of 146% adipocyte differentiation relative to BM-MSC (Fig. 13B). Hence, we tested whether SKPs isolated with no-stress (NS-SKPs) or only fibroblast cultures could differentiate into adipocytes (Fig. 14). Fig. 14A indicates that fibroblast cultures directly exposed to adipocyte differentiation medium showed sporadic cell differentiation containing lipid droplets at day 21, whereas numerous cells exhibited large lipid vesicles in adipocytes derived from NS-SKP and pH-SKP. Digital determination of the percentage of adipocytes present in the different samples showed that only 13% of the fibroblasts were able to differentiate into adipocytes (Fig. 14B). In contrast, 112% of the NS-SKP and 141% of the pH-SKP were capable of adipocyte differentiation relative to BM-MSC (Fig. 14B). These results demonstrate that SKPs were competent to differentiate into adipocytes, with the efficiency depending on the method of isolation. Furthermore, the differentiation of rare adipocytes in the fibroblast cultures indicates that those few cells most likely originate from the pre-existing SKPs in the fibroblast cultures.

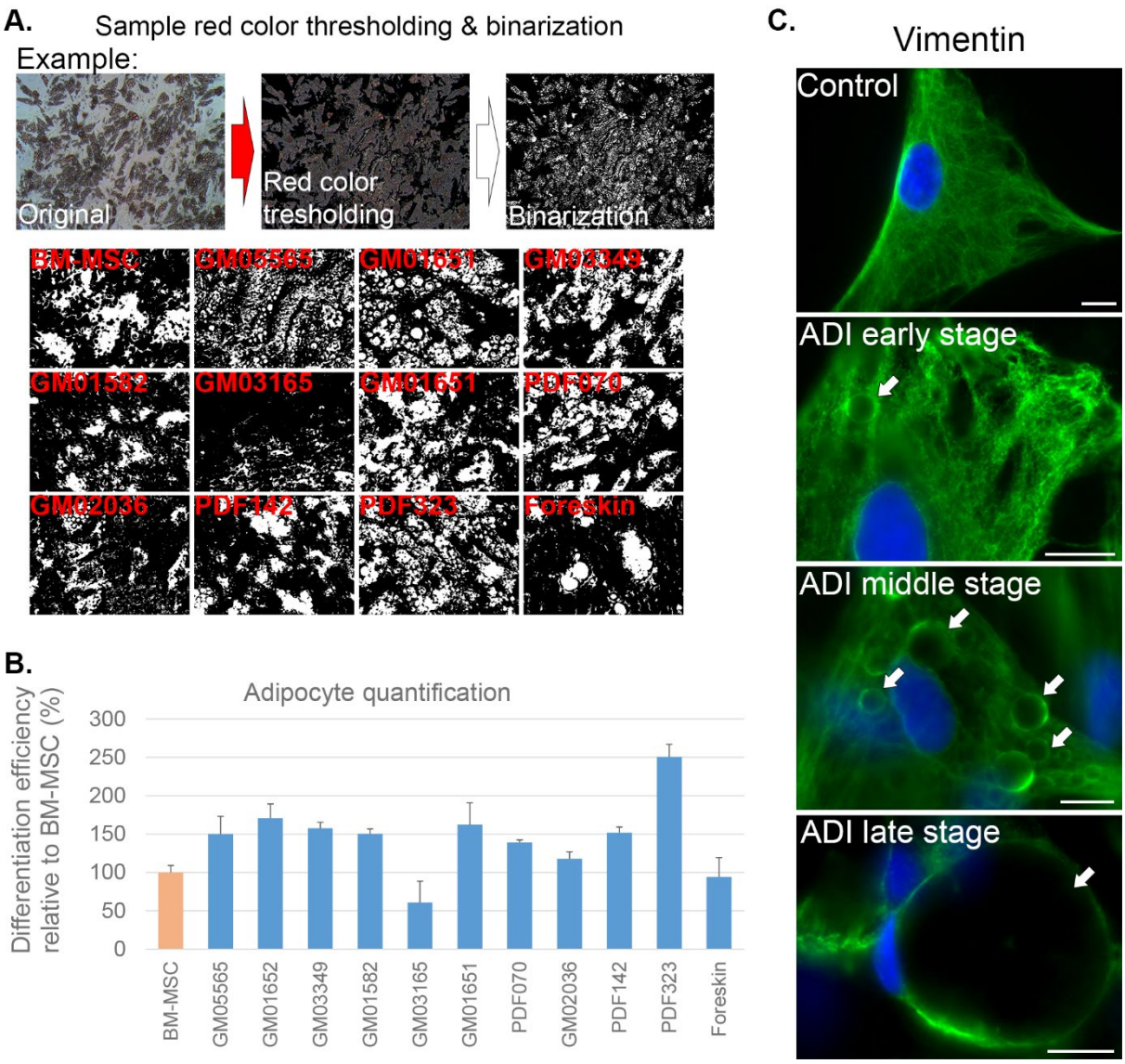

Fig. 13. pH-SKPs efficiently differentiated into adipocytes and showed vimentin network remodeling. (**A**) Oil red O (ORO) color threshold analysis of adipocyte-differentiated pH-SKPs isolated from 11 different fibroblast cell lines and control BM-MSC. The top panel shows an example of the methodology of color thresholding; with the initial isolation of red color followed by binarization, where white represents stained lipids. The bottom panel shows a representation of the indicated cell line at day 28 of adipocyte differentiation after digital processing. (**B**) A graph illustrating the red color analysis, representing an estimate of the lipid percentage in a field of 1,317 × 1,317 µm per cell line. Data are normalized to the BM-MSC and expressed as the mean ± SD (n = 3). (**C**) Representation of vimentin status during the development of adipocytes. Control fibroblasts and early-, middle-, and late-stage adipocytes were immunolabeled for vimentin (green) and counterstained for DNA with DAPI (blue). The arrows indicate vimentin-encaged lipids. Scale bar: 10 µm. Abbreviation used: ADI = adipocyte.

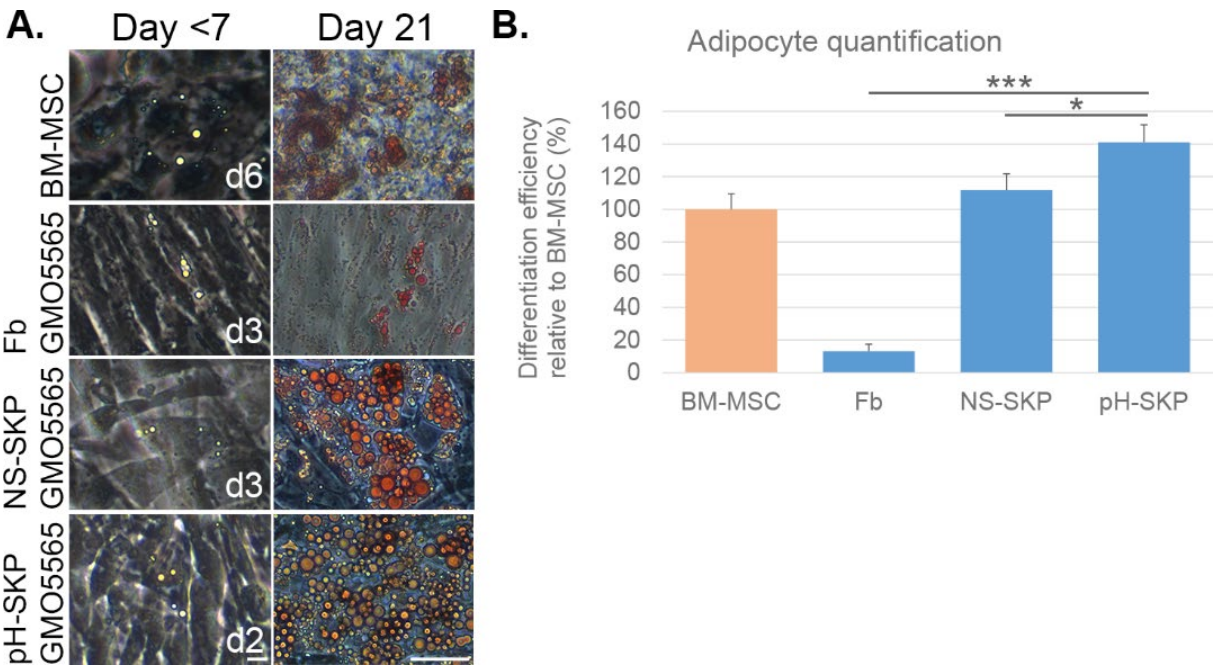

Fig. 14. Adipocyte differentiation efficiency of pH-SKPs, NS-SKPs, and fibroblasts. (**A**) Adipocyte differentiation of BM-MSCs, GM05565 fibroblasts (Fb), no-stress SKPs (NS-SKP), and low pH stress SKPs (pH-SKPs). The first column (day <7) shows the first lipids detection, scale bar: 10 µm. The day 21 column shows oil red O (ORO) staining at day 28, scale bar: 50 µm (n = 4). (**B**) ORO color threshold analysis at day 21 of adipocyte differentiation was performed with BM-MSC, GM05565 Fibroblasts (Fb), no-stress SKPs (NS-SKP), and acidic stress (pH-SKPs). Data are expressed as the mean ± SD relative to the positive control BM-MSC (***$P < 0.0005$, *$P < 0.05$; n = 4).

Next, vimentin, a type III intermediate filament protein, was analyzed to follow the reorganization of the cytoskeleton in pH-SKP cells at different stages of adipocyte differentiation as previously reported [53, 178]. Adipocytes were immunolabeled for vimentin at day 28 of differentiation. At this time point, early-, middle-, and late-stage adipocytes were present because not all cells from an adhered spheroid initiated the differentiation simultaneously (Fig. 13C). At the early stages of adipocyte differentiation, minor reorganization of vimentin filaments was observed enveloping the lipids with a spherical caged structure (Fig. 13C). At the middle stages of differentiation, the cells showed a further reorganization of the vimentin filaments, as indicated by the increased vimentin-positive sphere-like formation in the cytoplasm. At later stages, large lipid droplets formed and were totally wrapped with vimentin filaments (Fig. 13C).

These findings indicate that pH-SKP spheroids isolated from primary fibroblasts can re-organize their vimentin network around the developing lipid droplets upon the induction of adipocyte differentiation. These results further support the multipotency and plasticity of pH-SKP cells.

1.4.7 pH-SKP cells can differentiate into smooth muscle and fibroblast cells

To further assess the multipotent potential of pH-SKP cells, smooth muscle and fibroblast differentiation were induced. A schematic representation of the SMC differentiation protocol is shown in Fig. 15A. Briefly, pH-SKP spheroids at day 5 were allowed to adhere and then induced to differentiate as described in the Materials and Methods (pages 61–68). SMCs derived from pH-SKP cells were fixated between days 10 and 12 post-induction and immunolabeled for smooth muscle α-actin (αSMA), calponin, and smooth muscle myosin heavy chain (SM-MHC): proteins that are typically expressed in SMCs [145]. All SMC markers were expressed in SMCs derived from pH-SKPs at day 10 under SMC differentiation conditions (Fig. 15B). We also evaluated the potency of SMC differentiation of NS-SKPs and fibroblast cultures relative to pH-SKPs (Fig. 16A). The results showed that all SMC markers (αSMA, calponin, and SM-MHC) were absent on day 0 of SMC differentiation but were detected at day 11 (Fig. 16A). However, the differentiation efficiency was very variable with only 15% SMCs detected in the fibroblasts, 29% in NS-SKPs, and 76% in pH-SKPs cultures (Fig. 16B). These results indicate that pH-SKPs were more competent to differentiate into SMCs compared to NS-SKPs (Fig. 16B). Only a few cells in the fibroblast cultures showed potency to differentiate into SMCs. These findings indicate that SMCs induced from the primary fibroblast cultures might originate from the pre-existing SKPs present in those cultures.

In addition to SMC differentiation, pH-SKP cells were also able to differentiate into fibroblast cells. A schematic representation of the fibroblast differentiation protocol is shown in Fig. 15C. Briefly, after adherence, pH-SKP cells were cultured in fibroblast culture medium as described in the Materials and Methods (pages 66–68). After 3 to 5 passages, the morphology of differentiated pH-SKP cells was similar to that of normal fibroblasts (Fig. 15D). Moreover, fibroblasts derived from pH-SKPs were positive for the fibroblast marker prolyl-4-hydroxylase beta (P4HB): An enzyme involved in collagen synthesis localized in the endoplasmic reticulum [127] (Fig. 15D).

In summary, our findings indicate that a 30-min exposure of primary fibroblast cultures to pH 5.7 induces rapid cell proliferation and spheroid development when grown in SKP medium compared to previously reported methods [71, 185]. The generation of pH-SKP spheroids occurred faster, showed clonal expansion ability (Fig. 17), and provided a 4-fold higher SKP yield compared to previous procedures, therefore, obviating long-term culture. Moreover, the pH-SKPs expressed typical multipotent stem cell markers and showed potency to differentiate into adipocytes, SMCs, and fibroblasts *in vitro*. Additionally, pH-SKP isolation, expansion, and differentiation were replicated using various primary dermal fibroblast cell lines, independent of donor age, biopsy site, or *in vitro* passage number.

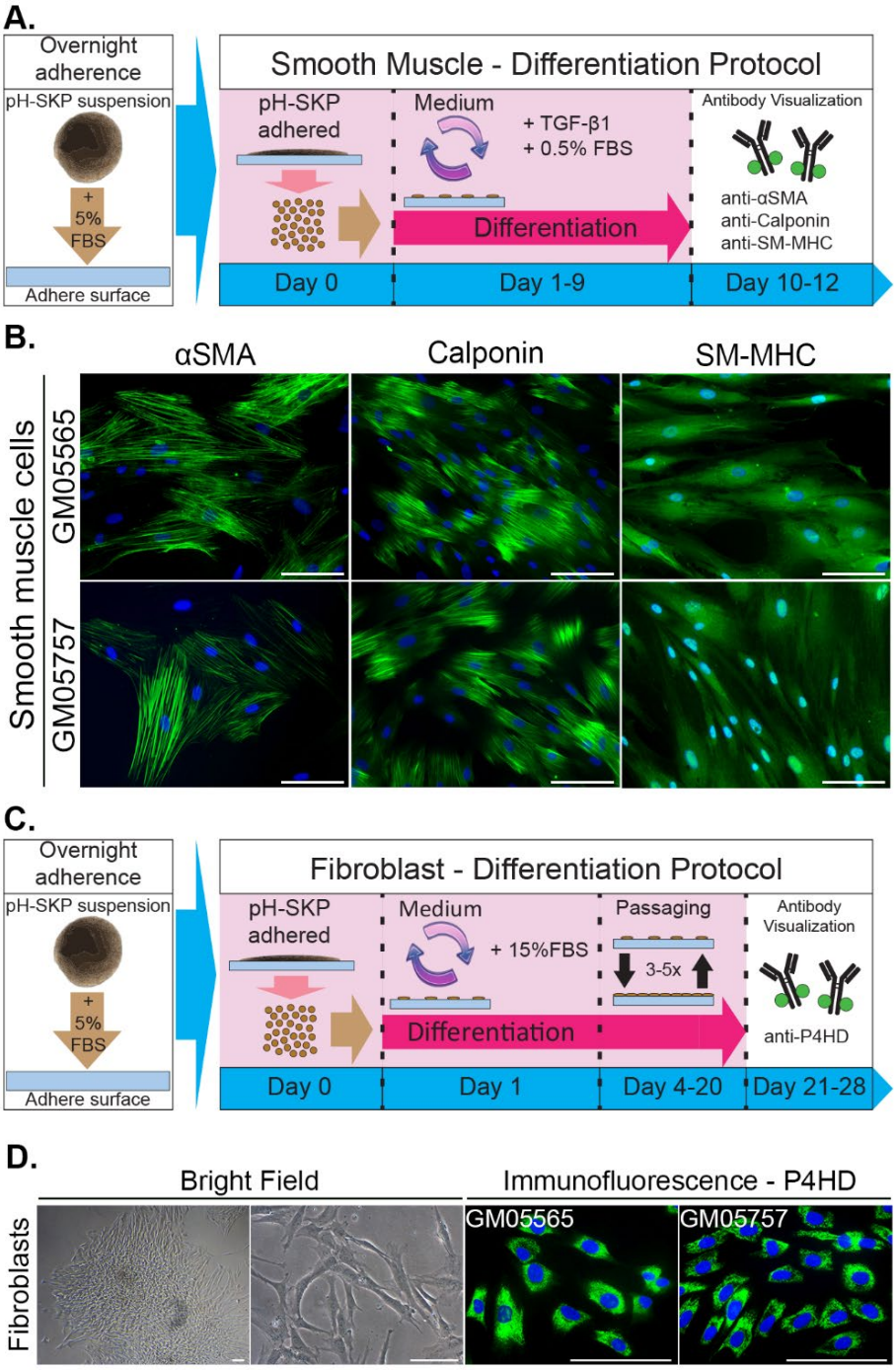

Fig. 15. pH-SKP cells can differentiate into smooth muscle cells and fibroblasts. (**A**) Schematic overview of the pH-SKP SMC differentiation protocol. Briefly, pH-SKP spheroids were first adhered for 16–18 h in SKP medium supplemented with 5% FBS. The spheroids were then dissociated and re-seeded at low density, followed by SMC differentiation induction in SMC medium for 10 to 12 days. (**B**) SMC differentiation was assessed by immuno-labeling of αSMA, calponin, and SM-MHC as indicated. Representative images of SMCs derived from pH-SKP cells, isolated from GM05565 and GM05757 fibroblasts, at day 10 are shown. DNA was counterstained with DAPI (blue). Scale bar: 100 µm. (**C**) Schematic overview of the pH-SKP fibroblast differentiation protocol. Briefly, after adherence and low-density re-seeding, pH-SKP cells were cultured in 15% FBS-supplemented medium followed by 3 to 5 passages. Cells were immunolabeled for the fibroblast marker P4HD. (**D**) Representative images of fibroblasts differentiated from pH-SKP cells isolated from GM05565 and GM05757 fibroblast lines are shown. On the left, the bright field shows the morphology of an adhered pH-SKP spheroid and the fibroblast morphology of pH-SKP cells directed to differentiate into fibroblast cells at passage four. The right images are fibroblasts derived from pH-SKP differentiation labeled for P4HD (green) and counterstained with DAPI for DNA (blue).

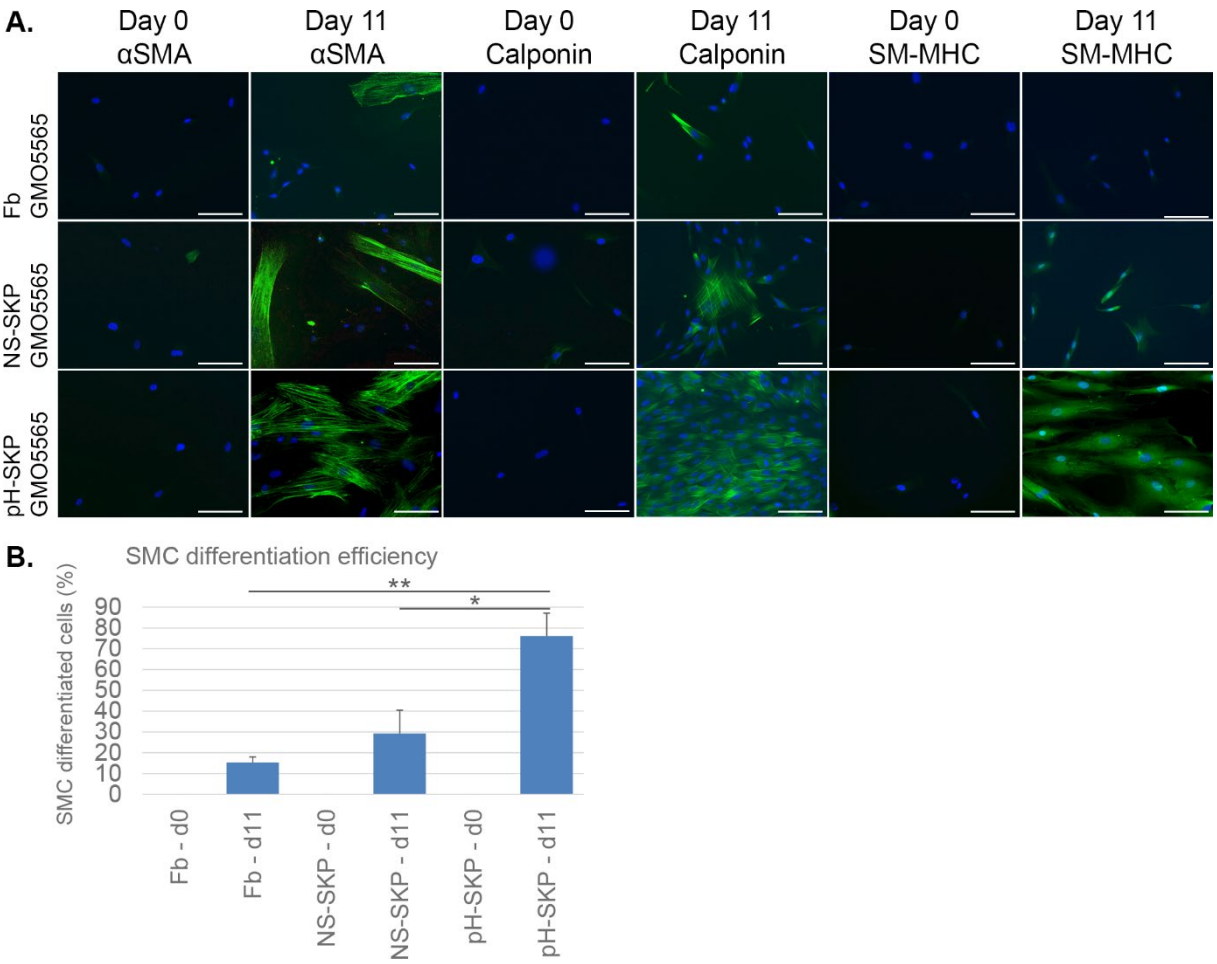

Fig. 16. SMC differentiation efficiency of pH-SKPs, NS-SKPs, and fibroblasts. (**A**) SMC differentiation of GM05565 Fibroblasts (Fb), no-stress SKPs (NS-SKP), and low pH stress SKPs (pH-SKPs) were monitored at day 0 and 11 by immunohistochemistry with antibodies for αSMA, Calponin, and SM-MHC (all in green). DNA was counterstained with DAPI (blue). Scale bar: 100 µm. (**B**) Quantification of SMC differentiation was determined with the percentage of calponin-positive cells in indicated samples. The percentage was determined by a direct count of at least 300 cells per coverslip in triplicate and from three independent experiments. Data are expressed as the mean ± SD (***P < 0.0005, *P < 0.05; n = 3).

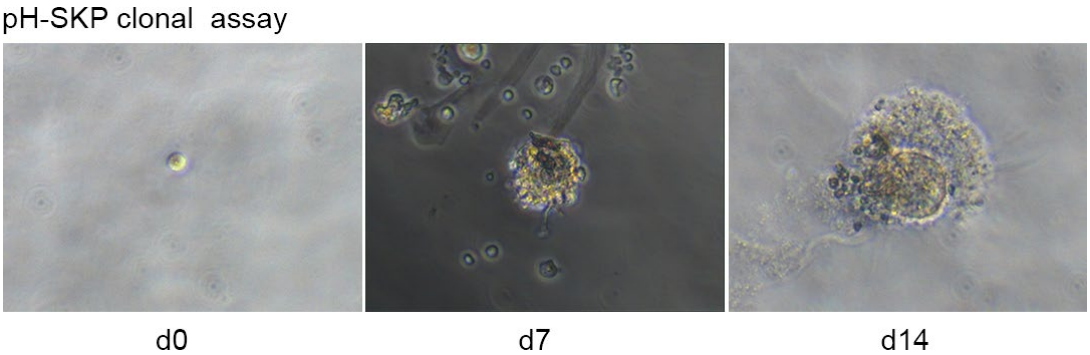

Fig. 17. Clonal growth of a single pH-SKP cell. A single cell derived from GM05565 pH-SKP at day 5 via dissociation. The cell was followed for a total of 14 days.

1.5 Discussion

Current isolation methods of skin-derived precursor (SKP) cells are thwarted by certain limitations. The classic isolation method introduced by Toma et al. requires fresh skin tissue and long culture times to isolate SKPs [169]. A second strategy for SKP isolation [71, 185] circumvents the need for fresh skin tissue by using pre-established dermal fibroblast cultures available from commercial cell banks. However, limitations such as long-term culture, low yield, and requirement of early cell passage reduce the utilization of this method, highlighting the need for further improved isolation strategies.

In this study, we present a novel SKP isolation procedure as an alternative that overcomes the limitations of previous methods. We report that exposure of human primary dermal fibroblast cultures to acidic stress (pH 5.7) for 30 min at 37°C induces rapid spheroid formation and expansion of SKP cells, termed pH-SKPs, within 5 days *in vitro*. These pH-SKPs express stem cell markers such as nestin, Oct4, Sox2, and NANOG, as well as, CD9, C-Myc, and Klf4, and exhibit multipotent properties. Moreover, pH-SKPs showed higher ability to differentiate into SMCs and adipocytes compared to SKPs isolated with the no-stress method. No derivation of neuronal lineage was attempted and remains to be investigated in the future. Additionally, we found that fibroblast cultures directly exposed to SMC or adipocyte medium exhibited a few differentiated cells. We propose that these rare cells that are present in the primary fibroblast cultures might be the pre-existing SKPs.

The pH has long been known to influence cellular functions such as cell growth and protein synthesis [109]. Regulation of the intracellular pH (pHi) is therefore crucial to maintain cell function. One regulator of the pHi is NHE, which removes intracellular acid via exchange of a proton for an extracellular sodium ion [3]. The first isoform discovered was NHE1 and is located in the plasma membrane [86, 160]. When the pHi drops below a certain threshold level, the NHE1 protein is directly activated via an internal allosteric proton-binding regulatory site. In turn, NHE1 affects various cell functions such as cell survival, proliferation, and cytoskeleton and actin filament assembly [41, 84, 119]. Interestingly, we found that short exposure to an acidic extracellular pH (pHe) of 5.7 induced a significant increase of NHE1 expression in fibroblast cultures. Additionally, the short acidic stress exposure resulted in a rapid proliferation of SKPs. Although outside the scope of the present study, we suggest that NHE1 activation might play a significant role in the pH-SKP isolation method, and further studies are needed to characterize this process fully. More detailed investigations on the mechanisms underlying the signaling pathways elicited by acidic pH stress will undoubtedly offer new opportunities for further improvements of SKP isolation and possibly other adult stem cell populations present in tissues other than the skin.

The rapid expansion of pH-SKPs might hold great potential for clinical or translational purposes. For example, pH-SKP differentiation into functional insulin-producing islet-like cells

could be applied for the development of future diabetes therapy [118]. Another area for further investigation is the utilization of pH-SKP cells in drug and disease modeling. For example, SKP cells can be isolated from the skin of patients suffering from diseases such as Hutchinson-Gilford progeria syndrome [71, 185] and Hirschsprung's disease [90]. The use of fibroblast cultures for expansion and storage would obviate the need for repeated skin biopsies, which would significantly elevate patient stress. Moreover, for fundamental science and other applications, fibroblasts can be easily purchased from commercial biorepositories and used for pH-SKP isolation and differentiation into various cell types without the need for surgical interventions.

In conclusion, we report an efficient method for rapid SKP cell isolation using a short acidic stress treatment of pH 5.7 on primary dermal fibroblasts. Ready-to-use pH-SKP preparations were obtained four times faster compared to previously reported methods and exhibited typical stem cell markers and differentiation potencies. Furthermore, pH-SKPs can be isolated from fibroblast preparations derived from all ages, body sites, and even late culture passages. In all cases, the isolated pH-SKPs showed similar spheroid expansion, morphology, stemness markers, and differentiation potential within 5 days of *in vitro* culture. Thus, this pH-SKP isolation method is an efficient, rapid, and standardized method to generate large numbers of SKPs. We acknowledge that the potential use for *in vivo* applications will require further *in vivo* studies to determine their safety, survival, function, and differentiation. Nevertheless, pH-SKPs can become valuable tools for basic and translational research and possibly one day in regenerative medicine.

Chapter 2

Full Area Mosaic Imaging Techniques for Analysis of Microscopic Targets

A novel imaging technique to generate mosaic images of a macro-scale area such as a 48-well-plate well of 12,000 µm diameter containing all microscopic targets at high-resolution.

In this chapter, the development and application of two mosaic imaging techniques are described. Previously, Chapter 1 shortly described the motorized mosaic imaging (MMI) technique and its application. In Chapter 2, the full mechanics and reasoning behind MMI are discussed. Additionally, the novel video mosaic imaging (VMI) technique is discussed as well.

2.0.1 Abstract

Whole-sample imaging and data acquisition for numerical analysis using microscopy are often impossible or cumbersome tasks in most laboratories. Existing systems and approaches are either very expensive or complicated. Therefore, two mosaic imaging techniques were developed, termed motorized mosaic imaging and video mosaic imaging. During the development, the focus was placed on simplicity and low-cost and create high-quality mosaic images of complete samples while magnified. To test both techniques, cellular and synthetic microscopic sample types, residing in a 48-well plate, were imaged. These samples included cellular spheroids at days 5, 7, and 10 and glass beads. The technical limitations and optimal settings were investigated by using various image overlap percentages and video record durations. These images were then processed by image processing software. We found that both techniques could generate mosaic images from both sample types. For motorized mosaic imaging, mosaics could be generated for samples with an image overlap between 76% and 42% for the y-axis and 82% and 57% for the x-axis, depending on particle number and spread. For video mosaic imaging, 120 seconds of recording was found most optimal for obtaining mosaics. Finally, microscopic targets of the mosaic images could be quantified in number and size. In sum, we report the successful application of two mosaic imaging techniques that are easy-to-use and low-cost, providing new approaches for a broad public to digitally record microscopic samples to analyze microscopic targets at a macro-scale.

Keywords: biological analysis, imaging techniques, macro microscopy, mosaic imaging, spheroid culture

2.0.2 Abbreviations

Abbreviation	Meaning
CTRL	Control
DMEM	Dulbecco's modified Eagle medium
EGF	Epidermal growth factor
FBS	fetal bovine serum
FGF	Fibroblast growth factor
h	hours
min	minutes
MMI	Motorized mosaic imaging
PBS	phosphate buffered saline
SKP	skin-derived precursor
pH-SKP	low pH isolated skin-derived precursor cells
RT	room temperature
s	seconds
SKP	Skin-derived Precursor
VMI	Video mosaic imaging

2.1 Background and Introduction

In this subchapter, the general information, basic components, and related investigative techniques are discussed for Chapter 2. The purpose of this subchapter is to provide fundamental information for readers unfamiliar in the field and provide means to increase their comprehension of the thesis' content and conclusions. The discussed topics will provide various answers to specific questions: "What are microscopic targets?" "How are they visualized and imaged?" "Which dimensions are used for mosaic imaging, and how do they relate to each other?" "How are images used for quantification purposes?" etc. Additionally, the principles behind investigative techniques are discussed as well. However, details such as step-by-step protocols, material references, or machine models are not discussed in this subchapter. For this information, I kindly refer to the Materials and Methods subchapter of this chapter.

2.1.1 Microscopic targets

Microscopic targets are structures that are too small to be seen with the naked eye alone but large enough to be seen with a microscope. These targets can be organic structures such as mammalian or plant tissue, including, for example, cells present in skin (e.g., fibroblasts, adipocytes, or melanocytes) or plant components (e.g., the cell wall or chloroplasts). Another large field involved with microscopic targets are micro-organisms, including bacteria, archaea, fungi, and viruses. Furthermore, microscopic targets can also be inorganic structures, including, for example, stones and minerals or crafted materials such as metals or textiles. In general, the application of microscopy is more broadly applied to microscopic biological targets due to the plethora of biological variance in nature. Additionally, there is considerable interest and benefit studying the microscopic targets of biological origin. Obtaining information at this level provides a myriad of possibilities to study pathological diseases and fundamental cellular mechanisms, and the opportunity to develop new therapies for human benefit in disease and health.

2.1.2 Fundamental basics of microscopy

The application of microscopy itself to obtain images of microscopic targets has been used for almost 400 years and remains of high-value in science today. Over the years, many other types of microscopic techniques have been developed. Some of these types include bright field, dark field, fluorescent, phase contrast, confocal, multiphoton, and electron microscopy. In this chapter, I focus on the application of bright field microscopy specifically.

Bright field microscopy is the first developed microscopy technique, which is the most basic and widely used one. This technique uses a set of lenses to diffract the light and magnify a microscopic target of interest. In general, the sample containing the microscopic target(s) is illuminated by a light source, which then reflects the light. The reflected light is guided through an objective that contains a set of lenses to diffract and guide it further. Then, it travels through an ocular that also contains a set of lenses to refract light. Both the objective and ocular refract the light in such a way that the image of the microscopic target becomes magnified. The total magnification of the target depends on the magnification of the objective and ocular. For example, with a 20× objective and 10× ocular, a total magnification of 200× is acquired. Alternatively, the refracted light could be guided toward a camera to digitize the received light via a complementary metal-oxide-semiconductor (CMOS) or charged-coupled device sensor to generate a digital image of the magnified microscopic targets.
In current modern days of digitalization, the digital recordings of microscopic targets are in high demand. As a result, the digital acquisition of a specific field of view in microscopy with digital cameras has been well established and widely applied. Such an acquisition of an image from a microscopic target reveals that the acquired image itself is limited to the extent of the field of view. After all, after the image is acquired, one cannot look further anymore to see objects outside the acquired view. This field of view is determined by the components used for magnification such as the objective and the ocular. The field of view represents the diameter of the sample that can be seen at any given point. For instance, while the total sample could be in centimeters, the magnified and visual image that can be seen through the ocular is only a small portion of the total macro area.
The lack of ability to make a complete magnified image of the whole sample leads to a loss of information. This because the immediate drawback of microscopy is that the often-large amounts of microscopic targets reside in a large area such as a cell culture plate, tissue section (e.g., mouse brain), or blood smear (e.g., for diagnostics). These large areas cannot be captured in one standard microscopic image due to the restricted field of view inherent to the technique. However, the acquisition of a digital recording from the whole sample is highly beneficial as it allows digital storage and retrieval of whole-sample images representing entire experiments for full sample data analysis and comparative studies.

2.1.3 Mosaic imaging

By using multiple images covering the whole area, a whole image of microscopic targets in a macro-scaled area can be acquired. Such an image generated from multiple sub-images is termed a panoramic or mosaic image. The principle behind mosaic imaging is that image 1 contains completely new information of a piece from the target to image. Then, image 2 contains partly new but also partly already acquired information from image 1 of the image

target. So, image 1 and 2 share a part of the same information. This information can be used to overlap and stitch the images together. Then, image 3 contains partly old (from image 2) and new information again of the target. This process is continued until the whole macro target is captured into one mosaic image.

Currently, there are various techniques and systems that approach the overlap/scanning mosaic imaging principle. One of such systems is the Surveyor from Meyer Instruments (patent no. US 5612819 A), which scans slides containing sections of tissue to create mosaics. Another system is the Zeiss Axiovert with the mosaiX module (patent no. EP 0199573 A2). Both examples are often for general purposes and require complete one-set systems, including specialized microscopes, camera, table, incubation chamber, and software. These one-set systems result in high-cost and low flexibility, which are significant drawbacks as it reduces the accessibility to other laboratories. There are also more specific approaches that use, for example, various custom algorithms and processing techniques modeled for applications such as multiphoton microscopy [140], but also for approaches to amend certain limitations of sample scanning [94]. Furthermore, a manual and straightforward approach has also been developed to create nematode mosaics. Unfortunately, it is limited to only a few images, making it unsuitable for macro-scale areas [46]. The above examples illustrate the demand and applicability of macro-scale imaging of microscopic targets. However, these existing systems and techniques are not widely applicable due to high-cost and accessibility. As such, additional mosaic imaging options are needed.

2.1.4 Motorized and video mosaic imaging

In this chapter, I describe the development of two mosaic imaging techniques, termed MMI and VMI. Both methods are easy-to-use, low-cost, and can generate high-quality mosaic images that represent a digital recording of all microscopic targets residing in a large area. For MMI, the basic strategy is to place the sample on a motorized table to image the area of interest automatically. The MMI technique was implemented in the study from Chapter 1 to acquire a digital recording of all spheroids of a sample for analysis. Then, for VMI, the basic strategy is to video record the area of interest to obtain images from the video frames. As proof of principle, MMI and VMI were investigated by whole-well imaging of a 12,000-µm diameter well containing various sample types and target numbers, including cellular spheroids and synthetic glass beads.

2.2 Methodology Used

Various methods and analysis approaches were employed to develop and establish a functional macro mosaic imaging technique. In this subchapter, the background and principles behind those approaches are shortly discussed. After this subchapter, a detailed step-by-step protocol for each method mentioned in this chapter is followed. This includes exact material references to provide the means and full understanding for repetition and validation by other scientists.

2.2.1 Used microscopic targets

The original purpose of developing the mosaic imaging technique was to circumvent the traditional cellular spheroid analysis and avoid the high-cost of existing mosaic systems. Here, traditional analysis represents the simple counting-by-hand approach, which uses a small representative and not the complete sample. This approach is less accurate and becomes more cumbersome when dealing with a high number of targets in samples (e.g., SKP spheroids). In this chapter, concerning the development of mosaic imaging, SKP spheroids were used as biological imaging microscopic targets.
Mosaic imaging techniques provide large mosaic images of macro areas, which are then used for analysis. In the process of analysis, various dimensions and units such as light, pixels, and frames are converted to calculate relevant data such as size in µm. To have a reference for analysis, glass beads were used as synthetic particles. These microscopic targets have a known diameter size and can be used to validate the techniques and analysis method.

2.2.2 Dimensions – µm, pixels, and frames

Mosaic imaging can be used for quantitative analysis of microscopic targets thanks to the conversion of various dimensions and units. These include light to pixels (including video frames) thanks to the CMOS sensor in the microscope camera, followed by pixels to µm. The presented mosaic imaging techniques—MMI and VMI—both use the size of the inner-well diameter of a 48-well-plate well as a size reference. This diameter represents 1.2 cm or 12,000 µm. When the complete mosaic is generated, it is cropped into a square that fits the inner-well size and is then resized to 5,000 × 5,000 pixels. The 12,000 µm diameter represents then 5,000 pixels, which equals 2.4 µm to 1 pixel (Fig. 1). When the microscopic targets are measured from the image in pixels, the size in µm can be calculated and used for quantification purposes. This conversion approach will be validated with the use of microscopic targets from which the size is known (synthetic glass beads).

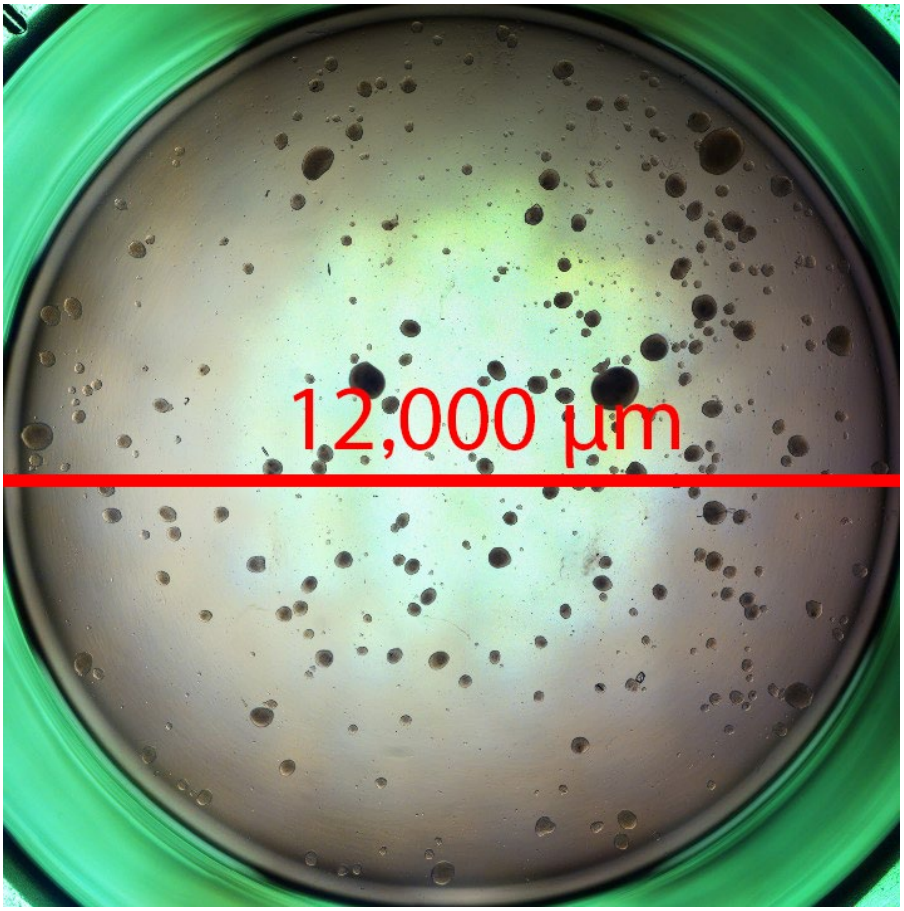

Fig. 1. Whole-well mosaic image. This image was obtained via the motorized mosaic imaging method. In the mosaic image, half of the spheroids from an SKP preparation can be clearly seen in the well while under magnification. This image can be used for zooming in while retaining image quality.

2.3 Materials and Methods

In this paragraph, the materials and methods used in this chapter are described in detail. First in an overview and then as an exact step-by-step protocol. The step-by-step protocol is provided because the focus of this thesis lays on method and technique development. Knowledge for precise execution is therefore required. By following the step-by-step protocol, one can exactly repeat the performed experiments. In addition to the step-by-step protocol, the specific reagents and media will also be provided.

2.3.1 Microscopic imaging targets

2.3.1a Synthetic microscopic targets

Glass beads were used as synthetic targets with a known diameter size between 425 and 600 µm in diameter (Sigma, G-8772). Two sample conditions were made by weighing 30 and 60 mg of glass beads as separate samples, in which 30 mg represents a half full well and 60 mg a full one, both based on a 48-well-plate well (Nunc, diameter: 1.2 cm). The glass beads were transferred to the well with 1,000 µL Milli Q (MQ) water.

2.3.1b Biological microscopic targets

Biological targets consisted of pH-SKP spheroids (GM05565, Coriell Institute). Primary fibroblast cultures were collected with trypsin. The cell suspension was pelleted at 450 × g for 5 min at room temperature (RT) and was washed with sterile PBS. One million cells were resuspended in 500 µL of pH-adjusted HBSS (ThermoFisher-Gibco, 14175053) buffer. The pH of the HBSS buffer was adjusted with HCl (Merck, 1.00319.2500, Hohenbrunn, Germany) to a pH of 5.7. Cells resuspended in HBSS pH 5.7 were incubated for 25 min at 37°C and 5% CO_2 and agitated every 5 min. Thereafter, the cell suspensions were centrifuged 450 × g for 5 min at RT. In total, the cell suspensions were exposed for 30 min to the HBSS (pH 5.7), including a 25-min incubation and 5-min centrifugation. Next, each pellet was resuspended in 6 mL of classic SKP medium (4:1 – Dulbecco modified Eagle medium [DMEM, ThermoFisher-Gibco, 21885025]: F12 [ThermoFisher-Gibco, 21765029], 20 ng/mL EGF [ThermoFisher-Gibco, PHG0311], 40 ng/mL bFGF [ThermoFisher-Gibco, PHG0026], 2% v/v B27 [ThermoFisher-Gibco, 17504044], 0.5 µg/mL Fungizone [ThermoFisher-Gibco, 15290018], and 100 U/100 µg/mL penicillin/streptomycin [ThermoFisher-Gibco, 1514022]) and divided equally over two T25 non-treated flasks. Cells were fed every other day with 10× SKP medium (10× EGF, bFGF, and B27), diluted to a final concentration of 1× in culture medium and agitated daily by pipetting up and down to prevent clumping and cell adherence to the plastic flask.

Low pH SKP isolation and culture (pH-SKPs): step-by-step protocol.

Required media:

Table 1. 1× SKP medium – used for SKP isolation.

	Total volume	10,000	µL		
	Times concentrated	1			
	Material			**End concentration**	
1	DMEM (low glucose) Gibco, 21885-025	7,255.5	µL		
2	F12 Gibco, 21765-029	2,418.5	µL		
3	EGF (0.1 mg/mL) ThermoFisher-Gibco, PHG0311	2	µL	20	ng/mL
4	bFGF (0.1 mg/mL) ThermoFisher-Gibco, PHG0021	4	µL	40	ng/mL
5	B27 ThermoFisher-Gibco, 17504044	200	µL	2%	v/v
6	Fungizone (250 µg/mL) ThermoFisher-Gibco, 15290018	20	µL	0.5	µg/mL
7	Pen/Strep (10,000 U/10,000 µg/mL) ThermoFisher-Gibco, 1514022	100	µL	100 U/100	µg/mL

Table 2. 10× SKP medium – used for SKP feeding.

	Total volume	10,000	µL		
	Times concentrated	10			
	Material			**End concentration**	
1	DMEM (low glucose) Gibco, 21885-025	5,865	µL		
2	F12 Gibco, 21765-029	1,955	µL		
3	EGF (0.1 mg/mL) ThermoFisher-Gibco, PHG0311	20	µL	200	ng/mL
4	bFGF (0.1 mg/mL) ThermoFisher-Gibco, PHG0021	40	µL	400	ng/mL
5	B27 ThermoFisher-Gibco, 17504044	2,000	µL	20%	v/v
6	Fungizone (250 µg/mL) ThermoFisher-Gibco, 15290018	20	µL	0.5	µg/mL
7	Pen/Strep (10,000 U/10,000 µg/mL) ThermoFisher-Gibco, 1514022	100	µL	100 U/100	µg/mL

Stock preparation notes for SKP medium:

See for detailed descriptions of stock preparation, the notes of Chapter 1 page 31–32.

Hank's balanced salt solution (HBSS) pH 5.7:

1. The pH of HBSS (Gibco, Life Technologies, 14175-053) was adjusted to 5.7 by using HCl (Merck, 1.00319.2500, Hohenbrunn, Germany).
   Note: The following steps took 1 to 2 days.
2. A 500-mL HBBS bottle was emptied into a 1-L beaker and HCl was added until the desired pH level (pH 5.70) was reached and stable for at least 1 h. If the pH would change again in this period, it was adjusted again, followed by a 1-h attempted wait again.
3. The final solution was filtered by a 0.2 µm Minisart (Sartorius Stedim, 16534) filter to sterilize it.
4. The filtered HBSS was then aliquoted in 50- and 15-mL tubes and stored at 4°C until use. It is recommended to re-measure the pH after 1 year.

Low pH SKP protocol (pH-SKPs):

1. At least 2 days before following the pH-SKP isolation protocol, pH-adjusted HBSS was prepared, see above.
2. Before starting the isolation protocol, pH-adjusted HBSS was placed at RT to acclimatize.
3. Primary fibroblasts were used that were previously cultured with normal fibroblast medium (DMEM: 15% FBS, 1% Glutamine, 1% Pen/Strep [10,000 U/10,000 µg/mL], and 2 mL Gentamicin).
4. The used cells for SKP isolation were at least 60% confluent and not above 80%. Importantly, for all SKP conditions the monoculture cells never reached or had reached a confluent state of above 90% in their culture history.
5. When the cells were ready, they were detached via the trypsin protocol, described previously (page 29). Briefly, the culture medium in the cell culture dish was aspirated followed by the addition of 8 mL of sterile PBS. The dish was rinsed by carefully tilting it. Then the PBS was aspirated, and to each dish, 0.5 mL of trypsin was added. All dishes were then placed into the cell incubator providing 37°C. After 10 min of incubation, the cells were collected in fibroblast culture medium, transferred to a 50-mL tube and centrifuged 450 × g for 5 min at RT.
6. The supernatant was aspirated, and the cells were resuspended in sterile PBS. The volume of PBS was usually around 20 mL per tube. This cell suspension was then used to determine the cell concentration via a cell hemocytometer. This was done either via the Muse viability assay according to the manufacturer’s instructions or a counting chamber (Neubauer Chamber) in which 5 µL of cell suspension was inserted to each side.

7. After determining the cell concentration, the cells were transferred with one million per 15-mL tube. These cells were then centrifuged 450 × g for 5 min at RT. The supernatant was then aspirated.
8. The cells were resuspended in 500 µL of HBSS and carefully mixed with a 1000-µL pipet tip while avoiding any bubble formation. The 15-mL tubes were then placed vertically into a cell incubator at 37°C and 5% CO_2.
9. The cells were agitated every 5 min to homogenize the descended cells again.
10. After 25 min, the cells were placed in a centrifuge and centrifuged 450 × g for 5 min at RT. In sum, the total incubation time in pH-adjusted HBSS solution was in total 30 min.
11. After centrifugation, the acidic supernatant was carefully removed via aspiration. The cells were then gently resuspended in 6 mL of SKP medium per 15-mL tube (see Table 2). Per T25 flask, 3 mL of the cell suspension was transferred, totaling the cell number at 0.5 million per flask.
12. The cap of the flasks was left partially unscrewed to allow air circulation. The flasks were then placed into a cell incubator for culture.
13. Every day the cells were resuspended once by using a 5- or 10-mL pipet and gently spraying the medium over the bottom of the flask to promote a suspension culture.
14. After 2 days of culture, the cells were fed by adding 10× concentrated SKP medium (including 10× EGF, FGF and B27, see Table 3) by diluting it with the main previously volume (e.g., 3 mL previous volume + 333 µL 10× SKP medium). The feeding was repeated every other day.
15. At days 3, 5, and 7, the spheroids were taken out for mosaic imaging analysis to determine the culture yield.

2.3.2 Sample preparation for imaging

Before imaging, spheroid samples (per T25 flask) were first transferred and divided over two 48-well-plate wells with a volume between 1.5 and 2.5 mL per well. Air bubbles were removed after transfer, and spheroids were randomly pipetted with a 1000-µL pipet tip to promote a homogenous spread. Spheroids were then allowed to settle at the bottom of the well for 5 min. For all biological samples, the temperature and CO_2 levels were left at room conditions to minimize biological activity during long periods of imaging in our experimental setup. Glass beads were spread as homogeneously as possible via tilting of the plate. The 30-mg glass beads were centered in the middle of the well because all beads went in one direction during tilting due to the size and smoothness of the glass bead surface.

Sample preparations: step-by-step protocol.

The following protocol describes the use of one flask for imaging by the MMI or VMI method. This method can also be applied to multiple flasks.

1. On the designated day, the flask containing spheroids was retrieved from the incubator and placed in a sterile biosafety cabinet.
2. For VMI, the bottoms of the 48-well-plate wells were first covered with vertical lines made with a fine tip Lab marker from VWR International (cat 52877–398). The space between the lines was approximately 1 mm. For MMI, the 48-well plate was not marked.
3. The medium inside the flask was taken with a 5-mL pipet and used to carefully spray the plastic surface bottom to detach any attached spheroids. Then, the complete solution was collected in the 5-mL pipet and divided over two 48-well-plate wells. Depending on the culture day, the total volume to divide was between 3 and 3.5 mL. Note: The top row and first column of the wells from the 48-well plate were not used due to obstruction of the microscope table on those locations.
4. After the transfer of spheroids into the 48-well plate, they were allowed to descend to the bottom of the well. Depending on the spheroid size, this would take approximately 1 to 3 min as larger spheroids descended faster.
5. After the spheroids descended, approximately 1 mL of the medium from each well was taken back into the 5 mL pipet. This medium was used to rinse the flask again and collect any remaining spheroids. These remaining spheroids (the suspension) were divided over the same two wells.
6. The spheroids were mixed in each well with a 1000-µL pipet tip to promote a homogenous spread over the well's surface. This was followed by allowing the spheroids to descend again. For the best imaging quality, the remaining bubbles on top of the liquid's surface were removed with a 1000-µL pipet and the volume level equalized between wells.
7. With the spheroids ready in each well, the imaging was performed. See for further imaging steps Chapter 2.3.3, Motorized mosaic imaging, and 2.3.4, Video mosaic imaging.
8. The spheroids were collected again after imaging by first using a 1000-µL pipet to pipet up and down on the well's surface to detach any attached spheroids, followed by the collection into a 5-mL pipet. From both wells, the spheroids were collected and transferred back into their respective flask.
9. The flask containing the spheroids was placed back into the cell incubator for the continuation of the spheroid culture.

2.3.3 Motorized mosaic imaging (MMI)

To generate overlapping sequential images, a motorized table was used (from the Axiovert 200M Zeiss microscope) along with a 5× objective and camera (AxioCam MRc5, Zeiss). The AxioVision software (AxioVs40 V4.8.2.0) was used to program the motorized table and the acquisition of images. To position the table holding the sample plate, various x- and y-axis coordinate settings were pre-calculated with the top left of the first well as point zero (0, 0). The coordinates were saved as a comma-separated values (CSV) file (see supplementary data files for the coordinate lists of four wells), which is a format readable for the AxioVision software. However, only a maximum of 800 coordinate positions was used per CSV file due to software limitations. Additionally, the z-axis coordinate was corrected for each well after manual adjustment to generate the sharpest image of the microscopic target. The adjusted CSV file was then imported into the AxioVision "Multidimensional acquisition" and loaded into the "Position list" tool. Before imaging, Köhler illumination was applied and optimized for both sample types to obtain optimal optical acquisition. Then, various additional hardware and software parameters were set. First, a white illumination strength at voltage 5–6 was used for the lamp, which was higher or lower based on sample volume because more medium required more light. Second, a camera white balance adjustment was done with the AxioVision software, and a 1292 × 968-pixel resolution with the fast color acquisition was set for image capture.

MMI: step-by-step protocol.

In the following step-by-step protocol, various components of the microscope are mentioned. An overview of the specified microscope is shown in Fig. 2 after the protocol below. For additional information regarding the microscope components and functions, please refer to the Axiovert200M Manual available online from Zeiss.

1. The microscope (motorized) table was placed from a top perspective at the farthest (lowest x-axis) to the left and farthest to the bottom (lowest y-axis). The table was then placed from a front perspective to the bottom (lowest z-axis). This position was used to calibrate the table and was set as home and point zero for all axes. In the software, this was done as follows: go to "multidimensional acquisition" > "Positionlist" tab (XY short) > "MarkFind" > "Stage" tab > "Home" > click yes, yes. For the z-axis, click in the same Mark and Find window the focus tab and click "home" followed by yes, yes.
2. The color camera was selected and configured by going to the "work area," clicking on cameras, and then clicking on the desired mounted camera. The AxioCam camera with color was used for all image acquirements.

3. In the camera configurations, in the “Adjust” tab, the “Auto Snap” and “Auto Live” options were deselected.
4. Then, in the “Frame” tab, the resolution was set at a 1292 × 968-pixel resolution with fast color.
5. The table was then placed closest to an opening of the incubator chamber, which was mounted on the microscope. In this case, the table was moved to the farthest to the right bottom, based from a top perspective. The plate containing the microscopic targets was then carefully mounted on the microscope stage (the motorized table).
6. A well containing microscopic targets was centered above the 5× objective using the table positioner. The samples were then put into focus by using the focusing drive of the microscope, see Fig. 2 for schematic details.
7. The Köhler illumination method was applied. First, the luminous-diaphragm was closed with the setting lever until the light beam became more condensed.
8. With the setting knob for vertical adjustment of the condenser, the shape of the condensed light was altered until a clear and sharp hexagonal shape was seen.
9. By using both centering screws for the condenser, the condensed hexagon shaped light was centered in the middle of the visual field through the ocular.
10. The setting knob for vertical adjustment of the condenser was then used to open the condenser again fully.
11. The illumination intensity was set at a voltage of 5–6 using the toggle switch for illumination. The exact number of voltage depended on the liquid volume present in a well (a larger volume of liquid required more light).
12. For each well, the focus was determined, and the corresponding z-axis noted from the software.
13. Then, in the coordination lists, the respective z-axis value was altered per well to have each well in focus (these lists can be found in the supplementary data). This was simply done with the find and replace function of notepad. The old z-axis value was replaced with the new measured value.

    Note: This has to be repeated each time the plate has been mounted or re-mounted on the microscope stage.
14. The coordinate lists were configured in the “Mark and Find” window. The CSV coordinate lists were the only format compatible with the AxioVision software. Click on “New” then on “Import Positionlist…” and select the desired coordinate list.
15. The white balance was set for the first well by first clicking on the “Live” button in the main icon menu and then by clicking on the “White balance” button.
16. With all settings ready for bright field imaging, an image was acquired automatically from each of the coordinates included in the list.

Axiovert 200M Microscope

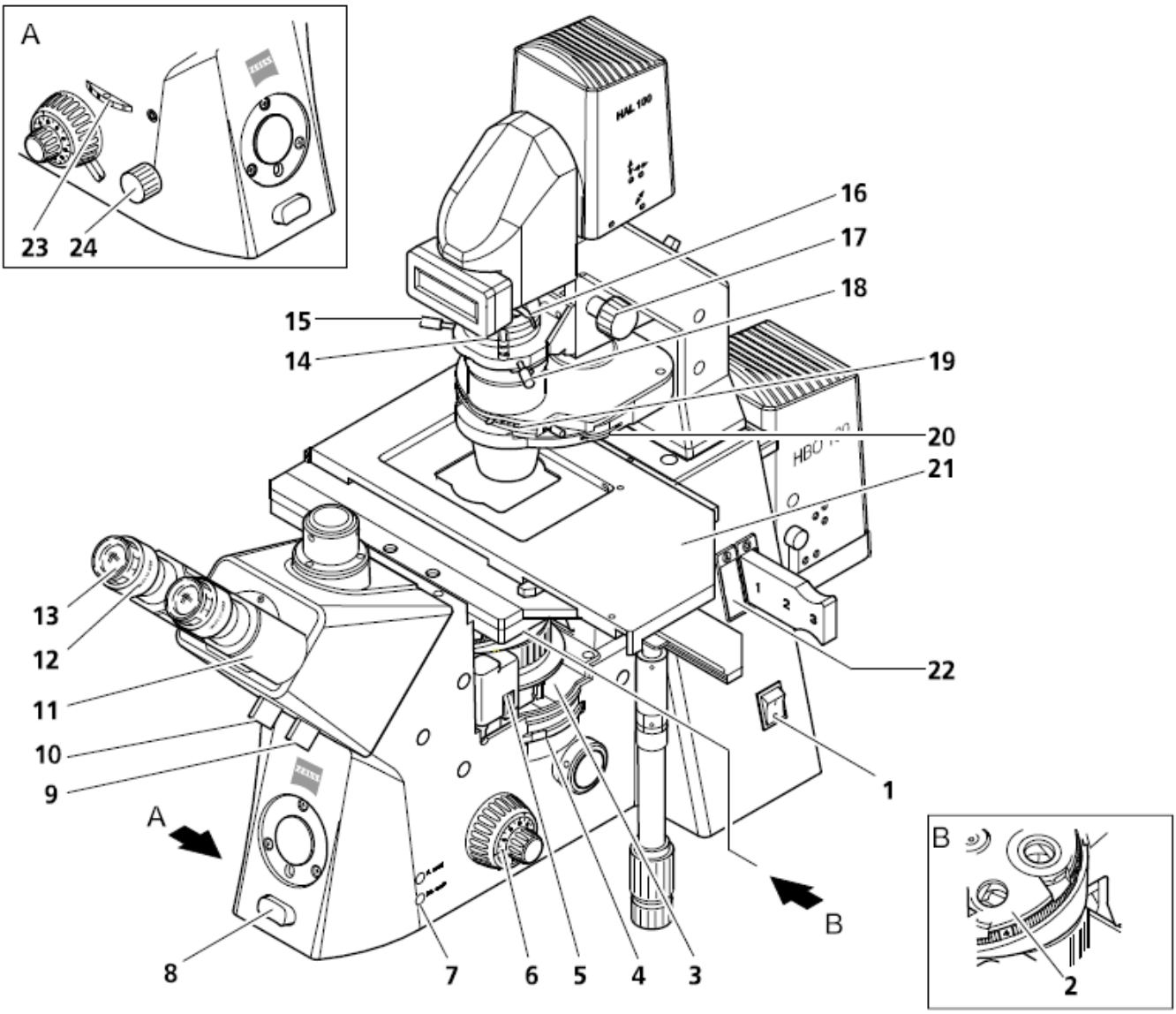

1 On / Off switch
2 Objective nosepiece
3 Compartment for slider Analyzer
4 Setting wheel for Optovar turret
5 Reflector turret
6 Focusing drive coarse / fine
7 HAL on / off switch
8 Toggle switch for illumination intensity
9 Turning or sliding knob for vis / doc beam splitting
10 Turning or sliding knob for Bertrand lens and manual shutter
11 Binocular tube component
12 Setting ring of the eyepiece
13 Eyepiece
14 Polarizer D with 2-position filter changer
15 Centering screw for condenser
16 Setting lever for luminous-field diaphragm
17 Setting knob for vertical adjustment of the condenser
18 Centering screw for condenser
19 Turret disk of condenser
20 Setting wheel for aperture diaphragm on the condenser
21 Microscope stage
22 Compartment for aperture diaphragm slider
23 Setting wheel for Sideport
24 Setting knob for Frontport / Baseport

Fig. 2. Schematic image of the Zeiss Axiovert 200M microscope used for MMI.

2.3.4 Video mosaic imaging (VMI)

VMI used a standard setup, including a light microscope (Zeiss Axiovert 40 CFL inverted), 5× objective, and camera (AxioCam MRc5, Zeiss). The camera was used via the AxioVision software (AxioVs40×64 V4.8.3.0) to obtain a live feed of the sample on the computer screen. The "live speed control" of the camera was set to fast, which determined the refresh rate of the live feed. Then, the screen capture software Debut Video Capture Software (DVCS) was used to record the live feed screen shown by the AxioVision software. This resulted in a custom video resolution of 1168 × 872 pixels containing only the live feed area of the sample. To video record this area, the recording setting "Fast capture" was used in DVCS at 30 frames per second. The resulting video file was in the audio video interleave (or AVI) format.
Prior to sample placement, straight red marker lines were drawn approximately 1 mm apart from each other on the bottom of the 48-well plate to establish a guiding path during VMI recording. Finally, each well was recorded while manually moving the plate by starting at the top left and following the marked red lines on the plate. Recording durations of 30, 60, 90, and 120 seconds were obtained for the whole well for all samples.

<u>Video mosaic imaging: step-by-step protocol.</u>

1. The Axiovison software was started, followed by the activation of the live feed by clicking on "Live" in the main icon menu.
2. The live feed refresh rate was set to fast. This option can be found right next to the "Snap" button in the Live window.
3. The plate with the samples was then placed on top of the microscope table (Zeiss Axiovert 40 CFL inverted). A well with targets was centered above the 5× objective.
4. Both the "Exposure" and "White balance" buttons were clicked and set.
5. The DVCS or any other screen capture software was started.
6. The DVCS software was used to capture the on-screen images of the computer monitor. The live feed of the AxioVision software was set to the maximum screen size. The screen capture software was then set to only capture the live feed view at 30 frames per second. This resulted in a custom video resolution of 1168 × 872 pixels.
7. With the live feed window open, the first 48-well-plate well was orientated with the top left first in view. The screen capture software was started to record, and the well was moved upwards, resulting in a downwards motion on the camera. Then, at the bottom of the well, it was moved one line to the right followed by a downwards motion of the plate, which resulted in an upwards motion on the camera. At the top of the well, it was moved one line to the right again. This process was continued for the whole well. The motion speed was dependent on the recording durations determined before the experiment. The used record durations were 30, 60, 90, and 120 seconds.

2.3.5 Mosaic generation

Images for each well were stored in separate folders to prepare MMI obtained images for mosaic generation. These images were then converted into JPEG files via the export function of the AxioVision (SE64 Rel. 4.9.1) software. To prepare VMI recordings for mosaic generation, image frames were obtained via Photoshop CC (Adobe) using the import function “Video Frames to Layers.” With the option “Limit to Every X Frames,” the frame extraction per well was limited as close as possible to 500 frames and not more due to software limitations of Photoshop CC. These frames were then exported via the export function “Layers to Files” to JPEG, resulting in one folder containing all the VMI images per well.

Mosaics were generated with the mosaic processing software Autopano Giga (64-bit, V4.2.3, from Kolor). One JPEG folder was used for one mosaic, representing one whole 48-well-plate well. The mosaic software was used with the manufacturer’s default settings for generating mosaics. Next, the mosaic image was cropped in a square configuration where the crop box contained only the inner well of the mosaic image. The cropped mosaic was then rendered into a JPEG (maximal quality at 300 DPI) image file. This was followed by a final step of resizing the mosaic image into a resolution of 5,000 × 5,000 pixels to correct for any small distortions.

2.3.6 Mosaic image processing and sample analysis

Microscopic targets of interest in the mosaic images were selected and isolated in Photoshop CC. All objects smaller than 20 pixels were ignored. After selection, targets were isolated into a separate layer and overlaid with black color before being saved as JPEG. This resulted in an image with all the microscopic targets in black and the background in white, which was used for further analysis.

ImageJ (Fiji) was used to obtain numerical data from the black targets. First, the image was set to 8-bit, and the threshold set to default with black and white (B&W) (bins 0 and 128), followed by the binary adjustments “Convert to mask” and “Watershed.” Then, the scale was set via “Set Scale” at 0.5 pixels representing 1.2 µm. Finally, the targets were analyzed with the “Analyze Particles” command—parameter size was set to 1000-infinity and circularity to 0.65–1.00. All steps were recorded as a macro code for automation analysis of multiple mosaics, presented after this paragraph. Together, the numerical data of all targets were obtained automatically in one Excel file.

Macro automation code for quantitative analysis of microscopic targets with ImageJ:

```
run("8-bit");
setAutoThreshold("Default");
//run("Threshold...");
//setThreshold(0, 128);
setOption("BlackBackground", false);
run("Convert to Mask");
run("Watershed");
run("Set Scale...", "distance=0.5 known=1.2 unit=um global");

dir = getDirectory("image");
name = getTitle;
index = lastIndexOf(name, ".");
if (index!=-1) name = substring(name, 0, index);
name = name + ".xls";

run("Analyze Particles...", "size=1000-Infinity circularity=0.65-1.00 show=[Overlay Outlines]
display");
saveAs("Results", dir+name);
print(dir+name);

close();
run("Close");
```

2.3.7 Statistical analysis

Results are presented as the mean ± standard deviation (SD) with a minimum of n = 3. Correlation analysis was performed using Pearson correlation in GraphPad Prism 6 (GraphPad Software). The sample sizes are indicated in the figure legends.

2.4 Results

2.4.1 Motorized mosaic imaging generates whole-well mosaic images

For MMI, a motorized table from a Zeiss Axiovert 200M microscope was used to make sequential overlapping images (Fig. 3A). Various distances between two consecutive images of the sample were investigated, which resulted in multiple MMI settings. Each MMI setting represents the distance in µm that the table with the sample will move before making the next image. A total of 18 different MMI settings were investigated, including various overlapping images with the y-axis overlapping between 20 and 80% and the x-axis between 40 and 90% (Table 3). The differences between the x- and y-axis were caused by the widescreen image acquisition of 1292 pixels for the x-axis and 968 pixels for the y-axis. As a result, a larger image overlap for the x-axis was obtained than the y-axis at the same MMI setting.

The MMI method successfully generated whole-well mosaic images of both biological and synthetic targets (Fig. 3B). A magnified window of the mosaic shows that high-quality and magnification were retained and that particles of 5–10 µm could be distinguished from the background, and thus, making the technique suitable for the analysis of cells.

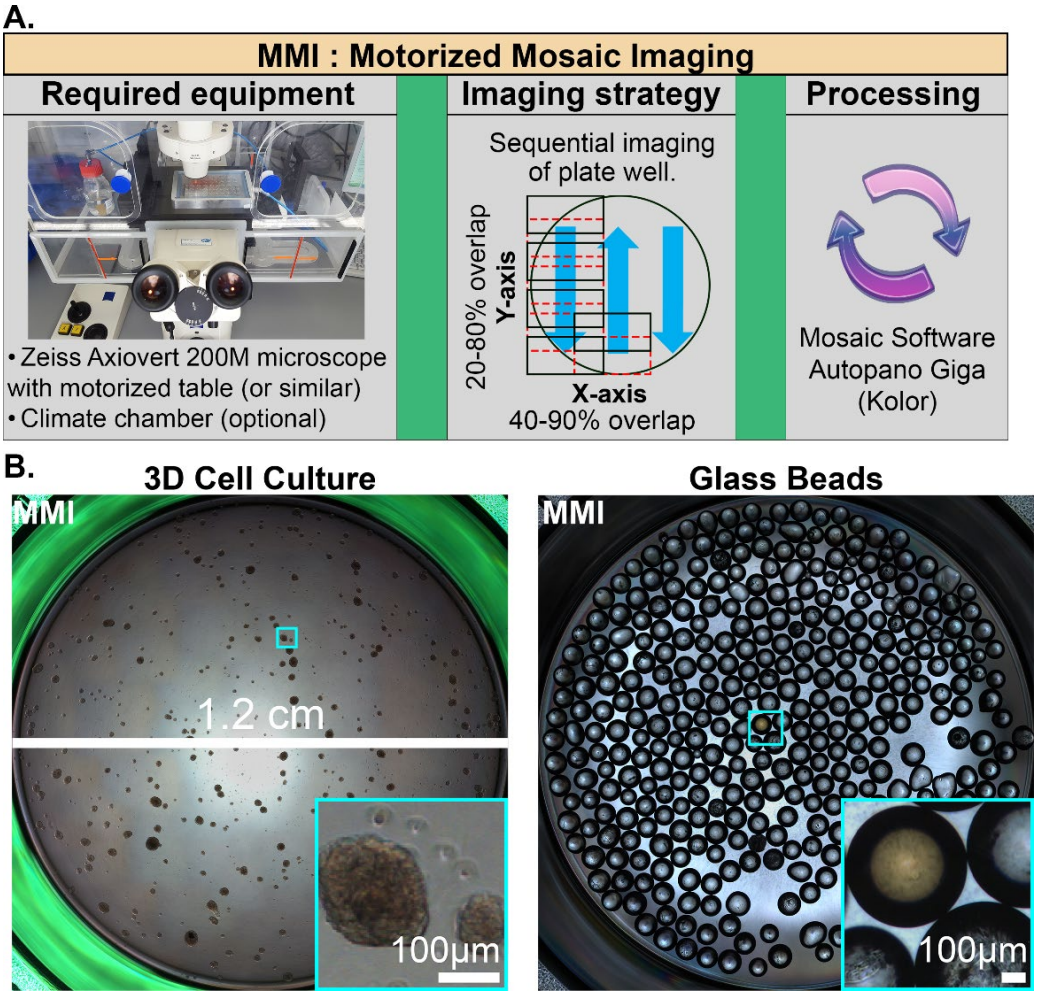

Fig. 3. MMI generates mosaics on a macro-scale from microscopic targets. (**A**) Principle of MMI. In the left column, the required equipment is shown, middle column the imaging strategy of sequential image overlapping, and the third column the processing step with mosaic software. (**B**) Representation of successfully generated MMI mosaic images of a pH-SKP cell culture at day 7 and 60-mg synthetic glass beads. Both were generated with the 600×600 MMI setting.

Table 3. MMI settings, image overlapping percentages, and durations.

MMI Setting	Y-Axis Change (µm)	X-Axis Change (µm)	Y-Axis Image Overlap (%)	X-axis Image Overlap (%)	Images (per well)	Time for Acquisition 1 well (mm:ss)	Total Time for Saving 1 Well (mm:ss)
500×500	500	500	76	82	575	14:05	2:28
500×1000	500	1,000	76	64	300	7:26	1:02
600×600	600	600	71	78	399	9:49	2:46
600×1000	600	1,000	71	64	252	6:13	0:29
700×700	700	700	66	75	323	7:58	0:59
700×1000	700	1,000	66	64	228	5:37	0:32
800×800	800	800	61	71	240	5:53	0:24
800×1000	800	1,000	61	64	192	4:50	0:19
900×900	900	900	57	68	195	4:51	0:19
900×1000	900	1,000	57	64	180	4:36	0:17
1000×1000	1,000	1,000	52	64	156	3:58	0:15
1100×1100	1,100	1,100	47	60	132	3:23	0:13
1200×1200	1,200	1,200	42	57	110	2:52	0:10
1300×1300	1,300	1,300	37	53	110	2:55	0:11
1400×1400	1,400	1,400	33	50	90	2:25	0:08
1500×1500	1,500	1,500	28	46	90	2:23	0:09
1600×1600	1,600	1,600	23	42	72	1:58	0:10
1700×1700	1,700	1,700	18	39	72	1:59	0:06

2.4.2 MMI mosaic generation is influenced by image overlap, microscopic target quantity, and spread

All MMI settings for 5-day-old spheroids resulted in successful mosaic generation (Fig. 4A). For 7-day-old spheroids, smaller image overlaps were investigated. Here, successful mosaic generation was possible up to MMI setting 1400×1400, while higher settings led to unsuccessful mosaics with image distortion (Fig. 4B). Typical distortions included warped images, missing pieces, or failure to generate a mosaic at all. For glass beads, 60 mg resulted in successful mosaic generation up to MMI setting 1600×1600 (Fig. 5A). In contrast, 30-mg glass beads showed minor warped image distortion at most MMI settings after 700×700 and large distortion after 1100×1100 (Fig. 5B).

Then, a different in-well sample configuration with particles more centered was used to investigate the effect of sample location on mosaic generation. Here, 30-mg glass bead samples resulted in mosaics up to MMI setting 1400×1400 (Fig. 5B). This showed that particle spread and positioning in the well influenced the success rate of mosaic generation for low-particle samples.

Together, these results show the importance of sufficient recognition points from one taken image to another. The software uses in-photo objects for recognition points to compare overlapping images with each other and stitch them together into a mosaic. Therefore, better spread and more sample particles in a well result in more successful mosaics at higher MMI settings (i.e., images with less overlap).

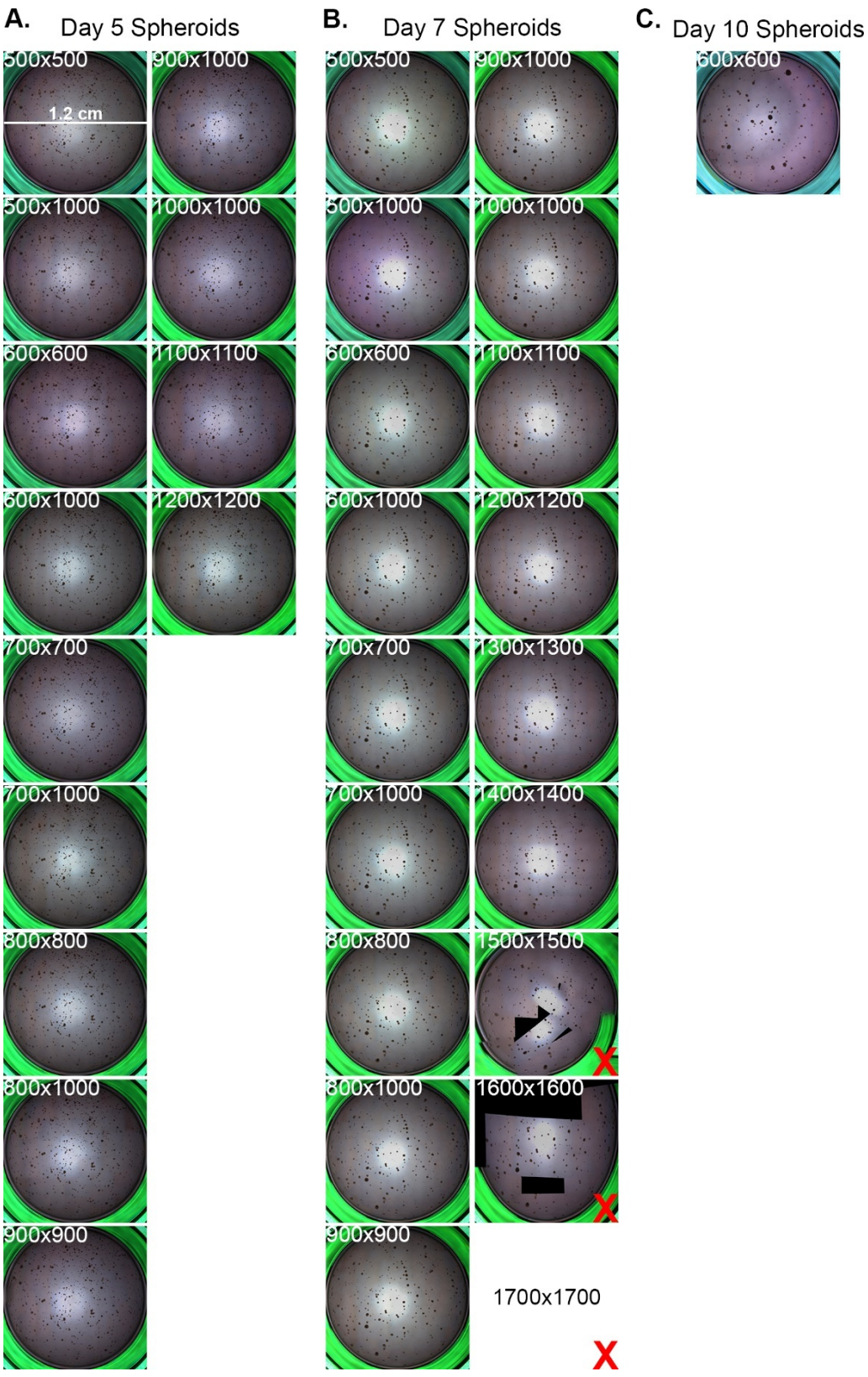

Fig. 4. Mosaic overview of all MMI settings with cellular spheroids. (**A**) MMI mosaics from one spheroid sample at culture day 5 are shown for MMI settings 500×500 to 1200×1200. (**B**) MMI mosaics from spheroid culture day 7 is shown for MMI settings 500×500 to 1700×1700. A red X indicates image distortions or failure of mosaic generation. (**C**) MMI mosaic of one spheroid sample from culture day 10 at MMI setting 600×600. Scale bar at the top left: 1.2 cm.

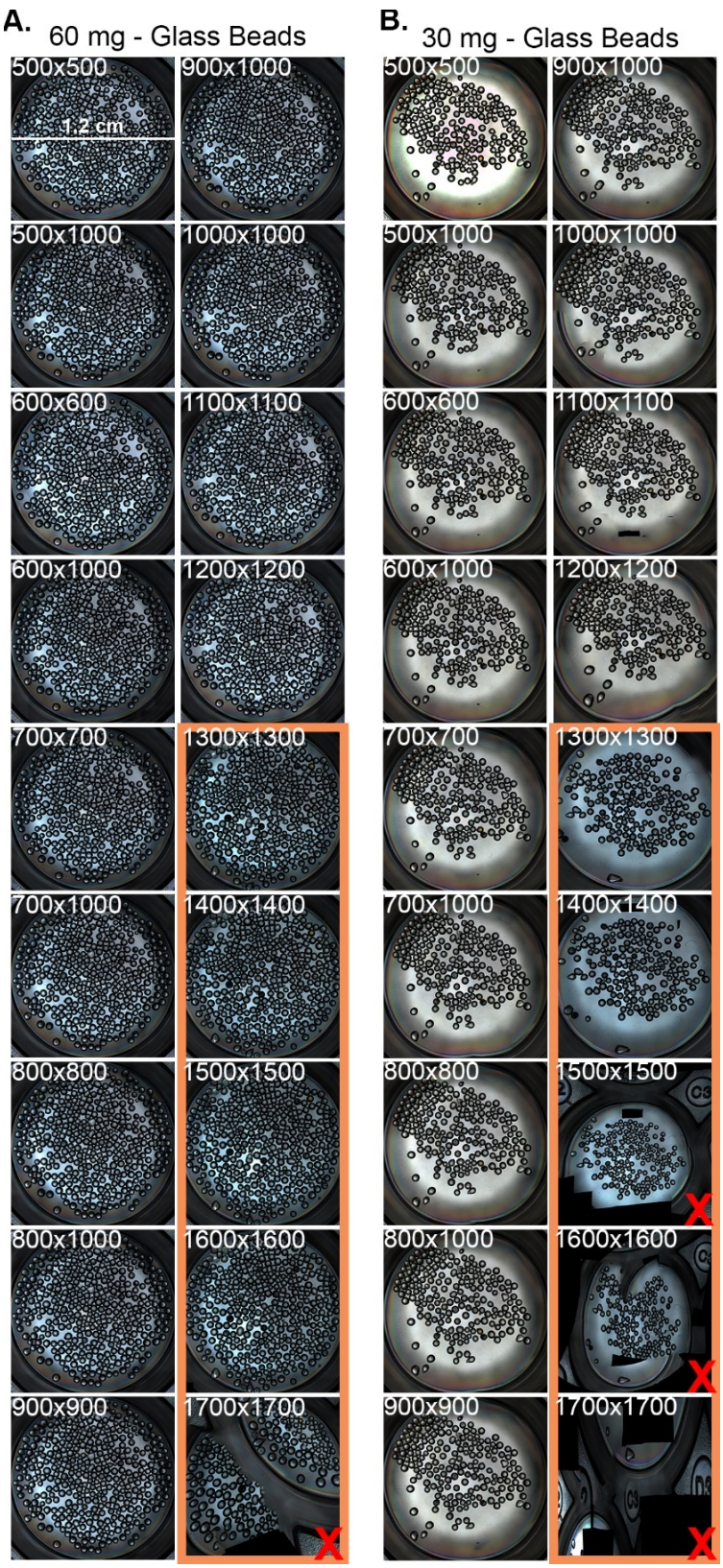

Fig. 5. Mosaic overview of MMI settings with glass beads. (**A**) MMI mosaics from the 60-mg glass bead samples are shown for MMI settings 500×500 to 1200×1200. For MMI settings 1300×1300 to 1700×1700, a more spread and centered configuration of beads were used. A red X indicates image distortions or failure of mosaic generation. (**B**) MMI mosaics from the 30-mg glass bead samples are shown for MMI settings 500×500 to 1200×1200. For MMI settings 1300×1300 to 1700×1700, a more spread and centered configuration of beads were used. Scale bar at the top left: 1.2 cm.

2.4.3 MMI mosaic generation can record and visualize cell movement

We next investigated whether MMI could be used to detect spheroid activity in mosaic images. One spheroid sample was imaged with MMI in 2-h intervals for a 6-h period. In this time-frame, various spheroids were found to travel a certain distance in the well. For example, two spheroids showed homing behavior and traveled to each other over a distance of approximately 65 µm in 6 h (Fig. 6). These results show that the MMI technique can also be used for biological target tracking and provides the potential for the time-lapse recording of whole-well samples.

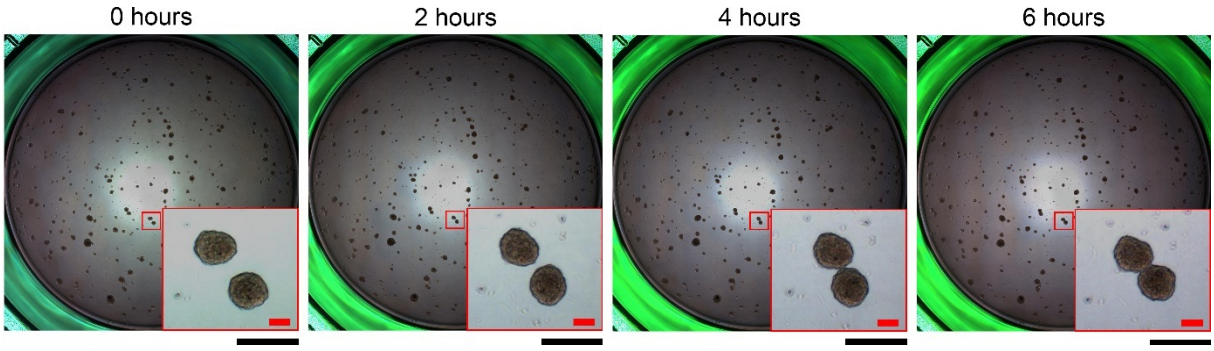

Fig. 6. Cellular trafficking of 7-day-old spheroids. Four whole-well mosaics were compared against each other with 7-day-old spheroids at a 2-h interval MMI imaging. The magnified window represents an example of spheroid trafficking. Red scale bar: 100 µm, and black scale bar: 0.25 cm.

2.4.4 Sample quantity and sample size influence mosaic image generation

The Autopano Giga mosaic software provides various parameters that can be used to gain further insight into the mosaic quality and generation principles. An indicator of overall quality of the mosaic is the so-called “root mean square (RMS),” which represents the error of alignment between two images used in a mosaic. The Global RMS is the average of all images present in a mosaic, and a higher value indicates a higher error, and therefore, lower mosaic quality. A second parameter is termed “control points” and represents the recognition points found between images based on identical in-photo objects. Then, the parameter “links between images” represents the links made between control points of images to stitch the mosaic together based on the overlapping parts of images.

To investigate the software parameters in relation with MMI settings and sample types, MMI settings 500×500 to 1200×1200 were compared. First, higher MMI settings resulted in less acquired images than lower MMI setting because with each higher MMI setting the motorized table will travel a larger distance before the next image acquisition, resulting in a lower image overlap (Fig. 7A). Therefore, fewer images are taken compared to shorter distances (lower MMI settings) that require more steps to cover the whole sample. As a result, the Global RMS value showed an increasing trend for all samples and conditions at higher MMI settings,

indicating lower mosaic quality (Fig. 7B). Additionally, the lower image overlaps with higher MMI settings resulted in less identical in-photo object information between two images for control points (Fig. 7C). This lower amount of control points was directly related to fewer links between images that are made between control points for image stitching (Fig. 7D). The image stitching is directly correlated to mosaic generation, and its quality was evidently reduced in relation to a lower image overlap at higher MMI settings.

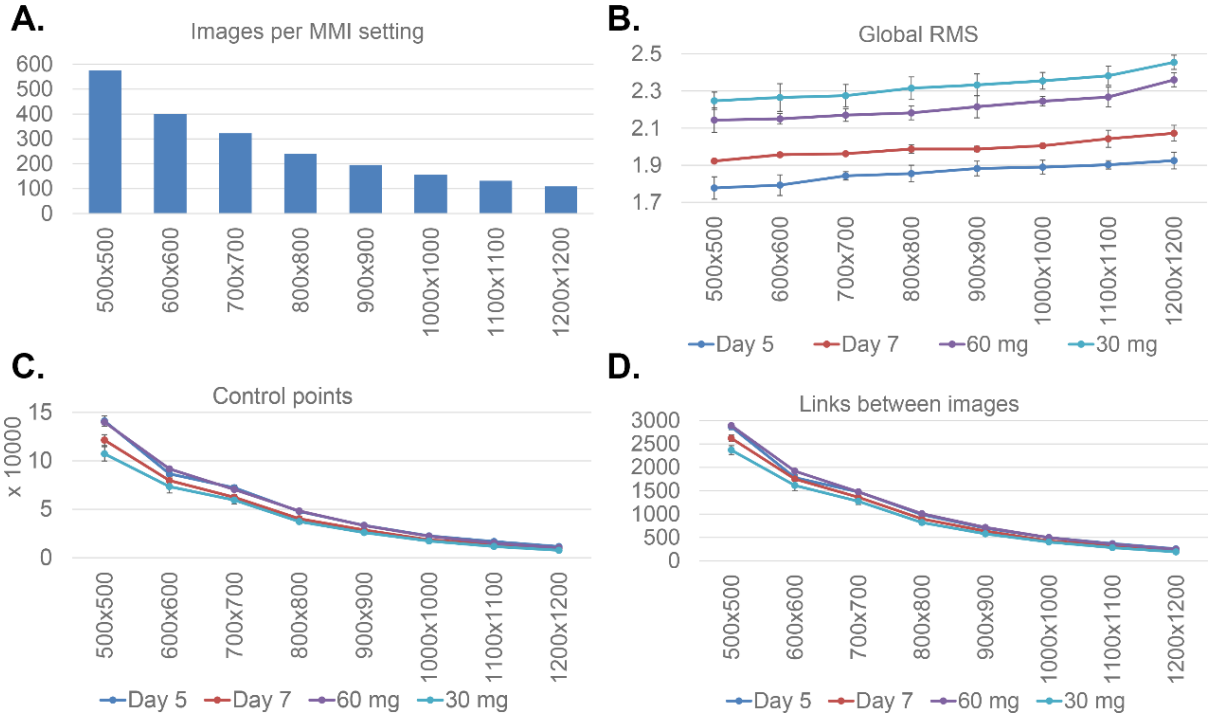

Fig. 7. MMI generates mosaics on a macro-scale of microscopic targets. (**A**) Image number that is acquired per MMI setting between MMI setting 500×500 and 1200×1200. (**B**) Global RMS value per MMI setting for day 5 and 7 spheroids and 60- and 30-mg glass beads. (**C**) Control points per MMI setting and sample, representing the found identical points between overlapping images by the mosaic software. (**D**) Links between images per MMI setting and sample type, representing links used to stitch images between control points. For all panels, data represent the mean ± SD (n = 4).

In addition to MMI settings, sample type and condition also influenced mosaic quality but did not significantly affect successful generation. For example, 5-day- and 7-day-old spheroids showed that the Global RMS was higher for day 7 with all MMI settings, indicating poorer quality (Fig. 7B). In the experimental setup, a longer culture time resulted in fewer spheroids due to the lack of temperature and CO_2 regulation during imaging periods (see Materials and Methods, pages 103 to 104). Therefore, less in-photo objects were present in older spheroid preparations in the used experimental setup, resulting in fewer control points found by the software at day 7 compared to day 5 with the same MMI settings (Fig. 7C). Consequently, fewer links between images for stitching were found for day 7 as well (Fig. 7D). Similar results were found for glass beads. The 60-mg glass bead mosaics had consistently better quality than the 30-mg ones. With more objects per well at 60 mg, more control points were found,

and more links between images can be made, resulting in a higher mosaic quality. When comparing spheroids with glass beads, spheroids at both time points had better quality due to more objects (spheroids and cells) in the well (Fig. 7A).

A significance in the Pearson correlation coefficient was found between image number per MMI setting and Global RMS. The correlation was strongest between MMI settings 500×500 to 1000×1000 with R = −0.96 for day 5 spheroids (P = 0.002), R = −0.99 for day 7 spheroids (P = 0.0002), R = −0.88 for 60-mg glass beads (P = 0.019), and R = −0.93 for 30-mg glass beads (P = 0.007) (Fig. 8). These results indicate that the correlation between image overlap and Global RMS (mosaic quality) became stronger and more significant with fewer objects/particles (i.e., spheroids or glass beads). Thus, lower MMI settings (representing more images) are more beneficial and important for samples with a lower number of particles for mosaic quality.

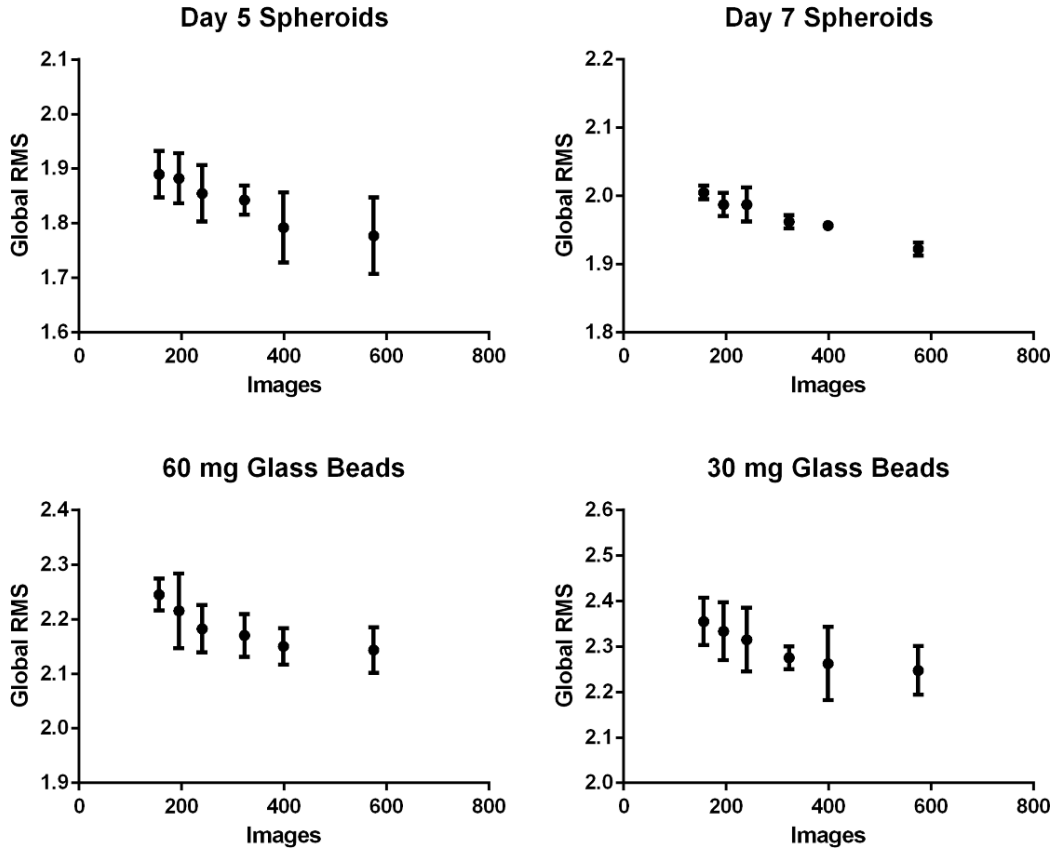

Fig. 8. Pearson correlation shows a strong correlation between Global RMS and image number. Representation of the Pearson correlation plot of Global RMS to the number of images used per MMI setting for MMI mosaics of day 5 and 7 spheroids and 60- and 30-mg glass beads. Data are expressed as the mean ± SD (n = 4).

Overall, these results show that MMI mosaic generation is dependent on image overlap percentage and sample particle quantity. Additionally, image overlap and sample particles share a correlative relation in which higher overlap percentages are required with lower amounts of particles per well.

2.4.5 Video mosaic imaging generates whole-well mosaic images

VMI is a mosaic imaging technique based on sample video recording with a standard light microscope and camera. The obtained video frames are used to generate mosaics of 48-well-plate wells. The effect of recording duration length was tested on the mosaic generation and quality by using spheroids and glass beads targets (Fig. 9A). VMI mosaic generation was determined as successful when the complete well was visible with no major distortion or large missing parts in crucial areas (see for example Fig. 9B).

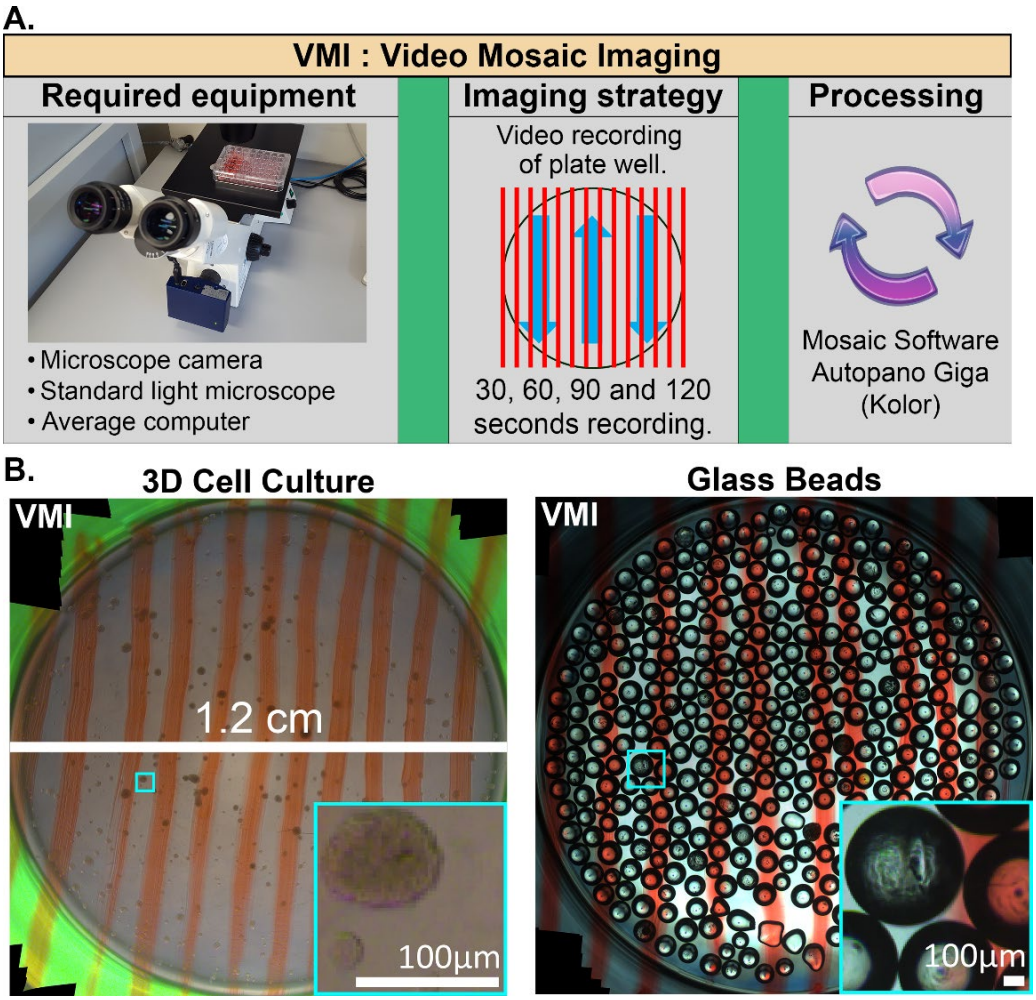

Fig. 9. VMI generates mosaics on a macro-scale of microscopic targets. (**A**) The principle of VMI is shown. In the left column, the required equipment is shown. In the middle column, the imaging strategy of sequential overlapping to generate overlapping images is shown. Finally, in the third column, the processing step with mosaic software is shown. (**B**) Representation of a successfully generated VMI mosaic image of 7-day-old spheroids and 60-mg glass beads, both at the 120-second recording duration.

For all samples, mosaic formation was optimal with 120-second video recording durations per well (Fig. 10). An exception was 30-mg glass beads, of which none of the durations resulted in a complete mosaic generation—most likely caused by large empty spaces in the well. Similar to MMI, mosaics from VMI had higher quality and chance of successful generation when the in-well particle amount was higher. This was evidenced for day 5 spheroids (Fig. 10A) and 60-mg glass beads (Fig. 10B). Here, both sample types generated mosaics at multiple recording durations compared to their lower particle counterparts (day 7 spheroids and 30-mg glass beads).

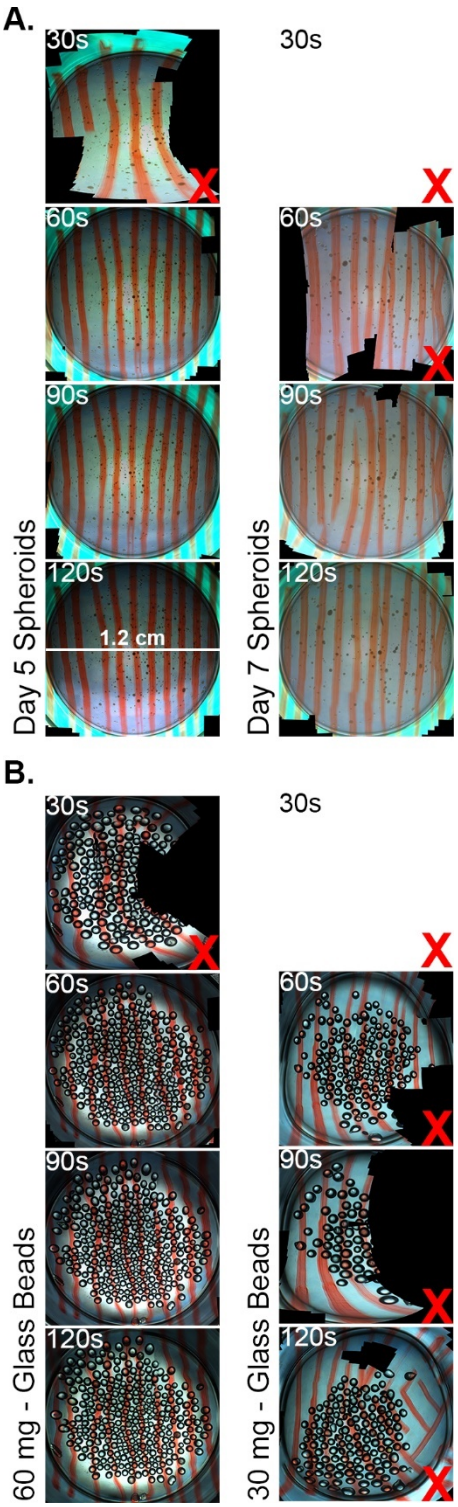

Fig. 10. Mosaic overview of VMI recording durations for cellular spheroids and glass beads. (**A**) VMI mosaics of 5-day-old and 7-day-old spheroids, with VMI recording durations of 30, 60, 90, and 120 seconds. A red X indicates the failure of more than one mosaic caused by large artifacts or incomplete rendering for that specific VMI duration. (**B**) VMI mosaics of 60- and 30-mg glass beads with duration settings of 30, 60, 90, and 120 seconds. Scale bar is represented in panel A, 120s day 5 spheroids: 1.2 cm.

2.4.6 VMI mosaic image generation is influenced by sample quantity and size

For VMI, the mosaic properties according to the provided parameters were also investigated, which included “total sub-mosaics found,” “Global RMS,” “control points,” and “links between images.” First, the total sub-mosaics found parameter, which represents the number of unsuccessful sub-mosaics generated from the source images (obtained from the video recording) of one well, was evaluated. This parameter showed that shorter durations resulted in more sub-mosaics and less with longer durations (Fig. 11A). Longer recording durations also resulted in an improvement of Global RMS (Fig. 11B). Additionally, control points and links between images increased at longer durations as well, leading to more stitches between images, and therefore, better mosaic generation and quality (Fig. 11C and D). Overall, longer recording durations showed improvement for all parameters compared to shorter durations.

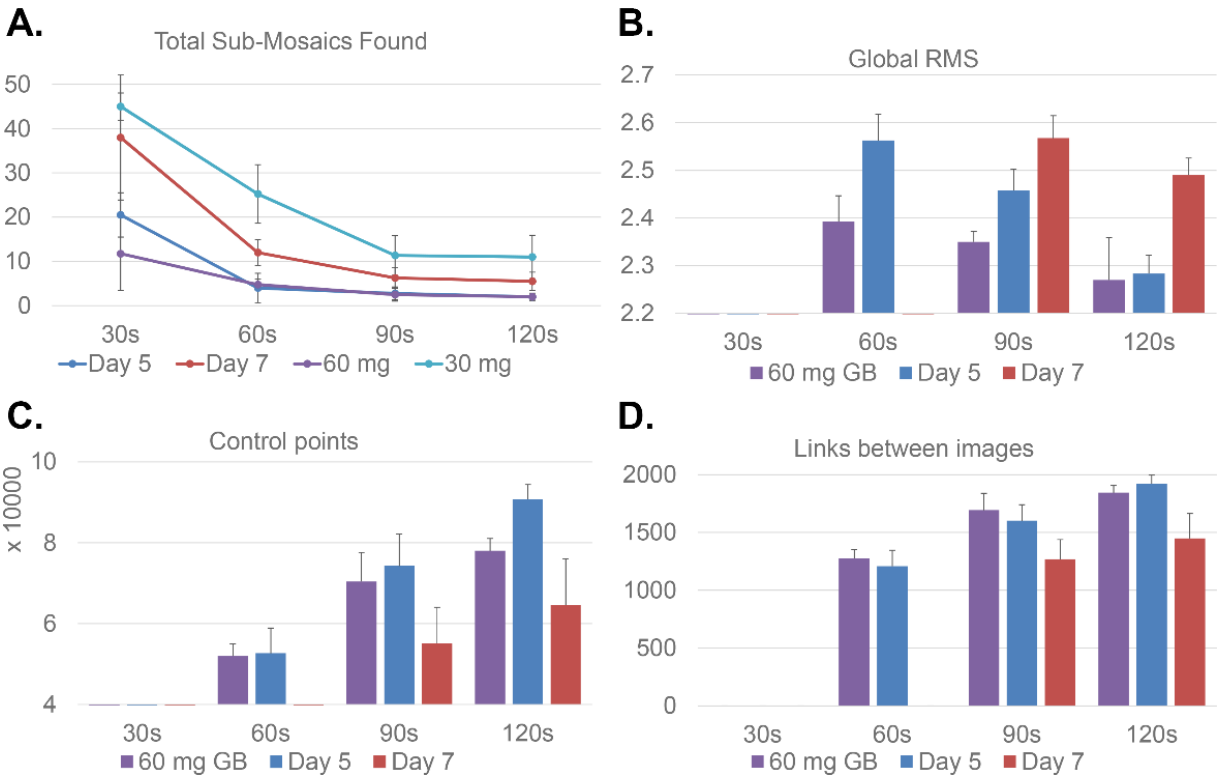

Fig. 11. VMI generates mosaics on a macro-scale of microscopic targets. (**A**) Graph illustration of total sub-mosaics found during mosaic processing of the images acquired with recording durations of 30, 60, 90, and 120 seconds for 5- and 7-day-old spheroids and 60- and 30-mg glass beads. (**B**) Global RMS value per VMI recording duration that generated successful mosaics for 5- and 7-day-old spheroids and 60- and 30-mg glass beads. (**C**) Control points per VMI duration and sample that represent the identical points found between overlapping images by the mosaic software. (**D**) Links between images per VMI duration and sample type, representing links used to stitch images between control points. The data represent the mean ± SD (n = 4).

In contrast to MMI, longer VMI recordings did not result in more images for mosaic generation due to the 500-frame limit (see Materials and Methods, page 109). Image number and overlap do therefore not increase (Fig. 12A). Nevertheless, mosaic quality was found to still improve with longer VMI durations. This is presumably caused by the reduced speed in movement. Longer recording durations allow a slower movement to record the whole well, and therefore, probably result in less motion-blur affected video image frames; the mosaic software cannot use blurred images to identify control points with sharp images. As a result, shorter VMI recording durations have more images lost than longer ones (Fig. 12B).

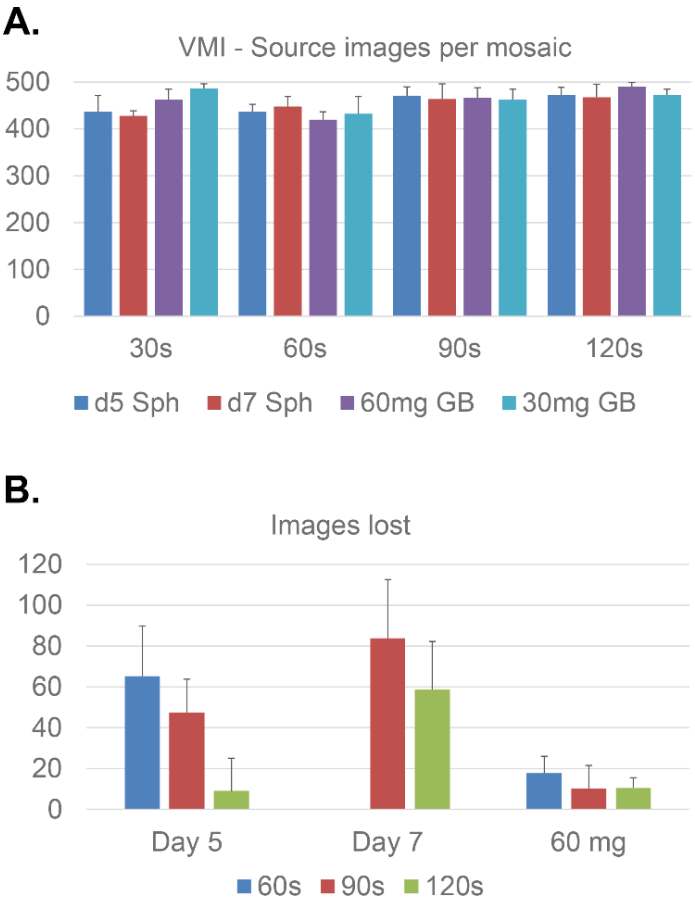

Fig. 12. Overview of source images obtained per VMI setting and images lost at mosaic generation. (**A**) Graph illustration of the number of source images obtained from video frame extraction per VMI setting for 5- and 7-day-old spheroids, and 60- and 30-mg glass beads. (**B**) Number of images lost and not used in a complete mosaic per VMI duration for 5- and 7-day-old spheroids, and 60- and 30-mg glass beads. For panels A and B, data are expressed as the mean + SD (n = 4).

In addition to VMI recording duration time, sample type and conditions also influenced VMI mosaic parameters. Similar to MMI, high-particle containing samples (e.g., 5-day-old spheroids and 60-mg glass beads) resulted in the lowest number of sub-mosaics and highest mosaic quality (Fig. 11A, 11B). Here, samples with fewer particles (e.g., 7-day-old spheroids and 30-mg glass beads) were more dependent on VMI recording duration. For example, the total sub-mosaics generated was reduced more drastically with longer recording durations compared to the particle-rich samples. Fewer particles also resulted in fewer control points (Fig. 11C), links between images (Fig. 11D), and more lost images during VMI mosaic generation (Fig. 12B). Thus, in addition to particle amount and spread for an optimal mosaic generation, VMI mosaic generation was also dependent on the recording duration. Low-particle samples required longer recording durations to reach similar quality mosaics as high-particle samples.

2.4.7 Numerical data can be obtained from whole-well mosaics

A key advantage of whole-sample imaging by MMI and VMI is the possibility to quantify and compare targets of interest in the samples. As a proof of principle, spheroids and glass beads were isolated in the mosaic images with Photoshop CC. These were then analyzed via a macro automation code (see Materials and Methods) in ImageJ (Fiji). As a result, the numerical data of each particle present in each whole sample, including the size and number, was obtained (Fig. 13).

For the biological samples, three time points were investigated, including 5-, 7-, and 10-day-old spheroids. For synthetic samples, 60- and 30-mg of glass beads were analyzed. Based on the obtained data, the size frequency of particle diameter was determined by categorization into the following diameter sizes: <100, 100–250, 250–400, and >400 µm for spheroid samples and <400, 400–500, 500–600, and >600 µm for glass bead samples (Fig. 13B). For spheroids, their number was highest for day 5 and then decreased until day 10. Furthermore, during further culture days, the presence of smaller sized spheroids decreased, while larger ones increased, indicating spheroid growth and amalgamation. For glass beads, a more consistent pattern was observed. The majority of glass beads were between 400 and 600 µm in diameter, which was in accordance with the manufacturer's specifications (Fig. 13B). As expected, a clear linear correlation was seen between the used mass of glass beads and found bead number. The 30-mg glass bead sample had about half the number of beads compared to the 60-mg one and showed a similar size frequency ratio (Fig. 13B).

The total spheroid yield was calculated by combining the measured surface area of all spheroids to gain a better indication of spheroid growth. Interestingly, while a reduction of almost 50% in spheroid number—between day 5 and 7—was found (Fig. 13B), this was not the case for spheroid yield. Instead, only a ~30% reduction was seen for the spheroid yield (Fig. 13C). This indicates that although spheroid numbers decreased, the spheroids themselves became larger. The total yield represents, therefore, a more informative value for biological samples. In contrast, half the amount of glass beads resulted in half the number and also half the total yield (Fig. 13B and C). Overall, these results show that mosaic images of a macro-scale area with microscopic targets can be processed and used to obtain representative numerical data. These data are not limited by a sampling estimate but include all the targets per sample. Thus, full-mosaic imaging with MMI and VMI provide additional and crucial data, such as total yield, which provides a more complete and reliable analysis for comparative studies.

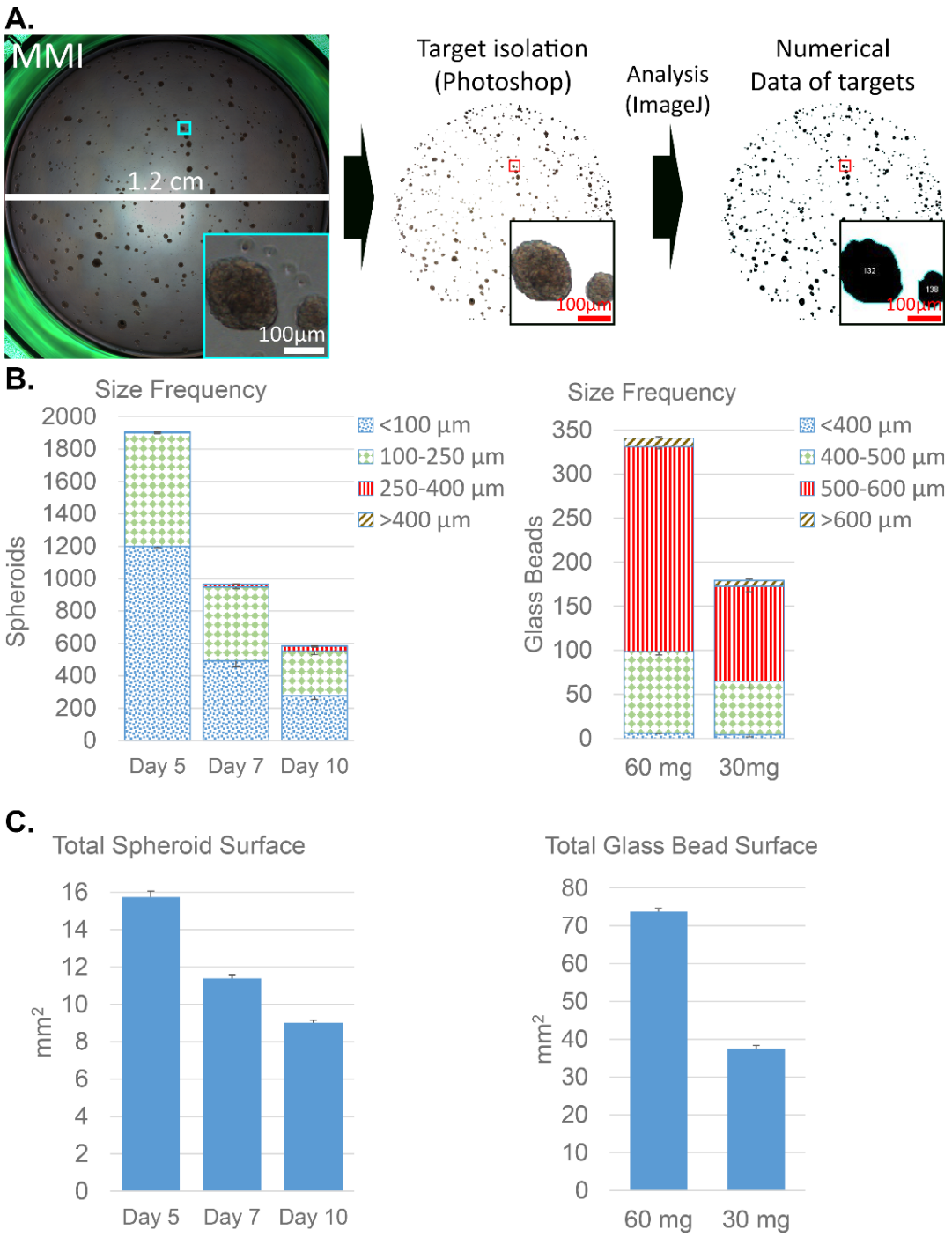

Fig. 13. Mosaics from spheroids and glass beads can successfully be processed and analyzed to obtain sample quantification. (**A**) A representation of data extraction from whole-well mosaics. MMI setting 600×600 was used with 5-day-old spheroids as an example. Microscopic targets of interest were isolated from the mosaic image via Photoshop selection, followed by isolation into a separate layer used for ImageJ particle analysis. (**B**) Graph illustrations of diameter size frequency from 5-, 7-, and 10-day-old spheroids and 60- and 30-mg glass beads. All sample data was obtained from mosaics made with the 600×600 MMI setting. All data are expressed as the mean with the three smallest size categories −SD and the largest category +SD. (**C**) Total surface area calculation of 5-, 7-, and 10-day-old spheroids and 60- and 30-mg glass beads, all shown in mm^2. Data are expressed as the mean +SD. For panel B and C, spheroids represent n = 6 for mosaic analysis and n = 3 for biological sample analysis. For glass bead analysis, 60- and 30-mg samples represent n = 4 for mosaic analysis and sample analysis.

Table 4. Successful mosaic generation vs. MMI setting. Top values represent each MMI setting. Green cells represent tested and successful mosaic generation. All samples resided in a 48-well-plate well during imaging.

	500 x 500	600 x 600	700 x 700	800 x 800	900 x 900	1000 x 1000	1100 x 1100	1200 x 1200	1300 x 1300	1400 x 1400	1500 x 1500	1600 x 1600	1700 x 1700
5-day-old spheroids													
7-day-old spheroids													
30-mg glass beads													
60-mg glass beads													

Table 5. Successful mosaic generation vs. VMI record duration time. Top values represent VMI record duration in seconds (s). Green cells represent tested and successful mosaic generation. All samples resided in a 48-well-plate well during imaging.

	30 s	60 s	90 s	120 s
5-day-old spheroids				
7-day-old spheroids				
30-mg glass beads				
60-mg glass beads				

2.5 Discussion

Mosaic imaging provides various benefits compared to standard microscopy. One is the ability to encompass a macro-scale area including the whole sample while retaining magnification. In both diagnostic and scientific fields, the obtainment of whole-sample image recordings will have great beneficial implications. Major examples are that one can refer back to a digitally recorded sample state made in the past, reduce physical storage space of fixated samples, and perform full sample quantification analysis.

Current approaches and techniques to obtain a mosaic image of microscopic targets at a macro-scale are costly and have low accessibility. For example, mosaic imaging by Surveyor from Meyer Instruments and Zeiss MosaiX require complete specialized systems. Other approaches are either with high complexity requiring various algorithms, custom-software, or manual placement of images [45, 46, 94, 140]. Additional reported mosaicking applications for biology, X-ray, and oceanology are complex and require specialized equipment and advanced image processing code [9, 106, 113]. Together, these limitations show a need for alternative mosaic imaging techniques that are easy-to-use, low-cost, and provide high-quality mosaic images.

In this study, two mosaic imaging techniques are presented that provide an easy-to-use and low-cost approach to obtain high-quality mosaics. These techniques, termed MMI and VMI, obtain digital microscopic images that overlap with each other and cover the complete macro-scale area. The images are then used to generate a single high-resolution mosaic image of the whole sample. We focused on the use of the commercially available software Autopano Giga, which is originally developed for photography. The use of commercial software significantly lowers complexity and removes limitations seen in custom in-house-build mosaic software that requires specific tacit knowledge [29]. Additionally, Autopano Giga uses in-photo objects to create mosaics as opposed to other available mosaic systems; therefore, it provides high-flexibility in imaging approaches. So, by combining bright field microscopy and two imaging approaches with simple software, we designed two low-cost and highly accessible techniques to provide a robust mosaic imaging method suitable for microscopic imaging in most laboratories.

As a proof of principle, we investigated the acquisition of whole-well mosaic images from cellular spheroids and synthetic glass beads residing in a 48-well plate. The optimal settings, limitations, and principles regarding sample type and condition were determined. Both mosaic imaging techniques were able to generate whole-well mosaic images (see Table 2 and 3 for a summary overview). Additionally, MMI and VMI were dependent on several principles, which affected generation success and quality (Fig. 14). First, there are three general principles for both techniques, which include that larger image overlap (Fig. 14, No. 1), higher particle number (Fig. 14, No. 2), and increased particle spread (Fig. 14, No. 3) result in a lower Global

RMS and thus higher quality mosaics. Additionally, for MMI, a larger number of particles or greater particle spread is required—when a lower image overlap is used—to maintain the Global RMS value (Fig. 14, No. 4). For VMI, an increased video record duration results in a lower Global RMS (Fig. 14, No. 5) and less incomplete sub-mosaics (Fig. 14, No. 6).

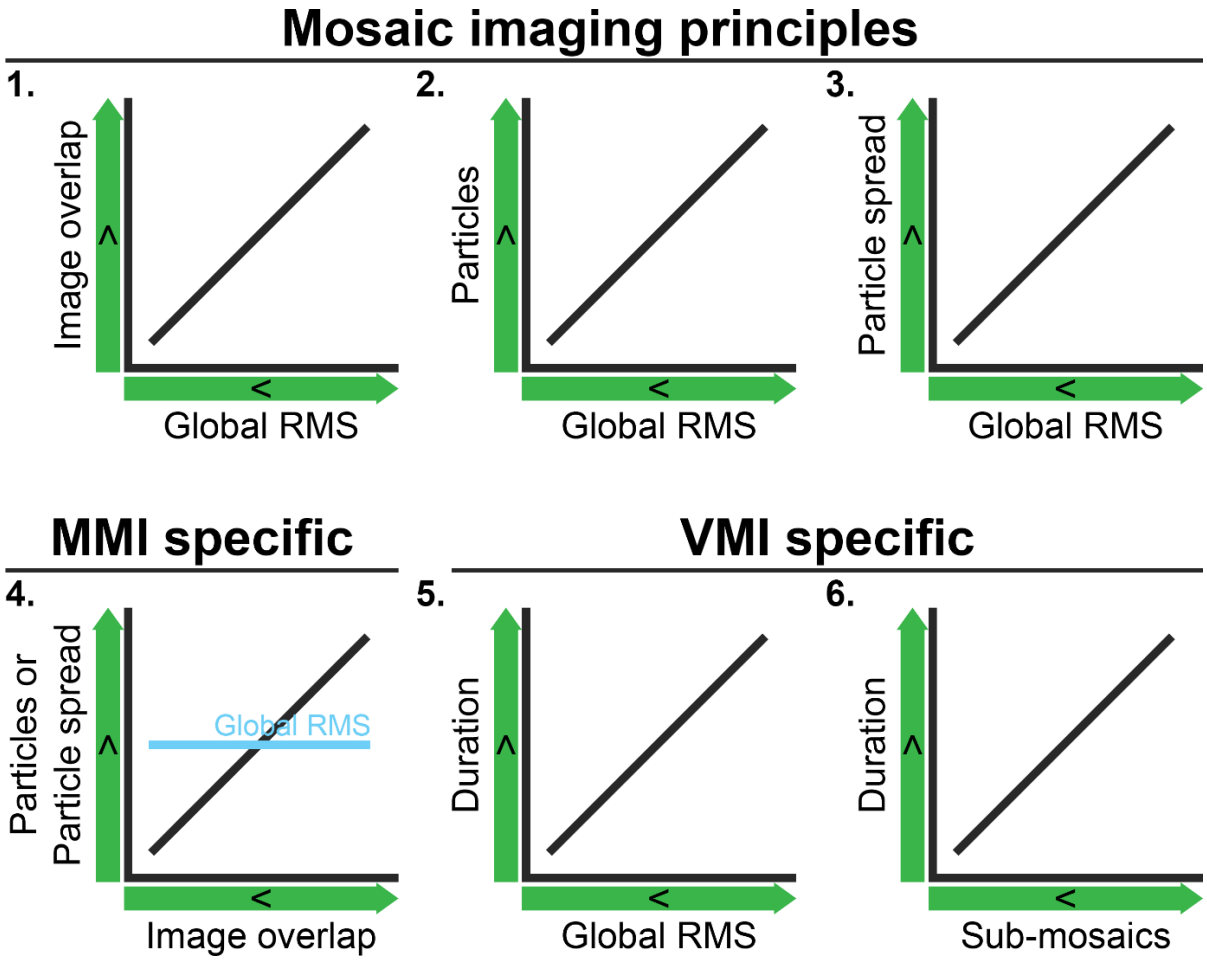

Fig. 14. MMI and VMI techniques depend on six principles that affect mosaic generation and quality. First, the three general principles for both MMI and VMI include the following: (**1**) as the image overlap increases, the Global RMS decreases (better mosaic quality); (**2**) as the number of particles increases, the Global RMS decreases; and (**3**) as the particle spread increases, the Global RMS decreases. Second, the MMI-specific principle is as follows: (**4**) To maintain the Global RMS value, more particles or higher particle spreads are required with fewer images. Third, the VMI-specific principles include the following: (**5**) as the video recording duration increases, the Global RMS decreases; and (**6**) longer video recording durations result in fewer sub-mosaics. Abbreviations include MMI: motorized mosaic imaging, VMI: video mosaic imaging, and RMS: root mean square.

Together, the MMI and VMI principles can act as guidelines to optimize sample screening and experimental setup. For example, when 10 wells have to be imaged containing high-particle numbers, an MMI setting of 1500×1500 would suffice. This setting requires only 25 min for

imaging, while in comparison, the MMI setting 500×500 requires approximately 3 h for imaging. Another example would be when particle number is low. Instead of using a 48-well plate, one could use a 96-well plate to increase particle density and simultaneously decrease imaging time. Similar optimization approaches are applicable for VMI. Therefore, while most mosaic settings and sample conditions resulted in complete mosaics, applying the principles can provide significant advantages, and therefore, demonstrates the flexibility of MMI and VMI. Overall, only these clear principles are needed to optimize experiments and mosaic imaging, with no need for an in-depth understanding of mosaic programming thanks to the low-cost commercial software.

In conclusion, we show that MMI and VMI are two appropriate and accessible techniques for the acquirement of mosaic images that encompass complete macro-scale areas containing all microscopic targets. We were able to successfully create mosaic images of 48-well-plate wells of 1.2 cm in diameter, which contained either cellular or synthetic samples. These could also be analyzed in a quantifiable manner for sample comparison. Therefore, we believe that the MMI and VMI techniques are broadly applicable for microscopy analysis and screening thank to their easy-to-use, high-flexibility, and low-cost properties, and therefore, will be of great value to scientists.

Chapter 3

Adipocyte Development of HGPS Stem Cells from pH-SKP Spheroids

Primary dermal fibroblasts cultures obtained from Hutchinson-Gilford progeria syndrome (HGPS)-suffering subjects can provide pH-SKP spheroids *in vitro* of which the stem cells have the remarkable ability to differentiate into adipocyte cells *in vitro*. This while patients themselves lack adipose tissue due to the disease.

3.0.1 Abstract

HGPS is a rare premature aging disease in children and is caused by a mutated form of the nuclear lamina protein lamin A, termed progerin. These children appear frail and old-aged and suffer symptoms such as subcutaneous fat loss, alopecia, and bone changes, resulting in a premature death between the 13th and 17th life year due to stroke or heart attack. A cure and various tools to investigate the disease are both lacking and scarce, respectively. In this chapter, the application of the novel pH-SKP isolation method was investigated with pre-established dermal HGPS fibroblasts as a tool to obtain naïve multipotent HGPS stem cells. HGPS pH-SKP spheroid formation was confirmed and analyzed for stemness at day 5 of culture. Stem cell markers nestin, CD9, Sox2, Oct4, and NANOG were investigated by immunohistochemistry and were found positive in HGPS pH-SKP spheroids. Multipotency was confirmed by *in vitro* differentiation of HGPS pH-SKPs into smooth muscle cells, fibroblasts, and remarkably also into adipocytes. Overall, our results show the applicability of pH-SKP isolation on pre-established dermal fibroblasts from a rare disease, and we propose this method as a cellular model for HGPS investigation to promote the development of a cure.

Keywords: adipocytes, adult stem cells, HGPS, pH-SKP isolation, progeria

3.0.2 Additional information

In this chapter, the novel pH-SKP method described in Chapter 1 is applied to HGPS-affected primary dermal fibroblast cultures to investigate the potential stem cell isolation and multipotent capability [15]. A less quantitative approach was taken in this third chapter compared to Chapter 1, and a higher focus was placed on a positive or negative outcome, such as whether HGPS fibroblasts can provide multipotent pH-SKPs cells or not. Additional quantitative data such as a range of different HGPS cell lines, spheroid yield, or differentiation efficiencies were reserved for future investigations as obtainment of such data was not possible due to the additional required time that exceeded what was available for this thesis.

3.0.3 Abbreviations

Abbreviation	Meaning
-CSIM	cysteine, serine, isoleucine, and methionine
Dex	dexamethasone
DNA	deoxyribonucleic acid
CTRL	control
DMEM	Dulbecco's modified Eagle medium
DNA	deoxyribonucleic acid
EGF	epidermal growth factor
FACE-1	farnesylated-proteins converting enzyme 1
FBS	fetal bovine serum
FGF	fibroblast growth factor
h	hours
HGPS	Hutchinson-Gilford progeria syndrome
IBMX	3-IsoButyl-1-MethylXanthine
ICMT	isoprenylcysteine carboxyl methyltransferase
IHC	immunohistrochemistry
min	minutes
mRNA	messenger ribonucleic acid
P4HD	prolyl-4-hydroxylase beta
PBS	phosphate buffered saline
pH-SKP	low pH stress isolated skin-derived precursor cells
RCE-1	Ras converting CAAX endopeptidase 1
RT	room temperature
s	seconds
SDS-PAGE	sodium dodecyl sulfate-polyacrylamide gel electrophoresis
SKP	skin-derived precursor
SMC	smooth muscle cells
SM-MHC	smooth muscle myosin heavy chain
ZmpSte24	zinc metallopeptidase STE24 homolog

Background and Introduction

In this subchapter, relative general information, basic components, and other related investigative techniques are discussed for Chapter 3. The results obtained for this project are mainly a culmination of previous chapters, and various page redirections will be made for previously described general or methodological information. The purpose of this subchapter is to provide fundamental information for readers unfamiliar in the field and provide means to increase their comprehension of the thesis' content and conclusions. The discussed topics will provide various answers to certain questions: "What is HGPS?" "How do people get it?" "What have previous studies shown?" etc. Additionally, the principles behind investigative techniques will be shortly discussed as well. However, details such as step-by-step protocols, material references, or machine models are not discussed in this subchapter. For this information, I kindly refer to the Materials and Methods subchapter of this chapter.

3.1.1 The nuclear lamina

The nuclear lamina is a dense network layer composed of intermediate filaments between the inner nuclear membrane and peripheral heterochromatin providing structure to nuclei found in almost all metazoans [40]. The nuclear lamina network consists mainly out of A- and B-type lamins, including A, C, B1, and B2, where lamin A and C are both A-type and lamin B1 and B2 B-type [120]. The study of the lamina network has become an important aspect as increasing evidence shows its multifaceted role not only in nuclear structural support but also for DNA replication, transcription, chromatin regulation, mitosis, and others [110, 139, 159]. Mutations in the lamin genes have shown to cause a broad range of diseases, collectively known as laminopathies. Multiple tissues have been found to be affected by laminopathies, including neuron, vascular, muscle, bone, and adipose tissue [123, 139]. An example of a laminopathy is the rare but well-known devastating premature aging disease HGPS, which is caused by the expression of a mutated lamin A, and will be the main subject of this chapter.

3.1.2 Lamin A

The transcription of lamin A originates from the LMNA gene, which also accounts for lamin C via alternative exon splicing [102]. The LMNA mRNA for lamin A is first translated as the precursor protein prelamin A and undergoes multiple post-translational modifications to reach its mature form lamin A [141]. Prelamin A contains a -CAAX motif (amino acids -CSIM: cysteine, serine, isoleucine, and methionine) at its C-terminal and can be farnesylated at the cysteine by farnesyltransferase. This step is followed by proteolytic cleavage of the -AAX (-

SIM) motif by the Ras converting CAAX endopeptidase 1 (RCE-1) or zinc metallopeptidase STE24 homolog (ZmpSte24, also known as FACE-1: farnesylated-proteins converting enzyme 1). The remaining farnesylated cysteine undergoes carboxymethylation by the isoprenyl-cysteine carboxyl methyltransferase (ICMT). Finally, ZmpSte24 removes the farnesyl moiety by proteolytic cleavage of the last 15 C-terminal amino acids, creating a nonfarnesylated mature lamin A [33, 128]. Certain anomalies in one of these steps can result in severe consequences. For example, when lamin A remains its farnesyl moiety, due to either a loss of the second cleavage site for ZmpSte24 or loss of ZmpSte24 itself, it causes the detrimental laminopathy disease HGPS [8, 47].

3.1.3 Hutchinson-Gilford progeria syndrome

HGPS—also known as progeria disease—is a rare premature aging laminopathic disease that mainly occurs in children. This mortal disease develops within 1 in every 4 to 8 million new-born babies worldwide [52]. Affected children appear healthy at birth but start to show phenotypic abnormalities between the first and third year in their development. These abnormalities include among others loss of subcutaneous fat, alopecia (loss of hair), bone changes, narrow nasal bridge, high-pitched voice, nail dystrophy, progressive joint contractures, and dental crowding [6, 61]. Even though a rare disease, it is relatively well-known because of various media coverage over the years and the apparent devastating premature aging effects on children. Therefore, a cure is highly desired and supported by many people.

HGPS is categorized as a laminopathy because its main perpetrator is progerin, an aberrant form of the nuclear lamina protein lamin A. As mentioned above, this nuclear protein is transcribed as a precursor protein from the LMNA gene, termed prelamin A, and normally undergoes multiple post-translational modifications before reaching maturation (lamin A) [141]. Here, two key post-translational processes are the farnesylation of prelamin A and the proteolytic cleavage of the same farnesyl moiety in a later stage by the zinc metalloproteinase enzyme ZmpSte24 [141]. The exact functioning of this temporary farnesyl moiety is not fully understood or at which stages its presence is most crucial; however, evidence suggests that the farnesyl moiety gives prelamin A higher affinity in order to be correctly located at the nuclear envelope for its incorporation into the nuclear lamina [24]. Failure to remove this farnesyl moiety at later stages from prelamin A results in the disruption of the nuclear lamina and nuclear membrane [22, 184]. As a consequence, aberrations in mitosis, DNA regulation, and other cellular mechanisms, such as DNA damage and the increase of harmful reactive oxygen species, cause a pathological phenotype [125, 126, 181].

The failure to remove the farnesyl moiety from prelamin A is the main cause for HGPS, see for a detailed description Prokocimer et al. [141]. Here, a *de novo* silent point mutation in the

LMNA gene (1824C > T, p. G608G) activates a cryptic splice site in the mRNA of the transcribed prelamin A and results in a 150-nucleotide mRNA loss. Within this loss, the recognition site for ZmpSte24 is included but not the CAAX motif required for farnesylation [39, 47]. As a result, during the post-translation modifications, prelamin A becomes permanently farnesylated. This mutant prelamin A protein is termed progerin and disrupts the nuclear lamina and causes blebbing of the nuclear membrane: a typical cellular phenotype of HGPS (Fig. 1). On the macro level, progerin particularly affects tissues of mesodermic origin such as fat, hair, skin, bone, teeth, blood vessels, and others [6, 61]. Overall, HGPS results in accelerated aging and premature death between the 13th and 17th life year, which is primarily caused by accelerated atherosclerosis and cardiovascular complications such as stroke or heart attack [6].

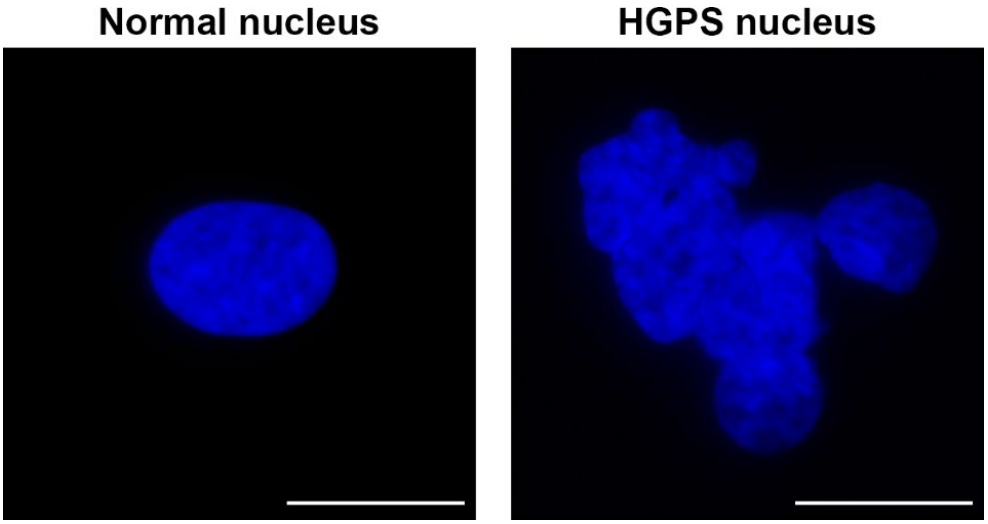

Fig. 1. HGPS nuclear blebbing. Image comparison between a normal nucleus and an HGPS-affected nucleus. DNA is stained with DAPI. Scale bar: 10 µm.

3.1.4 Adipose tissue and HGPS

Adipose (fat) tissue is widely seen as an unwanted type of tissue due to aesthetic values and increasing obesity prevalence in modern society. However, it has an underappreciated crucial role in the human body. Adipose itself is a loose fibrous connective tissue with fat harboring cells known as adipocyte cells. The main known function of adipocytes is the storage of triglycerides (fats), and the uptake or release depends on the energy available to the organism. In recent years, additional important functions of adipocytes have been discovered, including the secretion of hormones, growth factors, and pro-inflammatory cytokines that regulate various processes such as blood pressure, reproductive function, immune response, and angiogenesis among others [2, 35, 107]. Furthermore, secretion of so-called adipokines (e.g., Leptin) by adipocytes have shown to play a role in various obesity-related cancers, involving breast, prostate, and colon cancer [73, 161]. With all of these important functions, adipose tissue is now recognized as an endocrine/metabolic organ of the human body [192].

Adipose tissue can be divided into three main types: white, brown, and beige (also called brite). For a detailed review of these adipose types, please refer to [58, 150]. Briefly, white adipose tissue (WAT) is mainly responsible for energy storage in the form of fat. When the host has a higher energy intake than energy expenditure, WAT adipocytes increase in size and number. When the host has a lower energy intake than energy expenditure, WAT adipocytes reduce in size and number due to the fat energy usage. Brown adipose tissue (BAT), on the other hand, is mainly responsible for non-shivering thermogenesis [69, 150]. BAT adipocytes use their stored energy to generate heat from thermogenesis. This occurs when the host is directly exposed to a cold environment and requires BAT activation to maintain its internal body temperature. BAT levels are suggested to be highest in newborns in so-called BAT depots, which are located in the interscapular regions and around the kidney. These depots help newborns survive cold temperatures as they do not have enough muscle tissue for shivering to generate warmth. Finally, the beige adipose tissue, which also has the main function of non-shivering thermogenesis to generate heat [58]. The difference between beige and BAT tissue is that beige adipocytes are located in WAT tissue and are derived from WAT precursors [79]. Beige adipocyte differentiation is induced when the host is repeatedly exposed to cold, also in adults [79]. In this thesis, the focus was on WAT—from this point on referred to as adipose or adipocytes—and its influence, role, and status in HGPS patients.

Children suffering from HGPS lose and lack eventually adipose tissue in their first few years [64]. This partial or complete loss of adipose tissue is generally characterized as lipodystrophy and known among others to be caused by genetic disorder [2, 21, 179]. For example, mutations in the LMNA gene for lamin A have been associated with various lipodystrophy diseases such as Werner's syndrome, mandibuloacral dysplasia, and Dunnigan type familial disease, which all cause abnormalities in adipose phenotype [12, 20, 21, 151]. Similarly, mutations in the LMNA gene responsible for HGPS result in a lipodystrophy phenotype due to the loss of subcutaneous fat as well [64]. As mentioned previously, adipose tissue has a broad range of regulatory functions and improving adipose presence in HGPS might, therefore, aid the promotion of the children's health. Another interest to investigate HGPS and its lipodystrophy is the possible relation between the lack of cancer development seen in HGPS patients and mouse models [38, 50, 83, 190]. The mechanisms of this relationship might provide additional insight into cancer prevention and treatment related to obesity and adipokines [13]. Furthermore, understanding the relationship between prelamin A, lamin A, and progerin on adipose inhibition might provide information for therapy development against obesity. Overall, a further understanding of adipose development and its lack in HGPS patients will provide valuable insights for future therapies.

3.1.5 Normal aging and prelamin A

In normal aging, farnesylated prelamin might also play a crucial role. However, most studies have focused mainly on the presence or integrity of abnormal lamin A or prelamin A in a pathological viewpoint. This is most likely because the LMNA gene is known for a broad range of possible mutations and that abnormal lamins are the primary cause of nuclear lamina integrity malfunction [36]. However, the few studies available have shown that elevated prelamin A levels in certain pathological traits were not caused by mutation. For instance, a study performed by Candelario J. et al. showed that elevated levels of wild-type prelamin A of 10% in human fibroblasts caused progeroid phenotypes and increased cellular senescence [17]. They also found significantly increased prelamin A levels in aged but normal cells, and high prelamin A levels and progeroid phenotypes in fibroblasts from old-age individuals were reported. In contrast, such high levels were absent in fibroblasts from young individuals. This indicates that lamin A metabolism might represent an important role in normal human aging [17]. Furthermore, a study from Ragnauth C.D. et al. showed that prelamin A accumulation was found in atherosclerotic lesions from aged individuals and co-localized with senescent and degenerate vascular smooth muscle cells [142]. Additionally, the mutant form of lamin A (progerin) that causes HGPS was found to be a biomarker of cellular aging in human skin [115]. Progerin is also involved in the cardiovascular pathology of HGPS, and a correlation has been found with the vascular pathology of normal aging [132]. These data have shown that the prevalence of prelamin A on normal aging is important and that progerin is also involved in healthy people. Further investigation of the mechanisms of HGPS and the aberrant prelamin A protein progerin might reveal valuable information concerning normal aging as well.

3.1.6 HGPS treatment

HGPS is known as a mortal disease with no cure and results in the premature death of affected children. Since the first clinical description in 1886 and 1897 by Jonathan Hutchinson [78] and Hastings Gilford [57], respectively, progress for treatment has been slow. It was not until 2003 that the responsible gene and mutation was found; a breakthrough pushed by the Progeria Research Foundation [47]. This was immediately followed by new treatment strategies. The consensus became that prevention of the farnesyl moiety on prelamin A would prevent progerin formation, and thus, the aberrant incorporation and distortion of the nuclear lamina. The focus was placed on a drug termed lonafarnib, which was originally developed for cancer and known as a farnesyltransferase inhibitor (FTI). The drug provided the means to inhibit farnesyltransferase and suppresses the farnesylation of prelamin A [23]. Similar FTI-type drugs quickly advanced into clinical trials for HGPS patients with the first completed in 2012 by Gordon et al. [62]. The outcome was encouraging as statistical improvement in weight,

cardiovascular health, and bone mineral density was reported in most of the 26 patients. However, these improvements were modest, did not account for the whole group, included side effects (mild diarrhea, fatigue, nausea, and vomiting), and no improvement of adipose tissue formation was reported. Also, the clinical values were significantly lower than the normal values of similar aged healthy children. Nonetheless, in a recent survival study by Gordon et al. [63], it was reported that compared to untreated and treated HGPS patients, the treatment resulted in a significant increase of mean survival by 1.6 years for the treated patients. Seemingly small, this number does account for an average increase of 12% in lifespan, emphasizing the importance of clinical trials and the development of a treatment. In sum, more studies are required to investigate additional or complementary treatment options to improve HGPS children's living conditions and further increase their lifespan.

3.1.7 pH-SKP cells as an *in vitro* model for HGPS

While the strategy to prevent farnesylation of prelamin A with FTIs has shown some success, other strategies need to be sought to further improve the lives of HGPS patients. Therefore, further insights into the molecular and cellular mechanisms of HGPS cells are needed. We hypothesize that the pH-SKP isolation method (see Chapter 1) could also be applied to pre-established HGPS fibroblast cultures to isolate naïve multipotent HGPS pH-SKP stem cells. Such cells would provide a multitude of possibilities. For example, other cell types (e.g., neurons and smooth muscle cells) could be obtained without invasive biopsies. Additionally, highly-controlled *in vitro* conditions provide an optimal environment for fundamental studies and drug testing. Overall, successful isolation of HGPS pH-SKPs would bring many advantages, which includes the reduction of stress placed on children suffering from HGPS.

3.2 Methodology Used

In this study, the used methodology overlaps with the methodology of Chapter 1. Such methods include general fibroblast cell culture, pH-SKP isolation and culture, pH-SKP differentiation, and immunohistochemistry protocols. Those page numbers will be given in this chapter if the reader desires to read it. Additional information regarding the used methodology not discussed previously will be additionally discussed in this subchapter. This includes, for example, protein separation and detection by SDS-PAGE and western blot. After this subchapter, a detailed step-by-step protocol for each method mentioned is described in the Materials and Methods. This to provide the means and full understanding for exact repetition and validation by other scientists.

3.2.1 Culture of HGPS cell lines

The used biological material comprised of primary dermal fibroblast cell lines originally obtained from HGPS patients. The HGPS cell lines were obtained and cultured similarly as the normal fibroblast cell lines as described in Chapter 1 (pages 27 to 29). Differences between normal and HGPS were found in cell morphology and proliferation speed. HGPS cells showed more irregular shaped fibroblasts and required more time to attain a certain confluent state compared to normal fibroblasts (Fig. 2). When performing comparison experiments with normal and HGPS cell lines, the slower growth had to be taken into account when preparing experiments. For example, frozen samples of HGPS cell lines in vials were thawed and cultured earlier than normal cells to provide additional time for them. Additionally, HGPS cells grew at a lower density than what was possible with normal ones, and more dishes were required to reach a similar HGPS cell number compared to normal cells.

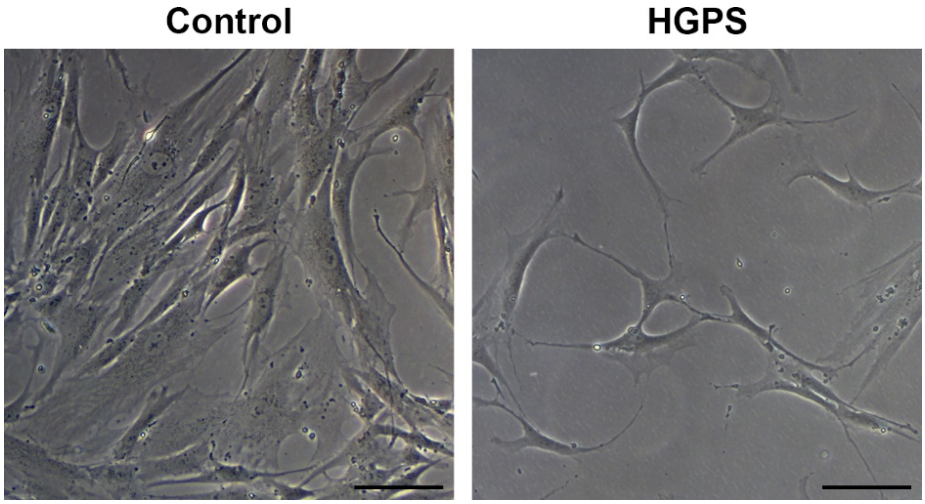

Fig. 2. Monocultures of control cells grow faster and more uniform than HGPS cells. Scale bar: 100 µm.

3.2.2 SDS-PAGE and western blot

Regarding HGPS cells, the key components of the disease are the aberrant protein progerin and lamin A but also the ratio relation with lamin C. Detailed analysis of these proteins is therefore required. This includes the methodology mentioned in previous chapters such as polymerase chain reaction (PCR) and immunohistochemistry. Additionally, in this HGPS chapter, additional analysis methods are introduced, such as SDS-PAGE (sodium dodecyl sulfate-polyacrylamide gel electrophoresis) and western blot. Here, three separate techniques are involved: protein acquirement and separation based on molecular protein size, protein transfer onto a membrane, and the visualization of the protein of interest via chemiluminescence. All three techniques' methodology and principles will be shortly described in this subchapter. Together, they provide quantitative data of the proteins of interest.

The first step of the SDS-PAGE and western blot protein quantification process is protein separation by SDS-PAGE. The cells are lysed to prepare a protein mixture and are then placed on top of an SDS-PAGE gel. Similar to the agarose gel electrophoresis for DNA separation, the SDS-PAGE also uses a gel containing a density matrix. This gel, however, stands vertically and is placed between two glass plates. A negative electrode is then placed at the top of the gel where the samples start and a positive one at the bottom of the gel. Because the protein mixture is negatively charged, it is pulled downwards into the gel. Large proteins will move slower through the gel due to the gel matrix and smaller proteins faster, which then results in protein separation. So, with our proteins of interest, lamin A (75 kDa) will remain the highest in the gel, followed by progerin, which has lost 50 amino acids, and then lamin C (70 kDa). However, these proteins cannot be seen with the naked eye inside the SDS-PAGE gel, and further steps are required for visualization and quantification.

The SDS-PAGE separated proteins are further processed by the western blot technique. With this technique, the proteins inside the SDS-PAGE gel can be transferred onto an Amersham Hybond-N membrane. The SDS-PAGE gel is placed between a sandwich of papers and the membrane. Then, a negative electrode is placed on the gel side of the sandwich and the positive electrode on the membrane side. The proteins are pulled toward the positive electrode and to the membrane and are then bound on it. After all the proteins have been transferred onto the membrane, they can be visualized by a bioluminescence technique.

The immunohistochemistry and bioluminescence techniques are applied to visualize proteins. After protein transfer by western blot, the proteins are on the Amersham Hybond-N membrane separated by their weight (in kDa). To visualize the proteins of interest, specific antibodies are used, which include a primary and secondary antibody. The second antibody contains a horseradish peroxidase (HRP) group, which upon contact with a chemiluminescence substrate provides a detectable bioluminescence signal. The obtained images from these signals can then be used to compare protein bands and provide quantitative data.

3.3 Materials and Methods

In this paragraph, the materials and methods used in this chapter are described in detail. First in an overview and then as an exact step-by-step protocol. The step-by-step protocol is provided because the focus of this thesis lays on method and technique development. Knowledge for precise execution is therefore required. By following the step-by-step protocol, one can exactly repeat the performed experiments. In addition to the step-by-step protocol, the specific reagents and media will also be provided.

3.3.1 Cell culture

The control primary dermal fibroblast cell line GM05565 was obtained from Coriell Institute (New Jersey, USA) and the HGPS cell line HGADFN003 and mandibuloacral dysplasia (MAD) PSADFN318 from the Progeria Research Foundation (Peabody, USA). The above cell lines were all human and established originally from skin biopsies and were used in experiments at passages between 12 and 21. The fibroblast cell lines were cultured as a monoculture in DMEM (Sigma, D6429) containing 15% fetal bovine serum (FBS, ThermoFisher-Gibco, 10270106), 1%L-glutamine (ThermoFisher-Gibco 25030081), 1% penicillin/streptomycin (ThermoFisher-Gibco, 1514022), and 0.4% gentamycin (ThermoFisher-Gibco, 15710049). Fibroblasts were cultured and used when approximately 80% confluent. All fibroblasts cultures were maintained in a humidified cell incubator (Binder, 9140-0046) at 37°C and 5% CO_2.

Cell culture: step-by-step protocol.

Required media:

Fibroblast culture medium:
The following was added to a bottle of 500 mL of DMEM (Sigma, D6429): 75 mL of FBS (final concentration 15%), 5 mL of penicillin/streptomycin (final concentration 1%), 5 mL of glutamine (final concentration 1%), and 2 mL of gentamycin (final concentration 0.4%). All the contents were mixed, and the bottle stored at 4°C until use.

Cell culture:

1. The vial containing the cells was taken out of the cryogenic storage and placed at room temperature (RT) to thaw. After approximately 10 to 15 min, the cells were transferred into a 50-mL tube containing 5 mL of fibroblast culture medium.
   Note: For HGPS cell lines this step was done 2–3 weeks earlier compared to the normal fibroblasts because of their slower proliferation.

2. The emptied vial was then rinsed once with 5 mL of culture medium. This volume was added to the 50-mL tube.
3. The 50-mL tube containing all the cells from the vial was then centrifuged at 450 × g for 5 min at RT to pellet the cells.
4. After centrifugation, the supernatant was aspirated. About 10 to 20 mL of sterile phosphate buffered saline (PBS) was added to wash the cells once. The previous centrifugation step was repeated.
5. After the second centrifugation step, the supernatant was aspirated, and the cells resuspended in fibroblast culture medium. The volume of this medium depended on the number of dishes prepared for culture. In general, one vial was divided over five cell culture dishes or between 2×10^5 and 3×10^5 cells per dish. In this step, 10 mL of fibroblast culture medium was added to the cell pellet for resuspension and was then divided into 2 mL aliquots per dish. Before adding the cells, 6 mL of fibroblast culture medium was added to each new dish. The final volume including cells equaled 8 mL.
6. After adding the cells to the dishes, the dishes were gently agitated by a swirling motion to homogenize the cells throughout the medium and spread them over the dish.
7. The culture dishes were then placed into the cell incubator. This incubator was set at 37°C and 5% CO_2. Every Monday, Wednesday, and Friday, the medium was aspirated and refreshed with 8 mL of fresh fibroblast culture medium.
8. When the cells became approximately 80% confluent, they were either divided into more dishes or used for experimentation.

Dividing one cell culture population from one culture dish into multiple:

1. The dishes containing the cells were taken out of the cell incubator and placed in the biosafety cabinet that maintained a sterile working area.
2. The medium was aspirated from each dish, and 8 mL of sterile PBS was added to wash the cells and remove any FBS residue.
3. The dish with PBS was gently agitated via a swirling motion followed by aspiration.
4. Then, 0.5 mL of trypsin was added directly on top of the cells. The trypsin was spread over the whole dish by tilting it in all directions. The dishes with trypsin were then incubated for 10 min in a cell incubator at 37°C.
5. After incubation with the trypsin, fibroblast culture medium was added to each dish to stop the trypsin's enzymatic reaction and collect the cells. In general, 9 to 10 mL of fibroblast culture medium was added to the first dish. With this volume, the dish was gently sprayed to collect the cells and detach any remaining cells. The same suspension was then used for the next two or three dishes for cell collection. After those dishes, a fresh volume of 9 to 10 mL culture medium was added to the next dish. The

same process was repeated for all dishes. The total cell suspension of one cell line was then collected into a 50-mL tube.

6. After collecting all the cells, they were centrifuged 450 × g for 5 min at RT.
7. The supernatant was aspirated and the cells resuspended in fresh fibroblast culture medium. The amount of volume depended on the number of dishes prepared. For each newly prepared dish, 2 mL of fibroblast culture medium was added to the cell pellet. For each new dish, 6 mL of fresh fibroblast culture medium was pre-deposited. In general, either 1 dish with cells was divided over 3 to 5 new ones (depending on the proliferation speed of the culture) or between 2×10^5 and 3×10^5 cells per dish. After mixing the cells in the freshly added culture medium via careful pipetting with a 5- or 10-mL pipet, 2 mL of the cell mixture was added to a new dish containing the pre-deposited fresh 6 mL medium. This mixture was then mixed via careful swirling.
8. The new dishes with cells were placed in the cell incubator providing 37°C and 5% CO_2. When 80% confluent, either above steps were completely repeated, or the cells were used for experimentation after step six.

3.3.2 Isolation protocol of HGPS pH-SKPs

Primary fibroblast cultures were collected by trypsin (≤80% confluent). The cell suspension was pelleted at 450 × g for 5 min at RT and then washed with sterile PBS. One million cells were resuspended in 500 µL of pH-adjusted HBSS (ThermoFisher-Gibco, 14175053) buffer. The pH of the HBSS buffer was adjusted with HCl (Merck, 1.00319.2500, Hohenbrunn, Germany) to a pH of 5.7. Cells resuspended in HBSS pH 5.7 were incubated for 25 min at 37°C and 5% CO_2 and agitated every 5 min. Thereafter, the cell suspensions were centrifuged 450 × g for 5 min at RT. In total, the cell suspensions were exposed for 30 min to the HBSS (pH 5.7), which included a 25-min incubation and a 5-min centrifugation step. Next, each pellet (containing one million cells) was resuspended in 6 mL of classic SKP medium (4:1 – DMEM [ThermoFisher-Gibco, 21885025]: F12 [ThermoFisher-Gibco, 21765029], 20 ng/mL EGF [ThermoFisher-Gibco, PHG0311], 40 ng/mL bFGF [ThermoFisher-Gibco, PHG0026], 2% v/v B27 [ThermoFisher-Gibco, 17504044], 0.5 µg/mL Fungizone [ThermoFisher-Gibco, 15290018], and 100 U/100 µg/mL penicillin/streptomycin [ThermoFisher-Gibco, 1514022]) and divided equally over two T25 non-treated flasks. Cells were fed every other day with 10× SKP medium (SKP medium with 10× concentrated EGF, bFGF, and B27) diluted to a final concentration of 1× in culture medium and agitated daily by pipetting up and down to prevent clumping and cell adherence to the plastic flask.

Low pH SKP isolation and culture (pH-SKPs): step-by-step protocol.

Required media:

Table 1. 1× SKP medium – used for SKP isolation.

	Total volume	10,000	µL		
	Times concentrated	1			
	Material			**End concentration**	
1	DMEM (low glucose) Gibco, 21885-025	7,255.5	µL		
2	F12 Gibco, 21765-029	2,418.5	µL		
3	EGF (0.1 mg/mL) ThermoFisher-Gibco, PHG0311	2	µL	20	ng/mL
4	bFGF (0.1 mg/mL) ThermoFisher-Gibco, PHG0021	4	µL	40	ng/mL
5	B27 ThermoFisher-Gibco, 17504044	200	µL	2%	v/v
6	Fungizone (250 µg/mL) ThermoFisher-Gibco, 15290018	20	µL	0.5	µg/mL
7	Pen/Strep (10,000 U/10,000 µg/mL) ThermoFisher-Gibco, 1514022	100	µL	100 U/100	µg/mL

Table 2. 10× SKP medium – used for SKP feeding.

	Total volume	10,000	µL		
	Times concentrated	10			
	Material			**End concentration**	
1	DMEM (low glucose) Gibco, 21885-025	5,865	µL		
2	F12 Gibco, 21765-029	1,955	µL		
3	EGF (0.1 mg/mL) ThermoFisher-Gibco, PHG0311	20	µL	200	ng/mL
4	bFGF (0.1 mg/mL) ThermoFisher-Gibco, PHG0021	40	µL	400	ng/mL
5	B27 ThermoFisher-Gibco, 17504044	2,000	µL	20%	v/v
6	Fungizone (250 µg/mL) ThermoFisher-Gibco, 15290018	20	µL	0.5	µg/mL
7	Pen/Strep (10,000 U/10,000 µg/mL) ThermoFisher-Gibco, 1514022	100	µL	100 U/100	µg/mL

Stock preparation notes for SKP medium:

See for detailed descriptions of stock preparation the notes of Chapter 1 page 60.

Hank's balanced salt solution (HBSS) pH 5.7:

1. The pH of HBSS (Gibco, Life Technologies, 14175-053) was adjusted to 5.7 by using HCl (Merck, 1.00319.2500, Hohenbrunn, Germany).
   Note: The following steps took 1 to 2 days.
2. A 500-mL HBBS bottle was emptied into a 1-L beaker and HCl was added until the desired pH level (pH 5.70) was reached and stable for at least 1 h. If the pH would change again in this period, it was adjusted again, followed by a 1-h attempted wait again.
3. The final solution was filtered by a 0.2 µm Minisart (Sartorius Stedim, 16534) filter to sterilize it.
4. The filtered HBSS was then aliquoted in 50- and 15-mL tubes and stored at 4°C until use. It is recommended to re-measure the pH after 1 year.

Low pH SKP protocol (pH-SKPs):

1. At least 2 days before following the pH-SKP isolation protocol, pH-adjusted HBSS was prepared, see above.
2. Before starting the isolation protocol, pH-adjusted HBSS was placed at RT to acclimatize.
3. Primary fibroblasts were used that were previously cultured with normal fibroblast medium (DMEM: 15% FBS, 1% Glutamine, 1% Pen/Strep [10,000 U/10,000 µg/mL], and 2 mL Gentamicin).
4. The used cells for SKP isolation were at least 60% confluent and not above 80%. Importantly, for all SKP conditions the monoculture cells never reached or had reached a confluent state of above 90% in their culture history.
5. When the cells were ready, they were detached via the trypsin protocol, described previously (page 29). Briefly, the culture medium in the cell culture dish was aspirated followed by the addition of 8 mL of sterile PBS. The dish was rinsed by carefully tilting it. Then the PBS was aspirated, and to each dish, 0.5 mL of trypsin was added. All dishes were then placed into the cell incubator providing 37°C. After 10 min of incubation, the cells were collected in fibroblast culture medium, transferred to a 50-mL tube and centrifuged 450 × g for 5 min at RT.
6. The supernatant was aspirated, and the cells were resuspended in sterile PBS. The volume of PBS was usually around 20 mL per tube. This cell suspension was then used to determine the cell concentration via a cell hemocytometer. This was done either via the Muse viability assay according to the manufacturer’s instructions or a counting chamber (Neubauer Chamber) in which 5 µL of cell suspension was inserted to each side.

7. After determining the cell concentration, the cells were transferred with one million per 15-mL tube. These cells were then centrifuged 450 × g for 5 min at RT. The supernatant was then aspirated.
8. The cells were resuspended in 500 µL of HBSS and carefully mixed with a 1000-µL pipet tip while avoiding any bubble formation. The 15-mL tubes were then placed vertically into a cell incubator at 37°C and 5% CO_2.
9. The cells were agitated every 5 min to homogenize the descended cells again.
10. After 25 min, the cells were placed in a centrifuge and centrifuged 450 × g for 5 min at RT. In sum, the total incubation time in pH-adjusted HBSS solution was in total 30 min.
11. After centrifugation, the acidic supernatant was carefully removed via aspiration. The cells were then gently resuspended in 6 mL of SKP medium per 15-mL tube (see Table 2). Per T25 flask, 3 mL of the cell suspension was transferred, totaling the cell number at 0.5 million per flask.
12. The cap of the flasks was left partially unscrewed to allow air circulation. The flasks were then placed into a cell incubator for culture.
13. Every day the cells were resuspended once by using a 5- or 10-mL pipet and gently spraying the medium over the bottom of the flask to promote a suspension culture.
14. After 2 days of culture, the cells were fed by adding 10× concentrated SKP medium (including 10× EGF, FGF and B27, see Table 3) by diluting it with the main previously volume (e.g., 3 mL previous volume + 333 µL 10× SKP medium). The feeding was repeated every other day.
15. At days 3, 5, and 7, the spheroids were taken out for mosaic imaging analysis to determine the culture yield.

3.3.3 Real-time quantitative PCR (qPCR) of lamin A and C

For the qPCR, the reactions occurred in volumes of 15 µL. This 15 µL consisted out two parts. One part contained the primers and reaction mix and the other cDNA and water (please see for an example Chapter 1, page 51). In each 15 µL of volume, 20 ng of estimated cDNA was used per reaction as starting material for the PCR amplification. Additionally, each reaction contained 300 nM of each primer, see Table 3 for further primer information. All samples were performed in triplicate per unique sample and placed in the qPCR apparatus (Mx3000P, Agilent Genomics) that executed the PCR program, as shown in Table 4.

Table 3. Primer design.

Primer (5' to 3')	Target Gene	Product Size (base pairs)	Primers (nM)	Info
FW: CTCTGCTCCTCCTGTTCGA REV: TTAAAAGCAGCCCTGGTGAC	GAPDH	144	300 300	[59]
FW: CTGAGTACAACCTGCGCT REV: GAGTGACCGTGACACTGG	Lamin A	141	300 300	
FW: GTGGTAGCCGCCGCTGAG REV: TTGGCACGGGGAGGCTGG	Lamin C	85	300 300	

qPCR: step-by-step protocol.

1. See qPCR Chapter 1, pages 39 to 45 and 50 to 53 for detailed instructions.

3.3.4 Cryosectioning and immunohistochemistry of HGPS pH-SKPs

The same techniques were used for HGPS pH-SKPs as for normal pH-SKP spheroids. For detailed spheroid cryosectioning and immunohistochemistry methods, please see pages 53 to 58.

3.3.5 Western blot analysis

Cell pellets were resuspended extensively in Laemmli sample buffer (Bio-Rad, 161-0737), and western blots were performed as described previously [114]. After protein separation and transfer onto the Amersham Hybond membrane, bound proteins were incubated for 1 h at RT with the primary antibodies. These included the 1:4,000 diluted anti-lamin A/C (Thermo Fischer, mab636), which also binds to progerin, and the 1:1,000 diluted anti-GAPDH (Sigma, G8795). The membranes were then incubated with the corresponding second antibody containing horseradish peroxidase (Jackson ImmunoResearch Laboratories) and incubated 1:5,000 for 1 h at RT. Proteins were visualized using chemiluminescence detection (ECL substrate, Bio-Rad 1705061). The signal was recorded with the Chemidoc MP Imaging System (Bio-Rad) and analyzed with Image Lab 5.2.1 software (Bio-Rad). Protein signals were quantified by normalizing to GAPDH as indicated.

3.3.5A Western blot analysis, sample preparation: step-by-step protocol.

Required media:

Table 4. The components of LB-buffer.

Component	Amount
LaemmLi sample buffer (Bio-Rad, 161-0737)	5.7 mL
β-mercaptoethanol (Bio-Rad, 161-0710)	300 µL
Protease inhibitor cocktail (Sigma, P8340)	60 µL
200 mM Phenylmethylsulfonyl fluoride (Sigma, 000000010837091001)	30 µL

Sample preparation for western blot with monocultures:

1. Control cells were first obtained from fibroblast cultures that were also used for pH-SKP isolation. About one million cells were collected optimally for western blot and 0.2 minimally. The remaining cells were used for pH-SKP isolation (requiring 1 million to make two flasks).
2. The trypsin detachment protocol was used to obtain adhered cells, see Chapter 1, page 29.
3. After obtaining detached cells in suspension, they were washed with PBS and transferred into a 1.5-mL Eppendorf tube.
4. This tube was centrifuged 450 × g for 5 min at RT to pellet the cells. The supernatant was aspirated, and 200 µL of LB-buffer (Table 4) was added.
5. The pellet was thoroughly mixed by pipetting 20–30× up and down with a 100-µL pipet tip. Bubble formation was avoided as much as possible. In general, cell pellets from monocultures quickly dissolved at this point.
6. The sample was then incubated 1 min on a 95°C heat-block.
7. Samples were then vortexed for 10 s. Step 5 was repeated if the sample was not completely dissolved.
8. The sample was then incubated 2 min on a 95°C heat-block.
9. The sample was placed on a vortex again for 10 seconds to mix.
10. The sample was allowed to cool for 15 min before placement in a −20°C freezer.

Sample preparation for western blot with spheroid cultures:

1. After pH-SKP isolation, the spheroids were collected into a 50-mL tube and washed with PBS.
2. The supernatant was partly aspirated. Then, the spheroids were transferred into a 1.5-mL Eppendorf tube.

3. The tube was centrifuged 450 × g for 5 min at RT to pellet the spheroids and aspirate the supernatant.
4. Then, 200 µL of LB-buffer (Table 4) was added.
5. The pellet was thoroughly mixed by pipetting with a 100-µL pipet tip (20–30×). Bubble formation was avoided.
6. The sample was then incubated 1 min on a 95°C heat-block.
7. Afterward, the sample was vortexed for 10 seconds. For spheroids, the lysis step in LB-buffer always proved to be very difficult, and extensive pipetting was required in general. This could take up to 15–30 min of total pipetting per sample.
8. The sample was then incubated again for 2 min on a 95°C heat-block.
9. Afterward, the sample was vortexed for 10 seconds again. If the sample was still not completely dissolved, it was pipetted again extensively, but the heating steps were not repeated again to prevent damage to the proteins.
10. The sample was allowed to cool down for 15 min before placement in a −20°C freezer or used for dot-blot analysis and SDS-PAGE protein separation (as described below).

3.3.5B Western blot analysis and dot-blot analysis: step-by-step protocol.

The protein concentration was determined by dot-blot analysis before SDS-PAGE. Dot-blot analysis uses a bovine serum albumin (BSA) standard with known protein concentrations, see Table 5. The unknown samples (e.g., origin fibroblasts and pH-SKPs) were compared with these values to determine the protein concentration. Based on this determined concentration 30 µg protein was prepared for each sample for the SDS-PAGE.

Table 5. BSA standard.

Standard	**End concentration**	**Laemmli buffer**	**BSA solution (ThermoFisher, 23209)**
S1	2,000 µg/mL	0 µL	300 µL BSA Stock (2,000 µg/mL)
S2	1,500 µg/mL	125 µL	375 µL BSA Stock (2,000 µg/mL)
S3	1,000 µg/mL	325 µL	325 µL BSA Stock (2,000 µg/mL)
S4	750 µg/mL	175 µL	175 µL S2
S5	500 µg/mL	325 µL	325 µL S3
S6	250 µg/mL	325 µL	325 µL S5
S7	125 µg/mL	325 µL	325 µL S6
S8	25 µg/mL	400 µL	100 µL S7
Blank	0 µg/mL	400 µL	0 µL

1. Before protein concentration determination, the BSA standard series were made according to Table 5. The BSA standard was stored at RT and could be used for up to 1 year, or when the blue color of Laemmli buffer changed into green or yellow.
2. Frozen protein samples were first allowed to thaw at RT for up to 0.5–1 h.

3. A piece of 6 × 8 cm Amersham Hybond blotting membrane paper (VWR, 10061-494) was cut and kept dry.
4. The samples and BSA standard were vortexed 3 × 10 seconds to mix.
   Note: The samples were always thoroughly mixed to reduce protein aggregation and precipitation and promote homogenization.
5. The samples were diluted 1 to 5 by adding 2 µL of sample with 8 µL of Laemmli buffer.
6. The dots were made by placing a 2 µL drop of BSA standard, pure sample, or 1:5 diluted sample on top of the membrane. Here, the BSA standard was placed in quadruplicates and the sample as one pure one with next to it the diluted ones in triplicate, as shown in the following scheme:

BSA Standard		**Samples (pure / dilutions)**
OOOO S1 (A, BSA 2,000 µg/mL)	OOOO S6 (F, 250 µg/mL)	O OOO (sample 1)
OOOO S2 (B, 1,500 µg/mL)	OOOO S7 (G, 125 µg/mL)	O OOO (sample 2)
OOOO S3 (C, 1,000 µg/mL)	OOOO S8 (H, 25 µg/mL)	O OOO (sample 3)
OOOO S4 (D, 750 µg/mL)	OOOO Blank (I, 0 µg/mL)	O OOO (sample 4)
OOOO S5 (E, 500 µg/mL)		O OOO (sample 5, etc.)

Note: The last four BSA standard concentrations (marked orange in the scheme) were marked by pencil because the washing steps would render them invisible.

7. The dotted membrane was completely dried at RT or shortly in a drying incubator set at 37°C. This drying process would bind the proteins in the placed dots to the Amersham Hybond blotting membrane.
8. After drying, the membrane was placed in Milli Q water to gently wash away the blue color from the LB-mix (if needed the Milli Q water was refreshed).
9. The membrane was then transferred to a container with Ponceau S solution (Sigma, P7170). The amount of solution added was enough to cover the membrane completely.
10. For several minutes, the membrane was stained. After staining, the Ponceau S solution was re-collected for re-use for another membrane.
11. The membrane was then washed in Milli Q water until the background became white. The previously placed dots containing protein material should stay purple. The dot would be more purple and intense with more protein compared to dots with less protein.
12. After washing, the membrane was placed inside the Chemidoc MP Imaging System (Bio-Rad) and then analyzed with the help of the Image Lab 5.2.1 software (Bio-Rad).

3.3.5C Western blot analysis with Image Lab 5.2.1 software: step-by-step protocol.

1. After placing the membrane inside the Chemidoc MP Imaging System, the software Image Lab was started. Then, “new file” was chosen, followed by “single channel,” “application,” “blot,” “colorimetric,” and then “position gel.”
2. The membrane was placed correctly in front of the camera. Then, “run protocol” was selected in the software.
3. After obtaining the images of the dots in black and white, “Lane and Bands” was selected in the Analysis Tool Box.
4. For each column, a lane was added, and for each dot, a band was added.
5. Then, in “Quantity Tools” the concentration values for each BSA standard dot were inserted per respective dot.
6. By clicking on the menu option “Standard Curve,” the standard curve created by the BSA standard series was generated. This window was then used to remove any abnormal values to improve the accuracy of the slope.
7. Then, by clicking on the menu option “Analysis Table,” the values of each sample were shown. The column “Abs. Quantity” represented the protein concentration of a specific band in a specific lane that included the protein sample dot.
8. The obtained concentrations per sample were used for a 30-µg protein preparation required for the SDS-PAGE protein separation.

3.3.5D Western blot analysis and SDS-PAGE: step-by-step protocol.

Table 6. 10× running buffer.

Component	**Amount**	**Final concentration**
Glycin (Sigma, G7126)	144 g	1.92 M
Tris-Base (Sigma, T1503)	30 g	248 mM
SDS (Sigma, 3771)	10 g	1%
Milli Q water	1 L	-

1. A 10× running buffer solution was made according to Table 6.
2. From the 10× running buffer, a 1 × solution was made by adding 100 mL 10× running buffer to 900 mL Milli Q water.
3. A 4–20% Mini-Protean TGX precast gel (Bio-Rad, 4561093) was prepared by unpacking it and removing the green tape at the bottom of the gel.
   Note: Removal of the green tape is essential and can be easily forgotten.
4. The gel was placed in the gel holder with the openings of the slots toward the inner chamber.

5. The inside of the chamber (the area between two fixed gels) was filled with 1× running buffer until the slots were submerged. In this phase, there was the opportunity to inspect for any leaks. In case of leaks, the gels were re-fixed in their respective holders.
6. Samples for the SDS-PAGE were prepared as a 30 µL volume containing 30 µg protein by diluting pure protein sample with Laemmli buffer. The concentrations of the pure protein samples were obtained during dot-blot analysis (see page 148 and 150).
7. All samples were then mixed thoroughly by vortex before gel loading.
8. First, 6 µL of protein marker (Bio-Rad, #1610394) was added in the first slot.
9. Then, a total of 30 µL of sample was added with a 10-µL pipet and tip. (The 10-µL pipet was used to improve accuracy.)
10. After loading the gel, the chamber was carefully placed on the desired location. The outer chamber was then filled with 1× running buffer.
11. The gel was run at 200V for 70 min, or until the 20 kDa marker line of the protein marker reached the black line located on the plastic of the gel cast.
12. If the protein transfer occurred on the same day, preparations were made while running the SDS-PAGE, see below “protein transfer: step-by-step protocol” step 1 to 4.
13. After completion of the run, the gel was released from its contraption. The plastic encasing was carefully removed, and the SDS gel itself released in a container with Milli Q water.

    Note: Parts of the gel that were not required were cut off. This included 2–3 cm from the slots (top) and bottom and 1 cm from both sides. Additionally, a non-essential corner was cut off from the gel as an indicator for sample orientation.
14. The gel was left to soak in Milli Q water before protein transfer (western blot).

3.3.5E Western blot analysis and protein transfer: step-by-step protocol.

Table 7. 10× transfer buffer.

Component	Amount	Final concentration
Glycin (Sigma, G7126)	144 g	1.5 M
Tris-Base (Sigma, T1503)	30.30 g	250 mM
SDS (Sigma, 3771)	10 g	1%
Methanol (AppliChem A3493,2500GL)	200 mL	20%
Milli Q water	800 mL	-

1. A 10× transfer buffer solution was made according to Table 7.
2. From the 10× transfer buffer, a 1 × solution was made by adding 100 mL 10× running buffer to 900 mL Milli Q water.
3. A piece of 6 × 8 cm of Amersham Hybond blotting membrane paper (VWR, 10061–494) was cut and placed in Milli Q water to soak.

4. The other two components of the western blot sandwich included 2× fiber pad and 2× filter paper. These were placed in 1× transfer buffer in the container to soak.
5. The western sandwich was stacked according to the depiction on the right. First, the fiber pad was placed on top of the black side of the gel holder cassette, then the filter paper followed and then the gel (the gel was placed mirrored). Finally, the membrane, filter paper, and fiber pad were added.

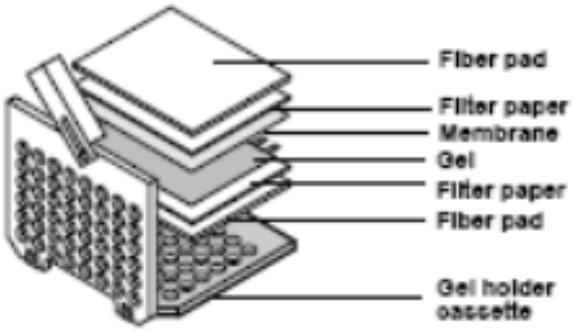

   Note: It was imperative to remove all bubbles between layers of the gel, especially between the gel and membrane. Bubbles could be removed by using a 15-mL Falcon tube as a roller and a piece of filter paper to avoid direct contact between the plastic, membrane, or gel.
6. The cassette was firmly closed and placed in the holder with the black side facing the electrode. Additionally, an ice pack and magnetic flow were added.
7. The container was placed on the magnetic stir plate and filled with 1× transfer buffer.
8. The protein transfer was performed at 400 mA for 80 min.
9. After the transfer, the membrane was removed and stained with Ponceau S to determine the success and amount of the protein transfer. A strong and smooth purple staining showing many bands with a white background was most optimal. If the bands included interruptions or spots, then the membrane would not be used for antibody staining as the transfer was not completely successful. (Repetition was then required.)
10. The membrane was washed 10 to 15 min in Milli Q water to wash out the Ponceau S.
11. Then, the membrane was submerged in a container with milk buffer blocking medium (0.6 g milk powder, 50 mL PBS, and 150 µL Tween) for 1 h at RT to block unspecific binding of future antibody incubation. The container and content were placed on a tilting device that continuously tilted up and down to cover the membrane with the liquid.
12. The membrane was ready to be used for antibody staining. Alternatively, it could be dried and stored at −20°C for future use.

3.3.5F Western blot analysis, protein visualization, and analysis: step-by-step protocol.

1. If the membrane was frozen, it was first allowed to thaw in the fridge for 30–60 min.
2. The primary antibody Lamin A/C (Thermo Fisher Scientific, mab636) was diluted 1:4,000 in milk buffer to a total volume of 7.5 mL and was added to the membrane for overnight (o/n) incubation at 4°C. The container and content were placed on a continuous tilting device.

3. After incubation, the antibody solution was collected for future use. This solution could be re-used up to 3–5 times.
4. The membrane was washed 3× for 5 min with milk buffer.
5. The second antibody was made (1:5,000 in milk buffer) in 7.5 mL and added to the membrane. This was incubated at RT for 1 h and placed on a tilting device.
6. The second antibody was removed, and the membrane washed with 1× PBS/Tween (50 mL PBS and 150 µL Tween) 3 × 5 min.
7. After the successive washes, the membrane was placed inside the Chemidoc apparatus.
8. Then, 1,200 µL of ECL substrate (600 µL Clarity Western Peroxide Reagent and 600 µL Clarity Western Luminol/Enhancer Reagent, Bio-Rad 1705061) was directly added on top of the membrane.
   Note: It was crucial to spread the ECL substrate over the entire membrane.
9. After adding the ECL substrate, the software Image Lab was opened. Then, “new file” was chosen, followed by “single channel,” “application,” “blot,” “high-resolution,” and then “position gel.”
10. The membrane was placed correctly in front of the camera, and “run protocol” was selected. Additionally, a range of exposure times was selected depending on the band signal intensity. The best image was chosen from this image series.
11. The membrane was placed back in its washing container after image acquisition and then was washed with PBS for 5 min to remove the ECL substrate.
12. The second primary antibody GAPDH (Sigma, G8795) was diluted 1:1,000 in milk buffer and added in a volume of 7.5 mL to the membrane and incubated for 1 h at RT.
13. Steps 3 to 11 were repeated.
14. Optionally, a third primary antibody could be added. This was β-Actin (Sigma, A5441 clone AC-15), which was diluted 1:10,000 in milk buffer, and was added to the membrane in a volume of 7.5 mL. This was incubated for 1 h at RT.
15. Steps 3 to 11 were repeated.
16. After obtaining all the images, Image Lab was used for analysis.
17. First, “Image Tools” was selected in the Analysis Tool Box to crop the image, leaving only the bands of interest. This was either the lamin A/C area or GAPDH and β-Actin one.
18. Then, “Lane and Bands” was selected in the Analysis Tool Box.
19. For each column, a lane was added, and for each protein band, a band was added.
20. By selecting the menu option “Analysis Table,” the values of each sample were shown. The column “Volume (Int)” represented the band intensity of the band.

21. The “Volume (Int)” value was obtained for all bands (incl. Lamin A/C, GAPDH, and β-Actin).
22. To determine the difference of protein ratio between samples, the housekeeping protein (GAPDH or β-Actin) was used to obtain a normalization factor. See below for the calculation principle.

Example of the calculation principle:
If the GAPDH “Volume (Int)” value of sample 1 = 10, sample 2 = 12, and sample 3 = 8, the normalization factor would become for sample 1 = 1 (10 / 10), sample 2 = 1.2 (12 / 10), and sample 3 = 0.8 (8 / 10). The values indicate that sample 2 has 1.2× too much (added too much protein, possibly by pipetting errors) and sample 3 has 1.25× too little (added too little protein). To normalize the values, all “Volume (Int)” values for sample 2 need to be divided by 1.2 and all values for sample 3 multiplied by 1.25.

23. After normalization of all the values, the lamin A/C and progerin ratios could be calculated and differences between samples determined, see examples below.

Example of the lamin A/C ratio determination within one sample:
Sample 1 is a fibroblast origin sample and has after normalization a “Volume (Int)” value of 6 for lamin A and a value of 4 for lamin C. This means that the ratio equals to 60% lamin A (6 / 10 [the total] × 100%) and 40% lamin C (4 / 10 [the total] × 100%).

Example for lamin A/C difference determination between two samples:
To compare differences in protein levels between samples, the “Volume (Int)” values are compared. Sample 1 is the same as the previous example, but sample 2, the pH-SKP sample, has after normalization a “Volume (Int)” value of 4.5 for lamin A and a value of 6 for lamin C. This means that pH-SKP spheroids have 1.33 times less lamin A (6 [sample 1] / 4.5 [sample 2]) or only 75% of the level of the sample 1 origin fibroblasts (4.5 [sample 2] / 6 [sample 1] × 100%). For lamin C, there would be 1.5 times more lamin C in pH-SKP spheroids than in the origin fibroblasts or 150% of the level of the sample 1 origin fibroblasts (6 [sample 2] / 4 [sample 1] × 100%).

3.3.6 Immunohistochemistry and differentiation of HGPS pH-SKPs

Similar as in Chapter 1, immunohistochemistry labeling (Chapter 1.3.6, pages 55 to 58) and differentiation (Chapter 1.3.7, pages 59 to 68) were performed for HGPS pH-SKPs. Some differences in methodology were taken into account for HGPS samples compared to normal ones. For instance, spheroid adherence required in general more time for HGPS pH-SKPs than normal pH-SKPs—HGPS pH-SKPs required between 2 and 3 days to adhere before differentiation could be induced. This longer adherence incubation time often did not flatten or spread the HGPS spheroids similar to normal ones. Another difference taken into account was the ability of HGPS pH-SKP cells to spread and proliferate from the adhered spheroid. This affected SMC and fibroblast differentiation, where HGPS pH-SKPs required more culture time compared to normal cells. All other conditions remained the same between HGPS and normal pH-SKPs. The found differences in differentiation will be further reported in the result section.

3.3.7 Long-term adipocyte culture

To investigate the potential and stability of adipocytes, long-term culture was investigated after initial differentiation. First, pH-SKP spheroids of both HGPS and normal cells were stimulated for adipocyte differentiation for 1 month, see Chapter 1.3.7A, page 59 to 63. Then, the differentiation medium was exchanged for adipocyte sustain medium, which mainly included insulin to provide adipocyte nutrients and promote lipid sustainment, see Table 9. Adipocytes for long-term cultures were fed every 3–4 days by completely refreshing the medium. Oil red O (ORO) staining was performed according to the Thermo Fisher Scientific SC protocol 00011 to confirm lipid presence.

Table 9. Adipocyte sustain medium – used to maintain and sustain SKP spheroids differentiated into adipocytes.

	Total Volume (X µL)	10,000	µL		
	Material			**End concentration**	
1	DMEM (1 g/L glucose) Gibco, 21885-025	8,780	µL		
3	Insulin (100 × / 1.0 mg/mL) I2643-50MG Sigma	100	µL	10	µg/mL
6	Fungizone (250 µg/mL) ThermoFisher-Gibco, 15290018	20	µL	0.5	µg/mL
7	Pen/Strep (10,000U/10,000 µg/mL) ThermoFisher-Gibco, 1514022	100	µL	100 U/100 µg/mL	
8	FBS Gibco, 10270-106	1,000	µL	10%	v/v

3.3.8 Statistical analysis

Results are presented as the mean ± standard deviation (SD). Comparisons were performed using the Student's t-test. *P* values less than 0.05 were considered statistically significant. The sample sizes are indicated in the figure legends.

3.4 Results

To test our hypothesis that pH-SKP isolation can be successfully applied to pre-established HGPS primary fibroblasts, we investigated the stemness of acidic-stress-treated (pH 5.7) HGPS fibroblast preparations. From these, we also investigated the status and ratio of lamin A, C, and progerin via qPCR and western blot to determine possible differences between fibroblasts and pH-SKPs. Additionally, the results of an in-depth literature study of adipogenesis will be shown, which was performed to investigate its mechanisms and the possible implications for HGPS cells.

3.4.1 HGPS cells have the ability to form pH-SKP spheroids

The potential ability to isolate multipotent stem cells from HGPS pre-established fibroblast cultures was tested (Fig. 3). Here, HGPS fibroblast cells showed a much lower proliferation rate and required more culture dishes than the control to obtain sufficient cells for pH-SKP isolation (Fig. 3A). A total of one million cells was collected from each cell line and subjected to the acidic stress at a pH of 5.7 for 30 min. After placement in SKP medium, HGPS cells were able to form pH-SKP spheroids similar to control (Fig. 3B).

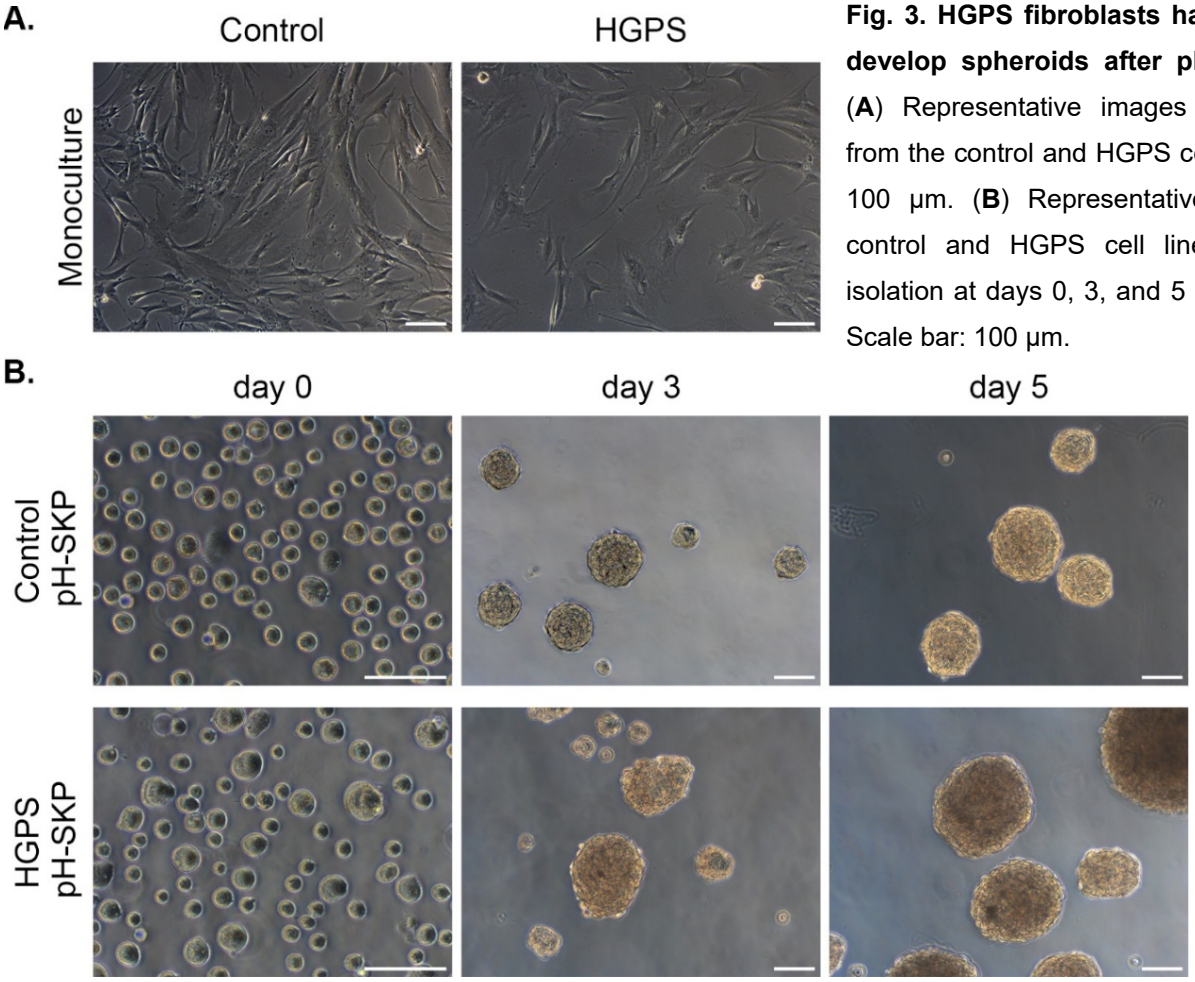

Fig. 3. HGPS fibroblasts have the ability to develop spheroids after pH-SKP isolation. (**A**) Representative images of monocultures from the control and HGPS cell line. Scale bar: 100 µm. (**B**) Representative images of the control and HGPS cell lines after pH-SKP isolation at days 0, 3, and 5 of culture (n = 3). Scale bar: 100 µm.

3.4.2 HGPS pH-SKP spheroids express multipotent stem cell markers

Expression of stem cell markers was evaluated by immunohistochemistry of 5-day-old spheroids to determine the stemness of HGPS pH-SKPs. Sections of HGPS spheroids were positive for the neuronal crest marker nestin [97] and the multipotent markers Sox2 [5], Oct4 [138], NANOG [122], and CD9 [80] (Fig. 4). These findings show that HGPS pH-SKP spheroids at day 5 in culture expressed stem cell markers and indicated that pH-SKP cells obtained from pre-established HGPS fibroblasts exhibit multipotent properties.

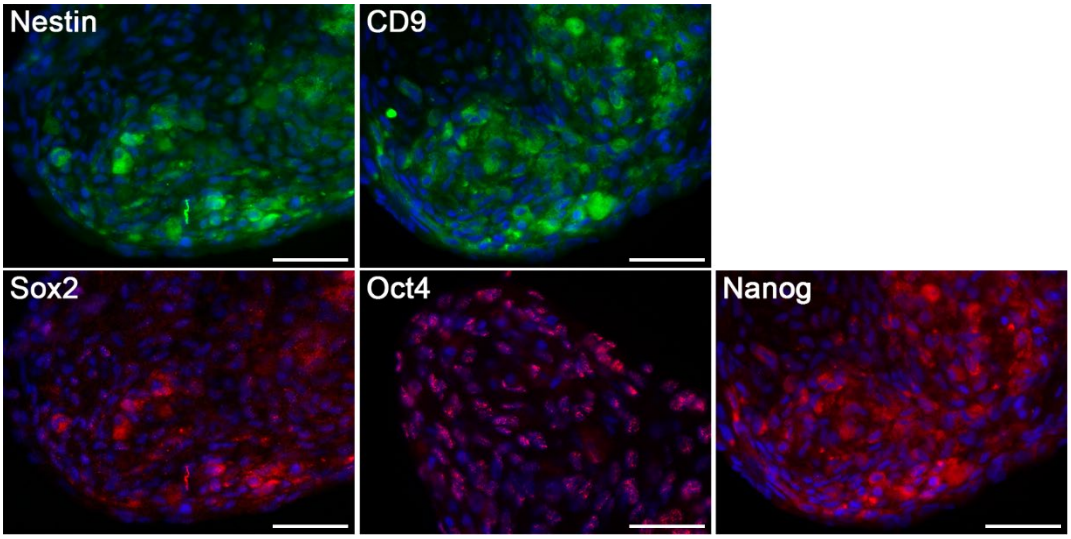

Fig. 4. HGPS pH-SKPs express the neuronal crest and multipotent stem cell markers. Immunohistochemistry of stem cell markers of 5-day-old HGPS pH-SKP spheroids obtained from HGPS cell line HGADFN003. The following stem cell markers were evaluated and labeled on 5-µm thick spheroid cryosections: nestin (green), CD9 (green), Sox2 (red), Oct4 (red), and NANOG (red). All cryosections were counterstained for DNA with DAPI (blue). Scale bar: 50 µm.

3.4.3 Control and HGPS pH-SKPs express lamin A and C mRNA similar to fibroblasts

The expression level of mRNA encoding for lamin A and C of pH-SKPs was determined next. This was done by reverse transcriptase PCR (RT-PCR) of total RNA followed by real-time quantitative PCR (qPCR) analysis of the messenger RNA (mRNA). RNA of the control and HGPS cells from the respective origin fibroblasts and 5-day-old pH-SKP preparations were isolated. The obtained real-time qPCR values were compared between pH-SKP spheroids and their corresponding origin fibroblasts (Fig. 5). Lamin A mRNA expression of control pH-SKPs showed an increase of 1.61× with *P* value 0.49 compared to origin fibroblasts. For HGPS pH-SKPs, lamin A expression decreased 3.6× (1 divided by 0.28× of control lamin A, see Fig. 5) with *P* value 0.06 compared to its origin fibroblasts. Both control and HGPS pH-SKPs showed no definite statistical significance for lamin A expression regarding their respective origin fibroblasts. This was similar for an increase of lamin C in pH-SKPs, where the control showed

1.20× (*P* = 0.07) and HGPS 1.58× (*P* = 0.41), shown in Fig. 5. These findings show that pH-SKP spheroids at day 5 have no statistically significant difference in lamin A and C expression compared to their respective origin fibroblast in our test setting. However, a higher number of samples (n > 3) could rule out the doubt of statistical significance concerning a reduced lamin A expression in HGPS pH-SKPs and an increased lamin C in control pH-SKPs—as those were closest to significance. Further investigation is needed to validate these observations.

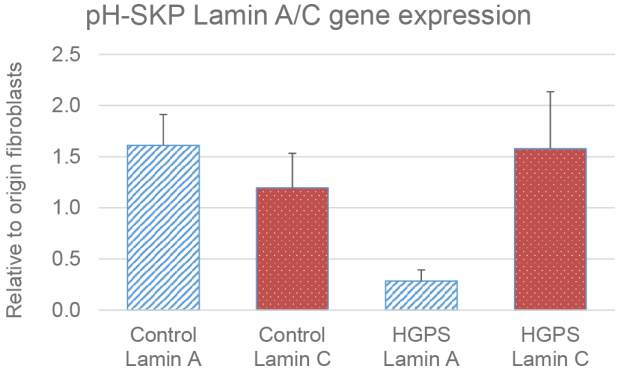

Fig. 5. Five-day-old control and HGPS pH-SKPs express similar levels of lamin A and C compared to their origin fibroblasts. RNA qPCR evaluation of lamin A and C of day 5 pH-SKP spheroids obtained from normal and HGPS fibroblasts. Data are shown as the expression in pH-SKP cells relative to the expression in corresponding origin fibroblasts. Values are the mean + SD (n = 3).

3.4.4 Control and HGPS pH-SKPs contain similar lamin A and C protein levels compared to fibroblasts

Protein levels of normal and HGPS pH-SKPs were analyzed via SDS-PAGE and western blot. Cell pellets from control and HGPS, including origin fibroblasts and pH-SKPs, were lysed, separated, and immunolabeled with anti-lamin A/C and anti-GAPDH (Fig. 6A). Colorimetric analysis of these bands showed a trend toward a higher lamin A ratio in both control and HGPS pH-SKPs and a higher progerin ratio for HGPS (Fig. 6B). However, further analysis showed that the ratio differences between control lamin A and C in fibroblasts compared to those of pH-SKPs did not reach a statistical significance with *P* = 0.07. This was neither the case for HGPS fibroblasts and pH-SKPs (lamin A: *P* = 0.97, lamin C: *P* = 0.13, and progerin *P* = 0.48). Then, the pH-SKP values were determined relative to their origin fibroblasts to determine the difference of protein levels in pH-SKPs (not the ratio levels, see Fig. 6B). The control showed a lamin A protein increase of 2.1× in pH-SKPs and 1.5× for lamin C compared to its respective origin fibroblasts (Fig. 6C). However, no significance was reached for lamin A with *P* = 0.06 and lamin C with *P* = 0.20. For HGPS, the lamin A protein level was 1.7× higher, lamin C 1.4×, and progerin 1.2× (Fig. 6D). Again, no statistical significance was reached for lamin A with *P* = 0.98, lamin C with *P* = 0.38, and progerin with *P* = 0.77. Previous data showed a similar trend (Fig. 6E). Overall, protein analysis did also not present significant differences for lamin A or C (and progerin for HGPS) levels in control or HGPS pH-SKPs compared to their origin fibroblasts. As such, further investigation is required to validate this observation.

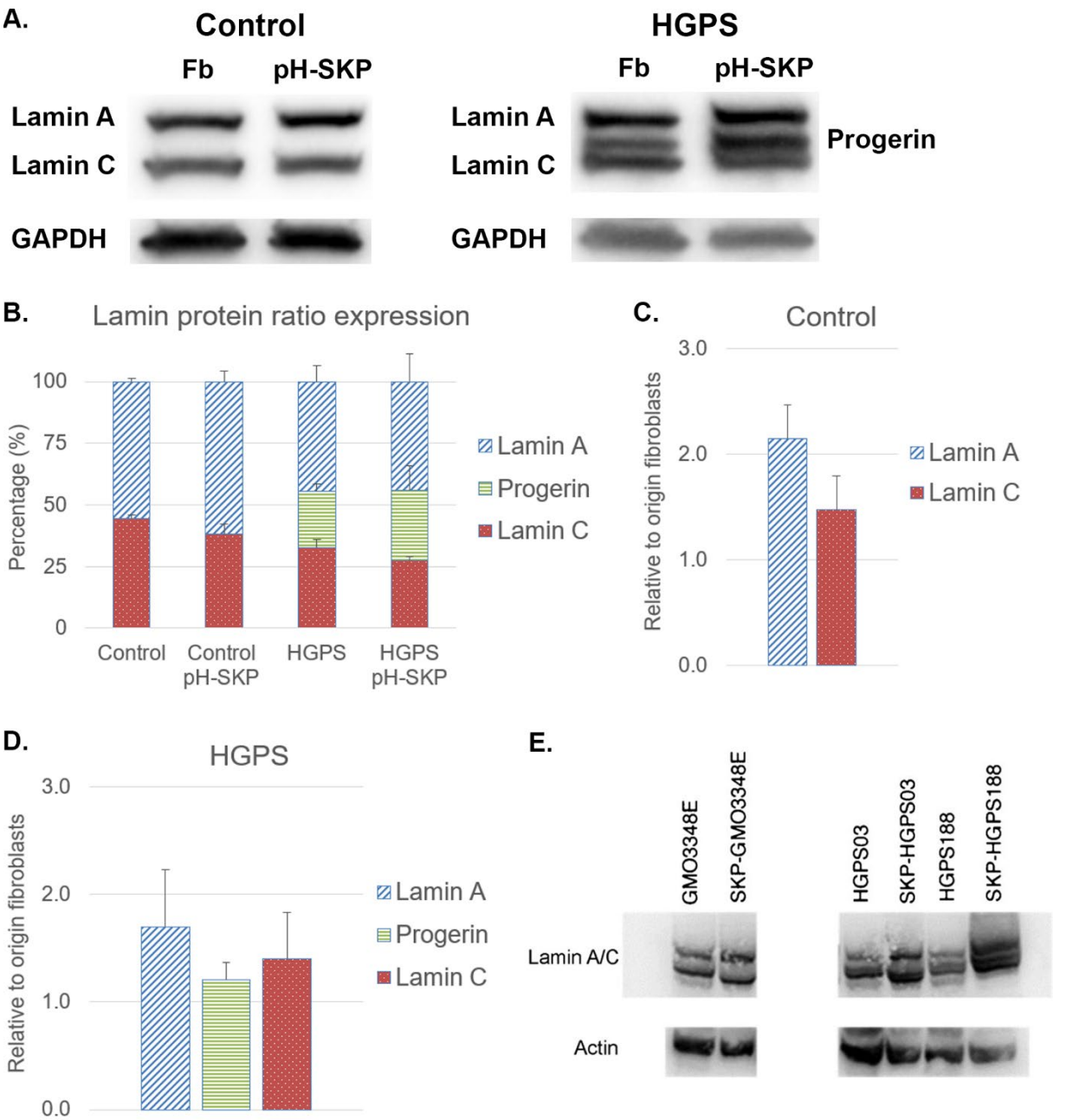

Fig. 6. Day 5 control and HGPS pH-SKPs contain similar levels of lamin A and C proteins compared to their respective origin fibroblasts. (**A**) Representation of lamin A, progerin, and lamin C proteins from lysed fibroblasts (Fb) and pH-SKP spheroids of control and HGPS via SDS-PAGE separation and western blot transfer. Anti-lamin A/C was used to visualize lamin A, C, and progerin with anti-GAPDH as a housekeeping gene for normalization. (**B**) Analysis of lamin A, progerin, and lamin C protein ratio per sample, including control fibroblasts, control pH-SKPs, HGPS fibroblasts, and HGPS pH-SKPs. Values represent the mean +SD (n = 3). (**C**) The analysis of lamin A and lamin C expression in control pH-SKPs relative to their respective origin fibroblasts. Values represent the mean +SD (n = 3). (**D**) Analysis of lamin A, progerin, and lamin C expression in HGPS pH-SKPs relative to their respective origin fibroblasts. Values represent the mean +SD (n = 3). (**E**) A previously published supplementary image by Wenzel et al. [186] showing lamin A, progerin, and lamin C of fibroblasts and Tr-SKPs for control (GM03348E) and HGPS (HGPS03 and HGPS188).

3.3.5 HGPS pH-SKPs have the ability to differentiate into fibroblasts, SMCs, and adipocytes

To investigate the multipotent potential of HGPS pH-SKP spheroids, fibroblast, smooth muscle, and adipocyte differentiations were induced and compared to control pH-SKP spheroids. For a schematic representation of the various differentiations, please refer to Chapter 1, page 82, Fig. 11; page 87, Fig. 15; and Chapter 1 page 59 to 68 for the differentiation methods. Briefly, for fibroblast differentiation, 5-day-old control and HGPS pH-SKP spheroids were adhered, and fibroblast culture medium was added to induce fibroblast differentiation. After 3 to 5 passages, the cells were immunolabeled with the fibroblast marker prolyl-4-hydroxylase beta (P4HB): an enzyme involved in collagen synthesis localized in the endoplasmic reticulum [127] (Fig. 7A). Both control and HGPS samples were found positive for P4HB, indicating fibroblast differentiation (Fig. 7A).

Next, HGPS pH-SKPs were subjected to SMC differentiation medium. Briefly, 5-day-old control and HGPS pH-SKP spheroids were allowed to adhere and then reseeded into a low single-cell density. The adhered cells were induced to differentiate into SMCs. The derived SMCs were fixated between day 10 and 12 post-induction of SMC differentiation and immunolabeled for smooth muscle α-actin (αSMA), calponin, and smooth muscle myosin heavy chain (SM-MHC)—proteins typically expressed in SMCs [145]. All SMC markers were found in SMCs derived from HGPS pH-SKPs at day 10 after differentiation induction; thus, showing their multipotent potential similar to control (Fig. 7B).

Finally, to further assess the multipotent potential of HGPS pH-SKP cells, adipocyte differentiation was induced. Briefly, 5-day-old control and HGPS pH-SKP spheroids were first allowed to adhere. For HGPS pH-SKPs, this period varied between 24 to 48 h as a slower adherence was observed compared to control pH-SKPs (Fig. 7C, first column). Then, the medium was replaced with differentiation medium containing adipocyte-inducing factors. Interestingly, the formation of lipid triglycerides—between three to eight small yellow lipid vesicles (droplets)—could generally be detected for both control and HGPS pH-SKP cells after 2 days of induction (Fig. 7C, second column). The number of lipid droplets increased after additional days (Fig. 7C, third column) and continued to increase in number and size, seen on day 17 (Fig. 7C, fourth column). In general, lipid size of control pH-SKPs became larger faster and the lipid number faster higher compared to HGPS pH-SKPs (Fig. 7C). Digital analysis of ORO-stained adipocytes (see page 70 to 72 for more information about digital ORO analysis) supported this by showing a 40% less red color presence for adipocyte-differentiated HGPS pH-SKPs compared to control (Fig. 7D). This indicates that HGPS pH-SKPs have approximately 40% fewer lipids than control cells after the same number of differentiation days.

Together, these findings show that HGPS pH-SKP spheroids have the ability to differentiate into fibroblasts and SMCs. Surprisingly, HGPS pH-SKPs were also able to differentiate into adipocytes but with a reduced potential. Interestingly, the first observation of lipids was for both the control and HGPS pH-SKPs the same at day 2 post-induction, but a difference became apparent showing a slower overall lipid development for HGPS pH-SKPs. Digital ORO analysis showed approximately 40% fewer lipids than control on the same day ($P < 0.005$) (Fig. 7D), further indicating some impairment of differentiation till at least day 17.

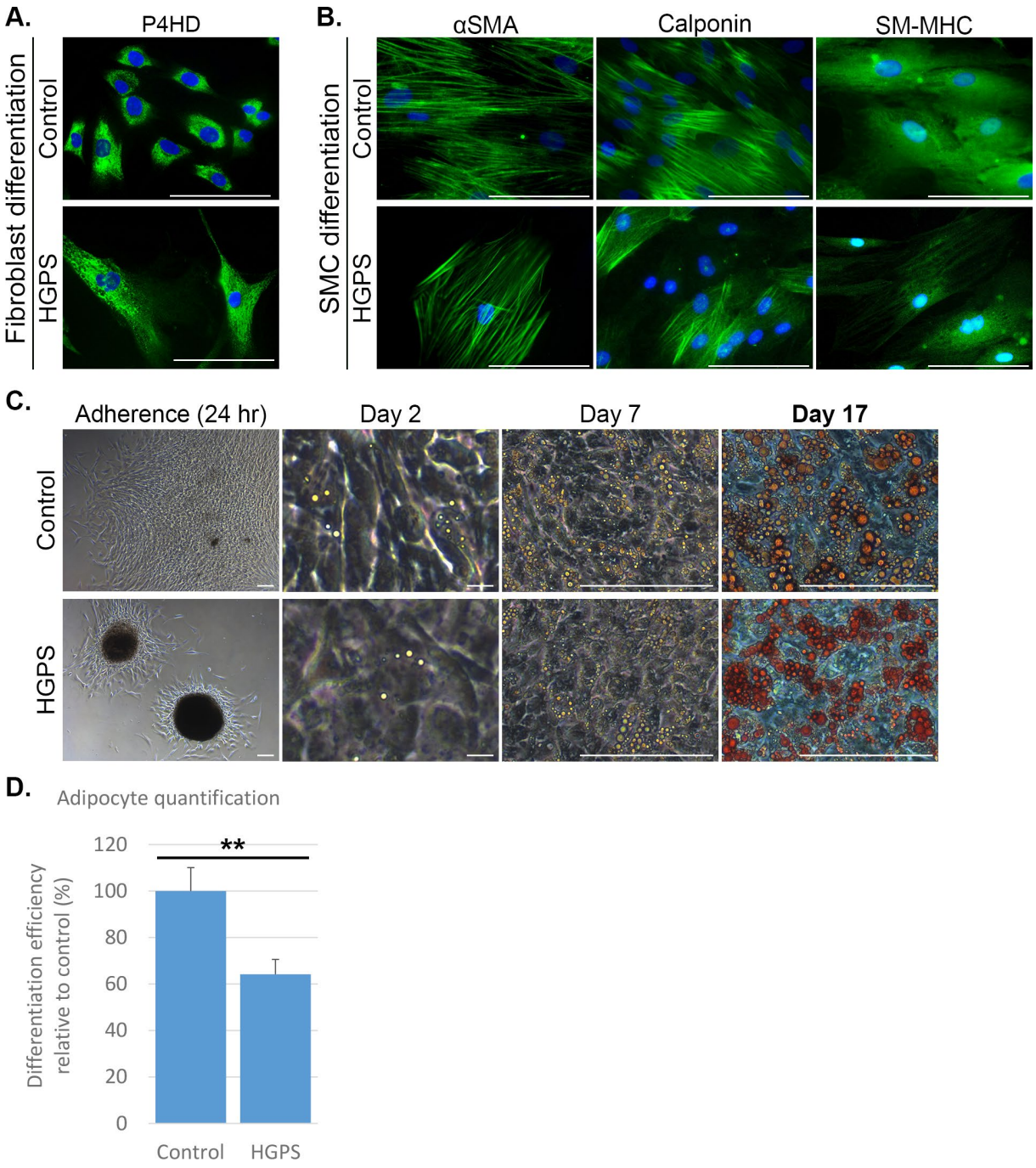

Fig. 7. HGPS pH-SKP spheroids can differentiate into fibroblasts, SMCs, and adipocytes. (**A**) Fibroblast differentiation of control and HGPS pH-SKP cells. The images show fibroblast-differentiated pH-SKP cells labeled for P4HD (green) counterstained with DAPI for DNA (blue). Scale bar: 10 μm (n = 3). (**B**) SMC differentiation at day 10 of control and HGPS pH-SKP cells, which are immunolabeled for αSMC, Calponin, and SM-MHC, all shown in green. DNA was counterstained with DAPI (blue). Scale bar: 100 μm (n = 3). (**C**) Control and HGPS pH-SKPs were differentiated into adipocytes. Adherence is shown after 24 h in adherence medium. The progress of lipid formation is shown for day 2 and 7. Oil red O staining was performed on day 17. Scale bar: first column, 100 μm; second column, 10 μm; and third and fourth column, 100 μm (n = 3). (**D**) Graph illustration of the red color analysis of ORO-stained adipocytes, representing an estimate in lipid percentage of a 1,317 × 1,317 μm field per cell line. Data are normalized to the control and expressed as the mean +SD (**P < 0.005; n = 4).

3.3.6 Pre-established fibroblasts of MAD (mandibuloacral dysplasia) patients have the ability to form pH-SKPs and differentiate into adipocytes

A pilot experiment—regarding the pH-SKP isolation method and potential stemness of pre-established fibroblasts obtained from MAD patients—was performed to investigate the application of the pH-SKP isolation method on a different disease. MAD is a rare disorder similar to HGPS but is distinguished by either a homozygous missense mutation (Arg527His) in the LMNA gene [129] or heterozygous mutation (Phe361fsX379 and Trp340Arg) in the zinc metalloproteinase (ZmpSte24) gene [1]. MAD fibroblasts from cell line PSADFN318, with mutations in the ZmpSte24 gene (heterozygous, Pro248Leu, and Trp450Stop), were cultured as monocultures followed by pH-SKP isolation (Fig. 8A, B). MAD-affected fibroblasts were able to form pH-SKP spheroids. These MAD pH-SKP spheroids were then subjected to adipocyte differentiation. Interestingly, they were able to differentiate into adipocytes as well (Fig. 8C). Differentiation was not seen until day 9 (Fig. 8C, first column), however, but steadily increased afterward (Fig. 8C, second column). However, after day 23, increased cell death and detachment of adipocytes was recorded (Fig. 8C, third column). Compared to HGPS adipocyte differentiation, MAD showed a higher impairment of adipocyte differentiation. Overall, these early results indicate that MAD fibroblasts are capable of forming pH-SKPs and adipocyte differentiation.

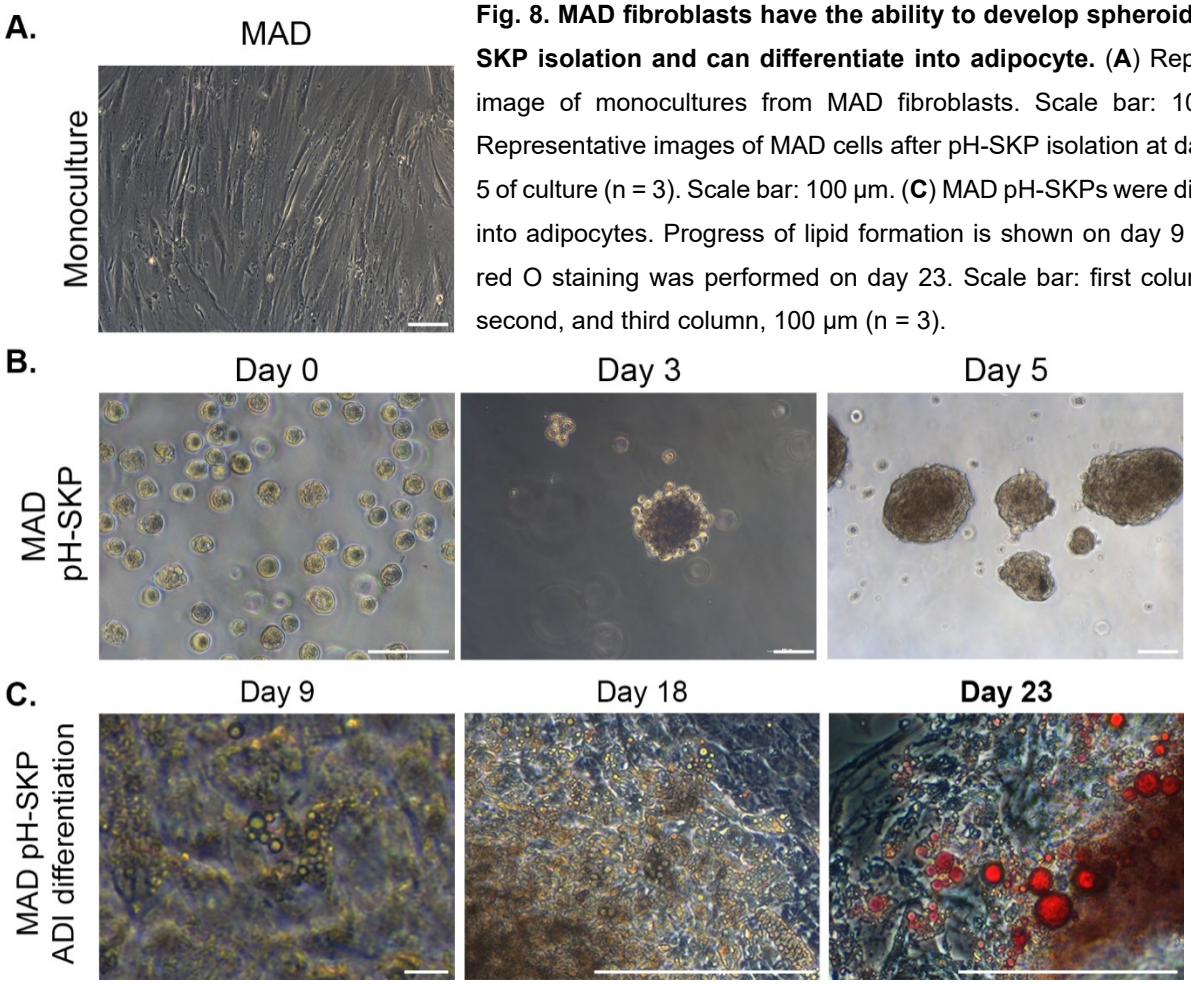

Fig. 8. MAD fibroblasts have the ability to develop spheroids after pH-SKP isolation and can differentiate into adipocyte. (**A**) Representative image of monocultures from MAD fibroblasts. Scale bar: 100 µm. (**B**) Representative images of MAD cells after pH-SKP isolation at day 0, 3, and 5 of culture (n = 3). Scale bar: 100 µm. (**C**) MAD pH-SKPs were differentiated into adipocytes. Progress of lipid formation is shown on day 9 and 18. Oil red O staining was performed on day 23. Scale bar: first column, 10 µm; second, and third column, 100 µm (n = 3).

3.3.7 Control and HGPS pH-SKPs are capable of long-term adipocyte culture

To investigate the stability of HGPS pH-SKP differentiated adipocytes, long-term adipocyte culture was tested *in vitro*. This investigation only focused on the ability of HGPS pH-SKP differentiated adipocytes to determine the long-term culture potential of such adipocytes in relation to a control counterpart.

As a first step, control and HGPS pH-SKPs were subjected to adipocyte differentiation induction medium for the first 28 days (see Materials and Methods). This was followed by adipocyte sustain medium for long-term culture (see Materials and Methods). Differentiated adipocytes from both control and HGPS pH-SKPs were able to maintain culture up to 120 days (Fig. 9). Interestingly, up to 42 days of culture, control and HGPS showed a standard morphology of lipid formation (Fig. 9, day 42), in which control had more and larger lipids than HGPS (also shown previously in Fig. 7). However, starting at day 70, a difference in status quo between their morphology and development became apparent (Fig. 9, day 70). First, the spread of adipocytes increased in control due to the increasing presence of left-over fibroblasts and their proliferation (Fig. 9, days 80 to 120). HGPS did not show this trend due to little or no increase of left-over fibroblasts and showed an adipocyte clustered area instead. HGPS fibroblasts are known in general to already proliferate slower in normal culture conditions compared to control fibroblasts due to their diseased conditions [18, 60, 187]. In this current study, the results indicate that the adipocyte sustain medium might have been too unfavorable—in addition to their already weakened state—for long-term culture regarding HGPS fibroblast growth (Fig. 9). This might be because adipocyte sustain medium has only 1 g/L glucose and no FBS compared to fibroblast culture medium, which has 4.5 g/L glucose and 15% FBS (see Materials and Methods). Furthermore, the control adipocytes reached a plateau in adipocyte size around day 70 (Fig. 9, day 70), while HGPS adipocytes showed an increasing number of irregular adipocytes with abnormally large lipids (Fig 9, day 120). Finally, both control and HGPS pH-SKP differentiated adipocytes showed cell death between days 120 and 140, which was less evident for control (Fig. 9, day 140). This indicated that between days 120 and 140 of adipocyte culture, a combination of *in vitro* limitation and abnormal growth resulted in the difference of observed cell death between control and HGPS adipocytes.

In summary, these results show the ability of control and HGPS pH-SKPs to differentiate into adipocytes and sustain their culture for long-term *in vitro*. Here, control pH-SKP-differentiated adipocytes reached a plateau in size around day 70. The culture contained more fibroblast proliferation and spread overall and showed a higher spread of adipocytes. In contrast, HGPS pH-SKP-differentiated adipocytes also reached a plateau in size around day 70 but showed an increase of abnormally large growing adipocytes around day 120. They also stayed more clustered, the culture showed fewer fibroblasts, and major cell death occurred around day 140.

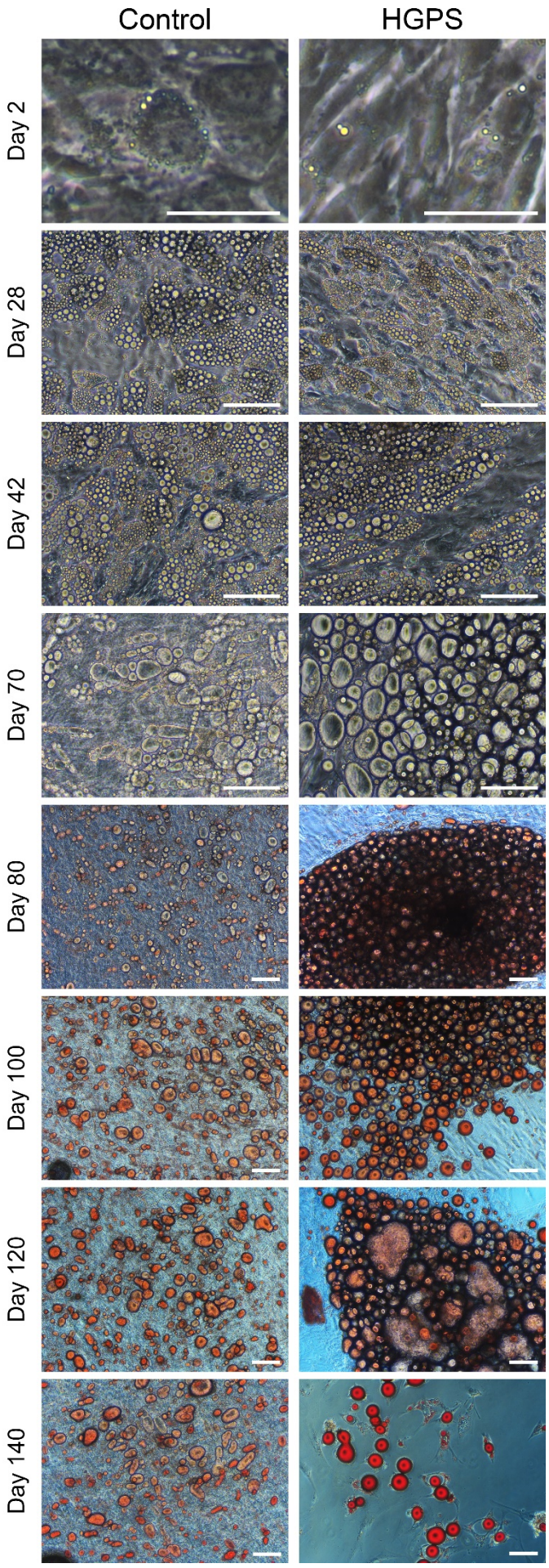

Fig. 9. Control and HGPS pH-SKP spheroids can sustain long-term adipocyte culture after differentiation. Representative images of control and HGPS pH-SKPs differentiated into adipocytes, which sustained a long-term culture. The progress of lipid formation is shown between days 2 and 140. The pH-SKP cells were subjected to adipocyte induction medium up to day 28. Afterward, cells were subjected to adipocyte sustain medium (see Method and Materials). Oil red O staining was performed on day 80, 100, 120, and 140. Scale bar: first row, 10 µm; remaining rows, 100 µm (n = 3).

3.4 Adipogenesis Pathway

3.4.0 The adipogenesis pathway model reveals five sub-pathways potentially related to HGPS pH-SKP adipocyte differentiation *in vitro*

A literature study was performed to unravel potential mechanisms of adipogenesis regarding HGPS pH-SKP differentiation. From these findings, an adipogenesis pathway map was constructed (Fig. 10). Here, the key protein required to initiate adipocyte differentiation is the peroxisome proliferator-activated receptor gamma (PPAR-γ) protein, shown black in the middle (Fig. 10) [26, 67, 93]. One of its direct stimulators, also shown in black, is the CCAAT/enhancer-binding protein alpha (C/EBP-α) protein that stimulates expression of PPAR-γ, which in turn stimulates C/EBP-α again, causing a positive feedback loop [103, 148, 171]. This feedback loop is initiated by the earlier transcription of the protein complex C/EBP-β and C/EBP-δ, both shown in black as well (Fig. 10) [19, 72]. Combined, these four proteins of the PPAR-γ core mechanism are essential for adipogenesis and are in the center of other stimulating or inhibiting pathways that are involved with adipocyte differentiation. There are in total six groups of such pathways, including the “Early differentiation initiators” in blue, “Wnt/β-catenin signaling” in purple, “TNFα and macrophage cytokines” in red, “Late-stage adipocyte promoting proteins” in yellow, “Notch” in green, and “DLK-1/Pref-1” in brown (Fig. 10). Please see Box 1 for a colorblind friendly description of Fig. 8. (Please see for further used abbreviations Fig.10.) Together, each of these groups plays a potential role in adipocyte differentiation *in vitro* in relation to HGPS pH-SKPs.

The first group to mention is the “Early differentiation initiators” group, shown in blue at the top left side (Fig. 10). This group is the only group that promotes adipogenesis and contains various sub-pathways, such as PKA and CREB, KLF4 and Krox2, and Smad-1, -5, -8 and p38 MAPK. All these proteins increase C/EBP-β and C/EBP-δ expression, and consequently, increase PPAR-γ and C/EBP-α. The *in vitro* used adipocyte differentiation medium focuses on the activation of these group members and include the following compounds: IBMX, Dex, indomethacin, insulin, and fetal bovine serum (Materials and Methods, page 60 and 61). Fig. 10 shows that these components directly influence the activation of the “Early differentiation initiators” group. IBMX increases PKA directly and CREB, KLF4, and Krox20 indirectly by inhibiting PDE. Then, the addition of Dex increases CREB directly, and indomethacin increases C/EBP-β and PPAR-γ directly. All these compounds are not naturally present *in vivo* in HGPS. Therefore, this data nominates the “Early differentiation initiators” group as a potential group where HGPS *in vivo* might lack sufficient activation.

The other pathway groups are only involved in the inhibition of adipogenesis. First is the “Wnt/β-catenin signaling” pathway group (Fig. 10, in purple, top middle of the pre-adipocyte). This signaling pathway is a major regulator of development throughout the animal kingdom

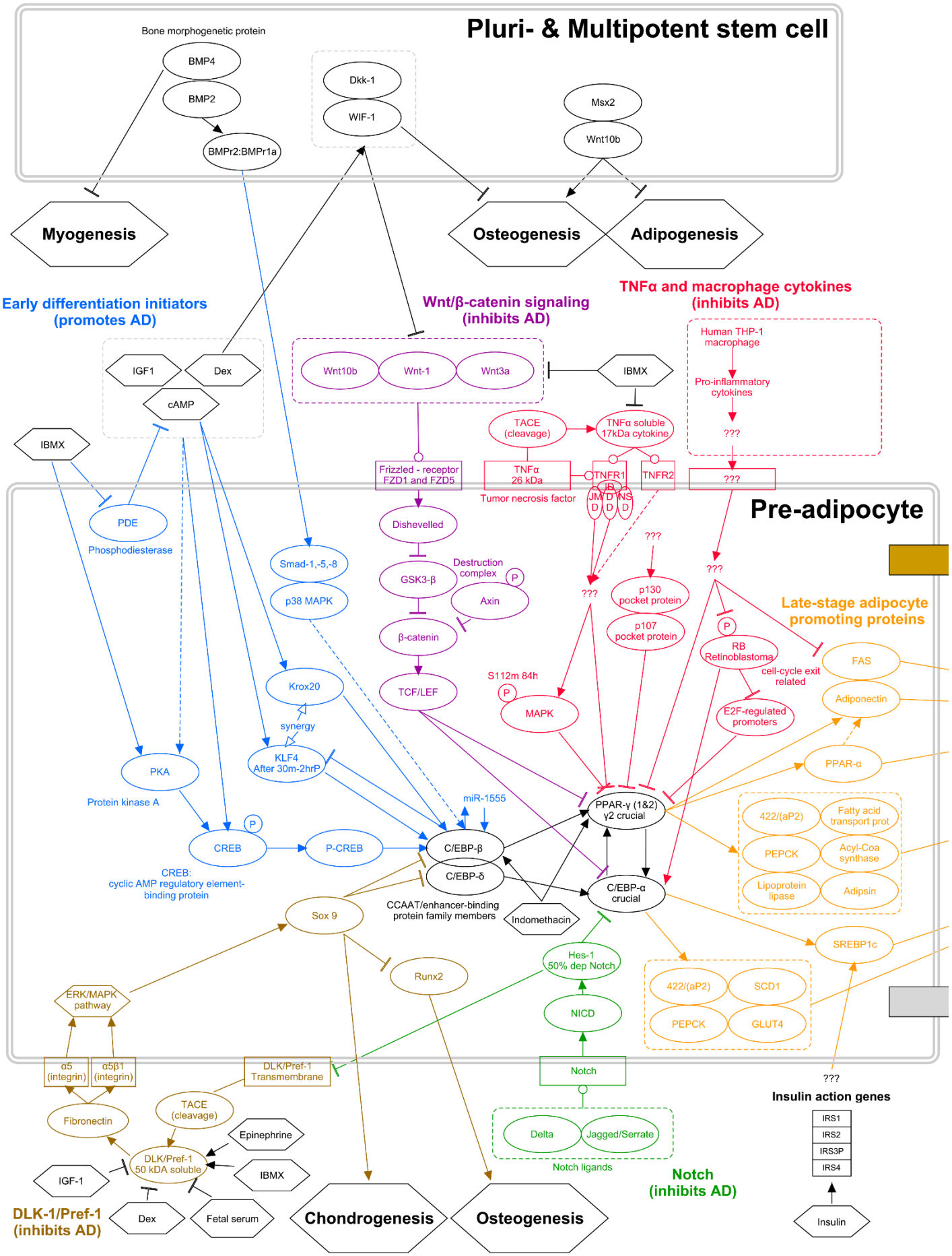
Pluri- & Multipotent stem cell
Bone morphogenetic protein
BMP4
BMP2
BMPr2:BMPr1a
Dkk-1
WIF-1
Msx2
Wnt10b
Myogenesis
Osteogenesis
Adipogenesis
Early differentiation initiators (promotes AD)
Wnt/β-catenin signaling (inhibits AD)
TNFα and macrophage cytokines (inhibits AD)
IGF1
Dex
cAMP
IBMX
Wnt10b
Wnt-1
Wnt3a
IBMX
Human THP-1 macrophage
Pro-inflammatory cytokines
???
TACE (cleavage)
TNFα soluble 17kDa cytokine
Frizzled - receptor FZD1 and FZD5
TNFα 26 kDa
Tumor necrosis factor
TNFR1
TNFR2
JMD
JBD
NSD
???
Pre-adipocyte
PDE
Phosphodiesterase
Dishevelled
Smad-1,-5,-8
p38 MAPK
GSK3-β
Destruction complex
P
Axin
β-catenin
TCF/LEF
???
p130 pocket protein
p107 pocket protein
???
Late-stage adipocyte promoting proteins
RB Retinoblastoma
cell-cycle exit related
E2F-regulated promoters
FAS
Adiponectin
PPAR-α
Krox20
synergy
KLF4 After 30m-2hrP
S112m 84h
MAPK
PKA
Protein kinase A
miR-1555
PPAR-γ (1&2) γ2 crucial
422/(aP2)
Fatty acid transport prot
PEPCK
Acyl-Coa synthase
Lipoprotein lipase
Adipsin
CREB
P-CREB
CREB: cyclic AMP regulatory element-binding protein
C/EBP-β
C/EBP-δ
CCAAT/enhancer-binding protein family members
C/EBP-α crucial
Indomethacin
Sox 9
SREBP1c
Runx2
Hes-1 50% dep Notch
NICD
422/(aP2)
SCD1
PEPCK
GLUT4
ERK/MAPK pathway
α5 (integrin)
α5β1 (integrin)
DLK/Pref-1 Transmembrane
Notch
???
Insulin action genes
IRS1
IRS2
IRS3P
IRS4
Insulin
TACE (cleavage)
Fibronectin
Epinephrine
DLK/Pref-1 50 kDA soluble
IGF-1
IBMX
Dex
Fetal serum
Delta
Jagged/Serrate
Notch ligands
Notch (inhibits AD)
DLK-1/Pref-1 (inhibits AD)
Chondrogenesis
Osteogenesis

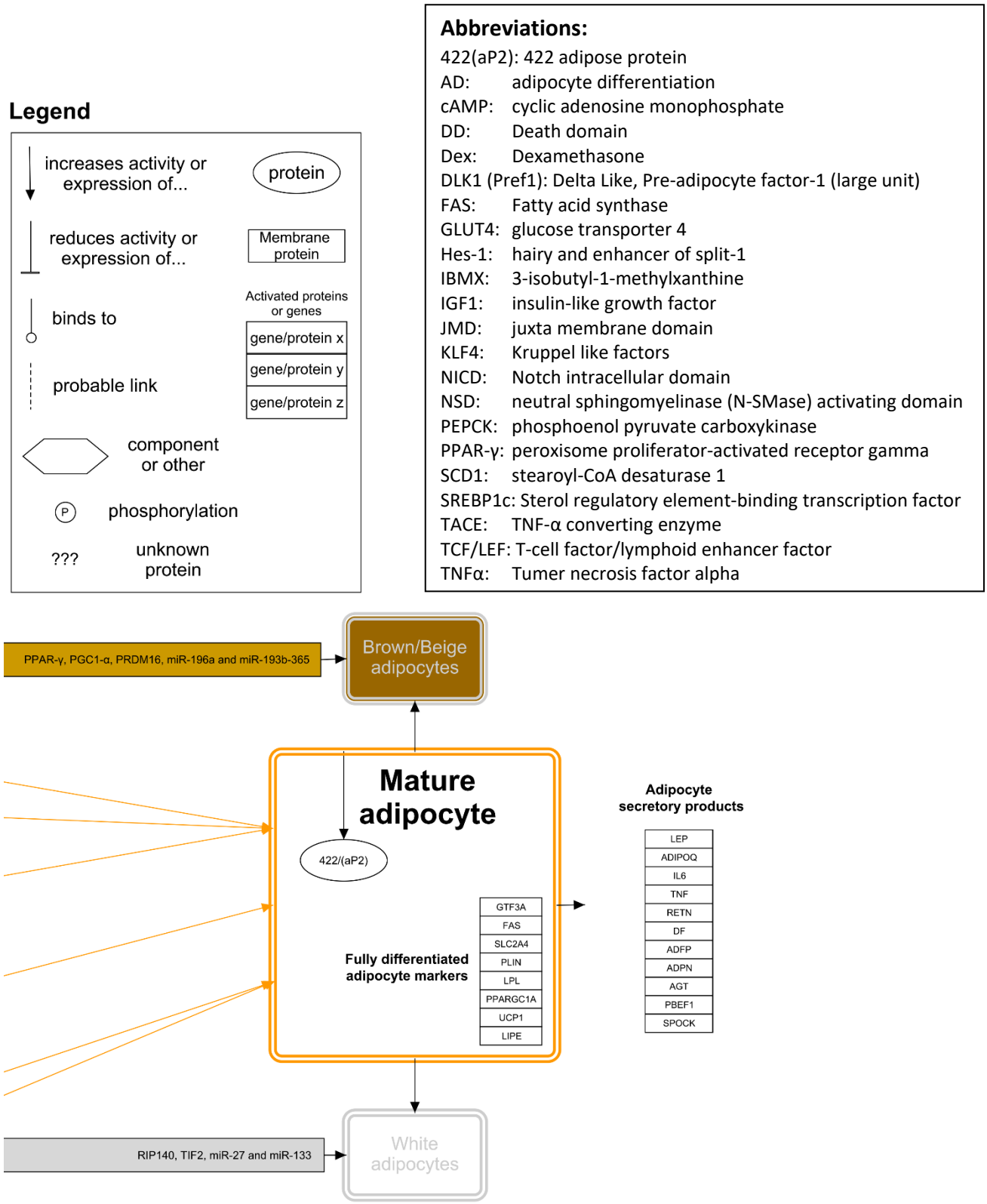

Fig. 10. Generated pathway map of adipogenesis with focus on *in vitro* and HGPS adipocyte differentiation. First, centered in the middle in black, the major components of adipocyte differentiation, including C/EBP-β, C/EBP-δ, C/EBP-α, and PPAR-γ. Then in blue, the adipocyte promoting pathway of early differentiation initiators. In purple, the adipocyte inhibiting pathway Wnt/β-catenin. In red, the adipocyte inhibiting pathways of inflammatory TNFα and macrophage cytokines. In brown, the adipocyte inhibiting pathway of DLK-1/Pref-1. In green, the adipocyte inhibiting pathway of Notch. And finally, in yellow, the late-stage adipocyte promoting proteins. (See Box 1 for a colorblind friendly description.)

Box 1. Colorblind friendly description of Fig. 10.

Early differentiation initiators (in blue), located in the top left of the pre-adipocyte:
PDE, SMAD-1,-5,-8, p38 MAPK, Krox20, KLF4, PKA, CREB, and P-CREB.

Late-stage adipocyte promoting proteins (in yellow), located at the middle and bottom right of the pre-adipocyte:
FAS, Adiponectin, PPAR-α, 422/(aP2), PEPCK, lipoprotein lipase, fatty acid transport protein, acyl0Coa synthase, adipsin, SREBP1c, SCD1, and GLUT4.

Wnt/β-catenin signaling (purple), located at the top middle of the pre-adipocyte:
Wnt10b, Wnt-1, Wnt3a, Frizzled-receptor FZD1 and FZD5, Dishevelled, GSK3-β, Axin, β-catenin, and TCF/LEF.

TNFα and macrophage cytokines (in red), located at the top right of the pre-adipocyte:
Human THP-1, pro-inflammatory cytokines, TACE, TNFα, TNFα soluble, TNFR1, TNFR2, ID, JMD, DD, NSD, P130 pocket protein, p107 pocket protein, RB retinoblastoma, E2F-regulated promotors, and MAPK.

Notch (in green), located at bottom middle of the pre-adipocyte:
Hes-1, NICD, Notch, Delta, and Jagged/Serrate.

DLK-1/Pref-1 (in brown), located at bottom left of the pre-adipocyte:
Sox9, Runx2, ERK/MAPK pathway, α5 integrin, α5β1 integrin, DLK/Pref1 transmembrane, DLK/Pref-1 soluble, TACE, and fibronectin.

and is involved in stem cell fate decisions (see for a review [130]). Concerning adipogenesis, this group is initiated by the activation of Frizzled membrane receptors FZD1 and FZD5 by Wnt10b, Wnt- 1, or Wnt3a. As a result, via the activation of Dishevelled, β-catenin is inhibited. This results in the increase of transcription factor TCF/LEF that then inhibits PPAR-γ and C/EBP-α and subsequently inhibits adipogenesis. However, the *in vitro* induction factors IBMX and Dex have an adipogenesis stimulating role in this situation. The addition of Dex indirectly decreases Wnt10b, Wnt-1, and Wnt3a by increasing their antagonists Dkk-1 and WIF-1. Then, the addition of IBMX further reduces the Wnt proteins by directly inhibiting them. TCF/LEF is then reduced, which results in the prevention of potential adipogenesis inhibition by the "Wnt/β-catenin signaling" pathway group.

The second identified group from the literature search results is the adipogenesis inhibiting "TNFα and macrophage cytokines" pathway, and it consists out of pro-inflammatory factors (Fig. 10, in red, top right of the schematic pre-adipocyte). First, TNFα is discussed, which is known for its role in the regulation of pro-inflammation and tumor cytotoxicity (see for a review [156]). TNFα fitted in the adipogenesis pathway model as it is increased in senescent cells and found in HGPS models [133]. In turn, this results in adipogenesis inhibition [25, 195]. In the pathway model, TNFα is cleaved by TACE creating a soluble TNFα, which in turn activates TNFR1 and TNFR2. This causes a direct inhibition of PPAR-γ via MAPK phosphorylation and other still unknown proteins (Fig. 10). Interestingly, IBMX was also found to directly decrease the presence of TNFα soluble, preventing another potential inhibitor of adipogenesis *in vitro*. The second part of the "TNFα and macrophage cytokines" pathway group are the pathways

activated by macrophage cytokines, which are involved in the innate immune system (see for a review [4]). Here, pro-inflammatory cytokines from human THP-1 macrophages have shown to inhibit adipogenesis [31]. A large part of this pathway group remains unclear in adipogenesis, but studies have shown that PPAR-γ is directly reduced by it and indirectly via inhibition of the phosphorylation of the retinoblastoma protein, which normally inhibits the PPAR-γ inhibitor E2F-regulated promoters. Additionally, when not inhibited, phosphorylated retinoblastoma protein promotes C/EBP-α, which then stimulates adipogenesis (Fig. 10). The macrophage cytokine pathway was included in this adipogenesis model for HGPS because none of the differentiation inducers (IBMX, Dex, fetal serum, insulin, or indomethacin) are known to intervene. Additionally, increased levels of inflammatory cytokines (IL-6 and CXCL1) have shown to be elevated in HGPS mouse models [133]. Together, the "TNFα and macrophage cytokines" pathway group signifies a potential role in the difference between differentiation of HGPS pH-SKPs *in vitro* and *in vivo*.

The third and fourth pathway groups, based on the literature search results, include "Notch" and "DLK-1/Pref-1," which are independently involved but also in relation with each other for adipogenesis inhibition. First, the "Notch" pathway is discussed, which is involved in signaling to regulate cell fate and stem cell differentiation [14]. It is activated by Notch ligands Delta and Jagged/Serrate, which activate the transmembrane protein Notch and causes the inhibition of C/EBP-α via Hes-1 (Fig. 10, in green, bottom middle of the schematic pre-adipocyte). Interestingly, "Notch" activation is necessary for early adipocyte differentiation to inhibit the "DLK/Pref-1" pathway via Hes-1 to promote adipogenesis but needs to be decreased again in later adipogenesis stages [149]. The "DLK/Pref-1" pathway itself is activated by cleavage of the DLK/Pref-1 transmembrane by TACE, resulting in DLK/Pref-1 soluble (Fig. 10, in brown, bottom left of the of the schematic pre-adipocyte). In turn, expression of fibronectin is increased, which activates α5 and α5β1 integrins. These, in turn, activate the ERK/MAPK pathway, resulting in expression of Sox 9, which directly inhibits the C/EBP-β and C/EBP-δ complex. Together, the "Notch" and "DLK/Pref-1" pathways are included in the adipogenesis model because progerin expression in HGPS stem cells has been found to activate downstream effectors of the Notch signaling pathway [154].

In sum, five pathway groups, including "early differentiation initiators," "Wnt/β-catenin signaling," "TNFα and macrophage cytokines," "Notch," and "DLK/Pref-1" where found based on the literature research results. Each pathway group signifies a potential role in the difference between HGPS stem cell adipocyte differentiation *in vitro* and *in vivo*, based on their involvement with the adipogenesis induction components or the effects of progerin.

3.5 Discussion – Chapter 3

HGPS is a rare and devastating premature aging disease for which mainly tissue biopsy, fibroblasts, and induced pluripotent stem cells are currently used to study the disease. These available tools are for various reasons less than optimal. First, tissue biopsy is undesirable since HGPS patients are children and only 350 to 400 are present at any time (estimated by the Progeria Research Foundation), causing high-stress on patients and insufficient tissue material for research [52]. Second, fibroblasts can be obtained and cultured easily and amassed in high amounts but do not represent the many other tissues and cell types affected in HGPS patients, such as adipocytes and smooth muscle cells (SMCs) [64, 154, 180, 200]. Third, induced pluripotent stem cells can become other cell types via directed differentiation but are difficult and labor intensive to obtain and maintain. Other complications such as spontaneous reversal to origin cell type and tumor formation could occur as well since these cells are genetically modified and not naïve [74, 117, 176]. Therefore, additional tools need to be investigated and tested to study rare diseases such as HGPS to promote the development of new therapies.

In this thesis, the application of pH-SKP isolation on HGPS fibroblasts was investigated as a new potential tool for HGPS research [15]. This technique, termed pH-SKP isolation, exposes pre-established dermal primary fibroblasts to temporary acid stress followed by culture with growth factors (EGF, FGF2, and B27), which results in multipotent SKP stem cells (pH-SKPs) after only 5 days. For more information about the pH-SKP isolation method, please see Chapter 1 page 34 to 36 or Budel et al. [15]. We report that HGPS acid-treated fibroblasts formed cellular spheroids similar to control after 5 days of culture with the pH-SKP isolation method. These HGPS pH-SKP spheroids were positively immunolabeled for the stem cell markers nestin, CD9, Sox2, Oct4, and NANOG, which indicates their multipotent potential. This was further confirmed by successful SMC and fibroblast differentiation. Furthermore, HGPS pH-SKPs were also able to differentiate into adipocytes: a cell type mostly absent in HGPS patients [64].

The expression of lamins (A and C) and progerin was also investigated. In general, lamin A expression is reported to be not or at low levels present in embryonic and adult stem cells and increases the more cells differentiate to their final cell type [32, 136, 137]. However, our results suggest that lamin A and other key molecular indicators of HGPS (lamin C and progerin) were higher expressed in pH-SKPs compared to their origin fibroblasts instead. And while there was no clear statistical significance with the sample group of three, observations indicated a possible increase in lamin A, C, and progerin in the isolated SKPs. Similar results were found in a study by Wenzel et al., where SKPs were isolated via trypsin stress [186]. An additional study disagrees with the consensus of no lamin A expression in embryonic cells and showed

data of detectable lamin A expression in such stem cells [44]. These studies indicating disagreement with lamin A expression in stem cells underline that there might be certain exceptions or conditions that influence lamin A expression. However, the data in this study are preliminary and require further investigation to contribute to the lamin A expression debate in adult stem cells.

Fibroblast monocultures (2D) and SKP spheroid (3D) cultures were compared together to determine expression differences for both Tr-SKP and pH-SKPs. The difference between culture methods might explain the found results of increased lamin expression in SKPs. Various studies have shown that culture style alone (2D vs. 3D) can significantly alter protein expression of many genes and that 3D culture represents *in vivo* conditions better [55, 87, 165, 204]. Additionally, immunofluorescent images of the nucleus and non-nucleus components of pH-SKP cells indicate that SKP cells are smaller compared to their origin fibroblast monoculture cells and that SKP cells contain much more nucleus material (Fig. S1). In the origin fibroblast monoculture, the nucleus represents a much smaller part of the total cell size (Fig. S1). Additional quantitative investigation needs to be performed; however, with these results, it can be speculated that monoculture fibroblasts have a lower nucleus to total cell size ratio (the nuclei are a smaller part of the total cells) than pH-SKP spheroid cells (the nuclei are almost the largest part of the cell). This could indicate that from 30 µg protein material, used in the western blot analysis, pH-SKPs will have more nucleus proteins (lamin A, C, and progerin), compared to its origin fibroblasts monoculture counterpart. Together, we recognize the indicated shortcomings of comparing 2D and 3D culture systems with each other. For future investigations, we propose the use of methylcellulose to generate fibroblast spheroids and compare such 3D fibroblasts with 3D pH-SKPs and determine the lamin A/C and progerin status more reliably in pH-SKPs [99, 112].

In this investigation, to our current knowledge, we report the first successful differentiation of naïve HGPS pH-SKP stem cells into adipocytes. Additionally, we report the first long-term adipocyte culture of HGPS-differentiated stem cells as well. This was confirmed up to 120–140 days of adipocyte culture for HGPS pH-SKPs and 130–140 days for control pH-SKPs, before observing cell death. Loss of the control in a similar time span indicates that *in vitro* limitations might be responsible for the observed cell death and that 3D or *in vivo* culture might prolong this span. Nevertheless, HGPS patients are reported to have a loss and lack of adipose tissue caused by impaired adipogenesis [64, 154]. Similarly, a previous study by Xiong et al. reported no or poor adipocyte differentiation from HGPS induced pluripotent stem cells and found a reduction in expression of key adipogenesis proteins: C/EBP-β, C/EBP-δ, C/EBP-α, and PPAR-γ [194]. An immediate difference between previous studies and our results is that we have used naïve stem cells obtained via our novel pH-SKP isolation method, while others used induced pluripotent stem cells [15, 194]. Further differences of Xiong et al. include that

our study's adipocyte medium contained 100× less insulin (10 µg/mL), 250× less dexamethasone (250 µM), 4× less indomethacin (50 µM), no pioglitazone, and only 10% FBS instead of knock-out serum. Another difference is that we also found that directly seeding pH-SKP spheroids (and not as a single-cell suspension) resulted in high-dense colonies after 24 to 48 h of spheroid adherence. This was found most optimal before adipogenesis initiation. The above-used conditions in this study compared to other studies might indicate that adjusted conditions are required to differentiate HGPS stem cells into adipocytes *in vitro*. However, with the overall consensus of impairment and lack of adipose tissue in HGPS patients, our *in vitro* data was surprising. Therefore, a literature study was performed with the focus on our *in vitro* manipulation method—including the adipogenesis-inducing supplements—in relation to *in vivo* conditions with progerin that lacks such supplements.

Based on the adipocyte literature study, an adipogenesis pathway map was constructed. This map revealed a main adipogenesis core system, including C/EBP-β, C/EBP-δ, C/EBP-α, and PPAR-γ. Besides the core system, five additional related sub-pathway groups of interest were found, including "Early differentiation initiators," "Wnt/β-catenin signaling," "TNFα and macrophage cytokines," "Notch," and "DLK-1/Pref-1." Together, with our pH-SKP differentiation method, results indicate that the "Early differentiation initiators" pathway group—responsible for adipogenesis activation—is functioning *in vitro* adequately in HGPS pH-SKP stem cells with progerin expression. Further direct evaluation of those respective proteins is required to confirm this statement. However, based on our adipogenesis pathway map, we speculate that the impairment and lack of adipose tissue found in HGPS patients is due to indirect inhibition of the "Early differentiation initiators" group and the PPAR-γ core system by progerin via direct or indirect interference of early activators present in the sub-pathway groups "Wnt/β-catenin signaling," "TNFα and macrophage cytokines," "Notch," and "DLK-1/Pref-1,"—all described in detail in Chapter 3.4, Adipogenesis Pathway [31, 133, 154].

In conclusion, we report the applicability of pH-SKP isolation with HGPS pre-established dermal primary fibroblasts. These HGPS pH-SKPs showed spheroid formation, stemness markers, and differentiation potential, including SMCs, fibroblasts, and adipocytes. Further studies based on the adipogenesis pathway map will be required to further investigate the potential of HGPS adipocyte-differentiated stem cells and their potential alterations. From such results, potential new therapeutic strategies to improve the lipodystrophy aspect of HGPS could be obtained. These findings might also provide insights and strategies concerning the treatment of obesity. Overall, the pH-SKP isolation method is a valuable tool that can be utilized for rare diseases such as HGPS and MAD and provides an attractive *in vitro* model for fundamental and translational research in general.

3.6 Supplemental Data

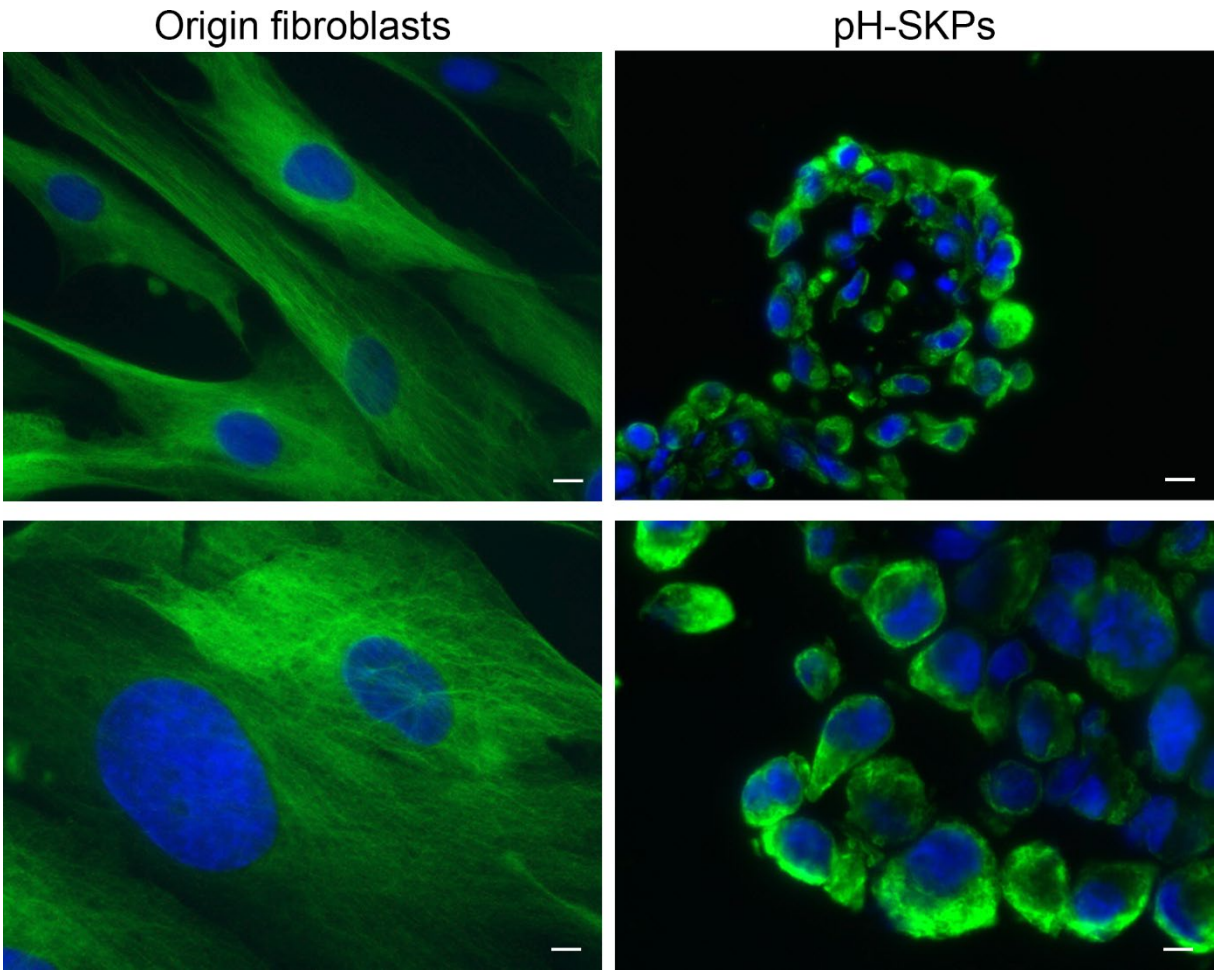

Fig. S1. Nucleus and non-nucleus cellular components are smaller with pH-SKP 3D culture. Representative images of origin fibroblasts and isolated pH-SKP spheroid cells are shown. Fibroblast 2D monocultures (left column) were immunolabeled with P4HD (green) and pH-SKP 3D spheroids (right column), after cryo-sectioning, with vimentin (green). All samples were counterstained for DNA with DAPI (blue). Scale bar: top row, 10 μm; bottom row, 5 μm (n = 3).

4.0 Acknowledgments

4.1A Acknowledgments (directly involved)

In this chapter, I would like to express my gratitude and thanks to the people who have supported me in one way or another regarding my Ph.D. I have divided my thanks into two main groups: people who were directly related to my Ph.D. and people who were indirectly related to it.

First of all, I would like to thank Professor Karima Djabali, my first advisor and boss during my Ph.D. When I first saw an expired Ph.D. vacancy position regarding Karima's group in 2013, I still tried to contact her, and I was fortunate enough to get a reply. This reply led to a Skype call—which was actually only audio due to technical difficulties—and eventually to a Ph.D. position at the Djabali group of Epigenetics of Skin Aging at the Technical University in Munich, Germany. For these successful events, I am very grateful to her. Then, during my Ph.D. and the pH-SKP paper writing, Karima provided strong critique, insight, guidance, an extension of my contract, and more, which have helped me to obtain the content of this thesis and eventually my Ph.D. Therefore, I would like to thank Karima for the opportunity to do my Ph.D. in her group, and all the help she provided, which is too much to mention all. And while the Ph.D. contained lots of challenges, hurdles, and hardships, it was also a pleasant time, with new experiences, and new people. Overall, my time in Djabali lab has made me into a better and stronger scientist and person. And for all of the above, I am very grateful to Karima as my first advisor and boss. Thank you again for the opportunity, which you made possible through your own hardships; your strong guidance; and for replying to my email on May 2nd, 2013, which made all of this possible. All of the supportive help and experiences described above will always be a major piece of my life to which I show my deepest gratitude to you.

Secondly, I also would like to thank Professor Burkhard Rost for taking the role as my second advisor and Professor Markus Ollert for taking up the role as my mentor, both which are necessary for the development and progress of the Ph.D. Furthermore, I thank Burkhard for attending my committee meetings, his well-structured feedback on my results and Ph.D., his pleasant but strong critiques, and his overall guidance for my Ph.D. He is a very busy person, and I express my gratitude to him for taking the position and also for reading and evaluating this thesis as part of the responsibilities of the second advisor. I also would like to thank Markus for attending my committee meetings (he had to travel from Luxembourg and is also a very busy person) and his critical questions and supportive feedback on my results.

Thirdly, I would like to mention the colleagues to whom I wish to express my gratitude. I would like to thank Dr. Vera Wenzel for helping me to start and get familiar with techniques such as

the Tr-SKP isolation method, cryosectioning, immunohistochemistry, and microscopy among others. As the successor of her project, she proved to be an insight of how to address technical difficulties and how to deal with them. Then, I would like to thank Dr. Diana Gabriel for helping me to get started with the western blot-related techniques, and the discussions and talks concerning the results but also for the non-scientific topics. I would like to thank Lu Xiang who started on the same date with his Ph.D. as I did. He was a great help for discussions regarding PCR-related and western blot experiments but also for critical discussions of the mosaic imaging results found in Chapter 2. On top of that, he is a good friend, and I enjoyed spending time with him during lunch and the cinema trips. Finally, I would like to thank Liu Chang who joined the group in the later stages of my Ph.D. Chang had a great insight for paper and data reviewing thanks to his previous experiences, which helped me to look at figures and data from a different and better viewpoint. Additionally, he has become a good friend, and I also enjoyed activities, such as movie watching in the cinema and having lunch, with him.

The following I would like to thank is Dr. Tobias Messemaker who played a big role directly and indirectly for my Ph.D. He was an external source that provided me with various great insights and help during my Ph.D. Tobias helped me significantly by reviewing and commenting on my proposal about the full-mosaic imaging techniques, which was submitted and approved by two reviewers of the International Conference on Engineering and Natural Sciences. This conference took place in Kyoto, Japan, and it was a crucial requirement for the TUM graduate school to obtain my Ph.D. I am very grateful for Tobias's help and feedback since I am also a big fan of Japan. It was my first time visiting and only made possible thanks to the approved conference proposal. My trip there was a big success and an enormous joy; something I will never forget. I also would like to thank Tobias for his critical reading of the first full manuscript version concerning the full-mosaic imaging techniques (Chapter 2 of this thesis), and other general feedback that helped me directly with my Ph.D.

Then, I also want to thank Tobias's indirect influences on my Ph.D., which is as one of my best and finest friends. I know him for almost 12 years now, and together we survived 4 years of bachelor, 2 years of master, 4 years of our Ph.D., and many hurdles in between. Additionally, I am not the most social-seeking person and appreciate my strong friendship with Tobias therefore only more. We pushed each other during our studies to strive for the best and at the same time supported one other—this also happened in squad Hotel. Without his friendship and support, my studies, and even Ph.D. would have been much harder and probably not as successful. For all of this, I am forever grateful to him. Thank you, my dear friend Tobias, for supporting me in all aspects of the Ph.D. before, during, and probably after too.

Finally, as part of my thanks focused on the people directly involved, I would like to thank all the people not specifically mentioned here. I am very grateful for every one of them that provided help, which has led to this thesis and eventually my official Ph.D. certificate.

4.1B Acknowledgments (indirectly involved)

In this section of the acknowledgments, I would like to thank all the people who have been indirectly involved with my Ph.D. but still supported me in some way. Such support has resulted in the wisdom, strength, stability, and perseverance within me to start, continue, and finish my Ph.D. I will start with my closest relatives whom I would like to thank, followed by friends, and others.

First of all, I would like to express my gratitude to my creators Merril Budel (father) and Gerda Budel-Fabriek (mother). Thanks to their efforts and struggles, they were able to provide an environment that has contributed to whom I have become today, for which I am grateful. Furthermore, I would like to thank my father for his feedback and insights as an English expert for whenever I had complicated grammatical questions or needed a sounding board regarding certain English sentence structures. Then, I would like to thank my mother for her always caring support and guidance, which gave me important hope and strength during the difficult and challenging periods. Finally, I also would like to thank them for helping me to move to Germany, for the financial support, for the help at the beginning with German letters, for the send boxes with Dutch specific foods, for the Skype calls, and for lots of other help and support not specifically mentioned here. Thank you. I appreciate all you have done a lot.

Next, I would like to thank my grandparents Jochem Fabriek (grandpa) and Gerda Fabriek (grandma). During my Ph.D., just like my parents, they offered a place and environment where I could go for relaxation, support, and fun. I would like to thank my grandparents for their wisdom on life and helpful alternative viewpoints on various topics. I also would like to specifically express my gratitude for their financial support, which made it possible for me to visit my family regularly and made my life financially more secure—or how they used to say, “You can do something fun with it for once in a while.” My grandparents were always there for me and always interested in the things I would do in the lab; even though it were difficult scientific topics. The effort I put into explaining those difficult topics to them have probably made me into a better scientist, as the level of understanding of an explanation by a layman reflects the level of the expert who did the explaining. Overall, their presence and support were highly appreciated during my Ph.D.

The following I would like to thank are my brothers Tristram Budel and Chanil Budel but also my aunt Olga Fabriek. Chanil and my aunt were often part of the Skype calls on Saturday afternoon together with my mother and grandparents. I always appreciated those Skype calls as it was a way to connect with my family and to express myself. I explained what I was roughly doing for my Ph.D. and always enjoyed their interest and compassion. Each of their unique traits was very appreciated. Then, I also would like to thank Tristram for his feedback, support,

insights, and interests concerning various things involved with doing my Ph.D. and the people around it.

Next, I would like to thank Aida Bitri, who has become, as my girlfriend, a mixture of family and friend. I met Aida eight months after I started my Ph.D. After that, she added an extra thick layer of happiness and joy to my life. And while we had our ups and downs during the development of our relationship, she was always there for me in the good and also the bad times during my Ph.D. In fact, she was my closest support and pillar during the hardships I encountered during the Ph.D. period. In such times of hardship and distress, Aida supported me also by doing things such as grocery shopping, cooking, and cleaning when I was too busy and stressed to do it myself during crucial periods of my Ph.D. I am very thankful to her for that. I am also thankful for her understanding and patience toward all the many and many evenings and weekends that we could have spent together but were sacrificed for the greater good instead—my Ph.D. The same applies to the lack of holidays together that were sacrificed as well due to a shortage of time and financial means. For all of the above things and simply the “dealing” with me, I will forever be grateful toward Aida.

I also would like to thank my other good friends Bas Appeldoorn, Robert-Jan Zandbergen, and Erik Schuszler. Simply their presence and interest have allowed me to unwind from time to time, allowing me to stay strong and focused during crucial moments of my Ph.D. The occasional online gaming with Robert-Jan and especially Bas, Chanil, and Tobias helped a lot to unwind and relax. For those times and their support as an outlet, I am very grateful. Furthermore, the visits of Robert-Jan, Bas, and Tobias at my place in Germany will always be appreciated and cherished. On top of that, Bas has visited me with four times the most, and his stable and down to earth mentality were always very pleasant to have around. He was always very interested and compassionate in my progress, and he always took the effort to get back in touch when I could not, due to very busy periods. For this, I am very grateful to him. Finally, I would like to thank Erik, my old swimming buddy, for his friendship and unfiltered feedback concerning my Ph.D. and other parts of life. Our talks and games of mobile chess and Word feud were (and are) all very much appreciated.

Finally, as part of my thanks focused on the people indirectly involved, I would like to thank all the people not specifically mentioned here. I am very grateful for each and every one of them that have provided some sort of support. Overall, there are most likely actions or things from the people mentioned here that I might not have described, but for the sake of not writing a bookwork with lots of references, I kept it concise and mentioned the things that stand out to me the most at the moment of writing. Nevertheless, I am grateful to everyone, because thanks to them, I had a nice time during my Ph.D. and the strength to finish it. Thank you.

Dankwoord

In deze paragraaf wil ik graag mijn dankwoord voor mijn grootouders Jochem Fabriek (Opa) en Gerda Fabriek (Oma) herhalen in het Nederlands. Tijdens mijn Ph.D., net zoals mijn ouders, boden zij een plek aan waar ik heen kon gaan voor ontspanning, ondersteuning en plezier. Graag wil ik mijn grootouders bedanken voor hun wijsheid over het leven en hulpvolle alternatieve standpunten van verschillende onderwerpen. Ik wil ook graag specifiek mijn dankbaarheid uiten voor hun financiële ondersteuning. Dit maakte mijn leven wat meer financieel zekerder—of zoals zij het zeiden, “Dan kan je er een keer wat leuks mee doen”. Mijn grootouders waren er altijd voor me en altijd geïnteresseerd in hetgeen wat ik deed in het lab; ook al waren dit moeilijke wetenschappelijke onderwerpen. De inspanning die ik deed om zulke moeilijke onderwerpen aan ze uit te leggen heeft mij waarschijnlijk een betere wetenschapper gemaakt, want het niveau van begrijpen door een leek reflecteert het niveau van de expert die het uitlegt. In het algemeen waardeerde ik hun aanwezigheid en ondersteuning tijdens mijn PhD zeer erg.

5.0 References

1. Agarwal, A.K., et al., *Zinc metalloproteinase, ZMPSTE24, is mutated in mandibuloacral dysplasia.* Hum Mol Genet, 2003. **12**(16): p. 1995-2001.
2. Agarwal, A.K. and A. Garg, *Genetic disorders of adipose tissue development, differentiation, and death.* Annu Rev Genomics Hum Genet, 2006. **7**: p. 175-99.
3. Aickin, C.C. and R.C. Thomas, *An investigation of the ionic mechanism of intracellular pH regulation in mouse soleus muscle fibres.* . Journal of Physiology, 1977. **273**: p. 295-316.
4. Arango Duque, G. and A. Descoteaux, *Macrophage cytokines: involvement in immunity and infectious diseases.* Front Immunol, 2014. **5**: p. 491.
5. Avilion, A.A., et al., *Multipotent cell lineages in early mouse development depend on SOX2 function.* Genes and Development, 2003. **17**: p. 126-140.
6. Baek, J.-H., T. McKenna, and M. Eriksson, *Hutchinson-Gilford Progeria Syndrome.* 2013.
7. Balaji, A.B., et al., *Pluripotent lineage of CD133 stem cells isolated from human skin samples.* Indian J Exp Biol, 2013. **51**(2): p. 107-15.
8. Barrowman, J. and S. Michaelis, *ZMPSTE24, an integral membrane zinc metalloprotease with a connection to progeroid disorders.* Biol Chem, 2009. **390**(8): p. 761-73.
9. Beck, J.C., et al., *Computer-assisted visualizations of neural networks: expanding the field of view using seamless confocal montaging.* Journal of Neuroscience Methods., 2000. **98**(2): p. 155-163.
10. Bi, D., et al., *Differentiation of human multipotent dermal fibroblasts into islet-like cell clusters.* BioMed Central Cell Biology, 2010. **11**: p. 46.
11. Biernaskie, J.A., et al., *Isolation of skin-derived precursors (SKPs) and differentiation and enrichment of their Schwann cell progeny* Nature Protocol, 2006. **1**: p. 2803-2812.
12. Boguslavsky, R.L., C.L. Stewart, and H.J. Worman, *Nuclear lamin A inhibits adipocyte differentiation: implications for Dunnigan-type familial partial lipodystrophy.* Hum Mol Genet, 2006. **15**(4): p. 653-63.
13. Booth, A., et al., *Adipose tissue, obesity and adipokines: role in cancer promotion.* Horm Mol Biol Clin Investig, 2015. **21**(1): p. 57-74.
14. Bray, S.J., *Notch signalling: a simple pathway becomes complex.* Nat Rev Mol Cell Biol, 2006. **7**(9): p. 678-89.
15. Budel, L. and K. Djabali, *Rapid isolation and expansion of skin-derived precursor cells from human primary fibroblast cultures.* Biology Open, 2017. **6**(11): p. 1745-1755.
16. Campbell, N.A.R., Jane B.; Urry, Lisa A.; Cain, Michael L.; Wasserman, Steven A.; Minorsky, Peter V.; Jackson, Robert B., *Biology 9th edition ISBN 978-0-8053-6844-4.* 2009: p. 229.
17. Candelario, J., et al., *Perturbation of wild-type lamin A metabolism results in a progeroid phenotype.* Aging Cell, 2008. **7**(3): p. 355-67.
18. Cao, K., et al., *A lamin A protein isoform overexpressed in Hutchinson-Gilford progeria syndrome interferes with mitosis in progeria and normal cells.* Proc Natl Acad Sci U S A, 2007. **104**(12): p. 4949-54.
19. Cao, Z., R.M. Umek, and S.L. McKnight, *Regulated expression of three C/EBP isoforms during adipose conversion of 3T3-L1 cells.* Genes Dev, 1991. **5**.
20. Capanni, C., et al., *Altered pre-lamin A processing is a common mechanism leading to lipodystrophy.* Hum Mol Genet, 2005. **14**(11): p. 1489-502.
21. Capell, B.C. and F.S. Collins, *Human laminopathies: nuclei gone genetically awry.* Nat Rev Genet, 2006. **7**(12): p. 940-52.
22. Capell, B.C., et al., *Inhibiting farnesylation of progerin prevents the characteristic nuclear blebbing of Hutchinson-Gilford progeria syndrome.* Proc Natl Acad Sci U S A, 2005. **102**(36): p. 12879-84.

23. Capell, B.C., et al., *Inhibiting farnesylation of progerin prevents the characteristic nuclear blebbing of Hutchinson-Gilford progeria syndrome.* Proceedings of the National Academy of Sciences of the United States of America, 2005. **102**(36): p. 12879-12884.
24. Casasola, A., et al., *Prelamin A processing, accumulation and distribution in normal cells and laminopathy disorders.* Nucleus, 2016. **7**(1): p. 84-102.
25. Cawthorn, W.P. and J.K. Sethi, *TNF-alpha and adipocyte biology.* FEBS Lett, 2008. **582**(1): p. 117-31.
26. Chawla, A., et al., *Peroxisome proliferator-activated receptor (PPAR) gamma: adipose-predominant expression and induction early in adipocyte differentiation.* Endocrinology, 1994. **135**(2): p. 798-800.
27. Chiang, Y., et al., *EGF upregulates Na+/H+ exchanger NHE1 by post-translational regulation that is important for cervical cancer cell invasiveness.* J Cell Physiol, 2008. **214**(3): p. 810-9.
28. Chinnici, C.M., et al., *Isolation and characterization of multipotent cells from human fetal dermis.* Cell Transplant, 2014. **23**(10): p. 1169-85.
29. Chow, S.K., , , et al., *Automated microscopy system for mosaic acquisition and processing.* Journal of Microscopy, 2006. **222**: p. 76-84.
30. Clewes, O., et al., *Human epidermal neural crest stem cells (hEPI-NCSC)--characterization and directed differentiation into osteocytes and melanocytes.* Stem Cell Rev, 2011. **7**(4): p. 799-814.
31. Constant, V.A., et al., *Macrophage-conditioned medium inhibits the differentiation of 3T3-L1 and human abdominal preadipocytes.* Diabetologia, 2006. **49**(6): p. 1402-11.
32. Constantinescu, D., et al., *Lamin A/C expression is a marker of mouse and human embryonic stem cell differentiation.* Stem Cells, 2006. **24**(1): p. 177-85.
33. Corrigan, D.P., et al., *Prelamin A endoproteolytic processing in vitro by recombinant Zmpste24.* Biochem J, 2005. **387**(Pt 1): p. 129-38.
34. Crane, G.M., E. Jeffery, and S.J. Morrison, *Adult haematopoietic stem cell niches.* Nature Reviews Immunology, 2017. **17**: p. 573.
35. Cristancho, A.G. and M.A. Lazar, *Forming functional fat: a growing understanding of adipocyte differentiation.* Nat Rev Mol Cell Biol, 2011. **12**(11): p. 722-34.
36. database, T.u.m., *http://www.umd.be/LMNA/.* 2012.
37. De Kock, J., et al., *Characterization and hepatic differentiation of skin-derived precursors from adult foreskin by sequential exposure to hepatogenic cytokines and growth factors reflecting liver development.* Toxicol In Vitro, 2009. **23**(8): p. 1522-7.
38. de la Rosa, J., et al., *Prelamin A causes progeria through cell-extrinsic mechanisms and prevents cancer invasion.* Nat Commun, 2013. **4**: p. 2268.
39. De Sandre-Giovannoli, A., et al., *Lamin a truncation in Hutchinson-Gilford progeria.* Science, 2003. **300**(5628): p. 2055.
40. Dechat, T., et al., *Nuclear lamins.* Cold Spring Harb Perspect Biol, 2010. **2**(11): p. a000547.
41. Denker, S.P., et al., *Direct binding of the Na--H exchanger NHE1 to ERM proteins regulates the cortical cytoskeleton and cell shape independently of H(+) translocation.* Molecular Cell, 2000. **6**: p. 1425-1436.
42. Deutsch, M.J., et al., *Digital image analysis approach for lipid droplet size quantitation of Oil Red O-stained cultured cells.* Analytical Biochemistry, 2014. **445**: p. 87-89.
43. Dyce, P.W., et al., *Stem cells with multilineage potential derived from porcine skin.* Biochem Biophys Res Commun, 2004. **316**(3): p. 651-8.
44. Eckersley-Maslin, M.A., et al., *Lamin A/C is expressed in pluripotent mouse embryonic stem cells.* Nucleus, 2013. **4**(1): p. 53-60.
45. Edwards, C.S., et al., *Mosaicking of global planetary image datasets: 1. Techniques and data processing for Thermal Emission Imaging System (THEMIS) multi-spectral data. Journal of Geophysical Research: Planets.* Journal of Geophysical Research E: Planets, 2011. **116**(10).
46. Eisenback, J.D., *A technique for making high-resolution megapixel mosaic photomicrographs of nematodes.* Journal of Nematology, 2012. **44**(3): p. 260-263.

47. Eriksson, M., et al., *Recurrent de novo point mutations in lamin A cause Hutchinson-Gilford progeria syndrome.* Nature, 2003. **423**(6937): p. 293-8.
48. Fernandes, K.J.L., et al., *A dermal niche for multipotent adult skin-derived precursor cells.* Nat Cell Biol, 2004. **6**(11): p. 1082-1093.
49. Fernandes, K.J.L., et al., *A dermal niche for multipotent adult skin-derived precursor cells.* Nature Cell Biology, 2004. **6**: p. 1082-1093.
50. Fernandez, P., et al., *Transformation resistance in a premature aging disorder identifies a tumor-protective function of BRD4.* Cell Rep, 2014. **9**(1): p. 248-60.
51. Fitzgerald, R.C., M.B. Omary, and G. Triadafilopoulos, *Acid modulation of HT29 cell growth and differentiation. An in vitro model for Barrett's esophagus.* Journal of Cell Science, 1997. **110**: p. 663-671.
52. Foundation, P.R., http://www.progeriaresearch.org, 2018.
53. Franke, W.W., M. Hergt, and C. Grund, *Rearrangement of the vimentin cytoskeleton during adipose conversion: formation of an intermediate filament cage around lipid globules.* Cell, 1987. **49**(1): p. 131-141.
54. Fuchs, E. and T. Chen, *A matter of life and death: self-renewal in stem cells.* EMBO Rep, 2013. **14**(1): p. 39-48.
55. Ghosh, S., et al., *Three-dimensional culture of melanoma cells profoundly affects gene expression profile: a high density oligonucleotide array study.* J Cell Physiol, 2005. **204**(2): p. 522-31.
56. Gilbert., S.F., *Developmental Biology, 6th edition, ISBN-10: 0-87893-243-7.* 2000.
57. Gilford, H., *On a Condition of Mixed Premature and Immature Development.* Med Chir Trans, 1897. **80**: p. 17-46.25.
58. Giralt, M. and F. Villarroya, *White, brown, beige/brite: different adipose cells for different functions?* Endocrinology, 2013. **154**(9): p. 2992-3000.
59. Godinho, S.A., et al., *Oncogene-like induction of cellular invasion from centrosome amplification.* Nature, 2014. **510**(7503): p. 167-171.
60. Goldman, R.D., et al., *Accumulation of mutant lamin A causes progressive changes in nuclear architecture in Hutchinson-Gilford progeria syndrome.* Proc Natl Acad Sci U S A, 2004. **101**(24): p. 8963-8.
61. Gordon, L.B., W.T. Brown, and F.S. Collins, *Hutchinson-Gilford Progeria Syndrome*, in *GeneReviews((R))*, M.P. Adam, et al., Editors. 1993, University of Washington, Seattle University of Washington, Seattle. GeneReviews is a registered trademark of the University of Washington, Seattle. All rights reserved.: Seattle (WA).
62. Gordon, L.B., et al., *Clinical trial of a farnesyltransferase inhibitor in children with Hutchinson-Gilford progeria syndrome.* Proc Natl Acad Sci U S A, 2012. **109**(41): p. 16666-71.
63. Gordon, L.B., et al., *Impact of Farnesylation Inhibitors on Survival in Hutchinson-Gilford Progeria Syndrome.* Circulation, 2014.
64. Gordon, L.B., et al., *Disease progression in Hutchinson-Gilford progeria syndrome: impact on growth and development.* Pediatrics, 2007. **120**(4): p. 824-33.
65. Gudjonsson, T., et al., *Immortalization protocols used in cell culture models of human breast morphogenesis.* Cell Mol Life Sci, 2004. **61**(19-20): p. 2523-34.
66. Guo, W., et al., *Efficient differentiation of insulin-producing cells from skin-derived stem cells.* Cell Prolif, 2009. **42**(1): p. 49-62.
67. Gurnell, M., *Peroxisome proliferator-activated receptor γ and the regulation of adipocyte function: lessons from human genetic studies.* Best Practice & Research Clinical Endocrinology & Metabolism. **19**(4): p. 501-523.
68. Hayflick, L., *The cell biology of aging.* Clin Geriatr Med, 1985. **1**(1): p. 15-27.
69. Heeren, J. and L. Scheja, *Brown adipose tissue and lipid metabolism.* Curr Opin Lipidol, 2018. **29**(3): p. 180-185.
70. Hill, R.P., et al., *Generation and characterization of multipotent stem cells from established dermal cultures.* PLoS One, 2012. **7**(11): p. e50742.

71. Hill, R.P., et al., *"Generation and characterization of multipotent stem cells from established dermal cultures.".* PLoS One, 2012. **7**(11): p. e50742.
72. Hishida, T., et al., *The role of C/EBPdelta in the early stages of adipogenesis.* Biochimie, 2009. **91**(5): p. 654-7.
73. Howard, J.M., G.P. Pidgeon, and J.V. Reynolds, *Leptin and gastro-intestinal malignancies.* Obes Rev, 2010. **11**(12): p. 863-74.
74. Hu, Q., et al., *Memory in induced pluripotent stem cells: reprogrammed human retinal-pigmented epithelial cells show tendency for spontaneous redifferentiation.* Stem Cells, 2010. **28**(11): p. 1981-91.
75. Huang, H.-P., et al., *Epithelial cell adhesion molecule (EpCAM) complex proteins promote transcription factor-mediated pluripotency reprogramming.* Journal of Biological Chemistry, 2011.
76. Huang, H.I., et al., *Multilineage differentiation potential of fibroblast-like stromal cells derived from human skin.* Tissue Eng Part A, 2010. **16**(5): p. 1491-501.
77. Hunt, D.P., et al., *A highly enriched niche of precursor cells with neuronal and glial potential within the hair follicle dermal papilla of adult skin.* Stem Cells, 2008. **26**: p. 163-172.
78. Hutchinson, J., *Congenital Absence of Hair and Mammary Glands with Atrophic Condition of the Skin and its Appendages, in a Boy whose Mother had been almost wholly Bald from Alopecia Areata from the age of Six.* Med Chir Trans, 1886. **69**: p. 473-7.
79. Ikeda, K., P. Maretich, and S. Kajimura, *The Common and Distinct Features of Brown and Beige Adipocytes.* Trends in Endocrinology & Metabolism, 2018. **29**(3): p. 191-200.
80. International Stem Cell Initiative, *Characterization of human embryonic stem cell lines by the International Stem Cell Initiative.* Nature Biotechnology, 2007. **25**(7): p. 803-816.
81. Joannides, A., et al., *Efficient generation of neural precursors from adult human skin: astrocytes promote neurogenesis from skin-derived stem cells.* Lancet, 2004. **364**(9429): p. 172-8.
82. Joannides, A., et al., *Efficient generation of neural precursors from adult human skin: astrocytes promote neurogenesis from skin-derived stem cells.* Lancet, 2004. **364**: p. 172-178.
83. Jordan, B.F., F. Gourgue, and P.D. Cani, *Adipose Tissue Metabolism and Cancer Progression: Novel Insights from Gut Microbiota?* Curr Pathobiol Rep, 2017. **5**(4): p. 315-322.
84. Kapus A., et al., *Functional characterization of three isoforms of the Na+/H+ exchanger stably expressed in Chinese hamster ovary cells. ATP dependence, osmotic sensitivity, and role in cell proliferation.*
. Journal of Biological Chemistry, 1994. **23**: p. 23544-23552.
85. Kaur, G. and J.M. Dufour, *Cell lines: Valuable tools or useless artifacts.* Spermatogenesis, 2012. **2**(1): p. 1-5.
86. Kemp, G., H. Young, and L. Fliegel, *Structure and function of the human Na+/H+ exchanger isoform 1.*
Kemp G, Young H, Fliegel L. Channels (Austin), 2008. **2**(5): p. 329-336.
87. Kenny, P.A., et al., *The morphologies of breast cancer cell lines in three-dimensional assays correlate with their profiles of gene expression.* Mol Oncol, 2007. **1**(1): p. 84-96.
88. Kumar, R., et al., *Adult skin-derived precursor Schwann cells exhibit superior myelination and regeneration supportive properties compared to chronically denervated nerve-derived Schwann cells.* Experimental Neurology, 2016. **278**: p. 127-142.
89. Kuroda, Y., et al., *Unique multipotent cells in adult human mesenchymal cell populations.* Proc Natl Acad Sci U S A, 2010. **107**(19): p. 8639-43.
90. Kwok, C.K., P.K. Tam, and E.S. Ngan, *Potential use of skin-derived precursors (SKPs) in establishing a cell-based treatment model for Hirschsprung's disease.* Journal of Pediatric Surgery, 2013. **48**: p. 619-628.

91. Lavoie, J.F., et al., *Skin-derived precursors differentiate into skeletogenic cell types and contribute to bone repair.* Stem Cells development, 2009. **18**: p. 893-906.
92. Lebonvallet, N., et al., *Characterization of neurons from adult human skin-derived precursors in serum-free medium : a PCR array and immunocytological analysis. .* Experimental Dermatology, 2012. **21**: p. 195-200.
93. Lee, J.-E. and K. Ge, *Transcriptional and epigenetic regulation of PPARγ expression during adipogenesis.* Cell & Bioscience, 2014. **4**(1): p. 29.
94. Legesse, F.B., et al., *Seamless stitching of tile scan microscope images. Journal of microscopy.* Journal of Microscopy, 2015. **258**(3): p. 223-232.
95. Legg, J., et al., *Role of melanoma chondroitin sulphate proteoglycan in patterning stem cells in human interfollicular epidermis.* Development, 2003. **130**(24): p. 6049-6063.
96. Lehman, T.A., et al., *p53 mutations in human immortalized epithelial cell lines.* Carcinogenesis, 1993. **14**(5): p. 833-9.
97. Lendahl, U., L.B. Zimmerman, and R.D.G. McKay, *CNS stem cells express a new class of intermediate filament protein.* Cell, 1990. **60**: p. 585-595.
98. Lermen, D., et al., *Neuro-muscular differentiation of adult porcine skin derived stem cell-like cells.* PLoS One, 2010. **5**(1): p. e8968.
99. Leung, B.M., et al., *Media additives to promote spheroid circularity and compactness in hanging drop platform.* Biomater Sci, 2015. **3**(2): p. 336-44.
100. Li, L., et al., *Human dermal stem cells differentiate into functional epidermal melanocytes.* J Cell Sci, 2010. **123**(Pt 6): p. 853-60.
101. Limbourg, A., et al., *Genetic reporter analysis reveals an expandable reservoir of OCT4+ cells in adult skin.* Cell Regen (Lond), 2014. **3**(1): p. 9.
102. Lin, F. and H.J. Worman, *Structural organization of the human gene encoding nuclear lamin A and nuclear lamin C.* J Biol Chem, 1993. **268**(22): p. 16321-6.
103. Lin, F.T. and M.D. Lane, *CCAAT/enhancer binding protein alpha is sufficient to initiate the 3T3-L1 adipocyte differentiation program.* Proc Natl Acad Sci U S A, 1994. **91**(19): p. 8757-61.
104. Liu, Q., et al., *Muse Cells, a New Type of Pluripotent Stem Cell Derived from Human Fibroblasts.* Cell Reprogram, 2016. **18**(2): p. 67-77.
105. Liu, S., G. Dontu, and M.S. Wicha, *Mammary stem cells, self-renewal pathways, and carcinogenesis.* Breast Cancer Research, 2005. **7**(3): p. 86.
106. Loo, B.W.J., , , W. Meyer-Ilse, and S.S. Rothman, *Automatic image acquisition, calibration and montage assembly for biological X-ray microscopy.* Journal of Microscopy, 2000. **197**: p. 185-201.
107. Lowe, C.E., S. O'Rahilly, and J.J. Rochford, *Adipogenesis at a glance.* J Cell Sci, 2011. **124**(Pt 16): p. 2681-6.
108. Lu, T.-Y., et al., *Epithelial Cell Adhesion Molecule Regulation Is Associated with the Maintenance of the Undifferentiated Phenotype of Human Embryonic Stem Cells.* Journal of Biological Chemistry, 2010. **285**(12): p. 8719-8732.
109. Mackenzie, C.G., J.B. Mackenzie, and P. Beck, *The effect of pH on growth, protein synthesis, and lipid-rich particles of cultured mammalian cells.* Journal of Biophusical Biochemistry and cytology, 1961. **9**: p. 141-156.
110. Malhas, A., N.J. Saunders, and D.J. Vaux, *The nuclear envelope can control gene expression and cell cycle progression via miRNA regulation.* Cell Cycle, 2010. **9**(3): p. 531-539.
111. Mao, D., et al., *Skin-derived precursor cells promote angiogenesis and stimulate proliferation of endogenous neural stem cells after cerebral infarction.* Biomedical Research international, 2015. **2015**: p. 2015:945846.
112. Maritan, S.M., E.Y. Lian, and L.M. Mulligan, *An Efficient and Flexible Cell Aggregation Method for 3D Spheroid Production.* J Vis Exp, 2017(121).
113. Marks, R.L., S.M. Rock, and M.J. Lee, *Real-Time Video Mosaicking of the Ocean Floor. IEEE Journal of Oceanic Engineering.* IEEE Transactions on Pattern Analysis and Machine Intelligence, 1994. **20**(3): p. 229-241.

114. McClintock, D., L.B. Gordon, and K. Djabali, *Hutchinson–Gilford progeria mutant lamin A primarily targets human vascular cells as detected by an anti-Lamin A G608G antibody.* Proceedings of the National Academy of Sciences of the United States of America, 2006. **103**(7): p. 2154-2159.
115. McClintock, D., et al., *The mutant form of lamin A that causes Hutchinson-Gilford progeria is a biomarker of cellular aging in human skin.* PLoS One, 2007. **2**(12): p. e1269.
116. McClintock, D., et al., *The Mutant Form of Lamin A that Causes Hutchinson-Gilford Progeria Is a Biomarker of Cellular Aging in Human Skin.* PLoS ONE, 2007. **2**: p. e1269.
117. Medvedev, S.P., A.I. Shevchenko, and S.M. Zakian, *Induced Pluripotent Stem Cells: Problems and Advantages when Applying them in Regenerative Medicine.* Acta Naturae, 2010. **2**(2): p. 18-28.
118. Mehrabi, M., et al., *Differentiation of human skin-derived precursor cells into functional islet-like insulin-producing cell clusters.* In Vitro Cell Dev Biol Anim, 2015. **51**: p. 595-603.
119. Meima, M.E., et al., *The sodium-hydrogen exchanger NHE1 is an Akt substrate necessary for actin filament reorganization by growth factors.* Journal of Biological Chemistry, 2009. **284**: p. 26666-26675.
120. Melcer, S., Y. Gruenbaum, and G. Krohne, *Invertebrate lamins.* Experimental Cell Research, 2007. **313**(10): p. 2157-2166.
121. Mitalipov, S. and D. Wolf, *Totipotency, pluripotency and nuclear reprogramming.* Adv Biochem Eng Biotechnol, 2009. **114**: p. 185-99.
122. Mitsui, K., et al., *The homeoprotein Nanog is required for maintenance of pluripotency in mouse epiblast and ES cells.* Cell, 2003. **113**: p. 631-642.
123. Mounkes, L., et al., *The laminopathies: nuclear structure meets disease.* Curr Opin Genet Dev, 2003. **13**(3): p. 223-30.
124. Mozafari, S., et al., *Skin-derived neural precursors competitively generate functional myelin in adult demyelinated mice.* Journal of Clinical Investigation, 2015. **125**: p. 3642-3656.
125. Musich, P.R. and Y. Zou, *DNA-damage accumulation and replicative arrest in Hutchinson-Gilford progeria syndrome.* Biochem Soc Trans, 2011. **39**(6): p. 1764-9.
126. Musich, P.R. and Y. Zou, *Genomic instability and DNA damage responses in progeria arising from defective maturation of prelamin A.* Aging (Albany NY), 2009. **1**(1): p. 28-37.
127. Myllyharju, J., *Prolyl 4-hydroxylases, the key enzymes of collagen biosynthesis.* Mathematical Biosiences, 2003. **22**(1): p. 15-24.
128. Navarro, C.L., P. Cau, and N. Levy, *Molecular bases of progeroid syndromes.* Hum Mol Genet, 2006. **15 Spec No 2**: p. R151-61.
129. Novelli, G., et al., *Mandibuloacral Dysplasia Is Caused by a Mutation in LMNA-Encoding Lamin A/C.* The American Journal of Human Genetics, 2002. **71**(2): p. 426-431.
130. Nusse, R. and H. Clevers, *Wnt/b-Catenin Signaling, Disease, and Emerging Therapeutic Modalities.* Cell. **169**(6): p. 985-999.
131. Okamoto, T., et al., *Clonal heterogeneity in differentiation potential of immortalized human mesenchymal stem cells.* Biochemical and Biophysical Research Communication, 2002. **295**: p. 354-361.
132. Olive, M., et al., *Cardiovascular pathology in Hutchinson-Gilford progeria: correlation with the vascular pathology of aging.* Arterioscler Thromb Vasc Biol, 2010. **30**(11): p. 2301-9.
133. Osorio, F.G., et al., *Nuclear lamina defects cause ATM-dependent NF-kappaB activation and link accelerated aging to a systemic inflammatory response.* Genes Dev, 2012. **26**(20): p. 2311-24.
134. Pan, S., et al., *Application of a novel population of multipotent stem cells derived from skin fibroblasts as donor cells in bovine SCNT.* PLoS One, 2015. **10**(1): p. e0114423.
135. Patel, J., et al., *Foreign body-induced granulation tissue is a source of adult stem cells.* Transl Res, 2010. **155**(4): p. 191-9.

136. Pekovic, V. and C.J. Hutchison, *Adult stem cell maintenance and tissue regeneration in the ageing context: the role for A-type lamins as intrinsic modulators of ageing in adult stem cells and their niches.* J Anat, 2008. **213**(1): p. 5-25.
137. Peric-Hupkes, D., et al., *Molecular maps of the reorganization of genome-nuclear lamina interactions during differentiation.* Mol Cell, 2010. **38**(4): p. 603-13.
138. Pesce, M. and H.R. Scholer, *The homeoprotein Nanog is required for maintenance of pluripotency in mouse epiblast and ES cells.* Stem Cells, 2001. **19**: p. 271-278.
139. Politano, L., et al., *Advances in basic and clinical research in laminopathies.* Acta Myol, 2013. **32**(1): p. 18-22.
140. Price, D.L., et al., *High-resolution large-scale mosaic imaging using multiphoton microscopy to characterize transgenic mouse models of human neurological disorders.* Neuroinformatics, 2006. **4**: p. 65-80.
141. Prokocimer, M., R. Barkan, and Y. Gruenbaum, *Hutchinson-Gilford progeria syndrome through the lens of transcription.* Aging Cell, 2013. **12**(4): p. 533-43.
142. Ragnauth, C.D., et al., *Prelamin A acts to accelerate smooth muscle cell senescence and is a novel biomarker of human vascular aging.* Circulation, 2010. **121**(20): p. 2200-10.
143. Ramboer, E., et al., *Strategies for immortalization of primary hepatocytes.* J Hepatol, 2014. **61**(4): p. 925-43.
144. Rawlings, N.D. and A.J. Barrett, *Families of serine peptidases.* Methods Enzymol, 1994. **244**: p. 19-61.
145. Rensen, S.S., P.A. Doevendans, and G.J. van Eys, *Regulation and characteristics of vascular smooth muscle cell phenotypic diversity.* Netherland heart Journal, 2007. **15**(3): p. 100-108.
146. Rietze, R.L. and B.A. Reynolds, *Neural stem cell isolation and characterization.* Methods Enzymol, 2006. **419**: p. 3-23.
147. Rittie, L. and G.J. Fisher, *Isolation and culture of skin fibroblasts.* Methods Mol Med, 2005. **117**: p. 83-98.
148. Rosen, E.D., et al., *C/EBPalpha induces adipogenesis through PPARgamma: a unified pathway.* Genes Dev, 2002. **16**(1): p. 22-6.
149. Ross, D.A., P.K. Rao, and T. Kadesch, *Dual roles for the Notch target gene Hes-1 in the differentiation of 3T3-L1 preadipocytes.* Mol Cell Biol, 2004. **24**(8): p. 3505-13.
150. Saely, C.H., K. Geiger, and H. Drexel, *Brown versus white adipose tissue: a mini-review.* Gerontology, 2012. **58**(1): p. 15-23.
151. Sagelius, H., et al., *Targeted transgenic expression of the mutation causing Hutchinson-Gilford progeria syndrome leads to proliferative and degenerative epidermal disease.* J Cell Sci, 2008. **121**(Pt 7): p. 969-78.
152. Sangho, R. and P. Sang Kyu, *Modification of Pluripotency and Neural Crest-Related Genes' expression in Murine Skin-Derived Precursor Cells by Leukemia Inhibitory Factor (LIF).* International Journal of Oral Biology, 2012. **37**(4): p. 175-180.
153. Santini, R., et al., *SOX2 regulates self-renewal and tumorigenicity of human melanoma-initiating cells.* Oncogene, 2014. **33**(38): p. 4697-4708.
154. Scaffidi, P. and T. Misteli, *Lamin A-dependent misregulation of adult stem cells associated with accelerated ageing.* Nat Cell Biol, 2008. **10**(4): p. 452-9.
155. Schneider, S., et al., *Adipose-derived mesenchymal stem cells from liposuction and resected fat are feasible sources for regenerative medicine.* Eur J Med Res, 2017. **22**(1): p. 17.
156. Sedger, L.M. and M.F. McDermott, *TNF and TNF-receptors: From mediators of cell death and inflammation to therapeutic giants – past, present and future.* Cytokine & Growth Factor Reviews, 2014. **25**(4): p. 453-472.
157. Shim, J.H., T.R. Lee, and D.W. Shin, *Novel in vitro culture condition improves the stemness of human dermal stem/progenitor cells.* Mol Cells, 2013. **36**(6): p. 556-63.
158. Shu, B., et al., *Directed differentiation of skin-derived precursors into fibroblast-like cells.* International journal of clinical and experimental pathology, 2014. **7**: p. 1478-1486.

159. Shumaker, D.K., E.R. Kuczmarski, and R.D. Goldman, *The nucleoskeleton: lamins and actin are major players in essential nuclear functions.* Current Opinion in Cell Biology, 2003. **15**(3): p. 358-366.
160. Slepkov, E. and L. Fliegel, *Structure and function of the NHE1 isoform of the Na+/H+ exchanger.* Biochemistry and Cellular Biology, 2002. **80**(5).
161. Snoussi, K., et al., *Leptin and leptin receptor polymorphisms are associated with increased risk and poor prognosis of breast carcinoma.* BMC Cancer, 2006. **6**: p. 38.
162. Stegmüller, J., et al., *AN2, the mouse homologue of NG2, is a surface antigen on glial precursor cells implicated in control.* Journal of Neurocytology, 2002. **31**(6-7): p. 497-505.
163. Steinbach, S.K., et al., *Directed differentiation of skin-derived precursors into functional vascular smooth muscle cells.* Arteriosclerosis, Thrombosis, and Vascular Biology, 2011. **31**: p. 2938-2948.
164. Tai, M.H., et al., *Oct4 expression in adult human stem cells: evidence in support of the stem cell theory of carcinogenesis.* Carcinogenesis, 2005. **26**(2): p. 495-502.
165. Takagi, A., et al., *Three-dimensional cellular spheroid formation provides human prostate tumor cells with tissue-like features.* Anticancer Res, 2007. **27**(1a): p. 45-53.
166. Tian, T., et al., *Muse Cells Derived from Dermal Tissues Can Differentiate into Melanocytes.* Cell Reprogram, 2017. **19**(2): p. 116-122.
167. Toma, J.G., et al., *Isolation of multipotent adult stem cells from the dermis of mammalian skin.* Nature Cell Biology, 2001. **3**: p. 778-784.
168. Toma, J.G., et al., *Isolation of multipotent adult stem cells from the dermis of mammalian skin.* Nat Cell Biol, 2001. **3**(9): p. 778-84.
169. Toma, J.G., et al., *Isolation and characterization of multipotent skin-derived precursors from human skin.* Stem Cells, 2005. **23**: p. 727-737.
170. Toma, J.G., et al., *Isolation and characterization of multipotent skin-derived precursors from human skin.* Stem Cells, 2005. **23**(6): p. 727-37.
171. Tontonoz, P., E. Hu, and B.M. Spiegelman, *Stimulation of adipogenesis in fibroblasts by PPAR gamma 2, a lipid-activated transcription factor.* Cell, 1994. **79**(7): p. 1147-56.
172. Tracy, L.E., R.A. Minasian, and E.J. Caterson, *Extracellular Matrix and Dermal Fibroblast Function in the Healing Wound.* Adv Wound Care (New Rochelle), 2016. **5**(3): p. 119-136.
173. Uchida, N., et al., *Direct isolation of human central nervous system stem cells.* Proceedings of the National Academy of Sciences, 2000. **97**: p. 14720-14725.
174. van der Flier, L.G. and H. Clevers, *Stem cells, self-renewal, and differentiation in the intestinal epithelium.* Annu Rev Physiol, 2009. **71**: p. 241-60.
175. van Deursen, J.M., *The role of senescent cells in ageing.* Nature, 2014. **509**: p. 439.
176. Vaskova, E.A., et al., *"Epigenetic memory" phenomenon in induced pluripotent stem cells.* Acta Naturae, 2013. **5**(4): p. 15-21.
177. Vasudeva, V.S., Abd-El-Barr. M.M., and J.H. Chi, *Implantation of Neonatal Skin-Derived Precursor Schwann Cells Improves Outcomes After Incomplete Cervical Spinal Cord Injury in Rats.* Neurosurgery, 2015. **77**: p. N15-17.
178. Verstraeten, V.L., et al., *Reorganization of the nuclear lamina and cytoskeleton in adipogenesis.* Histochemical Cell Biology, 2011. **135**(3): p. 251-261.
179. Vigouroux, C., et al., *Molecular mechanisms of human lipodystrophies: from adipocyte lipid droplet to oxidative stress and lipotoxicity.* Int J Biochem Cell Biol, 2011. **43**(6): p. 862-76.
180. Villa-Bellosta, R., et al., *Defective extracellular pyrophosphate metabolism promotes vascular calcification in a mouse model of Hutchinson-Gilford progeria syndrome that is ameliorated on pyrophosphate treatment.* Circulation, 2013. **127**(24): p. 2442-51.
181. Viteri, G., Y.W. Chung, and E.R. Stadtman, *Effect of progerin on the accumulation of oxidized proteins in fibroblasts from Hutchinson Gilford progeria patients.* Mech Ageing Dev, 2010. **131**(1): p. 2-8.

182. Wakao, S., et al., *Multilineage-differentiating stress-enduring (Muse) cells are a primary source of induced pluripotent stem cells in human fibroblasts.* Proc Natl Acad Sci U S A, 2011. **108**(24): p. 9875-80.
183. Walsh, T., et al., *Bioreactor Expansion of Skin-Derived Precursor Schwann Cells.* Methods in Molecular Biology, 2016. **15.02**: p. 103-110.
184. Wang, Y., et al., *Blocking farnesylation of the prelamin A variant in Hutchinson-Gilford progeria syndrome alters the distribution of A-type lamins.* Nucleus, 2012. **3**(5): p. 452-62.
185. Wenzel, V., et al., *Na¨ıve adult stem cells from patients with Hutchinson-Gilford progeria syndrome express low levels of progerin in vivo.* Biology Open, 2012: p. 1-11.
186. Wenzel, V., et al., *Naive adult stem cells from patients with Hutchinson-Gilford progeria syndrome express low levels of progerin in vivo.* Biol Open, 2012. **1**(6): p. 516-26.
187. Wheaton, K., et al., *Progerin-Induced Replication Stress Facilitates Premature Senescence in Hutchinson-Gilford Progeria Syndrome.* Mol Cell Biol, 2017. **37**(14).
188. Wikipedia, *List of distinct cell types in the adult human body.* https://en.wikipedia.org/wiki/List_of_distinct_cell_types_in_the_adult_human_body, 2018.
189. Williams, I.R., *Fibroblasts A2 - Delves, Peter J*, in *Encyclopedia of Immunology (Second Edition)*. 1998, Elsevier: Oxford. p. 905-909.
190. Williams, S.C.P., *Link between obesity and cancer.* Proceedings of the National Academy of Sciences of the United States of America, 2013. **110**(22): p. 8753-8754.
191. Willis, M.A. and R.J. Fox, *Progressive Multiple Sclerosis.* Continuum (Minneap Minn), 2016. **22**: p. 785-798.
192. Wozniak, S.E., et al., *Adipose tissue: the new endocrine organ? A review article.* Dig Dis Sci, 2009. **54**(9): p. 1847-56.
193. Xiao, J., et al., *Isolation of Bovine Skin-Derived Precursor Cells and Their Developmental Potential After Nuclear Transfer.* Cell Reprogram, 2016. **18**(6): p. 411-418.
194. Xiong, Z.M., et al., *An inhibitory role of progerin in the gene induction network of adipocyte differentiation from iPS cells.* Aging (Albany NY), 2013. **5**(4): p. 288-303.
195. Xu, M., et al., *Targeting senescent cells enhances adipogenesis and metabolic function in old age.* Elife, 2015. **4**: p. e12997.
196. Yang, J.H., et al., *Generation of insulin-producing cells from gnotobiotic porcine skin-derived stem cells.* Biochem Biophys Res Commun, 2010. **397**(4): p. 679-84.
197. Yang, J.H., et al., *Skin-derived stem cells in human scar tissues: a novel isolation and proliferation technique and their differentiation potential to neurogenic progenitor cells.* Tissue Eng Part C Methods, 2010. **16**(4): p. 619-29.
198. Yang, L., et al., *Schwann Cells Transplantation Improves Locomotor Recovery in Rat Models with Spinal Cord Injury: a Systematic Review and Meta-Analysis.* Cellular Physiology and Biochemistry. **37**: p. 2171-2182.
199. Yang, Z., et al., *Isolation and characterization of SSEA3(+) stem cells derived from goat skin fibroblasts.* Cell Reprogram, 2013. **15**(3): p. 195-205.
200. Zhang, H., Z.M. Xiong, and K. Cao, *Mechanisms controlling the smooth muscle cell death in progeria via down-regulation of poly(ADP-ribose) polymerase 1.* Proc Natl Acad Sci U S A, 2014. **111**(22): p. E2261-70.
201. Zhao, M., et al., *Tracing the stemness of porcine skin-derived progenitors (pSKP) back to specific marker gene expression.* Cloning Stem Cells, 2009. **11**(1): p. 111-22.
202. Zhao, M.T., et al., *Deciphering the mesodermal potency of porcine skin-derived progenitors (SKP) by microarray analysis.* Cell Reprogram, 2010. **12**(2): p. 161-73.
203. Zhao, W., et al., *Embryonic stem cell markers.* Molecules, 2012. **17**(6): p. 6196-236.
204. Zschenker, O., et al., *Genome-wide gene expression analysis in cancer cells reveals 3D growth to affect ECM and processes associated with cell adhesion but not DNA repair.* PLoS One, 2012. **7**(4): p. e34279.